THE UNIVERSITY of TULSA

Department of Petroleum Engineering

DRILLING RESEARCH PROJECTS ADVISORY BOARD MEETING

EXECUTIVE SUMMARIES REPORTS

May 23-24, 2005

TULSA UNIVERSITY
Drilling Research Projects
(TUDRP)

Advisory Board Meeting
May 23-24, 2005

Executive Summaries
Reports

Doubletree Hotel at Warren Place
6100 South Yale
Tulsa, OK 74136
918/495-1000

THE UNIVERSITY of TULSA

College of Engineering and Applied Sciences
Petroleum Engineering
Tulsa **U**niversity **D**rilling **R**esearch **P**rojects

May 9, 2005

Dear TUDRP Member Companies:

This report is submitted to summarize TUDRP's research activities since our last meeting in November, 2004. This book contains:

- an agenda;
- a list of our member companies;
- a list of TUDRP's personnel;
- a list of our current graduate students, their reports and/or proposals.

All reports will be fully presented and discussed at the meeting on May 23rd and 24th, 2005.

The active technical and financial support provided by each of you has been the key to our success. With your support and dedication, TUDRP will always strive for academic excellence, high quality research, and will maintain its commitment of providing short and long term drilling technology needs to the oil and gas industry.

On behalf of The University of Tulsa, I would like to extend my genuine appreciation for your continued interest in and support of TUDRP.

Sincerely,

Stefan Miska
Director, Drilling Research Projects

AGENDA

THE UNIVERSITY OF TULSA
Drilling Research Projects
Advisory Board Meeting

Doubletree Hotel at Warren Place
6100 South Yale
Tulsa, OK 74136

FINAL AGENDA

Monday, May 23rd, 2005

CLASSIC CONTINENTAL BREAKFAST…….8:00 a.m.
Salon A& B Room (Formerly California Room)

INTRODUCTION
Stefan Miska ……8:30 a.m. - 8:55 a.m.

PROGRESS REPORTS

Ramadan Ahmed……...8:55 a.m. - 9:30 a.m.
Experimental Study and Modeling of Yield Power-Law Fluid Flow in Pipes and Annuli

Jimmy Lozano……..…9:30 a.m. - 10:15 a.m.
The Effect of Elongational Flow Through the Drill Bit Nozzle on the Rheology of Polymeric Drilling Fluids

Coffee Break ……10:15 a.m. - 10:35 a.m.

Duan Mingqin……..……10:35 a.m. - 11:15 a.m.
An Experimental Study of Small Sand-Sized Cuttings Transport in Horizontal and High Angle Boreholes

Sarita Simoes....……..…… ……..11:15 a.m. – 11:50 a.m.
The Effect of Tool Joints on ECD While Drilling with Polymeric Fluids

Mengjiao Yu……..……...11:50 a.m. – 12:00 p.m.
Update on New Research Proposals

LUNCH…….....12:00 p.m. - 1:15 p.m.
Salon C Room (Formerly Scottsdale Room)

Mohammad Oyarhossein ...…….. ……1:15 p.m. – 1:50 p.m.
Mathematical Modeling of Transient Wellbore Trajectory for Complex BHA

Sandeep Valluri ……...……1:50 p.m. – 2:15 p.m.
Study on Effective Hole Cleaning Using "Sweeps" in Horizontal Wellbores

Zhu Chen…….. ……2:15 p.m. - 2:50 p.m.
Study of Cuttings Transport with Foam under Elevated Pressure And Elevated Temperature Conditions

Christina Tryon…..……..…..2:50 p.m. - 3:00 p.m.
Rheology of Polymer-Stabilized Foams

Mark Pickell……...……..……..3:00 p.m. - 3:10 p.m.
Continuing Foam Rheological Characterization Studies Using the Foam Generator and Viscometer Apparatus

Coffee Break …….…….3:10 p.m. - 3:25 p.m.

Elie Barakat…...……..……..……3:25 p.m.- 3:50 p.m.
An Experimental Study and Modeling of The Effect of Hydraulic Vibrations on Axial Force Transfer in Horizontal Wellbores

Jennifer Schaffner.……...…..3:50 p.m.- 4:00 p.m.
Study of Cuttings Attachment to Air Bubbles in Lab-Scale Tests

RESEARCH – PROPOSALS

Augusto Garcia… ……..……...……4:00 p.m.- 4:20 p.m.
Determination of Cutting Lag in Horizontal and Deviated Wells

INDUSTRY PRESENTATION

Willie Iyoho……...……..……..…...……..…….……4:20p.m. - 4:40 p.m.
Data, Data Everywhere…What's an Engineer to do?

Budget and Closing Comments ……..…….…4:40 p.m. - 5:00 p.m.

ADJOURN …….……..……..5:00 p.m.

RECEPTION…….……..7:00 p.m. - 9:00 p.m.
Doubletree at Warren Place Warren II Building, 19th Floor Ballroom
6100 South Yale Tulsa, OK 74136

THE UNIVERSITY OF TULSA
Advisory Board Meeting

University of Tulsa
2450 E Marshall
Tulsa, OK 74110

FINAL AGENDA

Tuesday, May 24th, 2005 NORTH CAMPUS

FACILITY TOUR of NORTH CAMPUS
Mark Pickell……9:00 a.m.-11:00 a.m.
With Focus on: Progress on Flow Loop Elevation Modifications

ROUND TABLE DISCUSSION……..11:00 a.m. – 11:30 a.m.

LUNCH…… 11:45 p.m.-1:00 p.m.
Formal Lounge in ACAC on The University of Tulsa- SOUTH CAMPUS

INDIVIDUAL MEETINGS (if required**)**……1:30 p.m. – 5:00 p.m.

**********Next Advisory Board Meeting- November 14 -15th, 2005**********

MEMBER COMPANIES

ChevronTexaco	**1967**
PDVSA Intevep, S.A.	**1975**
BP Exploration	**1977**
Petrobras/Cenpes	**1984**
Statoil	**1985**
Abu Dhabi National Oil Company	**1986**
Halliburton Energy Services	**1996**
Baker-Hughes	**1997**
United States Department of Energy	**1997**
Schlumberger	**1997**
Total	**1998**
Weatherford	**2000**
Anadarko Petroleum	**2001**
ExxonMobil	**2002**
Aramco Services	**2003**
ConocoPhillips	**2003**

TUDRP PERSONNEL

TUDRP PERSONNEL

EXECUTIVE DIRECTOR/PI:
Stefan Miska

SR. ASSOCIATE DIRECTOR:
Nicholas Takach

ASSOCIATE DIRECTOR:
Mengjiao Yu

RESEARCH ASSOCIATE
Ramadan Ahmed

PROJECT ASSISTANTS:
Devra McManus
Paula Udwin – part-time

MECHANICAL TECHNICIAN:
Garrett Pierce

PROJECT ENGINEER:
Mark Pickell

PROJECT TECHNICIAN
Steven Turpin

RESEARCH ASSOCIATES:
Charles Alworth
Steven Tipton
J.J. Azar
Siamack Shirazi
James Sorem

RESEARCH ASSISTANTS:

Zhu Chen, Ph.D. Candidate
Mingqin Duan, M.S. Candidate
Jimmy Lozano, M.S. Candidate
Sandeep Valluri, M.S. Candidate
Augusto Garcia, M.S. Candidate
Mohammad Oyarhossein, M.S. Candidate
Christina Tryon, Undergraduate
Sarita Simoes, M.S. Candidate
Elie Barakat, M.S. Candidate
Yahya Hashemiandari, M.S. Candidate
Vahid Dokhani, M.S. Candidate
Hamidreza Shahabadif, M.S. Candidate
Jennifer Schaffner, Undergraduate

Mailing Address:
Drilling Research Projects
600 South College Avenue
Tulsa, Oklahoma 74104
Telephone: (918) 631-5171

Shipping Address:
Drilling Research Projects
2450 East Marshall Street
Tulsa, Oklahoma 74110
Facsimile: (918) 631-5009

EXECUTIVE SUMMARIES
And
REPORTS

Experimental Study and Modeling of Yield Power-Law Fluid Flow in Pipes and Annuli

Ramadan Ahmed

Experimental Study and Modeling of Yield Power-Law Fluid Flow in Pipes and Annuli

---

INVESTIGATOR: Ramadan Ahmed, Research Associate

INTRODUCTION: During the last TUDRP Advisory Board Meeting (November 2004), a research proposal for investigating flow of Yield Power-Law (YPL) fluids in pipes and annuli was presented and accepted by the members. This is the first report that presents flow loop development activities and research work conducted since November 2004. In order to carry out small-scale flow loop experiments, the dynamic testing facility (DTF) that was developed previously for foam characterization was modified to permit rheology and hydraulic investigations of modern drilling fluids. Flow loop instrumentations and a data acquisition system were installed and calibrated.

OBJECTIVES: The aim of this study is to develop a reliable hydraulic model that accurately predicts the frictional pressure losses in pipes and annuli under laminar, transitional and turbulent flow conditions. The research involves both mathematical modeling and experimental investigations. The effects of fluid properties (function of temperature and pressure), eccentricity, pipe roughness and pipe rotation on the relationship between frictional pressure losses and flow rate will be studied experimentally and theoretically.

APPROACH: Flow loop experiments were conducted on two Bentonite muds (6% and 9% Bentonite by weight) that have strong shear thinning property and high yield stress. For this investigation, fluid characterization was made using pipe and rotational viscometers Results indicate that measurements obtained from these two methods are comparable. Rheologies of these fluids best fit the yield power-law model. Bentonite muds exhibit minor time-dependent rheological behavior. Frictional pressure losses in the pipes are in agreement with analytical solutions. Annular pressure loss measurements are compared with predictions of the model by Kozicki and Tiu model. A satisfactory agreement is obtained between the observed and calculated pressure losses.

DELIVERABLES:

- Experimental database for flow of YPL fluids (synthetic/polymeric);
- Mathematical models that can predict frictional pressure losses of YPL fluids in pipes and annuli under different flow conditions (flow regimes, temperatures, pressures, eccentricities, pipe rotations and wall roughnesses);
- Computer code to predict frictional pressure losses in boreholes;
- Recommendations and guidelines in the use of YPL fluids for ECD management and hydraulics optimization.

TUDRP

Experimental Study and Modeling of Yield Power-Law Fluid Flow in Pipes and Annuli

Ramadan Ahmed, The University of Tulsa, Drilling Research Projects

This report is prepared for TUDRP Advisory Board Meeting, May 23-24, 2005, Tulsa, Oklahoma

---

Summary

During the last TUDRP Advisory Board Meeting (November 2004), a research proposal for investigating flow of Yield Power-Law fluids in pipes and annuli was presented and accepted by the members. This is the first report that presents flow loop development activities and research work conducted since November 2004. To conduct small-scale flow loop experiments, the dynamic testing facility (DTF) that was developed previously for foam characterization is modified to permit rheology and hydraulic investigations of modern drilling fluids. Flow loop instrumentations and data acquisition system are installed and calibrated.

Many modern drilling fluids such as synthetic/polymer based muds are of Yield Power-Law type fluids[1]. Currently, very limited hydraulic data is available for such fluids. The aim of this study is to develop a reliable hydraulic model that accurately predicts the frictional pressure losses in pipes and annuli under laminar, transitional and turbulent flow conditions. The research involves both mathematical modeling and experimental investigations. The effects of fluid properties (function of temperature and pressure), eccentricity, pipe roughness and pipe rotation on the relationship between frictional pressure losses and flow rate will be studied experimentally and theoretically.

This report presents experimental investigations conducted on the flow of drilling muds that have strong shear thinning property and high yield stress. For this investigation, fluid characterization was made using three pipe viscometers (0.5” [12.7 mm], 0.824” [20.9 mm] and 1.38” [35 mm]) and two rotational viscometers (Chan 35). A fully eccentric annular test section (0.675” × 1.38” [17 mm × 35 mm]) is attached to the DTF loop (Fig.

1) in series with the pipe sections (pipe viscometers) to simulate eccentric boreholes. During the experiment, flow rate was varied from 0.1 to 21.5 gpm [0 to 79.5 l/min].

Water and polymeric fluid tests were conducted first to test data acquisition system and establish confidence on the measurements. Two Bentonite muds (6% and 9% Bentonite by weight) were considered for this investigation. Rheological measurements obtained from pipe viscometers were compared with readings of rotational viscometers. Results indicate that measurements obtained from these two methods are comparable. A maximum discrepancy of about 20% is observed at low shear rates. Rheologies of these fluids best fit the yield power-law model. Bentonite muds exhibit minor time-dependent rheological behavior. Frictional pressure losses in the pipes are in agreement with analytical solutions. Annular pressure loss measurements are compared with predictions of Kozicki and Tiu[2] model. A satisfactory agreement is obtained between the observed and calculated pressure losses. Predicted values are approximately 10% higher than the measured data.

Introduction

Many synthetic/polymeric drilling fluids show Yield Power-Law type rheological behavior. In current practice, rotational viscometer measurements are used as inputs for hydraulic models to predict frictional pressure losses in the drillpipe and wellbore. However, comparisons of experimental data[3,4] and field measurements[5] with predictions of these models often show significant discrepancies that suggest the need for further investigations and improvements on the usage of rotational viscometer measurements of these fluids.

Yield Power-Law fluids such as polymer based muds and synthetic fluids have been widely applied in drilling operations with well-known benefits[6]. The rheology and hydraulics of these fluids are very essential for the design of hydraulic programs, cuttings transport and drilling optimization. The standard API-recommended methods[7] for drilling hydraulics assume either a Power-Law or Bingham Plastic rheology model. However, most drilling fluids obey the Yield Power-Law model. Often the API methods tend to underestimate drillstring pressure losses and overestimate annular pressure losses[8]. For this reason, it becomes very difficult to accurately estimate equivalent circulation density (ECD), which is important in controlling wellbore stability and formation damage.

It is well documented[3,10] that the rheology and hydraulics of synthetic/polymeric fluids are functions of fluid properties, which are, in turn, functions of temperature, pressure and drilling fluid compositions. Results from the previous research[3] clearly show that rheological parameters such as consistency index and yield stress are highly sensitive to temperature. Therefore, further study on rheology and hydraulics of fluids with Yield Power-

Law behavior under different temperature and pressure conditions is vital for successful and economical drilling operations.

Objective

The primary objective of this study is to conduct an experimental and theoretical study of the rheology and hydraulics of YPL (synthetic/polymeric) fluids under different temperature and pressure conditions (simulated downhole conditions). Results of this study have great potential to reduce the drilling cost using synthetic/polymeric fluids. The specific objectives of this study are as follows:

i) to verify and improve the usage of rotational viscometer for rheology measurements of YPL fluids;

ii) to determine the effects of temperature and pressure on flow properties of YPL fluids;

iii) to evaluate the predictions of existing YPL fluid rheology/hydraulics models;

iv) to investigate experimentally and theoretically (including CFD simulations) the effects of pipe rotation, eccentricity and pipe roughness on the hydraulics of YPL fluids;

v) to develop rheology and hydraulic models for YPL fluids that account for the effects of temperature and pressure;

vi) to present recommendations and guidelines in the use of YPL fluids for ECD management and hydraulics optimization.

Scope of Work and Methodology

This research includes experimental investigations and theoretical/numerical simulation studies on pipe and annular flows of YPL fluids under laminar, transition and turbulent flow conditions. The flowing research activities are involved in this investigation:

i) Literature review;

ii) Rheological characterization of representative YPL fluids under high temperature-high pressure conditions using rotational viscometers;

iii) Experimental investigation of the hydraulics of YPL fluids in smooth and rough pipes and annuli at different temperatures, pressures and eccentricity;

iv) Comparison of experimental results with predictions of currently available YPL hydraulic models that use rheological data obtained from rotational viscometers;

v) Development of rheology and hydraulic models for synthetic/polymeric fluids taking into account the effects of temperature and pressure on properties of the fluid.

Literature review

Pipe and annular flows of Yield Power-Law fluid is of great interests in drilling applications. This model describes the rheological behavior of drilling muds more accurately than Bingham Plastic and Power-Law models. The Yield Power-Law rheological model for all time-independent fluids is given by:

$$\tau = \tau_y + K\dot{\gamma}^m \tag{1}$$

Laminar Pipe Flow

Assuming no-slip condition at the pipe wall, the generalized flow equation can be expressed for laminar pipe flow of time-independent fluid as:

$$Q = -\pi \int_0^{\tau_w} \left(\frac{R}{\tau_w}\right)^3 \frac{dv}{dr} \tau^2 d\tau \tag{2}$$

where Q, R and τ_w are the volumetric flow rate, pipe radius and wall shear stress, respectively. Rabinowitsch[10] developed a generalized expression for the wall shear rate as:

$$f(\tau_w) = \dot{\gamma}_w = \frac{\tau_w}{4} \frac{d\left(\frac{8U}{D}\right)}{d\tau_w} + \frac{3}{4}\left(\frac{8U}{D}\right) = \frac{3N+1}{4N}\left(\frac{8U}{D}\right) \tag{3}$$

Accordingly, for a time-independent fluid, the shear rate is entirely independent of the fluid properties. Development of this equation is presented in Appendix A. Similar generalized relationship may be developed for other geometries such as narrow slot annuli.

An exact analytical solution for steady, isothermal pipe flow of Yield Power-law fluids under laminar conditions can be presented in the following form, when the no-slip condition is assumed at the wall[11]:

$$\frac{8U}{D} = \frac{(\tau_w - \tau_y)^{(1+1/m)}}{K^{1/m}\tau_w^3}\left(\frac{4m}{3m+1}\right)\left[\tau_w^2 + \frac{2m}{1+2m}\tau_y\tau_w + \frac{2m^2}{(1+m)(1+2m)}\tau_y^2\right] \tag{4}$$

A derivation of this equation is presented in Appendix B. The wall shear stress, τ_w, can be determined from the nominal Newtonian shear rate (8U/D) as:

$$\tau_w = \tau_y + K\dot{\gamma}_w^m = K'(8U/D)^N \tag{5}$$

The Fanning friction factor for laminar pipe flow, f = 16/Re, where the Reynolds number is expressed as:

$$\mathrm{Re} = \frac{\rho D^N U^{2-N}}{K' 8^{N-1}} = \frac{8\rho U^2}{\tau_w} \tag{6}$$

Laminar Annular Flow

Fredrickson and Bird[12] made a detailed analysis and presented an exact solution for laminar flow of Power-Law fluids in concentric annuli. Accordingly, the volumetric flow rate in a concentric annulus is correlated to the pressure drop by:

$$Q = \pi \cdot \left(\frac{n}{3n+1}\right) \cdot \left(\frac{D_o}{2}\right)^{\frac{3n+1}{n}} \left(\frac{1}{2K} \cdot \frac{\Delta P}{\Delta L}\right)^{\frac{1}{n}} \cdot \left[(1-\beta^2)^{1+\frac{1}{n}} - \kappa^{1-\frac{1}{n}}(\beta^2-\kappa^2)^{1+\frac{1}{n}}\right], \tag{7}$$

The parameter β represents the location of maximum velocity in annulus. The approximate value of β can be determined by:

$$\beta = 0.9904 \cdot \kappa^{0.4141} \cdot \mathrm{n}^{0.01238}, \tag{8}$$

where the diameter ratio, κ = Di/Do.

A number of numerical simulation studies[13-15] were conducted to investigate non-Newtonian fluid flow in eccentric annuli. Using numerically obtained results, Haciislamoglu and Langlinais[15] developed a relationship between friction pressure losses of eccentric and concentric annuli for Power-law fluids that have n values ranging from 0.4 to 1.0. This relationship is valid for eccentricities ranging from 0 to 0.95 and diameter ratio from 0.3 to 0.9. An extensive numerical study on power-low fluid was carried out by Escudier et al.[13] using a highly accurate finite-volume technique. The effect of pipe eccentricity was examined with and without pipe rotation. Results without pipe rotation indicated that the product of friction factor and Reynolds number (fRe) varies with eccentricity, diameter ratio and Power-law exponent.

Theoretical analysis of Bingham fluid flow in pipes and concentric annuli was conducted by Melrose et al.[16] to develop a convenient numerical procedure for hydraulic computations. Complex relationships of Bingham fluids flow in concentric annuli were transformed into expressions that are more compact by introducing reduced variables. Savins[17] investigated power-law fluid flow through a circular pipe and concentric annulus, and Couette flow between concentric rotating cylinders. This author presented correlations that relate different flow curves obtained from pipe and Couette viscometers.

At present, an exact analytical solution for laminar flow of YPL fluids in eccentric annulus is not available. However, there are hydraulic models[2,18-20] that can be used for approximate prediction of frictional pressure losses in eccentric annuli. Based on the generalized Rabinowitsch-Mooney wall shear rate equation (Eqn 2), Kozicki and Tiu[2] developed a generalized hydraulic equation for predicting frictional pressure losses in laminar flow of time-independent fluids in ducts of arbitrary shape. The model adopts the shear rate equation for pipe flow and similar expression for flow in slits to have the same form of the generalized shear rate equation, which

is applicable for other duct geometries. According to this approach, the Rabinowitsch-Mooney equation applicable to flow through pipes and slits is expressed as:

$$f(\tau_w) = \dot{\gamma}_w = a\tau_w \frac{d\left(\frac{8U}{D_h}\right)}{d\tau_w} + b\left(\frac{8U}{D_h}\right) = \left[\frac{a}{N} + b\right]\left(\frac{8U}{D_h}\right) \tag{9}$$

where a and b are geometric constants (a = 0.25 and b = 0.75 for pipes and a = 0.5, b = 1 for slits) and D_h is the hydraulic diameter. Kozicki and Tiu[2] assumed that a generalization of the above equation is applicable to any arbitrary geometry that has wall shear stress variation along the wetted parameter (p). Thus:

$$f(\bar{\tau}_w) = \frac{1}{p}\oint_p f(\tau_w)ds = a\bar{\tau}_w \frac{d\left(\frac{8U}{D_h}\right)}{d\bar{\tau}_w} + b\left(\frac{8U}{D_h}\right) \tag{10}$$

where $\bar{\tau}$ is the average wall shear stress. Consequently, the average wall shear rate for any arbitrary geometry is given by:

$$f(\bar{\tau}_w) = \bar{\dot{\gamma}}_w = \left[\frac{a}{N^*} + b\right]\left(\frac{8U}{D_h}\right) \tag{11}$$

Kozicki and Tiu[2] suggested the use of capillary viscometer data for determining the generalized flow behavior index, N^* of an arbitrary shaped duct. Similarly, rotational viscometer data may be used to obtain N*. However, iterative procedure is necessary in this case because the value of N* is determined from the wall shear stress as presented in Appendix B. Thus, Eqn (B-11) can be rewritten in this form:

$$N^* = \frac{mC_c^*}{3m(C_c^* - 1) + 1} \tag{12}$$

where

$$C_c^* = (1-x)\left[\frac{2m^2}{(1+2m)(1+m)}x^2 + \frac{2m}{1+2m}x + 1\right] \tag{13}$$

where

$$x = \frac{\tau_y}{\bar{\tau}_w} \tag{14}$$

Values of the geometric constants are assumed independent of properties of the fluid. Therefore, for eccentric annuli these constants can be determined from Newtonian flows. Kozicki et al.[18] provided the following two equations to evaluate the geometric constants:

$$\frac{8U}{D_h} = \frac{\bar{\tau}_w}{(a+b)\mu} \tag{15}$$

$$\frac{8U_{\max}}{D_h} = \frac{\bar{\tau}_w}{2a\mu} \tag{16}$$

where μ is viscosity of a Newtonian fluid. Expressions for geometric constants for different duct cross-sections (concentric annuli, rectangular and elliptic ducts, and isosceles triangular sections) were presented[2,18]. For eccentric annuli values of these constants vary with the diameter ratio (κ) and eccentricity of the inner cylinder. Using bipolar coordinate transformation, Piercy et al.[21] obtained an exact solution for laminar flow of Newtonian fluid in eccentric annuli. Šesták et al.[22] used this solution in determining the geometric constants (Tables 1 and 2) for eccentric annuli.

After obtaining the values of geometric constants the average wall shear rate can be determined from Eqn (11) and the corresponding shear stress can be determined from the constitutive equation:

$$\bar{\tau}_w = \tau_y + K\bar{\dot{\gamma}}_w^m \tag{17}$$

The generalized Reynolds number for arbitrary shaped duct is determined from the average wall shear stress as:

$$\mathrm{Re}_K = \frac{8\rho U^2}{\bar{\tau}_w} \tag{18}$$

The flow of a modified Herschel-Bulkley fluid through eccentric annuli is examined by Vinod and McIntire[20]. A numerical solution strategy is developed to simulate laminar and turbulent flow of non-Newtonian fluids through conduits of arbitrary cross section. Annular friction pressure loss in slim-hole drilling is significant and needs a hydraulic model that is more accurate. A new hydraulics model for slim-hole drilling applications has been proposed by Hansen et al.[19]. This model is based on theoretical analysis and experimental investigations that include the effect of eccentricity, drillstring rotation and fluid rheology. Recently, Zamora et al.[23] proposed a hydraulic model that can be used for flow of YPL fluids in pipes and annuli under different flow regimes. At high shear rate, the model treats YPL fluids as power-law fluid. Model predictions were compared with results of small-scale flow loop and field measurements. In general, model predictions showed a

satisfactory agreement with the measured data. However, in some cases, the discrepancies were significant. The authors attribute these differences to drill pipe rotation, pipe roughness, tool joint effect and drag reduction.

Experimental Investigation

The dynamic testing facility (DTF) that was developed previously for foam characterization is modified to permit rheology and hydraulic investigations of modern drilling fluids (foams, aerated muds, polymer based fluids and synthetic muds). Experimental investigations were conducted on the flow of two different drilling fluids (approximately 6% and 9% Bentonite by weight) that have strong non-Newtonian behavior. Rheologies of these fluids were tested using both pipe and rotational viscometers.

Experimental Setup

Dynamic testing facility is small-scale flow loop that is developed for foam characterization. The facility was constructed on a 16' x 2-½' skid with a Unistrut cage for supporting the pipe and other components. During the last ABM, the possibilities of using DTF for small-scale investigations that requires highly controlled experimental setups were discussed. In order to meet this object, an annular test section (0.675" × 1.38" [17 mm × 35 mm]) is attached to the DTF loop in series with three pipe sections (0.5" [12.7 mm], 0.824" [20.9 mm] and 1.38" [35 mm]) as shown in Fig. 2. A Moyno type pump with maximum flow capacity 22 gpm [83.27 l/min] circulates the test fluid through the loop. Test fluids are prepared in a 55-gallon [208 liter] tank that has a high-speed stirrer. Hot water is provided from a water boiler to facilitate the mixing of polymers and Bentonite. Each test section is about 18 ft [5.5 m] in length and easily replaceable to vary the roughness and eccentricity. The loop is equipment with computer based data acquisition system and measuring instruments (Table 3) that are necessary for conducting rheology and hydraulic investigations. Four differential pressure transmitters are installed to measure the frictional pressure loss across the test sections. Coriolis flow meter (F3) is placed upstream of the test section to measure the mass flow rate. Two magnetic flow meters (F1 and F2) are installed downstream of the test section to verify Coriolis flow meter readings. Test section inlet and outlet pressures and temperatures are monitored during the test.

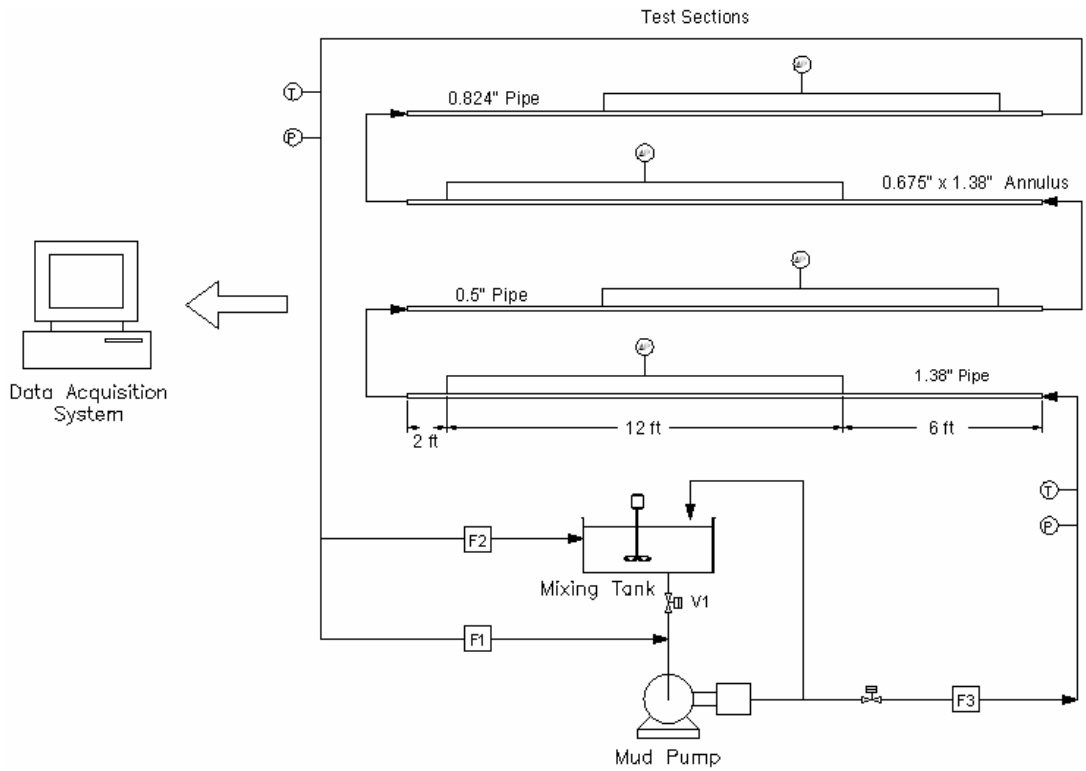

Fig. 2 Simplified Schematic of Experimental Setup

Wall roughnesses of the annulus and pipe sections were measured using a roughness-measuring instrument (Surftest 401). Wall roughnesses of the pipes were found to very low (smooth), when the measurements were taken along the pipe axis. This indicates that patterns of roughness groves are mostly parallel to the pipe axis. Therefore, tests were performed at 15° inclination from the pipe axis. In this case, the roughnesses of all the test sections were found to be approximately 5 μm.

Procedure

Flow loop experiment begins by blending warm water and a viscosifying agent (polymer or Bentonite) in the mixing tank. The inlet valve (V1) should be closed before introducing the viscosifying agent to the tank. This is to protect lumps from entering to the flow loop and clog the piping. After sufficient time of mixing, a homogeneous suspension (dispersion) forms. The suspension may contain small amount of air bubbles. Hence, additional agitation at lower mixer speeds should be necessary for deaerating the fluid. After sufficient deaeration, the inlet value should be open to allow the pump to circulate the fluid. The data acquisition system is turned on to monitor test parameters. The pump should start circulating the fluid at the lowest speed (146 rpm). The pump speed is increased to the maximum level to vent air pockets from the system. As the same time, test fluid in the pressure transmitter lines is displaced by injecting water. Test fluids such as Bentonite mud clog the pressure transmitter lines. When the steady state flow condition is established, fluid sample is taken from

the loop to conduct rheology test using rotational viscometers. Flow loop test begins immediately after rheology characterization of the fluid using rotational viscometers. Each test flow rate is maintained until steady state flow conditions are established; then, the data acquisition system begins recording measurements at the rate of one sample per second for two to five minutes duration.

Flow Loop Testing and Calibration Experiments

After modifying the DTF flow loop, several tests were conducted to evaluate and verify the reliability of measurements obtained from the system. The first test was conducted using water. Results of this experiment are presented in Fig. 3 in form of Fanning friction factor vs. Reynolds number. Detailed results are presented in Table 4. The Reynolds numbers in all the test sections were above the critical Reynolds number (Re = 2100), indicating turbulent flow conditions. Measured friction factors are in agreement with predictions of Colebrook's equation for smooth pipes.

Additional experiment was conducted using 1.5% Hydroxyethyl Cellulose (HEC) suspension. This is to verify measurements under laminar flow conditions, for which analytical solutions to the Navier Stokes equations are available for both pipe and concentric annular flows. The rheologies of the test fluids (Table 5) were measured using two rotational viscometers that are presented in Appendix C. Pipe section measurements were agreement with the analytical solution. In order to verify results from the annular test section, measurements were compared with the predictions of Fredrickson and Bird[12] equation (Eqn 7). All the measurements were found to significantly (40 to 50%) less than the predicted values. The annular section was disassembled to examine the conditions of pipe centralizers. The examination revealed that the cause of the unexpected low frictional pressure was the failure of pipe centralizer in keeping the pipe fully concentric. Therefore, they were removed from the pipe and experiments were conducted in a fully eccentric annuls (100% eccentric). Investigation on other eccentricities, including concentric annulus will be conducted in future.

Experiment with 1.5% HEC was repeated after reassembling the annular test section. Results of this experiment are presented in Table 6. Figure 4 presents flow curves of 1.5% HEC obtained for three different pipe sections. It is apparent from the logarithmic plot that almost all the data points lie on a single straight line, indicating the material is a power-law fluid. It is accepted that without wall slip and end effects, different diameter viscometers should give a single flow curve for a given time-independent fluid, if the temperature and pressure in the viscometers are maintained the same. The plot confirms the power-law fluid rheology obtained from rotational viscometers. In order to compare measurements of pipe and rotational viscometers, apparent viscosities measured using these two different methods are presented in Fig. 5. In general, the two methods approximately show the same rheological measurements. Discrepancies are relatively high at low shear rates

with maximum difference of about 12% at a shear rate of 20/s. For further verification pipe section measurements, results are presented (Fig. 6) in form of fanning friction factor versus generalized Reynolds number. Measured data points predominately lie on the theoretical, f = 16/Re line, which forms straight line in a logarithmic plot.

Measurements from the annular section are compared with results of numerical simulation obtained by Escudier et al.[13]. Theses authors published fRe* values for different eccentric annuli. For comparison purpose, a simulation result that is obtained for eccentricity of 0.98, diameter ratio of 0.5 and n value of 0.5 is considered. The value of power-law index, n, is approximately 0.5 for 1.5% HEC (Table 7). The measured data is presented in Fig 7 in form of friction factor versus Reynolds number (Re*), where Re* is given by:

$$\mathrm{Re}^* = \frac{\rho D_h^n U^{2-n}}{K} \tag{19}$$

The figure clearly shows that measured friction factors are in agreement with numerical obtained friction factors. Hence, measurement reliability is reasonably established for the eccentric annular section.

Experimental Results

Two Bentonite muds were studied in the present investigation. Rheology measurements of the test fluids were carried out just before the flow loop experiments (Table 6). Densities of the muds (Table 7) were measured using a graduated cylinder. Detailed results of the flow loop experiment are presented in Table 8. Flow curves (i.e. shear stress versus shear rate) of 9% Bentonite mud, obtained from the pipe sections, are presented in Fig. 8 together with measurements of the rotational viscometer. The result indicates that all pipe section data lie approximately on a single curve. However, the data points do not form straight line on the log-log plot, indicating 9% Bentonite mud is not a power-law fluid over this range of shear rate. As the pipe-size decreases, the flow curves slightly shift to the left. This could be due Thixotropic behavior (Figs. 9 and 10) of Bentonite mud because the variation in temperature was minimal (Table 8). The arrows in the figures indicate chronological progress of the experiment. It is apparent from the figures that hysteresis exist in the flow curve. In addition to the flow rate, the stress history appeared to be affecting the resulting wall shear stress. This means that the flow curve is not unique like typical time-dependent fluids. Analysis of the result for a given flow rate shows 5 to 15% variations in the wall shear stresses due to the Thixotropic effect.

Wall shear stress measurements that are obtained from the smallest pipe (0.5” pipe) are very close to the rotational viscometer data. A maximum discrepancy of about 20% is observed at low shear rates. Analysis of pipe viscometric data using $\log(\tau-\tau_y)$ vs. $\log(\gamma)$ plot indicates that 9% Bentonite mud is well represented by the

yield power-law model with τ_y = 3.7 Pa, m = 0.65 and K = 0.43 Pas^m. Similar analysis of rotational viscometer data suggests yield power-law model with τ_y = 4.3 Pa, m = 0.59 and K = 0.7 Pas^m. Yield stress measurements obtained from these two methods exhibit a discrepancy of 16%. Figure 11 shows the plot of friction factor versus generalized Reynolds number. The flow is predominantly laminar, as shown by the very low values of generalized Reynolds number. Measured data points closely lie on the theoretical laminar friction factor line (f = 16/Re). The smallest pipe data at high Reynolds numbers (Re > 2000) begins to deviate from the theoretical line, which indicates the onset of transition to turbulent flow.

Measured frictional pressure loss for the annular test section is presented in Fig. 12 as the function flow rate. For comparison purpose, predictions of Kozicki and Tiu[2] model are included in the figure. Model predictions show a satisfactory agreement with the measured pressure losses. In general, predicted values are approximately 10% higher than the measured data.

Another fluid considered for this investigation was 6% Bentonite mud. The fluid was prepared by diluting the 9% Bentonite mud. Test temperature was ranging from ranging from 80 to 85°F [27 to 29°C]. Detailed experimental results are presented in Table 9. Flow curves that are obtained from the pipe and rotational viscometers are presented in Fig. 13. Measured data from pipe viscometers lie roughly on a single curve. Nonetheless, viscometric measurements do not form straight line on the log-log plot, indicating non-power-law fluid. At high shear rates (50 to 1000 1/s), rotational viscometer measurements are very close to that of pipe viscometers. Analysis of pipe viscometric data using $\log(\tau-\tau_y)$ vs. $\log(\gamma)$ plot shows that the data points best fits the yield power-law model with τ_y = 2.1 Pa, m = 0.67 and k = 0.26 Pas^m. Similar analysis of rotational viscometer data also suggests yield Power-law model with τ_y = 2.7 Pa, m = 0.63 and k = 0.34 Pas^m. Discrepancy in yield stress measurement is approximately 28%. For both viscometers, the precision of low shear rate measurements are relatively less; because for these measurements, instrument reading fluctuations and data-acquisition system noise are comparable to the measurements.

Figure 14 shows the log-log plot of Fanning friction factor versus generalized Reynolds number for 6% Bentonite mud. The laminar flow prevails for Reynolds number below 2100, which is the critical value for pipe flows. For laminar flows, measured data points generally lie on the theoretical line (f = 16/Re). The data points begin to deviate substantially from the laminar flow line when the Reynolds number reaches approximately the critical Reynolds number, which indicates the end of laminar flow and the beginning of the transition to turbulent flow. For Reynolds number between 3000 and 4000, the smallest pipe (0.5” pipe) data points fall between two bounding constant N lines (0.6 and 0.8) that are obtained form the Dodge and Metzner[24]

correlation. This is in agreement with the values of N that are obtained from the flow curve curves. N values determined from the flow curves vary from 0.74 to 0.75, for this range of Reynolds number.

Figure 15 presents measured frictional pressure losses and predictions of Kozicki and Tiu[2] model for the annular test section. Good agreement is obtained between model predictions and experimental results. A maximum discrepancy of approximately 12% is observed between predictions and measurements.

Measured and predicted pressure losses in the pipes for 9% Bentonite mud under laminar condition are presented in Figs. 16, 17 and 18. The predicted pressure losses are obtained using different rheological models (Bingham Plastic, Power-law and Yield Power-law). The rheological parameters (τ_y, n, K, PV) for Bingham Plastic and Power-law models are determined from rotational viscometer data measured at 300 and 600 rpm. The rheological parameters of YPL model are determined from full measurements (i.e. 1 rpm to 600 rpm) of the rotational viscometer. It is apparent from the figures that the YPL model performs well when compared with the other two models. The maximum discrepancy between measurements and predictions is 26% for YPL model; while the maximum discrepancies for Bingham Plastic and Power-law models are 260% and 74%, respectively. In general, the discrepancies increases as the pipe size increases and the flow rate decreases. This means that the discrepancies are significant at low shear rates. The effect of flow rate on predictions of YPL model is minimal.

Conclusion

The Dynamic Testing Facility is upgraded to conduct rheology and hydraulic investigations for advanced drilling fluids (polymeric and synthetic fluids). Measurement reliability is reasonably established by comparing measured data with exact solutions for Hydroxyethyl cellulose suspension (power-law fluid). Rheology characterizations were made for two Bentonite muds using pipe and rotational viscometers. Results indicate that measurements obtained from these two methods are similar. Rheology of these fluids best fit the yield power-law model. The Bentonite muds exhibit minor time-dependent rheological behavior that may not significantly affect rheology characterization.

Frictional pressure losses in the pipes were measured predominately under laminar flow conditions. These results are in agreement with analytical solutions. Annular pressure loss measurements are compared with predictions of Kozicki and Tiu[2] model, which is developed for arbitrary duct geometry. The model represents the duct geometry using two geometric constants, which are obtained from Newtonian flows. Comparison of annular measurements with model predictions indicates a satisfactory agreement.

Future work

i) Continuation of this investigation with YPL fluids (Bentonite, Polymeric/Synthetic fluids) under laminar conditions;

ii) Investigations on the effects of eccentricity, wall roughnesses, temperature, pressure and pipe rotation;

iii) Investigation at high Reynolds numbers (requires small pipe size viscometers and/or higher flow rate capacity);

iv) CFD simulations;

v) Development of guidelines for ECD management and hydraulics optimization.

Nomenclature

a = geometric constant

b = geometric constant

U = mean flow velocity

U_{max} = maximum flow velocity

v = local flow velocity

D = pipe diameter

D_h = Hydraulic diameter

N = Generalized Fluid's Behavior Index

N* = Generalized Fluid's Behavior Index for any duct geometry

L = Pipe Length

K= Fluid's Consistency Index

Q = Volumetric Flow Rate

P = Pressure

p = wetted perimeter

m = Fluid Behavior Index

Re = Reynolds Number

f = friction factor

Greek Letters

ε = surface roughness

τ = Shear stress

$\bar{\tau}$ = average shear stress

γ = Shear Rate

$\bar{\gamma}$ = average shear rate

Δ = difference

ω = rotational speed

ψ = diameters ratio,

Subscripts

eff = effective

i = inside

o = outside

y = yield

w = wall

References

1. Davison, J. M., Clary, S., Saasen, A., Allouche, M., Bodin, D. and Nguyen, V-A. "Rheology of Various Drilling Fluid Systems under Deepwater Drilling Conditions and the Importance of Accurate Predictions of Downhole Fluid Hydraulics" SPE paper 56632, presented at SPE Annual Technical Conference and Exhibition, 3-6 October, Houston.
2. Kozicki, W. and Tiu, C. 1986. Parametric Modeling of Flow Geometries in Non-Newtonian Flows. Encyclopedia of Fluid Mech. 7, 200-248.
3. Demirdal, B., 2001, "The Study of Flow of Paraffin Based Synthetic Drilling Fluid at Elevated Pressure and Elevated Temperature (EPET) Conditions", Master of Science Thesis, University of Tulsa.
4. Subramanian,R. and Azar, J.J., 2000, "Experimental Study on Friction Pressure Drop for Non-Newtonian Drilling Fluids in Pipe and Annular Flow" SPE paper presented at the SPE International Oil and Gas Conference and Exhibition in China held in Beijing, China, 7-10 November 2000.
5. White, W.W., Zamora, M. and Svoboda, C.F., 1997, "Downhole Measurements of Synthetic-Based Drilling Fluid in an Offshore Well Quantify Dynamic Pressure and Temperature Distributions", SPE paper 35057, SPE drilling and Completion, September 1997.
6. Friedheim, J.E. and Conn, H.L. 1996, "Second Generation Synthetic Fluids in the North Sea: Are They Better?", SPE paper 35061, Presented at IADC/SPE Drilling Conference held in New Orleans, Louisiana, 12-15 March.
7. "Recommended Practice on the Rheology and Hydraulics of Oil-Well Drilling Fluids", API Recommended Practice 13D, 3rd Edition, June, 1995.
8. Reed, T.D., Pilehvari, A.A., 1993, "A New Model for Laminar, Transitional and Turbulent Flow of Drilling Muds", presented in the SPE/IADC Drilling Conference held in Amsterdam, February 22-25 (SPE 25456).
9. F.B. Growcock, S.L. Andrews, and T.P. Frederick, 1994, "Physicochemical Properties of Synthetic Drilling Fluids" SPE paper 27450, presented at the 1994 IADC/SPE Drilling Conference held in Dallas, Texas, 15-18 February.
10. Rabinowitsch, B. Z., Physik. Chem., 145A, 1, 1929.
11. Miska, S.Z."Advanced Drilling", Teaching Note, University of Tulsa, 2004.
12. Fredrickson, A.G. and Bird, R.B., 1958, "Non-Newtonian Flow in Annuli", Ind. Eng. Chem., 50, 347-383.
13. Escudier, M.P., Gouldson, I.W., Oliveira, P.J. and Pinho, F.T. 2000. Effects of inner cylinder rotation on laminar flow of a Newtonian fluid through an eccentric annulus. Int. Journal of Heat and Fluid Flow, 21, 92-103.

14. Fang, P., Manglik, R.M. and Jog, M.A. 1999. Characteristics of laminar viscous shear-thinning fluid flows in eccentric annular channels. Journal of Non-Newtonian Fluid Mechanics, 84, 1-17.
15. Haciislamoglu, M. and Langlinais, J. 1990, "Non-Newtonian flow in eccentric annuli", Journal of Energy Resources, pp 163,169.
16. Melrose, J.C., Savins, J.G., Foster, W.R. and Parish, E.R., "A practical Utilization of the Theory of Bingham Plastic Flow in Stationary Pipes and Annuli" Petroleum Transaction, AIME, vol. 213, 1958.
17. Savins, J.G. "Generalized Newtonian (Pseudoplastic) Flow in Stationary Pipes and Annuli" Petroleum Transaction, AIME, vol. 213, 1958.
18. Kozicki, W., Chou, C.H. and Tiu, C. 1966. Non-Newtonian flow in ducts of arbitrary cross-sectional shape. Chemical Engineering Science, 21, 665-679.
19. Hansen, S.A., Rommetveit, R., Sterri, N., Aas, B. and Merlo, A. "A New Hydraulics Model for Slim Hole Drilling Applications" SPE paper 57579, presented at SPE/IADC Middle East Drilling Technology Conference, 8-10 November, Abu Dhabi.
20. Vinod, P.S. and McIntire, L.V. "Rheology Effects on Laminar and Turbulent Flow of Model Drilling Fluids Through Deviated Wells" SPE paper 28287, Society of Petroleum Engineers, 1994.
21. Piercy, N.A.V., Hooper, M.S. and Winny, H.F. 1933. Viscous flow through pipes with core. London Edinburgh Dublin Phil. Mag. J. Sci., 15 647-676.
22. Šesták, J.Í., Žitný, R., Ondrušová, J. and Filip, V. 2001. Axial flow of purely viscous fluids in eccentric annuli: Geometric parameters for most frequently used approximate procedures, 3rd Pacific Rim Conference on Rheology, Canadian Group of Rheology, Montreal.
23. Zamora, M., Roy, S. and Slater, K. "Comparing a Basic Set of Drilling Fluid Pressure-Loss Relationships to Flow-Loop" paper presented at the AADE 2005 National Technical Conference and Exhibition, Houston, April 5-7.
24. Dodge, D.W. and Metzner, A.B., 1959, "Turbulent Flow of Non-Newtonian Systems", AIChE journal, Vol. 5, No. 2, June, pp 189-204.
25. Tomita, Y., 1959, Bulletin of J.S.M.E., 2, 10-6.
26. Torrance, B.M., 1963 "Turbulent Flow in Smooth Pipes of Yield-psedoplastic Fluids", South African Mechanical Engineer, vol. 13, 89-96.
27. Metzner, A.B. and Reed, J.C., 1955, "Flow of Non-Newtonian Fluids-Correlation of the Laminar, Transition and Turbulent flow Regions", AIChE Journal, Vol. 1, No.4, December, pp 434-440.

Fig. 1 Modified Dynamic Testing Facility (DTF)

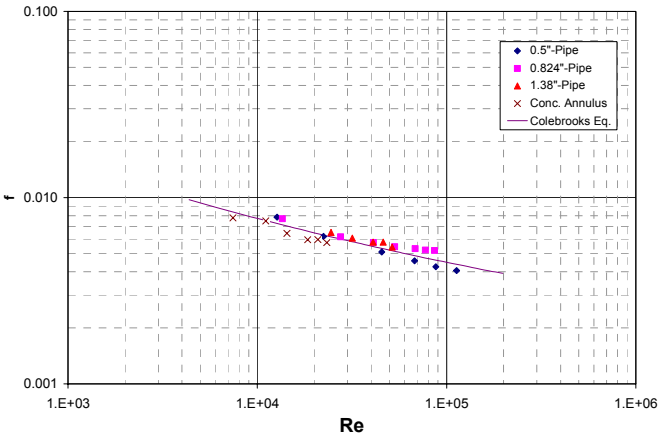

Fig. 3 Fanning Friction Factor vs. Reynolds Number for Water Test

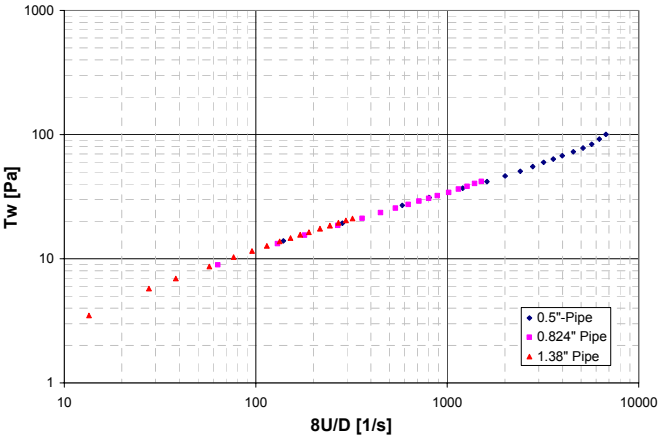

Fig. 4 Flow curves of 1.5% HEC in Three Different Pipe Sections

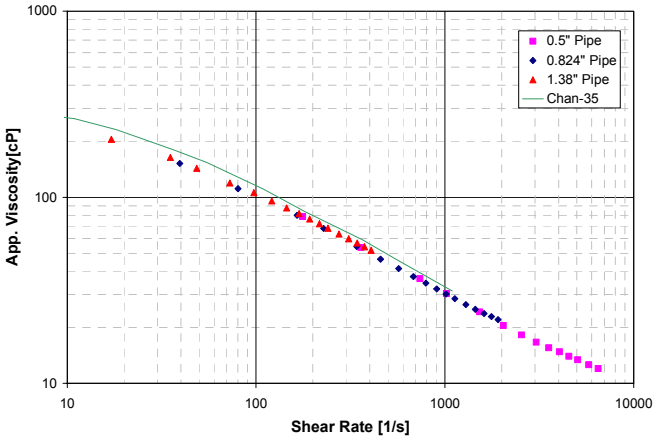

Fig. 5 Apparent Viscosities of 1.5% HEC Measured using Pipe and Rotational Viscometers

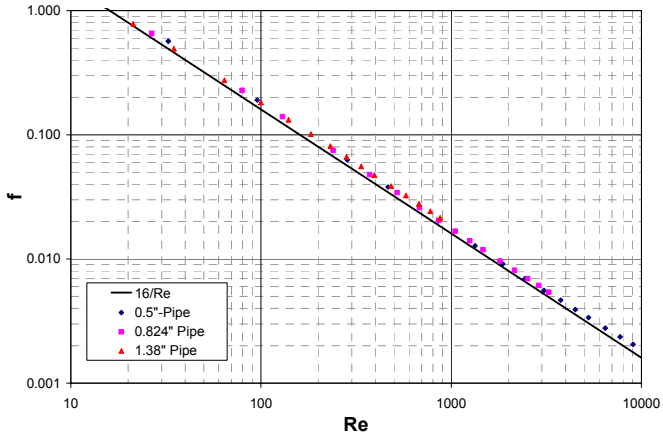

Fig. 6 Fanning Friction Factor vs. Generalized Reynolds Number for 1.5% HEC

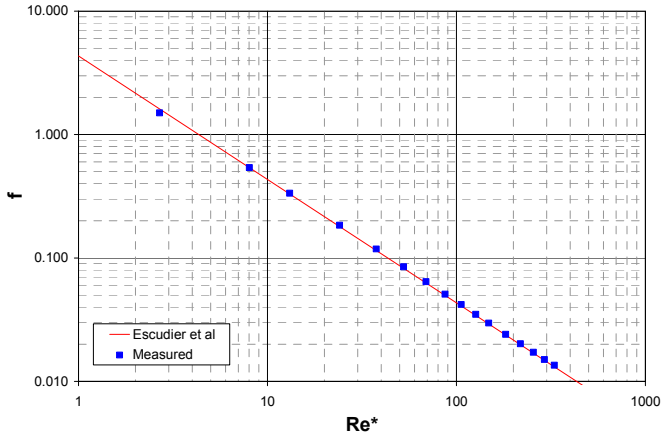

Fig. 7 Fanning Friction Factor vs. Reynolds Number (Re*) for Eccentric Annuls (1.5% HEC)

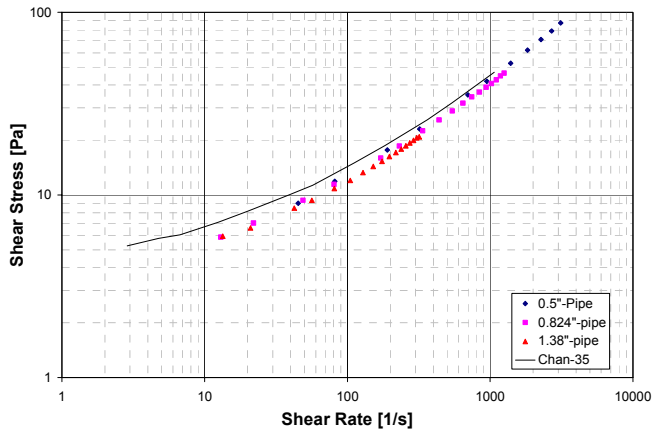

Fig. 8 Flow Curves Of 9% Bentonite Mud Using Pipe and Rotational (Chan 35) Viscometers

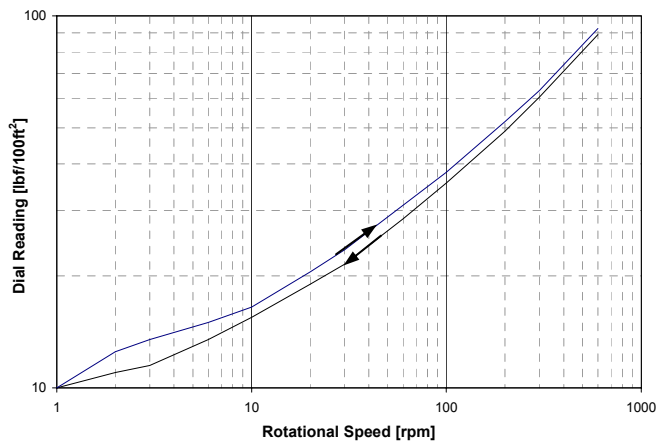

Fig. 9 Thixotropic Behavior of 9% Bentonite Mud Using Rotational Viscometer

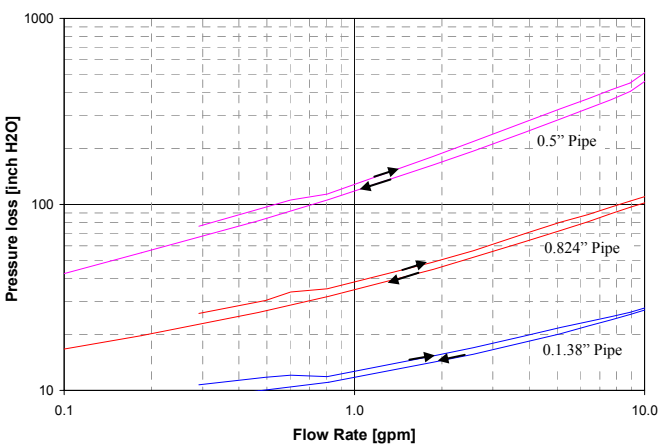

Fig. 10 Thixotropic Behavior of 9% Bentonite Mud Using Pipe Viscometers

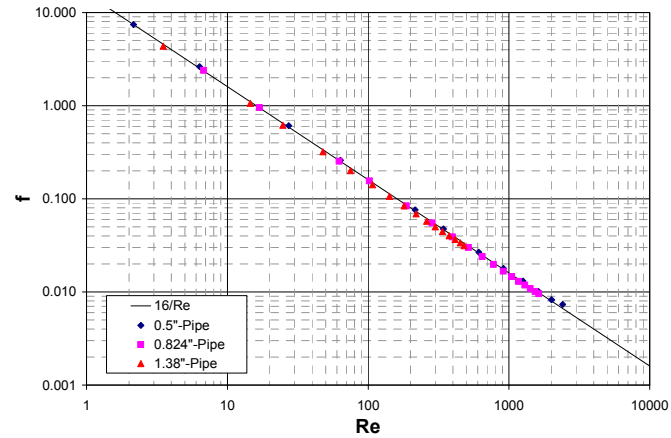

Fig. 11 Fanning Friction Factor vs. Generalized Reynolds Number For 9% Bentonite Mud

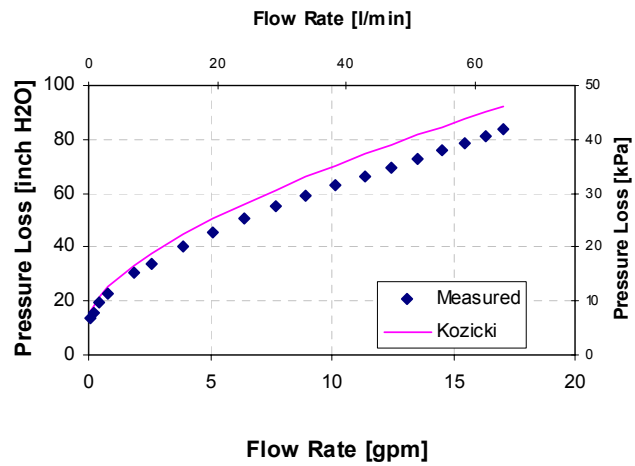

Fig. 12 Measured and Predicted Pressure Losses vs. Flow Rate for 9% Bentonite Mud in Fully Eccentric Annulus

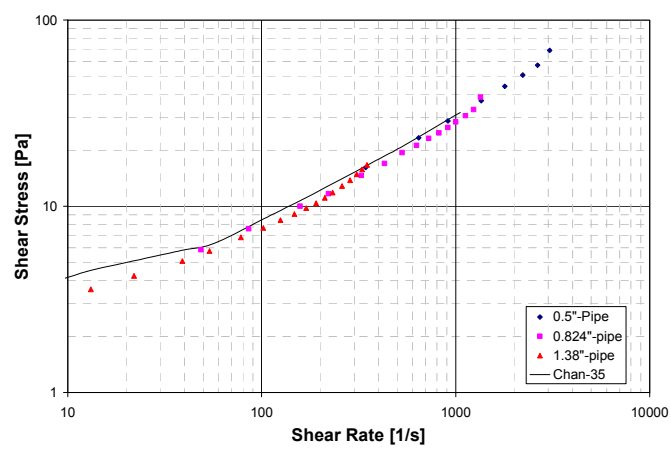

Fig. 13 Flow Curves of 6% Bentonite Mud Using Pipe and Rotational (Chan 35) Viscometers

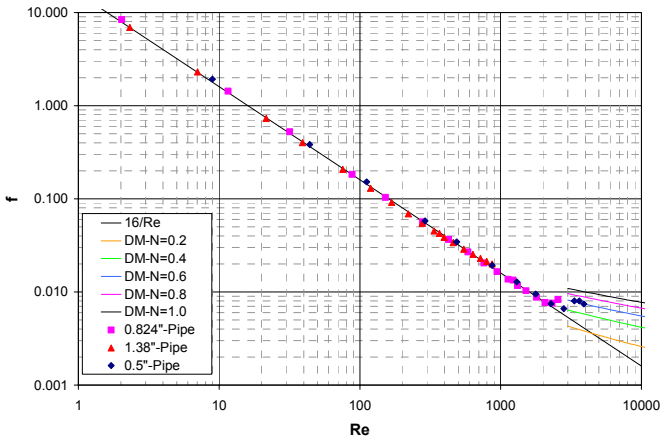

Fig. 14 Fanning Friction Factor vs. Generalized Reynolds Number for 6% Bentonite Mud

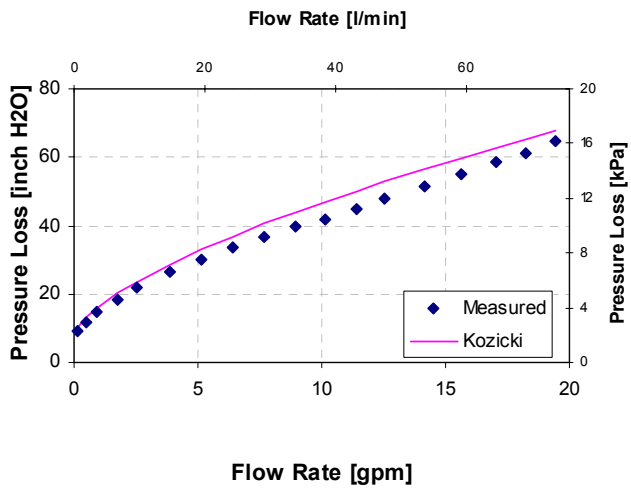

Fig. 15 Measured and Predicted Pressure Losses vs. Flow Rate for 6% Bentonite Mud in Fully Eccentric Annulus

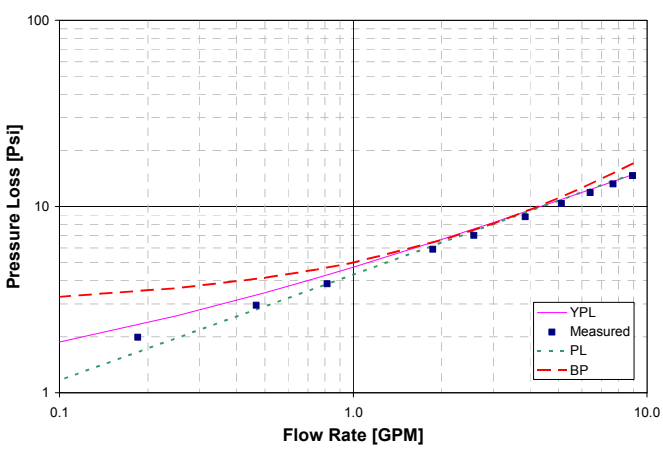

Fig. 16 Measured and Model Predicted Pressure Losses vs. Flow Rate for 9% Bentonite Mud in 0.5" pipe

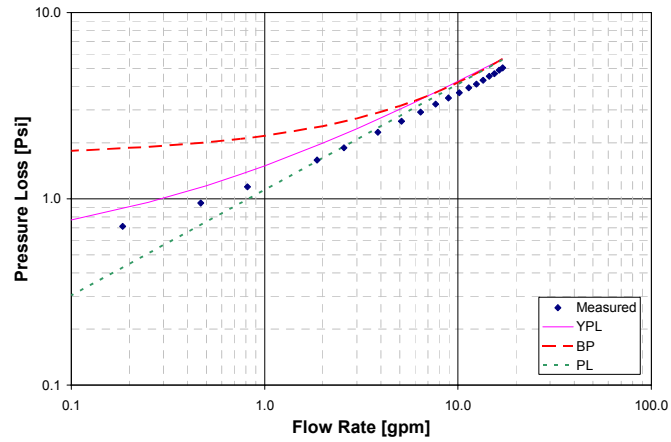

Fig. 17 Measured and Model Predicted Pressure Losses vs. Flow Rate for 9% Bentonite Mud in 0.824" pipe

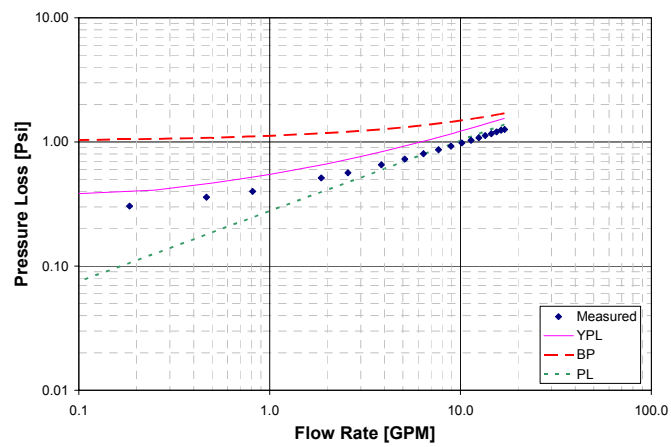

Fig. 18 Measured and Model Predicted Pressure Losses vs. Flow Rate for 9% Bentonite Mud in 1.38" pipe

Table 1 Geometric Constant "a" for Eccentric Annuli[22]

	$\varepsilon = 0.1$	$\varepsilon = 0.3$	$\varepsilon = 0.5$	$\varepsilon = 0.7$	$\varepsilon = 0.9$	$\varepsilon = 1.0$
$\kappa = 0.1$	0.391	0.316	0.268	0.236	0.216	0.209
$\kappa = 0.3$	0.408	0.309	0.246	0.204	0.176	0.165
$\kappa = 0.5$	0.412	0.302	0.233	0.187	0.155	0.142
$\kappa = 0.7$	0.413	0.298	0.225	0.177	0.144	0.131
$\kappa = 0.9$	0.413	0.296	0.223	0.173	0.139	0.126
$\kappa = 1.0$	0.413	0.296	0.222	0.173	0.139	0.125

Table 2 Geometric Constant "b" for Eccentric Annuli[22]

	$\varepsilon = 0.1$	$\varepsilon = 0.3$	$\varepsilon = 0.5$	$\varepsilon = 0.7$	$\varepsilon = 0.9$	$\varepsilon = 1.0$
$\kappa = 0.1$	0.992	0.976	0.884	0.772	0.677	0.641
$\kappa = 0.3$	1.040	1.009	0.877	0.726	0.595	0.541
$\kappa = 0.5$	1.056	1.020	0.872	0.704	0.559	0.499
$\kappa = 0.7$	1.062	1.024	0.869	0.695	0.544	0.482
$\kappa = 0.9$	1.064	1.026	0.869	0.692	0.539	0.476
$\kappa = 1.0$	1.065	1.026	0.869	0.692	0.539	0.476

Table 3 List of Measuring Instruments

	Instrument	Quantity	Manufacturer	Model
1	Magnetic Flow Meter	2	Omega	FMG-401/ FMG-403
2	Coriolis Mass Flow Meter	1	Micro Motion	ELITE® Mass Flow and Density Meters, CMF100
3	Differential Pressure Transmitters	4	Rosemount/Honeywell	Rosemount 3051CD/Honeywell ST 3000, STD125
4	Pressure Transmitter	1	Rosemount	3051C-Gauge
5	Temperature Transmitters	2	Rosemount	3144P
6	Data Acquisition Card	1	Omega	CIO-DAS48-PGA

Table 4 Detailed Results of Water Experiments

Flow Rate	Differential Pressure [inch H_2O]				Temperature [°F]		Pressure
[gpm]	0.5" Pipe	0.824" Pipe	Annulus	1.38" Pipe	Inlet	Outlet	[Psi]
1.84	15.31	1.62	1.02	0.26	71.31	70.69	3.01
3.22	36.76	3.76	1.64	0.30	72.45	72.08	6.02
6.43	121.27	12.02	3.91	0.99	74.55	72.12	13.20
9.63	243.07	25.10	8.41	2.16	73.95	72.41	25.30
12.68	391.99	41.28	12.52	3.49	71.74	72.36	42.92
15.63	More than 600	61.44	17.58	5.05	77.11	72.43	60.90
18.38	More than 600	83.28	24.41	6.97	72.18	69.40	84.91
20.76	More than 600	105.72	29.98	8.39	70.51	73.05	107.07

Table 5 Rheologies of Test Fluids Measured Using Rotational Viscometer (VIS#3)

RPM	Shear Stress					
	1.5% HEC @ 68°F [20°C]		9% Bentonite @ 74°F [23.3°C]		6% Bentonite @ 78°F [25.6°C]	
	[lbf/100ft^2]	[Pa]	[lbf/100ft^2]	[Pa]	[lbf/100ft^2]	[Pa]
1			10.00	4.79	6.00	2.87
2	2.50	1.20	11.00	5.27	6.50	3.11
3	3.00	1.44	11.50	5.51	7.00	3.35
6	5.50	2.63	13.50	6.46	8.50	4.07
10	8.00	3.83	15.50	7.42	9.50	4.55
20	12.50	5.99	19.00	9.10	11.00	5.27
30	16.00	7.66	21.50	10.29	12.00	5.75
60	23.00	11.01	28.50	13.65	17.00	8.14
100	29.00	13.89	35.50	17.00	22.00	10.53
200	41.00	19.63	49.00	23.46	32.00	15.32
300	48.50	23.22	60.50	28.97	40.00	19.15
600	65.00	31.12	89.00	42.61	60.50	28.97

Table 6 Summary of Yield Power-Law Rheological Parameters of Test Fluids

	1.5% HEC		9% Bentonite		6% Bentonite	
	Pipe	**Chan 35**	**Pipe**	**Chan 35**	**Pipe**	**Chan 35**
Yield Stress [lbf/100ft^2]	0.00 [0.00 Pa]	0.00 [0.00 Pa]	7.70 [3.70 Pa]	8.94 [4.3 Pa]	4.37 [2.10 Pa]	5.62 [2.70 Pa]
m	0.48	0.51	0.65	0.59	0.67	0.64
K [bf/100ft^{2}s^m]	2.6 [1.25 Pas^m]	2.2 [1.06 Pas^m]	0.88 [0.43 Pas^m]	1.46 [0.70 Pas^m]	0.54 [0.26 Pas^m]	0.71 [0.34 Pas^m]
Density [ppg/]	8.35 [1002 Kg/m^3]		8.68 [1040 Kg/m^3]		8.93 [1070 Kg/m^3]	

Table 7 Detailed Results of 1.5% HEC Experiment

Flow Rate	Differential Pressure [inch H_2O]				Temperature [°F]		Pressure
[gpm]	**0.5" Pipe**	**0.824" Pipe**	**Annulus**	**1.38" Pipe**	**Inlet**	**Outlet**	**[Psi]**
21.48	463.97	117.92	78.61	35.39	73.70	75.36	96.47
19.84	424.78	113.26	74.68	34.10	75.02	74.71	84.42
18.13	386.28	107.43	71.32	32.62	73.70	73.71	72.55
16.34	360.63	101.97	67.84	30.97	74.01	73.71	62.04
14.53	336.45	95.95	63.95	29.23	73.89	73.56	54.49
12.70	312.39	90.18	60.22	27.44	74.01	74.65	49.51
11.43	293.73	86.09	57.46	26.10	73.66	74.36	45.63
10.17	276.44	81.70	54.62	24.63	74.02	73.52	40.27
8.93	255.13	76.98	51.15	23.12	74.32	75.38	36.65
7.66	234.39	71.65	47.63	21.32	73.36	75.46	32.37
6.40	214.50	66.01	43.75	19.38	73.74	75.22	27.23
5.14	193.21	59.49	39.33	17.26	71.02	74.94	23.69
3.84	170.81	52.04	34.15	14.51	74.24	73.89	19.01
2.57	143.41	43.49	27.68	11.64	73.47	73.99	16.24
1.86	124.53	37.07	23.37	9.64	72.88	73.88	13.55
0.90	89.27	25.10	15.41	5.87	73.18	73.52	21.62
0.44	64.29	16.85	10.20	3.40	72.37	74.45	35.09

Table 8 Detailed Results of 9% Bentonite Mud Experiment

Flow Rate	Differential Pressure [inch H_2O]				Temperature [°F]		Pressure
[gpm]	**0.5" Pipe**	**0.824" Pipe**	**Annulus**	**1.38" Pipe**	**Inlet**	**Outlet**	**[Psi]**
17.03	More than 600	139.73	83.53	34.88	77.67	77.33	128.36
16.33	More than 600	135.86	81.44	34.46	78.68	78.01	118.33
15.44	More than 600	130.15	78.56	33.38	78.81	79.20	107.72
14.50	More than 600	125.81	76.10	32.29	77.35	78.40	99.21
13.50	More than 600	119.82	72.88	31.17	78.56	78.82	88.18
12.47	More than 600	114.40	69.53	29.91	79.09	79.20	74.23
11.37	More than 600	109.02	66.11	28.59	77.74	77.06	63.63
10.16	466.69	102.76	62.84	27.26	77.91	79.31	54.04
8.93	404.73	96.45	59.09	25.63	78.18	79.30	47.94
7.66	365.75	89.25	55.13	24.00	76.18	78.99	41.17
6.40	328.17	80.95	50.66	22.22	78.76	79.27	37.18
5.11	287.08	72.29	45.76	20.14	75.83	77.82	30.76

Flow Rate	Differential Pressure [inch H_2O]				Temperature [°F]		Pressure
[gpm]	0.5" Pipe	0.824" Pipe	Annulus	1.38" Pipe	Inlet	Outlet	[Psi]
3.85	243.35	62.98	40.45	18.16	79.02	78.38	26.23
2.57	193.70	51.96	33.79	15.66	78.64	77.37	20.51
1.87	163.12	44.69	30.33	14.18	77.48	77.92	17.65
0.82	106.23	32.11	22.67	11.07	77.47	77.10	26.96
0.47	81.52	26.27	19.24	9.95	77.22	77.69	39.18
0.18	54.92	19.71	15.32	8.41	76.01	76.46	48.42
0.10	41.64	16.47	13.53	7.90	76.33	76.61	51.74
0.29	76.37	25.92	19.72	10.74	75.82	75.44	44.62
0.49	96.64	30.42	22.59	11.78	75.08	74.56	38.12
0.60	105.81	33.85	24.70	12.09	75.32	74.81	33.65
0.81	113.79	35.25	24.68	11.87	75.24	74.00	28.50
1.85	180.54	48.72	33.28	15.30	74.99	74.16	19.70
2.57	217.96	56.45	37.61	16.97	74.28	74.46	23.70
3.86	276.53	69.59	44.97	19.65	75.47	75.49	30.28
5.13	326.05	80.12	50.32	21.78	73.20	75.36	34.27
6.39	370.11	88.29	54.99	23.43	73.99	74.89	40.49
7.66	413.53	96.82	59.78	24.89	72.77	74.19	44.97
8.91	449.24	104.10	64.03	26.31	74.01	75.93	48.78
10.13	516.26	110.70	67.50	27.87	73.50	75.71	58.95
11.37	More than 600	117.59	71.92	29.36	74.96	75.71	61.36
12.51	More than 600	123.92	74.95	30.79	74.91	75.71	73.30
13.49	More than 600	127.96	77.24	31.61	74.36	77.23	88.58
14.44	More than 600	131.88	79.50	32.60	77.26	77.34	98.59
15.38	More than 600	136.68	81.54	33.46	76.54	77.02	105.37
16.32	More than 600	140.54	83.83	34.73	76.82	77.95	117.75
17.16	More than 600	143.96	85.32	35.75	77.64	78.19	128.61

Table 9 Detailed Results of 6% Bentonite Mud Experiment

Flow Rate	Differential Pressure [inch H_2O]				Temperature [°F]		Pressure
[gpm]	0.5" Pipe	0.824" Pipe	Annulus	1.38" Pipe	Inlet	Outlet	[Psi]
19.41	More than 600	More than 150	64.65	27.97	81.92	82.23	146.70
18.26	More than 600	135.21	61.29	26.46	83.08	83.00	130.00
17.04	More than 600	108.00	58.52	24.89	82.82	82.73	112.88
15.65	More than 600	92.77	54.99	23.17	83.32	81.59	96.28
14.15	More than 600	86.01	51.46	21.52	81.27	83.53	85.21
12.55	More than 600	79.67	47.68	19.84	80.83	82.48	68.45
11.37	More than 600	74.36	44.79	18.60	81.23	83.08	58.90
10.80	More than 600	76.62	46.40	18.49	83.29	81.85	55.70
10.17	494.61	69.61	41.87	17.41	82.69	82.13	48.02
8.96	317.66	64.95	39.70	16.36	82.82	83.20	36.38
7.71	264.69	59.60	36.72	15.24	81.76	84.07	30.29
6.43	234.53	54.39	33.54	14.14	82.44	81.51	26.42
5.15	203.59	47.61	30.13	12.82	82.25	82.89	22.20
3.85	170.42	41.05	26.72	11.41	82.30	83.87	18.68
2.54	133.02	32.77	21.89	9.65	84.80	83.80	15.21
1.77	107.89	28.10	18.33	8.50	81.77	82.75	38.61

Flow Rate	Differential Pressure [inch H_2O]				Temperature [°F]		Pressure
[gpm]	0.5" Pipe	0.824" Pipe	Annulus	1.38" Pipe	Inlet	Outlet	[Psi]
0.91	74.82	21.22	15.00	7.08	81.10	82.54	20.36
0.48	53.22	16.40	11.77	6.01	81.19	81.10	35.59
0.17	33.85	12.14	9.21	4.94	79.56	83.61	45.15

Appendix A – Viscometric Pipe Flow

The volumetric flow rate for fully develop laminar pipe flow (Fig. B-1) under steady state conditions with velocity profile, v(r), can be expressed as:

$$Q = 2\pi \int_0^R vrdr \tag{A-1}$$

Integrating by parts and assuming that v(R) = 0 we get:

$$Q = -\pi \int_O^R r^2 \frac{dv}{dr} dr \tag{A-2}$$

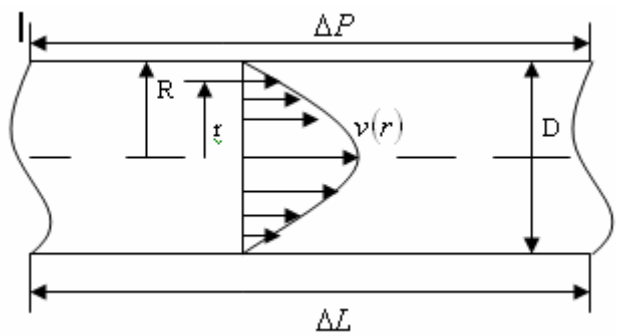

Fig. B-1 Viscometric Pipe Flow

We know that dv/dr is a function of shear stress τ. For steady state flow of fluid with constant density, we can write:

$$\frac{\tau(r)}{r} = \frac{\tau_w}{R} \tag{A-3}$$

The shear stress is given by:

$$\tau_w = \frac{R}{2}\frac{\Delta P}{\Delta L} \tag{A-4}$$

After changing variables, Eqn (A-2) takes form:

$$Q = -\pi \int_0^{\tau_w} \left(\frac{R}{\tau_w}\right)^3 \frac{dv}{dr} \tau^2 d\tau \tag{A-5}$$

Denoting dv/dr = f(τ), and differentiating with respect to τ_w and upon rearrangements, we obtain:

$$\frac{d\left(Q\tau_w^3\right)}{d\tau_w} = -\pi R^3 f\left(\tau_w\right)\tau_w^2 \tag{A-6}$$

Hence, the shear rate at pipe wall is:

$$f\left(\tau_w\right) = \left(-\frac{dv}{dr}\right)_R = \dot{\gamma}_w = \frac{1}{\pi R\tau_w^2}\frac{d\left(Q\tau_w^3\right)}{d\tau_w} \tag{A-7}$$

or

$$\dot{\gamma}_w = \frac{1}{\pi R^3}\tau_w\frac{dQ}{d\tau_w} + \frac{3Q}{\pi R^3} \tag{A-8}$$

Note that

$$\frac{Q}{\pi R^3} = \frac{U}{R} = \frac{2U}{D} \tag{A-9}$$

Therefore, Eqn (A-8) takes form:

$$\dot{\gamma}_w = \frac{\tau_w}{4}\frac{d\left(\frac{8U}{D}\right)}{d\tau_w} + \frac{3}{4}\left(\frac{8U}{D}\right) \tag{A-10}$$

Note that the following is true:

$$\tau_w\frac{d\left(\log\tau_w\right)}{d\tau_w} = \left(\frac{8U}{D}\right)\frac{d\left(\log\frac{8U}{D}\right)}{d\left(\frac{8U}{D}\right)} \tag{A-11}$$

From Eq (A-11) we get:

$$\frac{d\left(\frac{8U}{D}\right)}{d\tau_w} = \frac{\frac{8U}{D}}{\tau_w}\frac{d\left(\log\frac{8U}{D}\right)}{d\left(\log\tau_w\right)} \tag{A-12}$$

Substituting (A-12) to (A-10) we get expression for wall shear rate as:

$$\dot{\gamma}_w = \frac{1}{4}\left[3 + \frac{d\left(\log\frac{8U}{D}\right)}{d\left(\log\tau_w\right)}\right]\left(\frac{8U}{D}\right) \tag{A-13}$$

If we plot the wall shear stress (τ_w) against nominal Newtonian shear rate (8U/D) on a log-log scale, the generalized flow behavior index, N can be obtained from slope of the plot (flow curve) at a given shear rate by:

$$N = \frac{d(\log \tau_w)}{d\left(\log \frac{8U}{D}\right)} \tag{A-14}$$

Substituting (A-14) to (A-13) gives:

$$\dot{\gamma}_w = \left(\frac{3N+1}{4N}\right)\frac{8U}{D} \tag{A-15}$$

In general, one may write:

$$\tau_w = K'\left(\frac{8U}{D}\right)^N \tag{A-16}$$

Equation (A-16) is an equation of tangents to the flow curve. If the curve fits straight line on a log-log plot, we have power law fluid. In other words n = N and:

$$\tau = K\left(-\frac{dv}{dr}\right)^n \tag{A-17}$$

Appendix B – Laminar Flow of Yield Power Law in Pipes

The shear stress-shear rate relationship for Yield Power-law is expressed as:

$$\tau = \tau_y + K\left(-\frac{dv}{dr}\right)^m \tag{B-1}$$

For steady state flow of constant density fluid, the relationship between the shear stress and pressure gradient is given by:

$$\tau = -\frac{r}{2}\frac{dP}{dl} \tag{B-2}$$

Combining Eqs (B-1) and (B-2) gives

$$-\frac{dv}{dr} = \frac{1}{K^{\frac{1}{m}}}\left(-\frac{r}{2}\frac{dP}{dl} - \tau_y\right)^{\frac{1}{m}} \tag{B-3}$$

We observe that, for $-\frac{dv}{dr} \geq 0$ we need $-\frac{rdp}{2dl} - \tau_y \geq 0$. This occurs for $r = r_p$ that is given by:

$$-\frac{r_p}{2}\frac{dP}{dl} = \tau_y \tag{B-4}$$

In other words, in the range of $0 \le r \le r_p$ the shear rate is null and the fluid flows with constant velocity, v_p. The quantity, v_p, is called the plug flow velocity. Integrating Eqn (B-3) we get:

$$v(r) = \frac{1}{K^{\frac{1}{m}}}\left(-\frac{2dl}{dP}\right)\left(\frac{m}{m+1}\right)\left(-\frac{r}{2}\frac{dP}{dl} - \tau_y\right)^{\frac{1+m}{m}} + C \tag{B-5}$$

Assuming no slip at the pipe wall (i.e v(R) = 0):

$$v(r) = \frac{1}{K^{\frac{1}{m}}}\left(-\frac{2dl}{dP}\right)\frac{m}{m+1}\left[\left(-\frac{R}{2}\frac{dP}{dl} - \tau_y\right)^{\frac{1+m}{m}} - \left(-\frac{r}{2}\frac{dP}{dl} - \tau_y\right)^{\frac{1+m}{m}}\right] \tag{B-6}$$

Equation (B-6) is valid only for $r_p \le r \le R$. The plug velocity, v_p, can be obtained by setting $r = r_p$ in Eqn (B-6)

$$v_p = \frac{1}{K^{\frac{1}{m}}}\left(-\frac{2dl}{dP}\right)\left(\frac{m}{m+1}\right)\left(-\frac{R}{2}\frac{dP}{dl} - \tau_y\right)^{\frac{1+m}{m}} \tag{B-7}$$

The flow rate is given by:

$$Q = \pi r_p^2 v_p + \int_{r_p}^{R} 2\pi v(r) r dr \tag{B-8}$$

By substituting (B-6 and B-7) to (B-8) and evaluating integrals, the flow rate can be expressed as:

$$Q = \frac{\pi}{K^{\frac{1}{m}}}\left(\frac{R}{\tau_w}\right)^3\left(\frac{m}{m+1}\right)\left(\tau_w - \tau_y\right)^{\frac{1+m}{m}}\left[\tau_w{}^2 - \frac{2m}{1+2m}\tau_w\left(\tau_w - \tau_y\right) + \frac{2m^2}{(1+2m)(1+3m)}\left(\tau_w - \tau_y\right)^2\right] \tag{B-9}$$

Equation (B-9) can be written in terms of mean velocity as:

$$\frac{8U}{D} = \frac{(\tau_w - \tau_y)^{(1+1/m)}}{K^{1/m}\tau_w^3}\left(\frac{4m}{3m+1}\right)\left[\tau_w^2 + \frac{2m}{1+2m}\tau_y\tau_w + \frac{2m^2}{(1+m)(1+2m)}\tau_y^2\right] \tag{B-10}$$

Equation (B-10) can be written as follows:

$$\frac{8U}{D}\frac{1}{\dot{\gamma}_w} = \frac{4m}{3m+1}C_c = \frac{4N}{3N+1} \tag{B-11}$$

where

$$C_c = (1 - x)\left[\frac{2m^2}{(1+2m)(1+m)}x^2 + \frac{2m}{1+2m}x + 1\right] \tag{B-12}$$

where $x = \tau_y/\tau_w$. It is apparent from Eqn (B-10) that the wall shear stress cannot be expressed explicitly in terms of mean velocity. We need to apply an iterative procedure to obtain the wall shear stress for a given mean velocity. However, Eqn (B-10) is a nonlinear equation and may have more than one solution. The following

procedure gives a unique solution, if the mean velocity (U), pipe diameter, (D) and rheological parameters (τ_y, m and K) are known:

Step 1. Assume $C_c = 1$;

Step 2. Calculate wall shear rate (γ_w) from Eqn (B-11);

Step 3. Determine wall shear stress as:

$$\tau_{w,i} = \tau_y + K\dot{\gamma}_w^m;$$

Step 4. Calculate the value of x ($x = \tau_y/\tau_w$);

Step 5. Determine C_c form Eqn (B-12);

Step 6. Calculate wall shear rate (γ_w) from Eqn (B-11);

Step 7. Determine wall shear stress as:

$$\tau_{w,i+1} = \tau_y + K\dot{\gamma}_w^m;$$

Step 8. Repeat Steps from 4 to 7 until

$$\left|\frac{\tau_{w,i+1} - \tau_{w,1}}{\tau_{w,i+1}}\right| \le \sigma,$$ where σ is the tolerance limit

Step 9. Determine frictional pressure gradient as:

$$\frac{dp}{dl} = \frac{4\tau_w}{D}$$

Appendix C

Calibration of Rotational Viscometers

Two rotational viscometers (VIS#2 and VIS#3) were used. These instruments were calibrated using three different calibration oils (50 cP, 100 cP and 500 cP). Stress readings were corrected using the calibration curves. For the sake of simplicity, these curves are represented by correction factor equations. Stress reading correction factor, fc, for low range viscometer (VIS#2) is given by:

$$f_c = \frac{1.106\theta}{0.1053 + \theta} \tag{C-1}$$

Similarly, the correction factor for high range viscometer (VIS#3) is:

$$f_c = 1.0974 + 0.0001\theta \tag{C-2}$$

After correcting the measured shear stress, the shear rate is calculated as:

$$\gamma = \frac{2\varpi}{n'(\mathbf{1} - \psi^{2/n'})} \tag{C-3}$$

where

$$n' = \frac{d \ln \theta}{d \ln \varpi} \tag{C-4}$$

where ω is the rotational speed of the cup. Diameters ratio, ψ = di/do, which is 0.9365 for Chan 35.

The Effect of Elongational Flow Through the Drill Bit Nozzle on the Rheology of Polymeric Drilling Fluids

Jimmy Lozano

The Effect of Elongational Flow Through the Drill Bit Nozzle on the Rheology of Polymeric Drilling Fluids

INVESTIGATOR: Jimmy Lozano

INTRODUCTION:

No work has been done to investigate the effect of elongational flow through the drill bit nozzles on the rheology of polymeric fluids and the possible stretching and breaking of the molecular chains. This knowledge is of importance to understand the rheological properties of the polymeric fluid present in the annulus, and subsequently, its effect on cuttings transport, carrying capacity, and clay stabilization, among other functions

OBJECTIVE:

To analyze the effect of elongational flow occurring in the drill bit nozzle on the rheology of polymeric fluids (PAC, XCD, PHPA)

APPROACHES:

- Comparison of upstream pressure gradient and downstream pressure gradient
- Comparison of rheological properties of the fluid before and after experiments
- To determine if there is degradation or breaking of polymer chains as they flow through the nozzle by measuring the molecular weight
- Theoretical model that compares the strain rates developed at the nozzle vs. the strain rates required to stretch or break the molecular chains.

PROJECT STATUS:

Experiments were performed using three different polymers: PAC, XCD and PHPA; at three different concentrations: 0.25 PPB (0.7131 kg/m^3), 0.375 PPB (1.07 kg/m^3) and 0.5 PPB (1.427 kg/m^3). Three different nozzles were used: 18/32" (1.43 cm), 20/32" (1.59 cm) and 22/32" (1.75 cm).

Samples of the fluid before and after experiments were taken for rheological analysis to compare the effect of the pump and the three nozzles on the properties of the fluids.

The pressure drop through the nozzle was measured to determine the values of the discharge coefficients for the tested fluids.

Molecular weight distribution was performed to determine the effect of the positive displacement pump and nozzle 18/32" in four samples of XCD at 0.5 PPB.

A method was developed to compare the strain rates developed in the nozzles and the strain rates required to stretch and break the molecular chains of the polymers.

DELIVERABLES:

- Experimental Data Base
- Semi-annual Advisory Board Meetings Reports
- Theoretical Modeling (Strain Rate)
- Final Report

TUDRP

The Effect of Elongational Flow Through the Drill Bit Nozzle on the Rheology of Polymeric Drilling Fluids

Jimmy Lozano, The University of Tulsa, Drilling Research Projects

This report is prepared for TUDRP Advisory Board Meeting, May 23-24, 2005, Tulsa-Oklahoma.

Abstract

This report presents the analysis of experiments performed in the flow loop at the facilities of Tulsa University Drilling Research Projects (TUDRP). Experiments with PAC, PHPA and XCD at three different concentrations: 0.25 PPB (0.7131 kg/m^3), 0.375 PPB (1.07 kg/m^3) and 0.5 PPB (1.427 kg/m^3) were performed to investigate the effect of three different nozzles sizes: 18/32" (1.43 cm), 20/32" (1.59 cm) and 22/32" (1.75 cm) on the properties of the tested polymeric fluids.

The upstream and downstream pressure data obtained from the experiments was analyzed and compared. Samples of the fluid, upstream and downstream of the nozzle, were taken for rheological analysis to compare the effect of the pump and the three nozzles on the properties of the fluids.

The pressure drop through the nozzle was measured to determine the values of the discharge coefficients for the tested fluids and for comparison with those that are currently used in the drilling industry.

An analytical method was developed to compare the strain rates required to stretch or break a molecular chain of the polymeric fluids and the strain rates developed at the nozzle.

Also, molecular weight measurement was completed for four samples of XCD 0.5 PPB (1.427 kg/m^3). Results are presented comparing the effect of the pump and the nozzle on the molecular weight distribution of XCD.

Molecular weight markers were set to calculate the percentage of chains above or below in a polymeric solution (XCD 0.5 PPB) below or above a set molecular weight.

Project Status

Literature Review	100%
Loop Modifications	100%
Pump Up-Grade	100%
Water Experiments	100%
Polymer Experiments	100%
Molecular Weight Measurements	100%
Analysis of Data	100%
Modeling (Strain Rate Theory)	100%
Final Report	100%

Introduction

A polymer chain molecule experiences elongational flow when it is accelerated very quickly in a drill bit nozzle. When one end of a polymer chain is traveling at one velocity and the other end is being accelerated very rapidly, the chain will stretch and possibly separate, reducing the viscosity and molecular weight of the polymer.

As polymeric drilling fluid is accelerated through a drill bit nozzle, it can experience shear rates and strain rates in the order of 10^5 s^{-1}. Therefore, it is quite probable that the polymer chains are experiencing some form of deformation due to elongational flow. This knowledge is of importance to understand the rheological properties of the polymeric fluid present in the annulus and subsequently the cuttings transport, carrying capacity, and clay stabilization, among other functions.

Problem Statement

Polymers have been shown effective in reducing filtration, stabilizing clays, flocculating drilled solids, increasing carrying capacity, reducing drag, and serving as emulsifiers and lubricants[1]. However, little work has been done to investigate the effect of the extreme shear rates exerted by the drill bit nozzles on the rheology of polymeric fluids including the possible elongation and breaking of the molecular chains.

Experimental Facility

The indoor loop located at the north campus of The University of Tulsa and previously used by Asli Kilic[2] and Pier Alvarado[3] was modified to simmulate the flow of drilling fluids through the drill bit nozzle. A schematic of the loop is shown in Fig A-1.

A holder, shown in Fig A-2, was designed and constructed to hold the nozzle in place while running experiments. The nozzle holder is placed between two flanges that are attached to the pipe, separating it into two approximately equal sections: upstream and downstream.

The measured variables are summarized in table A-1.

Past Work

Water Experiments

The learning process of handling the experimental facility took place during this phase of the project. Water experiments were also performed for three major reasons:

1. To assure the operation of the experimental facility, including pressure transmitters and flow rate meter: Included in the thesis report and the ABM report of November 2004.
2. To calculate the roughness of the pipe, upstream and downstream of the nozzle: Included in the thesis report and the ABM report of November 2004.
3. To investigate cavitation downstream of the nozzle: Included in this report.

Cavitation

Cavitation is generally understood as the dynamic process of the formation and implosion of cavities in fluids. Cavitation occurs, for instance, when high flow velocities cause the local hydrostatic pressure to drop to a critical value that roughly corresponds to the vapor pressure of the fluid. Cavitation may occur in the nozzle, where there is significant gain in velocity as a consequence of a pressure drop. If cavitation is present, the fluid properties may change.

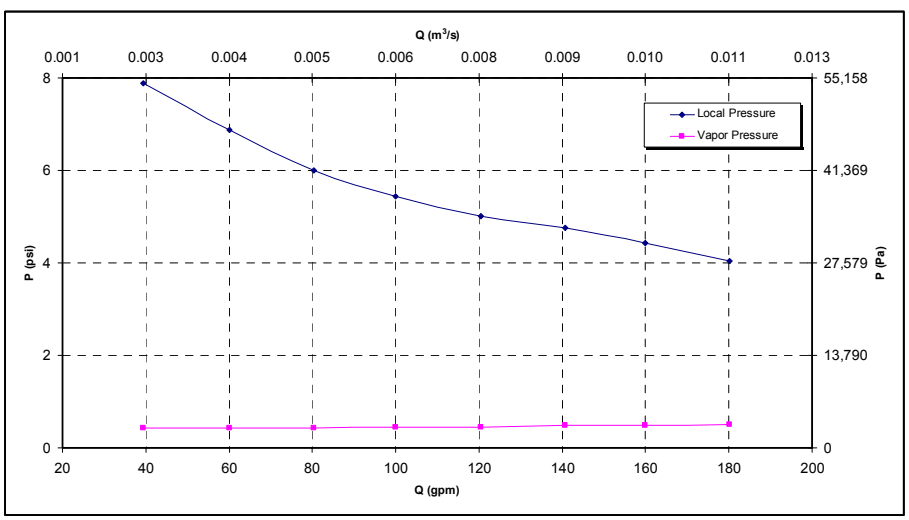

Figure 1: Investigation of Cavitation Downstream of the Nozzle

Tables of vapor pressure for polymeric fluids are not available, therefore in order to determine if cavitation was present or not, tables of water vapor pressure were used. The pressure at the outlet of the nozzle was compared with the vapor pressure at a given temperature.

Figure 1 is a plot of pressure vs flow rate for both, the vapor pressure and the pressure at the outlet of the nozzle. It demonstrates that the local pressure at the outlet of the nozzle is never below the vapor pressure and consequently cavitation is not present.

Polymer Experiments

Experiments were performed with three polymers at three different concentrations as described in the test matrix presented in Table A-2. Each fluid was circulated through the three different nozzle sizes, also included in the test matrix. Also, each fluid was circulated through the experimental section without a nozzle to investigate the effect of the pump on the properties of the fluids. The procedure for experiments with polymers and the experimental facility were included in the ABM report of November 2004. The polymeric test matrix is included in Appendix A.

Discussion of Results

When water is used as the circulating fluid, the difference between the upstream pressure gradient and the downstream pressure gradient is almost zero. But, if the upstream pressure gradient and the downstream pressure gradient are compared to a polymeric fluid, the difference is noticible.

Plots of pressure gradient vs. flow rate for polymeric fluids were included in the ABM report of November 2004. They showed that for a given flow rate, the upstream pressure gradient is higher than the downstream pressure gradient. This suggests that the fluid upstream or before the nozzle is different than the fluid downstream or after the nozzle.

It also suggests that the pressure required to flow the fluid through the upstream section is higher than the pressure required to circulate the fluid through the downstream section. This, consequently, is evidence of the thinning of the fluid due to elongational flow through the nozzle. Plots of PHPA 0.5 PPB and XCD are included in Appendix B as a reference. The plots of the other fluids are included in the thesis report and the database.

The terms “thinning” and “degradation” will be used through out the discussion. For the purpose of this report, “thinning” will refer to the alignment of polymeric chains (No breaking). The term “degradation” will refer merely to the breaking of chains.

Pressure Gradient Difference

The percentage pressure gradient difference was calculated using Eq.1 and used to compare the effect of different nozzles on a given fluid, and the effect of a nozzle on three different concentrations.

$$Difference = \left[\frac{\left(\frac{dP}{dL}\right)_{Up-Stream} - \left(\frac{dP}{dL}\right)_{Down-Stream}}{\left(\frac{dP}{dL}\right)_{Up-Stream}} \right] * 100 \quad \ldots\ldots\ldots\ldots \quad \text{Eq.1}$$

Effect of Nozzle Size on the Pressure Gradient Difference of a Given Fluid

Figure 2 is a plot of pressure gradient vs. flow rate using PHPA as polymeric fluid at a concentration of 0.5 PPB (1.427 kg/m^3). At 70 GPM, the pressure gradient difference is the highest and throughout the experiment this difference decreases until the last flow rate is achieved. The pressure difference at 70 GPM is about 15.5% for nozzle 18/32" (0.0142 m) compared to those of nozzles 20/32" (0.0158 m) and 22/32" (0.0174 m), which are 13.8% and 13%, respectively.

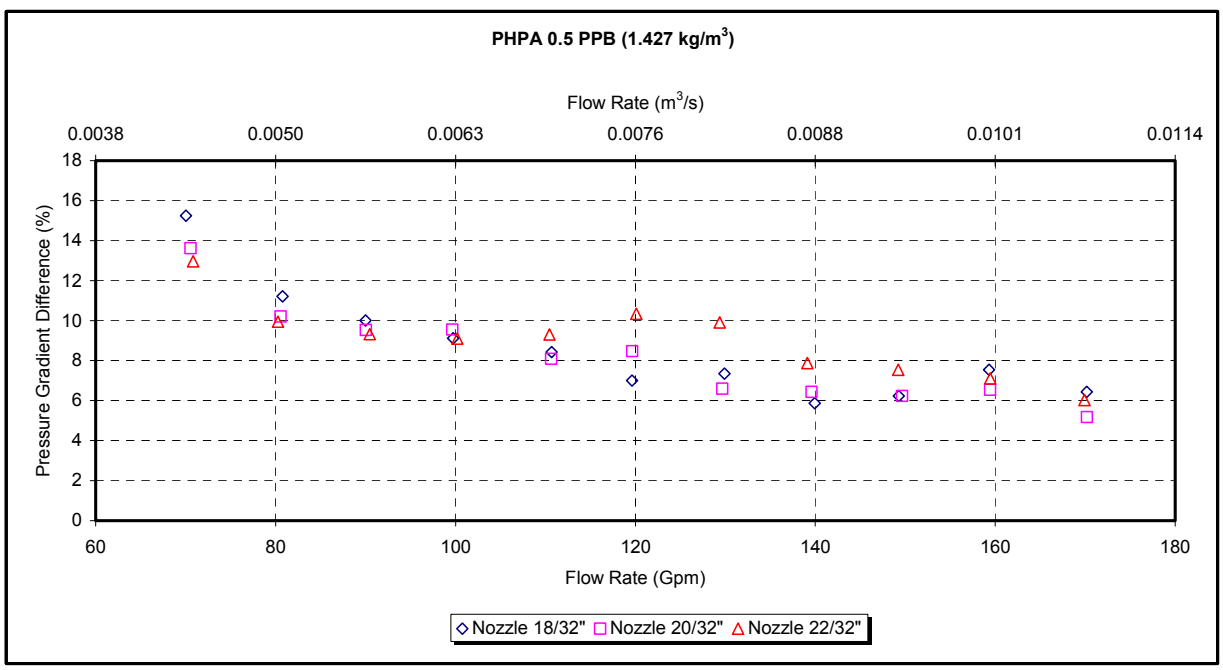

Figure 2: Pressure Gradient Difference vs. Flow Rate, PHPA 0.5 PPB

The pressure differences of the three nozzles decrease at flow rates higher than 140 GPM and tend to flatten out. This suggests that after some time the fluid is not affected any longer by the nozzles. If the experiment was to run for a longer time or at higher flow rates, the polymeric fluid will become thinner. Consequently, the pressure difference will likely turn out to be close to zero.

Plots of pressure gradient difference vs. flow rate are included on the thesis report for the other eight fluids. They also support the statement that the fluid reaches a state where it is not affected any longer by the experimental conditions and the curves flatten out.

Effect of Fluid Concentration on the Pressure Gradient Difference

Figure 3 is a plot of pressure gradient difference vs. flow rate for a given polymer and a given nozzle size. Three different concentrations are shown in the plot: 0.5 PPB (1.427 kg/m^3), 0.375 PPB (1.07 kg/m^3) and 0.25 PPB (0.7131 kg/ m^3).

From Figure 3 it is clear that the pressure gradient difference decreases as the flow rate increases. It suggests that the pressure gradient difference is higher for the highest concentration (PHPA 0.5 PPB). However, this trend is not followed by all the fluids.

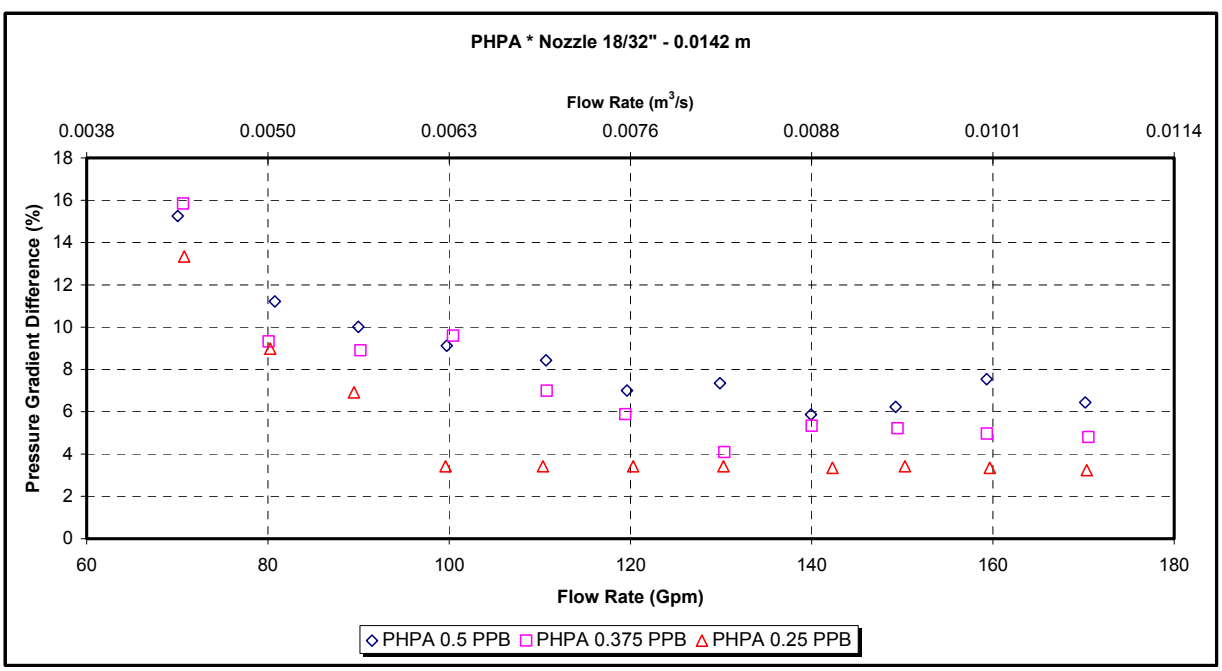

Figure 3: Pressure Gradient Difference vs. Flow Rate, PHPA * Nozzle 18/32"

Also, as in the previous case, it suggests that the fluid is thinning when it flows throught the nozzle. Plots for the other fluids are included in the thesis report.

Effect of Pump and Nozzles on the Rheology of Polymeric Fluids

Rheological parameters of the polymeric drilling fluids were determined with a Chan 3500 rotational viscometer. A comparison of the rheological parameters before and after each experiment provides an excellent insight into the effect of elongational flow through the nozzle on the rheology of the chosen polymeric fluids (PHPA, XCD and PAC). The following experiments were performed:

1. Without nozzle: To investigate the effect of the pump on the rheology of the fluid;
2. With nozzle: To investigate the effect of the pump and nozzle on the rheology of the fluid.

Plots of shear stress vs. shear rate were performed for each fluid. Each plot shows the rheological properties (K and n) for five different samples at a given concentration:

a. The original fluid right after mixing;
b. Fluid after experiment without nozzle (effect of the pump);
c. Fluid after experiment with nozzle 18/32” (0.0142 m);
d. Fluid after experiment with nozzle 20/32” (0.0158 m);
e. Fluid after experiment with nozzle 22/32” (0.0174 m).

Figure 4 shows that for a given shear rate, the shear stress of the initial fluid is the highest and the shear stress of the fluid after the pump is higher than those of the nozzles. For a given shear rate, the shear stress is lowest when the 18/32” nozzle is used. This implies that the thinning of the fluid when a 18/32” nozzle is used is the highest.

The second highest thinning occurs when a 20/32” nozzle is used. The third highest thinning occurs when a 22/32” nozzle is used. The pump affects the fluid, but the thinning is low compared to the thinning due to the nozzles. Plots for the other fluids are included in the thesis report. They revealed the same results. Table 1 summarizes the rheology for all the samples, before and after experiments.

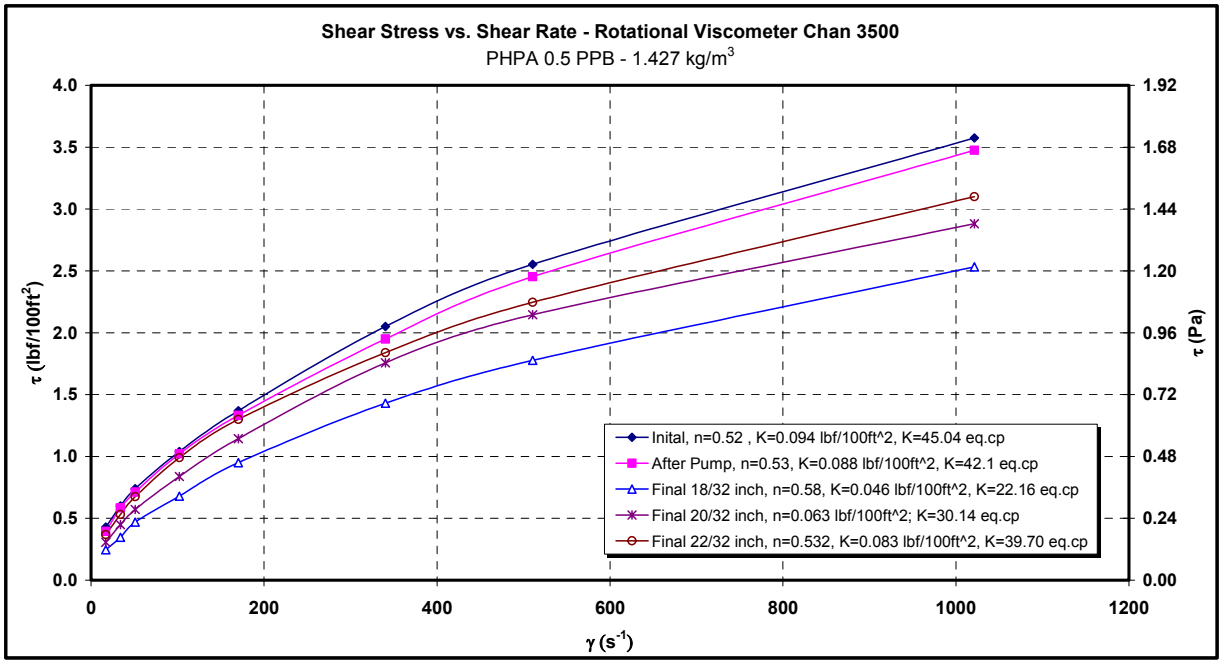

Figure 4: Shear Stress τ vs. Shear Rate γ. Fluid: PHPA 0.5 PPB - 1.427 kg/m^3

The parameters summarized in Table 1 are: Consistency index K, in three different units, and the flow behavior index, n. TD in Table 1 is the percentage of difference in consistency index K, between the initial fluid and the other four samples. TD was calculated with Equation 2. Even though TD is not the degradation, it gives an excellent insight into the effect of the pump and the nozzle on consistency index, K.

$$TD = \left(1 - \frac{K_{Initial}}{K_{Sample}}\right) * 100 \quad \text{(Eq.2)} \qquad ND = TD_{Sample-Nozzle} - TD_{Pump} \quad \text{(Eq.3)}$$

ND, in equation 3, is the percentage difference in consistency index K of the nozzle minus the percentage difference of the pump. This gives an idea of what percentage change in K is due to the nozzles.

Table 1 shows that the consistency index decreases while the flow behavior index, n, increases. Even though TD and ND give an idea of the percentage changes in K due to the pump and the nozzle, they do not present a relation between the changes in K and n.

Polymer	Concentration	Sample	K ($lbf.s^n/100ft^2$)	K ($Pa.s^n$)	K (eq.cp)	n	TD (%)	ND (%)
PHPA	0.5 PPB	Initial Fluid	0.0941	0.0450	45.04	0.52	0.00	N/A
		Pump	0.0879	0.0421	42.10	0.53	6.53	0.00
		Nozzle 18/32" - 0.0142 m	0.0463	0.0222	22.16	0.58	50.80	44.27
		Nozzle 20/32" - 0.0158 m	0.0629	0.0301	30.14	0.56	33.08	26.55
		Nozzle 22/32" - 0.0174 m	0.0829	0.0397	39.70	0.53	11.86	5.33
	0.375 PPB	Initial Fluid	0.0790	0.0378	37.84	0.55	0.00	N/A
		Pump	0.0630	0.0302	30.16	0.63	20.30	0.00
		Nozzle 18/32" - 0.0142 m	0.0440	0.0211	21.07	0.58	44.32	24.02
		Nozzle 20/32" - 0.0158 m	0.0526	0.0252	25.19	0.58	33.43	13.13
		Nozzle 22/32" - 0.0174 m	0.0603	0.0289	28.89	0.57	23.65	3.36
	0.25 PPB	Initial Fluid	0.0230	0.0110	11.02	0.70	0.00	N/A
		Pump	0.0191	0.0092	9.15	0.73	16.97	0.00
		Nozzle 18/32" - 0.0142 m	0.0061	0.0029	2.92	0.80	73.50	56.53
		Nozzle 20/32" - 0.0158 m	0.0106	0.0051	5.07	0.74	53.99	37.02
		Nozzle 22/32" - 0.0174 m	0.0141	0.0068	6.76	0.72	38.66	21.69
XCD	0.5 PPB	Initial Fluid	0.0580	0.0278	27.75	0.52	0.00	N/A
		Pump	0.0483	0.0231	23.13	0.55	16.65	0.00
		Nozzle 18/32" - 0.0142 m	0.0272	0.0130	13.00	0.56	53.15	36.50
		Nozzle 20/32" - 0.0158 m	0.0379	0.0182	18.16	0.57	34.56	17.91
		Nozzle 22/32" - 0.0174 m	0.0459	0.0220	21.98	0.55	20.79	4.14
	0.375 PPB	Initial Fluid	0.0407	0.0195	19.47	0.51	0.00	N/A
		Pump	0.0303	0.0145	14.51	0.54	25.48	0.00
		Nozzle 18/32" - 0.0142 m	0.0083	0.0040	3.99	0.70	79.51	54.03
		Nozzle 20/32" - 0.0158 m	0.0202	0.0097	9.66	0.59	50.39	24.91
		Nozzle 22/32" - 0.0174 m	0.0249	0.0119	11.90	0.52	38.88	13.41
	0.25 PPB	Initial Fluid	0.0150	0.0072	7.18	0.68	0.00	N/A
		Pump	0.0123	0.0059	5.90	0.73	17.83	0.00
		Nozzle 18/32" - 0.0142 m	0.0066	0.0031	3.14	0.75	56.27	38.44
		Nozzle 20/32" - 0.0158 m	0.0077	0.0037	3.71	0.74	48.33	30.50
		Nozzle 22/32" - 0.0174 m	0.0082	0.0040	3.95	0.71	44.99	27.16
PAC	0.5 PPB	Initial Fluid	0.0133	0.0064	6.35	0.81	0.00	N/A
		Pump	0.0120	0.0057	5.74	0.82	9.61	0.00
		Nozzle 18/32" - 0.0142 m	0.0081	0.0039	3.90	0.86	38.58	28.98
		Nozzle 20/32" - 0.0158 m	0.0088	0.0042	4.20	0.85	33.86	24.25
		Nozzle 22/32" - 0.0174 m	0.0096	0.0046	4.58	0.82	27.87	18.27
	0.375 PPB	Initial Fluid	0.0019	0.0009	2.73	0.90	0.00	N/A
		Pump	0.0019	0.0009	2.69	0.90	1.47	0.00
		Nozzle 18/32" - 0.0142 m	0.0019	0.0009	1.90	0.91	30.40	28.94
		Nozzle 20/32" - 0.0158 m	0.0019	0.0009	2.32	0.92	15.02	13.55
		Nozzle 22/32" - 0.0174 m	0.0019	0.0009	2.53	0.90	7.33	5.86
	0.25 PPB	Initial Fluid	0.0019	0.0009	2.12	0.91	0.00	N/A
		Pump	0.0019	0.0009	2.05	0.92	3.30	0.00
		Nozzle 18/32" - 0.0142 m	0.0020	0.0010	1.01	0.97	52.36	49.06
		Nozzle 20/32" - 0.0158 m	0.0020	0.0009	1.20	0.94	43.40	40.09
		Nozzle 22/32" - 0.0174 m	0.0019	0.0009	1.32	0.92	37.74	34.43

K: Consistency Index
n:Flow Behavior Index
TD: Difference due to pump and nozzle
ND: Difference due to nozzle

Table 1: Summary of Results

Apparent Viscosity

Apparent viscosity is a function of K and n, and therefore will be a better parameter to compare the fluid thinning through the three different nozzles for a given shear rate. Equation 4 determines the apparent viscosity at a given shear rate:

$$\mu_{Apparent} = K\gamma^{n-1} \qquad \text{(Eq.4)}$$

Plots of apparent viscosity vs. shear rate show that, in general, the apparent viscosity decreases as shear rate increases. For a given shear rate, the apparent viscosity of a given fluid is in the following order (1 for the highest and 5 for the lowest):

1. Initial fluid (Right after mixing);
2. Fluid without nozzle (effect of pump);
3. Fluid after experiment with nozzle 22/32”;
4. Fluid after experiment with nozzle 20/32”;
5. Fluid after experiment with nozzle 18/32”.

These plots can be found in the thesis report.

Pressure Drop Through the Nozzle

While running the experiments, pressure drop through the nozzle was collected. Even though analyzing the discharge coefficient C_d was not a priority in this particular project, having the data of measured pressure drop through the nozzle was a big advantage that needed to be used. The discharge coefficient can be obtained if the density of the fluid, flow rate, area of the nozzle and pressure drop are known. Eckel and Bielstein[4] determined the value of C_d to be 0.95 and Warren[5] determined it to be as high as 1.03.

$$C_d = \sqrt{\frac{8.311*10^{-5}*\rho*q^2}{A_t^2 \Delta P_b}} \qquad \text{(Eq.5)}$$

The units in equation 5 are:

ρ: Density of the fluid (lbm/gal);

q: Volumetric flow rate (gal/min);

A_t: Total area of the nozzle (in^2);

ΔP_b: Pressure drop through the nozzle (psi).

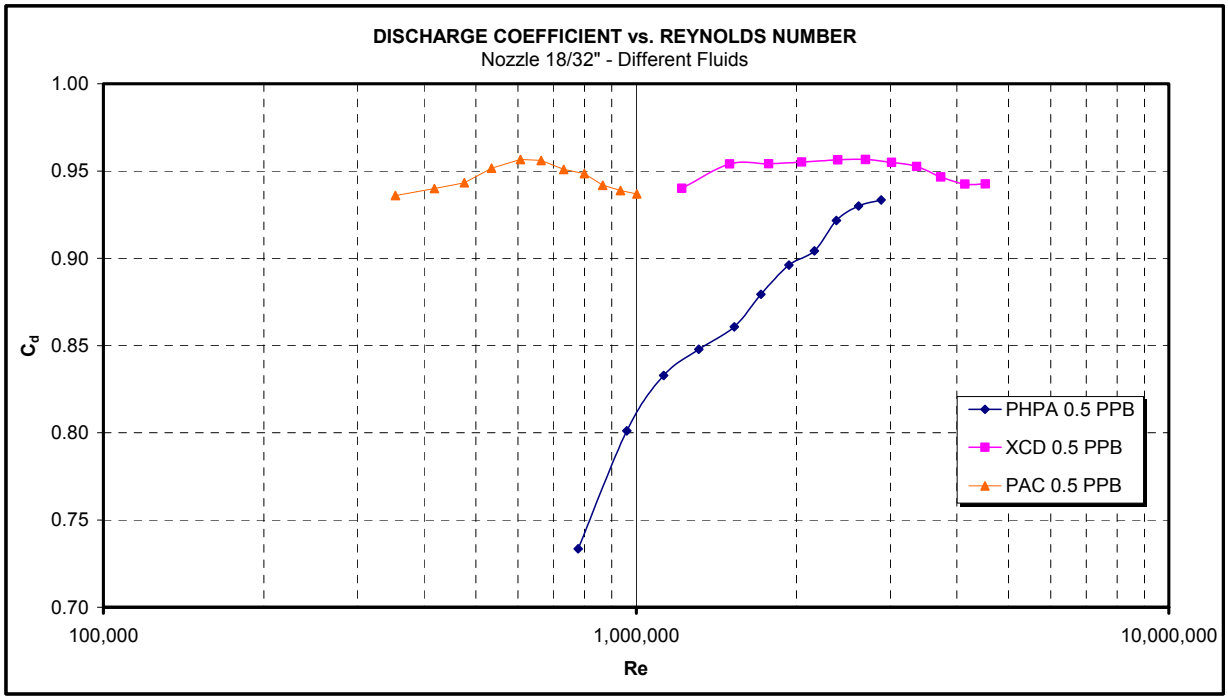

Figure 5: C_d vs. Re for a Given Nozzle Size of 18/32" and a Given Concentration of 0.5 PPB for Three Different Fluids

Figure 5 is a plot of discharge coeficient vs. Power Law Reynolds Number for XCD, PAC and PHPA at 0.5 PPB concentration and nozzle 18/32". This figure shows that the discharge coefficient of PAC increases from 0.935 to 0.96, where it reaches its peak, then decreases to a value of 0.935. The average is 0.945, which is fairly close to 0.95. The discharge coefficient of XCD increases from 0.94 to 0.96, where it reaches its peak, then decreases to a value of 0.94. The average C_d is 0.95, as determined by Eckel and Bielstein.

PHPA displays a much different trend. At the beginning of the experiment the discharge coefficient is about 0.73, which is 23% lower than 0.95. However, after recirculating the fluid, C_d increases and reaches a value close to 0.94 which is the last experimental point. This suggests that the final fluid is different than the initial fluid. The initial fluid requires more pressure to flow through the nozzle and consequently C_d is significantly lower than 0.95. The fluid, when it circulates, thins and behaves like water reaching a value of C_d close to 0.95. This is more evidence of the thinning effect of the nozzle.

Plots of C_d vs. Reynolds number for PAC and XCD at different concentrations and using the other nozzles present a value fairly close to 0.95. On the other hand, PHPA at the test concentrations and nozzle

included in the test matrix present a similar trend as the one shown in figure 5. These figures are available upon request.

Sink Flow Model (Metzner and Metzner[6])

Experimental and theoretical studies of the stretching and breaking of polymers in dilute solutions subjected to elongational flows have led to the following picture of the stretching process: at low strain rates, the polymer can be represented as a random coil, nearly undeformed by the applied flow field.

When the flow strain rate is further increased, the coil deformation is still rather weak. Eventually, a critical value of the strain rate is reached and the polymer undergoes an abrupt transition from the weakly perturbed coil to a nearly completely stretched state. The above transition can produce a significant modification of the flow field since, even in dilute solutions the contribution of the stretched polymers to the stress balance in the fluid can be quite considerable.

When the strain rate is increased even further, the tension (which is maximal at the center) in the stretched chain increases progressively until a second critical strain rate is reached, namely that corresponding to polymer fracture.

Several different analyses have been presented to describe the extensional flow of fluids through nozzles. The sink flow analysis, developed by Metzner and Metzner[6], assumes purely extensional flow and no shear component. Figure 6 represents contraction flow through a nozzle.

The sink flow analysis assumes:

1. Purely extensional flow
2. No Shear Component

Velocity Components, V_φ and V_θ are negligible compared to V_z:

$$V_\varphi = V_\theta = 0 \; ; \; V_z = \frac{Q}{A} \qquad \text{(Eq.7)}$$

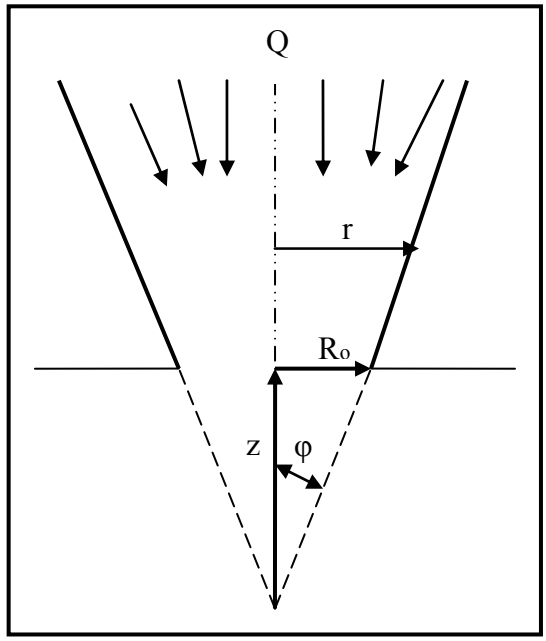

Figure 6: Flow Through Nozzle

where A is the cross-sectional area in the converging region, Q is the volumetric flow rate and V_z is the velocity along the axis of the nozzle. Eq.8 is the velocity along the z axis as a function of z, which can be derived to obtain the strain rate (Eq.9). Complete derivation can be found in Appendix B.

$$V_z = \frac{Q}{\pi z^2 (Tan\varphi)^2} \qquad \text{(Eq.8)}$$

$$\dot{\varepsilon} = \frac{dv_z}{dz} = -\frac{2Q}{\pi z^3 (Tan^2\varphi)} \qquad \text{(Eq.9)}$$

Eq.9 can be written as a function of the outlet radius of the nozzle.

$$\dot{\varepsilon} = -\frac{2Q\sin^3\varphi}{\pi R_o^3 (Tan^2\varphi)} \qquad \text{(Eq.10)}$$

Strain rate, in Eq.10, is a function of the flow rate Q, and the geometry of the nozzle (convergence of the angle, outlet radius of the nozzle). Therefore, it is necessary to use the inner dimensions of the nozzles to determine the convergence of the angle. Figure 7 is the schematic of the inner geometry of the nozzle. The inner and outer dimensions of the three nozzles are summarized in table A-3.

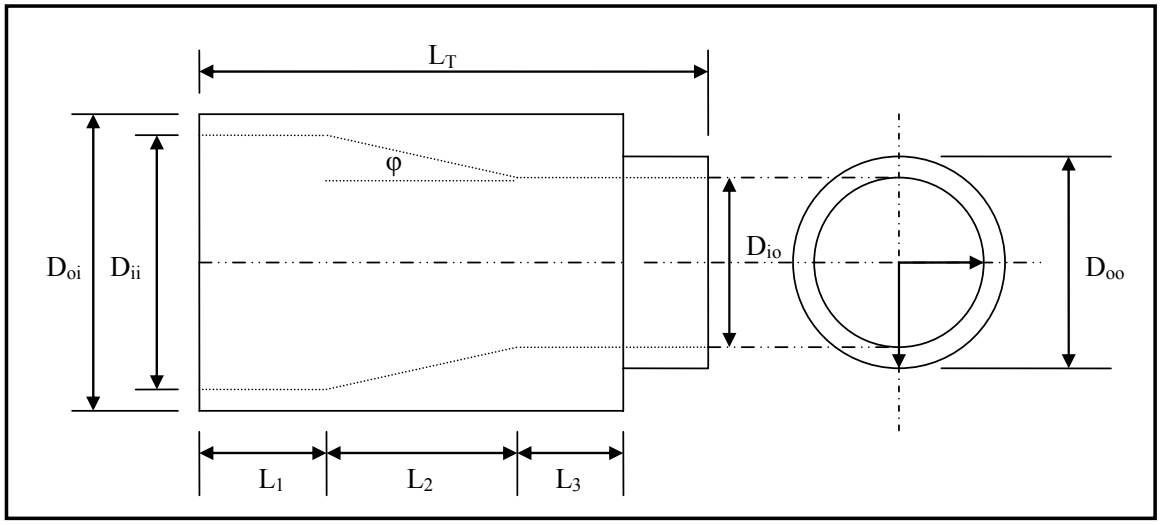

Figure 7: Geometry of Nozzle 18/32" (0.0142m) and Nozzle 20/32" (0.0158 m)

The convergence angle is equal to:

$$\varphi = Tan^{-1}\left(\frac{D_{ii} - D_{io}}{2L_2}\right) \qquad \text{(Eq. 11)}$$

Critical Strain Rate

De Gennes[7] predicted a coil-to-stretch transition in elongational flow at a critical strain rate:

$$\dot{\varepsilon}_c = \frac{0.5}{\tau_z} \qquad \text{(Eq.12)}$$

where τ_z is the longest relaxation time of the chain, which is given by Zimm's [8] relation:

$$\tau_z = \frac{M\eta_s[\eta]}{A_1 RT} \qquad \text{(Eq.13)}$$

where η_s is the solvent viscosity, [η] is the intrinsic viscosity, M is the molecular weight, R is the molar gas constant, and T is the absolute temperature. The constant A_1 has been experimentally obtained and has a value of 1.18.

Intrinsic viscosity can be obtained from:

$$[\eta] = KM^a \qquad \text{(Eq.14)}$$

where K and a can be found in the Polymer Handbook of Brandrup and Immergut for a specific polymer[9].

If $\dot{\varepsilon} > \dot{\varepsilon}_{cs}$, the molecular coil will completely stretch.

Fracture strain rate has been experimentally obtained for different ranges of molecular weight[9].

$$\dot{\varepsilon}_f = \dot{\varepsilon}_{cs}^{\ 1.02} \qquad \text{(Eq.15)}$$

If $\dot{\varepsilon} > \dot{\varepsilon}_{cs} > \dot{\varepsilon}_f$, the molecular coil will break.

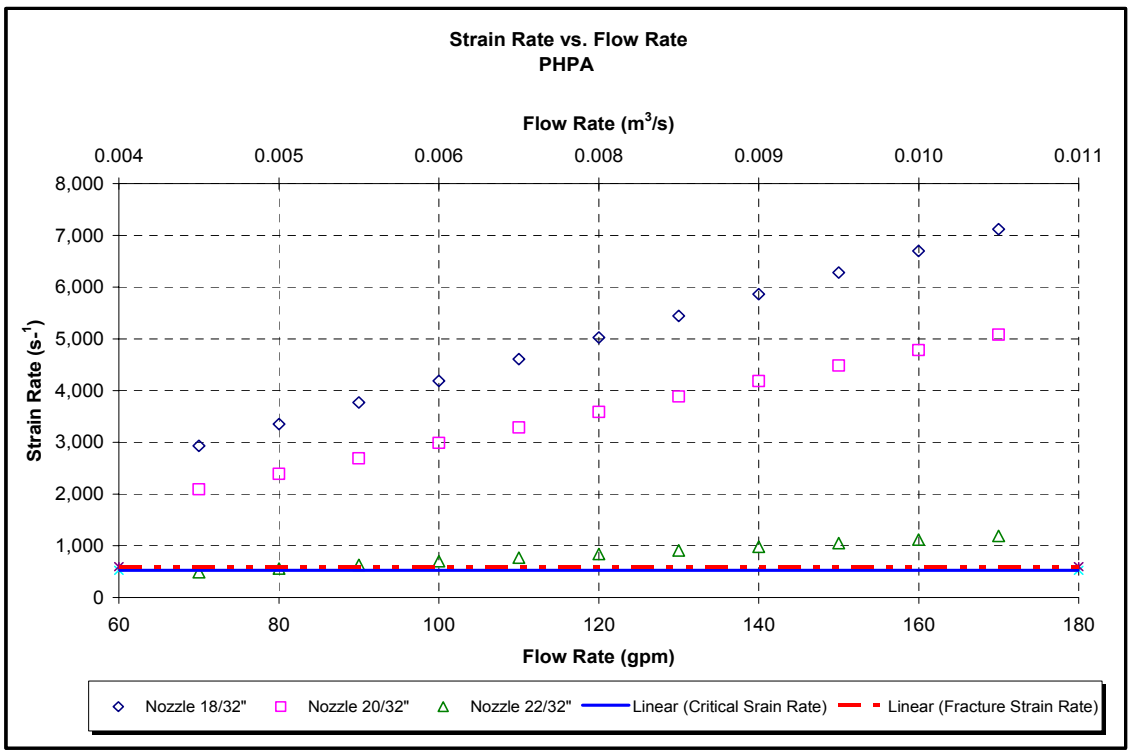

Figure 8: Strain Rate vs. Flow Rate. Critical and Fracture Strain Rate for PHPA

Figure 8 is a plot of Strain Rate vs. Flow Rate for three different nozzles. Critical strain rate and fracture strain rate are also plotted for PHPA. These two are only a function of intrinsic viscosity, which was obtained with equation 14, and molecular weight. For this purpose, 10 million Daltons was assumed as the MW of PHPA, 2 million Daltons as the MW of XCD and 1 million Daltons as the MW of PAC. These molecular weights are in the range of the molecular weights found in the literature. The figure suggests that for

the range of flow rates (70-170 GPM), nozzles 18/32" and 20/32" will stretch and break the molecular chains. Nozzle 22/32" will stretch the chains at a flow rate of 70 GPM and will break them at a flow rate of 80 GPM.

The comparison of the strain rates developed in the nozzles vs. the critical and fracture strain rates for XCD and PAC can be found in the thesis report.

Molecular Weight:

The results of molecular weight distribution and molecular weight markers included in this section were performed by Dr.Larry Harding of ConocoPhillips. Even though the findings are worthy of discussion, Dr. Larry Harding feels that the obtained data should be used with caution due to the lack of proper standards for absolute MW distribution

Background of Polymers:

The molecular weight of a polymer is controlled by the number of monomers in the chain, which affects the properties of the polymer. The molecular weight depends on the number of repeat units in the chain and is represented by:

$$M = n^* Mo$$

where n is the number of repeat units in the chain, and Mo is the molecular weight of each repeat unit.

Polymers can be divided into two major groups: those that are linear and those that are branched. The difference in the two is that linear polymers are made up of many units, which are joined together end to end to form a long chain. Branched polymers are essentially chain polymers that divide at certain points to form branches. These chains may be longer than 10,000 Å and 5 to 10 Å in diameter. Both groups are made up of hundreds, even thousands of unit cells called monomers, which join together to form macromolecules.

Each chain of a given polymer rarely has the same length or weight. Instead, a polymer sample is said to have a distribution of molecular weight, and typically the average value is given. The length of the chain has a large affect on the viscosity of a polymer, especially at high concentrations; this effect is caused by entanglements of the chains.

For every polymer there is a critical molecular weight, Mc, above which entanglements are more pronounced, and the shear viscosity rises more quickly with molecular weight. Below this critical molecular weight the increase in zero shear viscosity is almost linearly related to the increase in molecular weight.

The behavior of these chains is very difficult to model accurately, thus a number of models have been developed in order to examine the molecular responses. The simplest of these models, the Elastic Dumbbell

consists of two beads connected by a rod, which is taken to by elastic, is considered to represent two connected monomers.

When the connector is neither stretched nor compressed the dumbbell is in an equilibrium position. The dumbbell can be stretched or compressed depending on the surrounding conditions. The rate at which it returns to its equilibrium position is known as the relaxation rate. The relaxation rate varies depending on the degree of deformation and the strength of the bond between the "beads".

In general, the measurement of the molecular weight clearly reflects the breaking of molecular chains. The number-averaged molecular weight (M_n), the weight-averaged molecular weight (M_w) and the peak molecular weight (M_p) of the polymeric fluids before and after simmulation of flow through the nozzle can be measured. The M_n, M_w, and M_p measurements will help understand the dynamic behavior of the polymers that are used as drilling fluids.

XCD at 0.5 PPB(1.42651 kg/m^3) has been chosen to measure molecular weight distribution .

Calibration:

Size Exclusion Chromatography (SEC) gives the measurements of M_n, M_w, and M_p in a single run of a sample. Ideally samples should fit within the standard curve of a molecular weight standard. Unfortunately, the peak molecular weight of XCD is higher than the highest available molecular weight standard, which is 8 million Dalton.

This makes it necessary for the construction of a standard curve which can be extrapolated and still get good results. Figure 43 displays the obtained calibration curve.

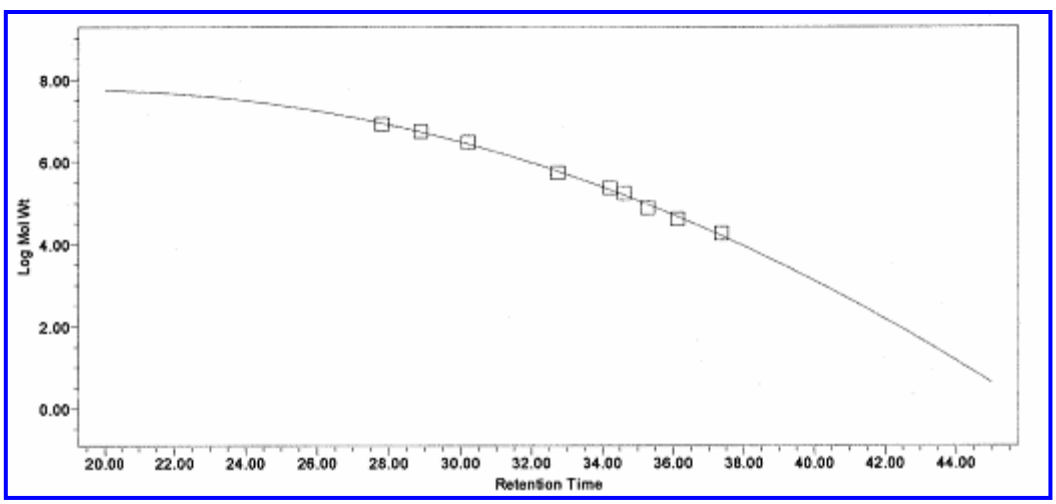

Figure 9: Log(Molecular Weight) vs. Retension Time

Once the standard curve has been calibrated, M_n, M_w, and M_p are obtained for the samples. The four samples include:

1. XCD 0.5 PPB (1.426 kg/m^3) right after mixing
2. XCD 0.5 PPB (1.426 kg/m^3) after letting the fluid flow for 45 minutes without a nozzle at 70 GPM fixed (0.0044 m^3/s) in order to establish the effect of the pump on the polymeric fluid
3. XCD 0.5 PPB (1.426 kg/m^3) at flow rates 70 GPM (0.0044 m^3/s) to 170 GPM (0.0107 m^3/s), in order to establish the effect of the pump on the polymeric fluid with the exact conditions of the experiments with nozzle.
4. XCD 0.5 PPB (1.426 kg/m^3) at flow rates 70 GPM (0.0044 m^3/s) to 170 GPM (0.0107 m^3/s), through a 18/32" (0.01429 m) nozzle.

The Chromatograms of the samples are shown in Figure 10. The first observation from this figure is that samples 1 and 3 overlap. This was expected since sample 3 was taken after sample 1 was flowed through the experimental facility. The overlapping also shows that these two samples had exactly the same concentration.

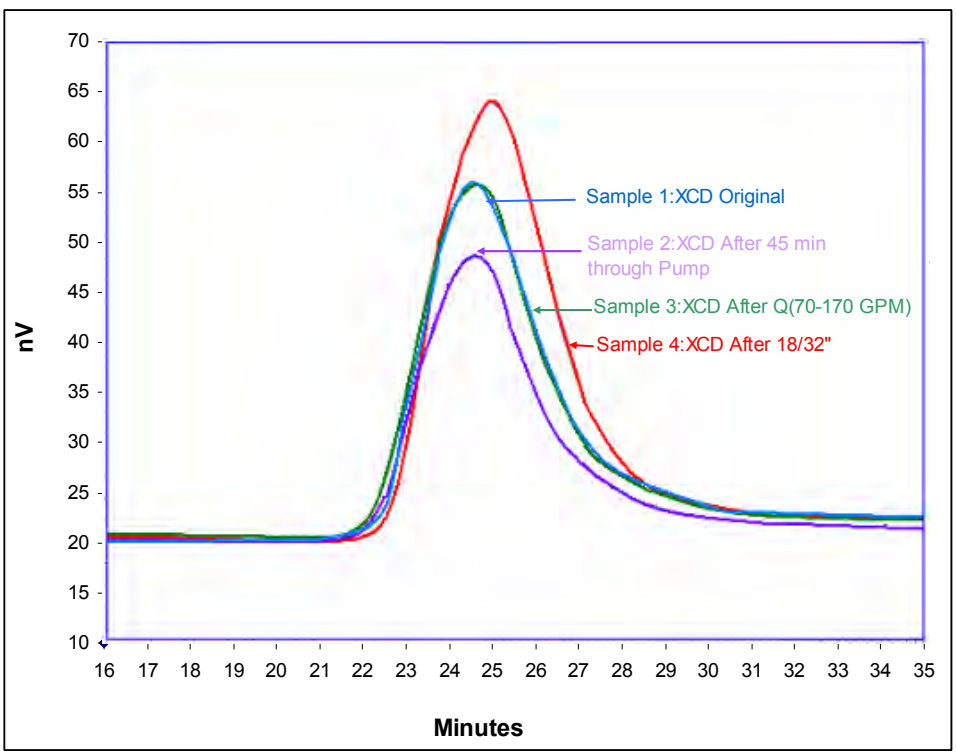

Figure 10: Gel Permiation Chromotography (GPC) for samples 1,2,3 and 4.

Sample XCD 0.5 PPB	M_n Daltons	M_w Daltons	M_p Daltons
1. Initial	21,433,000	25,197,000	27,364,000
2. After 45 min	22,417,000	25,824,000	26,279,000
3. After Rates	21,632,000	25,421,000	26,078,000
4. After 18/32"	19,013,000	23,023,000	24,097,000

Table 4: Molecular Weight of the four samples

Although the curve of sample 2 is lower than 1 and 3, it can be concluded that these three samples have a similar molecular weight. Since the MWD of sample 4 is shifted to the right, it reveals that the peak molecular weight MP is smaller compared to the other three samples. The explanation is that sample 4 has shorter chains than samples 1,2 and 3. It is known that shorter chains penetrate in between the small pores of the micro-porous system, while long chains move only through the larger pores.

Table 4 summarizes the number-averaged molecular weight (M_n), the weight-averaged molecular weight (M_w) and the peak molecular weight (M_p) for each of the samples. Table 4 shows the decreased values of M_n, M_w, and M_p for sample 4, which is the fluid that goes through the nozzle, compared to the other three samples. The other three numbers are very similar, but any interpretation should be subject to further analysis. However, this might suggest that molecular degradation takes place at the nozzle and that no degradation takes place at the pump. This last conclusion is based on the complete overlapping of samples 1 and 3; where sample 1 is the original fluid. Sample 3 is the fluid that was tested without a nozzle at similar conditions used in the nozzle experiments in order to investigate the effect of the pump.

Molecular Weight Markers:

Molecular weight markers were set to investigate the percentage of molecules below or above a determined MW.

MW_1 was set at 24,000,000 Daltons. Samples 1, 2 and 3 resulted in similar percentages (56.46%, 59.72% and 57.44%); while sample 4 (that went through the 18/32" nozzle) shows a lower percentage (45.89%). This means that only 45.89 % of the molecules of sample 4 are higher than 24 million Daltons, compared to samples 1, 2 and 3, which are all higher than 56 %. Consequently, sample 4 has more molecules below 24 million Daltons, which means that its peak molecular weight is less than those of samples 1, 2 and 3. This is further evidence of degradation of the polymer fluid that went through the nozzle.

MW_2 was set at 16,000,000 Daltons. Samples 1,2 and 3 have 84.99%, 86.93% and 85.43%, respectively, of molecules higher than 16 million Daltons. On the other hand, sample 4 has only 79.31 % of molecules higher than 16 million Daltons.

MW_3 was set at 8,000,000 Daltons, and sample 4 shows more molecules below this mark (3.62 %). Samples 1, 2 and 3 present fewer molecules below the mark of 8 million Daltons.

MW_4 was set at 4,000,000 Daltons, and sample 4 is the only one that has some percentage of molecules below this mark (0.37%). The other three samples have basically no molecules below 4 million Daltons (0.02%, 0.0%, 0.02%). This also supports the statement that the nozzle degradates the fluid.

	Sample: XCD 0.5 PPB - 1.07 kg/m^3			
	1. Original Fluid Right after mixing	2. After 45 min Fixed Q=70 GPM	3. Flow Rates 70 - 170 GPM	4. Effect of Nozzle Nozzle 18/32" - 0.0142
Peak Molecular Weigth MP (daltons)	27,364,489	26,279,258	26,078,402	24,097,767
%Molecules > MW1 MW1 = 24,000,000 Daltons	56.46	59.71	57.44	45.89
%Molecules > MW2 MW2 = 16,000,000 Daltons	84.99	86.93	85.43	79.31
%Molecules < MW3 MW3 = 8,000,000 Daltons	2.14	1.36	2.11	3.62
%Molecules < MW4 MW1 = 4,000,000 Daltons	0.02	0	0.02	0.37

Table 5: Markers of % Molecules

Conclusions:

a. The upstream pressure gradient is higher than the downstream pressure gradient for any given flow rate. This suggests that polymeric fluids get thinner when they flow through the nozzles.
b. The apparent viscosity is the lowest for the fluid that flows through the smallest nozzle.
c. The pump affects the rheology, but not as much as the nozzles. Consistency index K decreases and flow behavior index n increases.
d. The discharge coefficient is fairly close to 0.95 for XCD and PAC at the concentrations proposed in this project. PHPA presents discharge coefficients as low as 0.73 at the the beginning of the experiment.
e. Based on the strain rate model, all three nozzles 18/32”, 20/32” and 22/32” stretch and break the chains of PHPA. The chains of XCD and PAC will only stretch or break under given flow rates.
f. Based on the molecular weight distribution of XCD 0.5 PPB, the pump does not degrade or break the molecular chains of the polymer. On the other hand, nozzle 18/32” breaks some molecular chains.

Recommendations:

a. Tests should be performed with higher concentrations in the range of 0.5 to 1 PPB.
b. Tests should be performed at higher temperatures like those in the bottom hole to investigate thermo-degradation.

c. Tests should be performed at higher nozzle velocities like those of real drilling operations (400-600 ft/s).
d. It is necessary to separate the effect of flow rate and circulation time on the thinning or degradation of polymeric fluids.

Deliverables

1. Semi-Annual Advisory Board Meeting Reports
2. Experimental Database
3. Theoretical Model (Strain Rate)
4. Final Report

Acknowledgements:

The author sincerely acknowledges the support of Baker Hughes Inteq in providing the polymers used in this project and Baker Hughes Christiansen in providing the nozzles. Also, the support of ConocoPhillips and Dr.Larry Harding for the molecular weight measurements is truly appreciated.

References

1. Darley, H.C.H and Gray, George R.: "Composition and Properties of Drilling and Completion Fluids: Fifth Edition" Gulf Publishing Company, 1988, Chapter 4 and 11.
2. Kilic, Asli: "Experimental Investigation of Friction Pressure Reducers for Improved Drilling Hydraulics" University of Tulsa, Master Thesis, 2002.
3. Alvarado, Pier: "Experimental Study of Friction Pressure Reduction Under Elevated Temperature" University of Tulsa, Master Thesis, 2003.
4. Eckel, J.R., Bielstein, W.J.: "Nozzle Design and its Effects on Drilling Rate and Pump Operations" Drilling and Production Practice, API 1952, pp.28-42.
5. Warren, T.M.: "Evaluation of Jet-Bit Pressure Losses" SPE Drilling Engineering, Dec 1989, pp.335-340.
6. Metzner, A.B. and Metzner, A.P.: Stress Levels in Rapid Extensional Flows of Polymeric Fluids" Rheologica Acta 1970, 9, 174.
7. De Gennes, P.G.: Journal of Chemical Physics, 60:5030.
8. Zimm, B.H.: Journal of Chemical Physics, 24:269.
9. Brandrup, J. and Immergut E.H.: Polymer Handbook" John wiley & Sons, 1989.

Appendix A

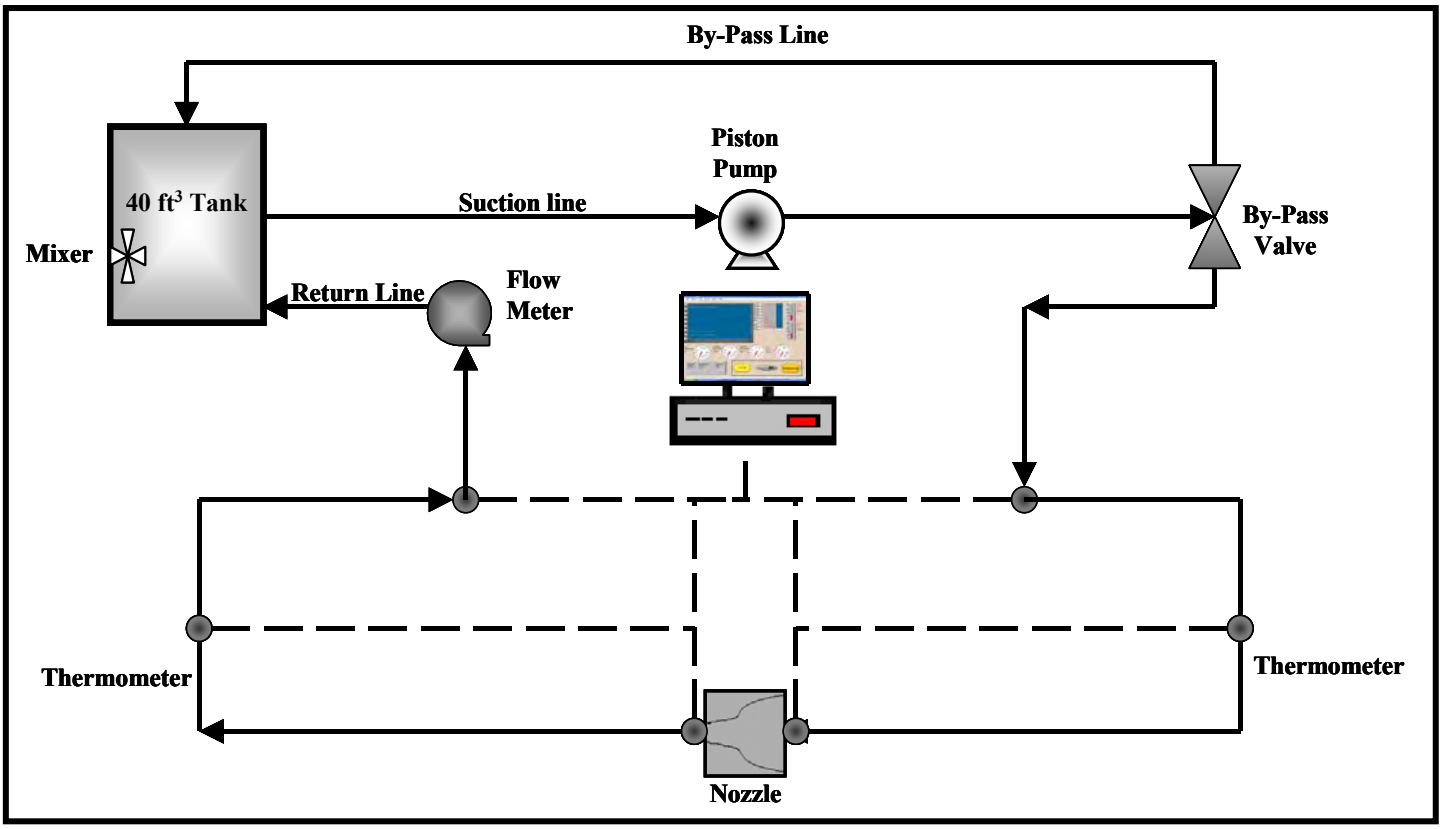

Figure A-1. Schematic Drawing of Experimental Facility

Measured Variables	
1	Pump Pressure
2	Upstream Pressure Drop
3	Upstream Temperature
4	Pressure Drop Through the Nozzle
5	Downstream Pressure Drop
6	Downstream Temperature
7	Mass Flow Rate
8	Density of the Fluid

Table A-1: Measured Variables

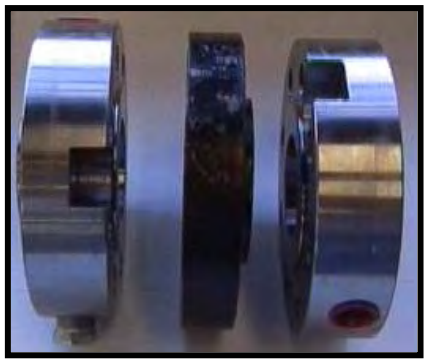

Figure A-2. Nozzle Holder

Fluid Type	Concentration		Fluid Flow Rate		Nozzle Diameter	
	PPB	kg/m^3	(GPM)	m^3/s	(inch)	m
PAC, PHPA, XCD			70	0.0044		
			80	0.0050		
	0.25	0.71325	90	0.0057	18/32	0.01429
			100	0.0063		
			110	0.0069		
	0.375	1.0699	120	0.0076	20/32	0.01588
			130	0.0082		
			140	0.0088		
	0.5	1.4265	150	0.0095	22/32	0.01746
			160	0.0101		
			170	0.0107		
Total Number of Tests :	**162**					

Table A-2: Test Matrix

		Nozzle 18/32" - 0.0142 m		Nozzle 20/32" - 0.0158 m		Nozzle 22/32" - 0.0174 m	
		Inches	cm	Inches	cm	Inches	cm
Total Length	L_T	1.3300	3.3782	1.3300	3.3782	1.0540	2.67716
Up-Length	L_1	0.3750	0.9525	0.3975	1.0097	0.2500	0.635
Middle Length	L_2	0.4550	1.1557	0.4570	1.1608	0.4225	1.07315
Down Length	L_3	0.5000	1.2700	0.4755	1.2078	0.3815	0.96901
Inlet Outer Diameter	D_{oi}	1.2915	3.2804	1.2915	3.2804	1.2915	3.28041
Inlet Inner Diameter	D_{ii}	1.1150	2.8321	1.1150	2.8321	1.1100	2.8194
Oulet Outer Diameter	D_{oo}	0.7900	2.0066	0.8000	2.0320	1.2915	3.28041
Outlet Inner Diameter	D_{io}	0.5550	1.4097	0.6250	1.5875	0.6875	1.74625

Table A-3: Dimenssion of the Nozzles

Appendix B: Derivation of Strain Rate:

Considering the isosceles triangle with the included angle φ (half angle of the convergence), the area at any point in the nozzle is given by:

$$A = \pi r^2 \qquad (1)$$

The radius, r, at the orifice of the nozzle is equal to:

$$R_o = zTan(\varphi) \qquad (2)$$

Therefore, the area at the orifice is equal to:

$$A = \pi z^2 (Tan\varphi)^2 \qquad (3)$$

where z is the radial coordinate distance. For small angles, the area at the orifice of the nozzle can be expressed as:

$$A = 2\pi z^2 (1 - Cos\varphi) \qquad (4)$$

However, equation 4 is only valid for small angles ($\varphi<15^o$) and the angles of the nozzles used in the experiments are larger than 15°. Consequently, equation 3 will be used to calculate the area at the orifice of the nozzle.

Substituting Equation 3 into equation $V_z = \frac{Q}{A}$:

$$V_z = \frac{Q}{\pi z^2 (Tan\varphi)^2} \qquad (5)$$

The extensional rate or strain rate at the orifice is equal to the derivative of V_z as a function of z:

$$\dot{\varepsilon} = \frac{dv_z}{dz} \qquad (6)$$

Deriving Equation 5, the strain rate is equal to:

$$\dot{\varepsilon} = \frac{dv_z}{dz} = -\frac{2Q}{\pi z^3 (Tan^2\varphi)} \qquad (7)$$

But z is equal to:

$$z = \frac{R_o}{Sin(\varphi)} \qquad (8)$$

Substituting equation 8 into equation 7.

$$\dot{\varepsilon} = -\frac{2Q\sin^3\varphi}{\pi R_o^3 (Tan^2\varphi)} \qquad (9)$$

An Experimental Study of Small Sand-Sized Cuttings Transport in Horizontal and High-Angle Boreholes

Duan Mingqin

An Experimental Study of Small Sand-sized Cuttings Transport in Horizontal and High-Angle Boreholes

INVESTIGATOR: Mingqin Duan

INTRODUCTION:

- Smaller cuttings seem to be more difficult to transport under certain conditions;
- Typical grain size of reservoir sands are on the order of 100 microns;
- Small cuttings transport behavior in a horizontal or highly inclined well is not well understood;

OBJECTIVES:

- Experimentally determine the influence of various combinations of drilling parameters on the required critical velocity for initiation of cuttings bed erosion, cuttings concentration and equilibrium bed height in horizontal and highly inclined wells;
- Develop models for small cuttings transport to predict critical transport velocities, cuttings concentration and bed height in horizontal and highly inclined wellbores.

PROJECT STATUS:

- Completed flow loop testing, upgrading and cuttings transport experiments. Ten percent work left for data analysis and model development. Sixty percent work left for final report.

RECENT PROGRESS:

- The mechanistic model for Critical Resuspension Velocity (CRV) was further improved to account for non-Newtonian shear flow;
- A computer code for CRV model was written. Modeling results were compared with experimental observations;
- Completed the remaining 48 experiments with 0.45 mm and 1.4 mm sands. The effects of the cuttings size, flow rate, hole inclination angle, drill pipe rotational speed and mud type on annular cuttings volumetric concentration and equilibrium bed height are discussed;
- Correlations for equilibrium bed heights and annular cuttings concentration were developed based on dimensional analysis;
- Completed 40% of the final report.

FUTURE WORK:

- Analyze the remaining experimental data and make necessary adjustments of the models if needed;
- Complete the final report.

EXPECTED COMPLETION DATE: August, 2005

TUDRP

An Experimental Study Of Small Sand-sized Cuttings Transport In Horizontal and High-Angle Boreholes

Mingqin Duan, The University of Tulsa, Drilling Research Projects

This report is prepared for TUDRP Advisory Board Meeting, May 23-24, 2005, Tulsa-Oklahoma.

Abstract

This report summarizes the improvement of the previously developed mechanistic model for Critical Resuspension Velocity (CRV) for small sand-sized cuttings transport in horizontal and high-angle boreholes. The model is extended from Newtonian uniform flow to non-Newtonian shear flow, which is closer to practical situations. This report also presents the experimental results with 0.45 mm and 1.4 mm cuttings on TUDRP LPAT flow loop. Effects of particle diameter, flow rate, hole angle, fluid type and drill pipe rotational speeds on cuttings volumetric concentration and equilibrium bed height are discussed. Correlations involving five dimensionless variables are also developed to predict annular cuttings volumetric concentration and bed height. More results and other details will be included in the final report (MS thesis).

Project Status

Tasks	Percentage Accomplished
Literature review and data gathering	95%
Flow loop operation training and system testing with fine sands	100%
Loop upgrading and modifications	100%
Test materials preparation	100%
Experimentation and Data analysis	90%
Model development	85%
Final report	40%

Objectives

- Experimentally determine the influence of various combinations of drilling parameters on cuttings concentration and bed height in horizontal and highly inclined wellbores and the critical velocity for initiation of cuttings bed erosion;
- Develop models for small cuttings transport to predict critical transport velocities, cuttings concentration and bed height in horizontal and highly inclined wellbores.

Statement of Problem

Field practice and experimental observations show that smaller cuttings are more difficult to transport under certain conditions.[1-3, 7, 11-13] Moreover, smaller particles tend to more easily cause stuck pipe due to their cohesive effects.[11 12]

Poor consolidated reservoir sands are known to be fine-grained particles with typical sizes on the order of 100μm.[13] However, very limited information is available for small cuttings transport under drilling conditions. The conclusions about the particle size effects on cuttings transport are also diversified, and even contradictory in some cases.[1-12] The experiments upon which these conclusions are based were conducted under incomparable conditions. It may not be correct, or at least not safe, to state explicitly that smaller cuttings are harder or easier to transport in horizontal wells compared with larger cuttings. The result depends on whether the sand bed has formed or not, as well as on various drilling parameters. Further experiments with small sand-sized particles are needed to understand why and under what conditions they are harder or easier to transport.

A Mechanistic Model for Critical Resuspension Velocity (CRV)

Critical Resuspension Velocity (CRV), is the minimum mean fluid velocity at which the first layer of small cuttings on top of a cuttings bed starts to be entrained into the flowing fluid. A preliminary model for CRV was developed based on force analysis applied to a protruding particle on a cuttings bed (Figure 1). Please refer to the progress report on 2004 May ABM for details. Further improvements are summarized here.

The forces exerted on a small cutting on a cuttings bed generate moments with respect to the contacting point with its neighboring particle. When the overall moment resulting from these forces is greater than zero, the particle begins to roll along its neighboring particles and then becomes entrained into the flowing fluid above it. Therefore, the critical condition is that the overall moment is zero. The mean fluid velocity at this critical condition is the CRV.

As depicted in Figure 1, the particle on the surface of the cuttings bed is subjected to three groups of forces: static forces, hydrodynamic forces and colloidal forces. Gravity, F_g, and buoyancy, F_b, are static forces

which are due to the properties of the particle and its surrounding fluid only and do not depend on the fluid flow. Drag, F_D, and lift, F_L, are hydrodynamic forces incurred by the fluid flow. Van der Waals dispersion forces, F_{van}, are colloidal forces existing between any neighboring particles. They become dominant forces when the diameter of two closely neighbored particles is below 0.1 mm. For the purpose of model simplification, all particles are assumed to be spheres.

Gravity F_g

$$F_g = \frac{\pi d_p^{\,3}}{6} \rho_p g \ , \tag{1}$$

where

ρ_p - particle density, kg/m^3,

d_p - particle diameter, m.

Buoyancy F_b

$$F_b = \frac{\pi d_p^{\,3}}{6} \rho_f g \ , \tag{2}$$

where

ρ_f - fluid density, kg/m^3.

Drag F_D and Lift F_L

The drag and the lift are obtained by solving drag coefficient, C_D, and lift coefficient, C_L, for a given shape of particle. C_D is defined as [24],

$$C_D = \frac{F_D}{0.5 \rho_f u^2 A} \ , \tag{3}$$

and C_L is defined as[24],

$$C_L = \frac{F_L}{0.5 \rho_f u^2 A} \ , \tag{4}$$

where u is the upstream velocity and A is the characteristic area of the particle. For a cutting on a cuttings bed, the characteristic area is defined as the projected area of the cutting above the mean bed surface when this cutting is projected to a plane perpendicular to force (drag or lift) direction. According to the original definition of the lift which is caused by pressure and shear stress distribution on the particle surface, buoyancy

should be included in the lift because it is due to the surface pressure distribution. However, buoyancy is listed as a separate force because of the way we obtain lift coefficient. Lift coefficient is obtained based on Saffman's lift [21] which exists only in a shear flow. It does not account for the buoyancy that is always present under any flow.

Various kinds of drag coefficients for a spherical particle have been developed. Standard Schiller-Neumann formula for extended Reynolds number was employed as the drag coefficient, C_{DuN} , in the preliminary model,[19]

$$C_{DuN} = \frac{24}{R_{epN}}(1 + 0.15 R_{epN}{}^{0.687}), \tag{5}$$

where R_{epN} is the particle Reynolds number for Newtonian fluids. It was developed for a sphere moving through a uniform Newtonian fluid, but extended to non-Newtonian fluids by simply redefining the particle Reynolds number. It is doubtful whether this extension is appropriate for a non-Newtonian fluid whose behavior index n is not close to 1. The improved model uses the drag coefficient developed for non-Newtonian fluids.

Various analytical, numerical and experimental techniques were employed to find the drag coefficient of a sphere moving in a power law fluid, which is only applicable to a low particle Reynolds number [27-30]. Graham and Jones (1994) [31] extended the coefficient to a finite Reynolds number up to 200 based on their numerical results, if fluid behavior index n is within 0.4 ~ 1. Combing their results, the overall equation for drag coefficient of a sphere in a power law fluid reads,

$$C_{Du} = \frac{24}{R_{ep}}(2-n), \qquad R_{ep} < 0.2(2^n),$$

$$C_{Du} = \frac{35.2}{(\frac{R_{ep}}{2^n})^{1.03}} + n(1 - \frac{20.9}{(\frac{R_{ep}}{2^n})^{1.11}}), \qquad 0.2(2^n) \le R_{ep} < 24(2^n),$$

$$C_{Du} = \frac{37}{(\frac{R_{ep}}{2^n})^{1.1}} + 0.25 + 0.36n \qquad 24(2^n) \le R_{ep} \le 100(2^n), \tag{6}$$

where R_{ep} is generalized particle Reynolds number, $R_{ep} = \frac{\rho_f V_r{}^{2-n} d_p{}^n}{K}$, V_r is the local velocity at the particle center, n is the fluid behavior index, and K is the fluid consistency index, all in SI units. Result of Eq. (6) shows a good agreement with that of Eq. (5) if n is set to be 1.

Based on the boundary layer analysis [25], the flow near the cuttings bed is shear flow. However, Eq. (6) was proposed for a uniform flow. Based on a three dimensional numerical simulation, R. Kurose and S. Komori

(1999) [32] studied the effects of fluid shear and sphere rotational speed on the drag. They noted that for a fixed value of R_{ep}, the actual drag coefficient C_D increases with the increase of fluid shear rate. The dependence of C_D on shear rate is more apparent at higher R_{ep}. The trend of C_D with shear rate is also in agreement with Dandy and Dwyer's observations [33]. Kurose and Komori proposed an expression for C_D of a rotating sphere under a shear flow at discrete particle Reynolds numbers.[32] Based on this expression and neglecting sphere rotation, C_D of a stationary sphere in a shear flow is obtained by curve fitting their discrete data. It reads,

$$C_D = C_{Du}[1 + (5\times10^{-4} R_{ep} + 0.0179)\alpha], \tag{7}$$

where C_{Du} is the drag coefficient in a uniform flow, which can be calculated from Eq. (6), α is the dimensionless shear rate, $\alpha = \frac{dV_r}{dy}\frac{d_p}{2V_r}$, and $\frac{dV_r}{dy}$ is the local velocity gradient. Eq. (7) indicates that, for a fixed shear rate, C_D is close to C_{Du} at low particle Reynolds numbers, but is higher than C_{Du} at high particle Reynolds numbers.

Wall effects can be safely neglected for small particles according to previous investigations. [20, 26] However, particle arrangements have great impact on the drag coefficient, as reported by Liang et al.[20] The actual C_D decreases with the decrease of particle separation distance depending on the flow direction. For the case of a particle on a cuttings bed, an average correction factor of 0.2 is assumed based on their experimental data. The following Eq. (8) considering the neighboring particle effects is employed as the drag coefficient for this model.

$$C_D = 0.2C_{Du}[1 + (5\times10^{-4} R_{ep} + 0.0179)\alpha]. \tag{8}$$

Because of the boundary layer existing near the cuttings bed, the flow approaching the particles is not a uniform flow. The velocity gradient along the surface of the particle produces an asymmetrical flow field which is responsible for the lift force. The most widely used equation for the lift on a small sphere in a slow shear flow was obtained by Saffman [21],

$$F_{Lsa} = 1.615 V_r d_p^{\,2}\sqrt{\rho\mu(\frac{dV_r}{dy})}. \tag{9}$$

All the units in this equation are SI units. Combining the definition of lift coefficient, C_L in Eq. (4), and setting u as the local fluid velocity, V_r, at the center of the particle, Saffman's lift coefficient is expressed as

$$C_{Lsa} = 4.11\sqrt{\frac{d_p}{R_{ep}V_r}\frac{dV_r}{dy}}. \tag{10}$$

Though this coefficient was used regardless of particle Reynolds number, R_{ep}, it is actually valid only when R_{ep} « 1. Dandy & Dwyer [33] reported numerical results for the shear lift at a larger R_{ep}. R. Mei [17] combined Saffman's analytical results at a small R_{ep} and Dandy & Dwyer's numerical results at a finite R_{ep}, and gave the following expression for the lift coefficient,

$$C_L = C_{Lsa}[(1-0.3314\alpha^{0.5})\exp(-\frac{R_{ep}}{10}) + 0.3314\alpha^{0.5}], \text{ for } R_{ep} \le 40, \text{ and}$$

$$C_L = C_{Lsa}[0.0524(\alpha R_{ep})^{0.5}], \text{ for } R_{ep} \ge 40, \tag{11}$$

where α is the dimensionless shear rate and C_{Lsa} is the lift coefficient calculated with Saffman's equation at the corresponding Reynolds number.

Both C_D and C_L are functions of particle Reynolds number R_{ep} and the dimensionless shear rate, α. In order to get R_{ep} and α, the local velocity, V_r, and the velocity gradient, $\frac{dV_r}{dy}$, must be obtained.

According to the boundary layer theory [25], the velocity profile in the viscous sublayer which is closest to the cuttings bed takes the following form,

$$u^+ = y^+ \qquad (y^+ \le 5), \tag{12}$$

where,

u^+- dimensionless local velocity, $u^+ = V_r/U_f$,

y^+- dimensionless distance from mean bed surface, $y^+ = yU_f^{\frac{2-n}{n}}(\frac{\rho_f}{K})^{\frac{1}{n}}$ for power law fluid [34],

y - distance from mean bed surface,

U_f- bed friction velocity, $U_f = (\tau_{bed}/\rho_f)^{0.5}$,

τ_{bed} - average bed shear stress.

Substituting u^+ and y^+ into Eq. (12) and rearranging it yields,

$$V_r = y(\frac{\tau_{bed}}{K})^{\frac{1}{n}}, \tag{13}$$

$$\frac{dV_r}{dy} = (\frac{\tau_{bed}}{K})^{\frac{1}{n}}. \tag{14}$$

If the particle protrudes into the buffer zone or the logarithmic layer above the viscous sublayer, the velocity profile takes the following form, [25]

$$u^+ = -1.076+1.445y^+ + 0.04885\, y^{+2} + 0.0005813\, y^{+3} \qquad (5 < y^+ \le 30), \tag{15}$$

$$u^+ = 2.5\ln y^+ + 5.5 \qquad (y^+ > 30). \tag{16}$$

The local velocity, Vr, and the local velocity gradient, $\frac{dV_r}{dy}$, can be solved from the above two equations by substituting the expression of u^+ and y^+.

By analogy to pipe flow, the average bed shear stress is defined in a similar way as follows,

$$\tau_{bed} = f_{bed}\frac{\rho U^2}{2}\ , \tag{17}$$

where U is the average fluid velocity in the open area above the cuttings bed and f_{bed} is the bed friction factor. By comparing Dodge & Metzner's friction factor correlation for non-Newtonian turbulent flow in smooth pipe and Colebrook's correlation for Newtonian flow in rough pipe [33], T. Reed and A. Pilehvari proposed an equation for non-Newtonian turbulent flow in rough pipe; it reads [35],

$$\frac{1}{\sqrt{f}} = -4\log\left(\frac{0.27\varepsilon}{D_{eff}} + \frac{1.26^{n^{-1.2}}}{(R_{e,gn} f^{(1-n/2)})^{n^{-0.75}}}\right), \tag{18}$$

where ε is absolute pipe roughness, D_{eff} is the effective diameter, $R_{e,gn}$ is the generalized Reynolds number, and $R_{e,gn} = \frac{D_{eff}{}^{n}\rho U^{2-n}}{8^{n-1}K}$. Replacing ε with the protruding particle height measured from the mean bed surface, this equation can be used to approximate the bed fiction factor. The mean bed roughness, ε, is expressed as a function of angle of repose, ϕ, and particle diameter, d_p (Refer to the report for 2004 May ABM for details).

$$\varepsilon = \frac{d_p}{2}(1+\sin\phi). \tag{19}$$

Denoting $C_\phi = \frac{(1+\sin\phi)}{2}$ as the correction factor of angle of repose for bed roughness, Eq. (18) is expressed as,

$$\frac{1}{\sqrt{f_{bed}}} = -4\log\left(\frac{0.27C_\phi d_p}{D_{eff}} + \frac{1.26^{n^{-1.2}}}{(R_{e,gn} f_{bed}{}^{(1-n/2)})^{n^{-0.75}}}\right). \tag{20}$$

Hydraulic diameter, d_{hyd} ,for the open flow area in a wellbore annulus is used to approximate D_{eff} when there is a cuttings bed in the annulus.

$$d_{hyd} = \frac{4A_f}{S_o + S_i + S_b}, \tag{21}$$

where A_f is the fluid flow area above cuttings bed, S_o is wetted perimeter of outer wellbore, S_i is wetted perimeter of inner drill pipe wall, and S_b is wetted perimeter of cuttings bed.

The bed friction for laminar flow is,

$$f_{bed} = \frac{16}{R_{e,gn}}, \tag{22}$$

However, turbulent flow is much more likely to happen than laminar flow in order to resuspend a particle in a cuttings bed. Once f_{bed} is obtained using Eq. 20 or 22, drag and lift can be calculated step by step.

Van der Waals Force F_{vanR}

Van der Waals forces are attractive forces acting between neutral atoms or molecules [14, 15]. Van der Waals forces were found to be dominant forces for closely contacted fine particles. A practical approximation for van der Waals force between two spherical particles is (Refer to the report for 2004 May ABM for details),

$$F_{van} = -\frac{Ad_p}{24s^2} \tag{23}$$

where A is the Hamaker constant, depending on the nature of the particles, A = 4.14×10^{-20} N.m for sand, d_p is particle diameter, and s is the separation distance between two particles.

A relationship between the particle separation distance and the particle diameter has been established recently by Yu *et al*. (2003) based on experimental observations [36],

$$s = 1.78\times10^{-5} d_p^{\,0.77} \tag{24}$$

Randomly choose a sand particle on a sand bed surface as a study object. Denote this particle as M. Experimental observations in this study show that the average number of sand particles neighboring particle M is six. Each neighboring particle applies a F_{van} to particle M, therefore, there are altogether six F_{van} applied to this particle. The total Van der Waals forces applied to particle M are the resultant forces from the six F_{van}. The direction of resultant Van der Waals forces is normal to the mean bed surface according to particles' arrangement, and the magnitude is,

$$|F_{vanR}| = 6\,|F_{van}|\sin\phi\ . \tag{25}$$

Once all the forces are obtained, the next step is to solve the moment equation for CRV.

Critical Resuspension Velocity (CRV)

Based on the rolling mechanism for a highly inclined wellbore, the critical state for particle movement on the cuttings bed is when the resultant moment with respect to the contact point, P, equals zero (Figure 1). The moment balance equation is expressed as,

$$\Gamma = d_p /2 \, [F_L \cos\phi + F_D \sin\phi - F_g \sin(\theta+\phi) - (F_b + F_{vanR})\cos\phi] = 0, \qquad (26)$$

where θ is the hole inclination angle and ϕ is cuttings' angle of repose. Substituting the equations derived for all the forces into the above equation, the CRV will be numerically solved. Procedures for CRV computation was proposed in the previous report.

The angle of repose ϕ for four different cuttings ranging from 0.15 mm to 3.3 mm was tested in air and water. If the cuttings are carefully piled up, this angle increases from 34º to 39º with particle diameter in the range of the particle size tested. However, when water is disturbed, this angle dramatically decreases to 5º -10º depending on the intensity of disturbance. This greatly changes particles' arrangement and makes the particles more difficult to roll along their neighboring particles because it is observed that these particles are "inserted" among other particles.

Figure 2 and 3 show comparison of the flow rate at the CRV calculated from this model with experimental data for 0.45 mm sand at different hole angles.

Experimental Results and Discussion

Seventy two experiments for 0.45mm and 3.3 mm cuttings with water and PAC have been completed on TUDRP LPAT flow loop. PAC concentration is 0.25 lb/bbl with a behavior index n of 0.72 and a consistency index k of 0.053 lbf .sn/100ft2 (0.0254 Pa.sn). Effects of five drilling parameters; namely, flow rate, cuttings size, hole angle, fluid type and drill pipe rotary speed, on annular cuttings volumetric concentration and bed height are discussed here. Experimental procedures are described in the report for 2004 May ABM.

Effects on Annular Cuttings Volumetric Concentration

Annular cuttings volumetric concentration is defined as the volume of the cuttings in the annulus at steady state divided by the annular volume. Figures 4-6 shows the volumetric concentration of three different cuttings at three different flow rates and three drill pipe rotational speeds in a horizontal well. Regardless of water flow rate, the concentration of the smallest sand-sized cuttings (0.45 mm) is about 7% * higher than that of the largest cuttings (3.3 mm) when pipe rotation is not present. However, with the increase of drill pipe rotational speed (Figures 4-6), the differences decrease, indicating that pipe rotation is more helpful for smaller

cuttings transport than for larger cuttings. In contrast with larger cuttings, smaller sand takes more time to settle back to the sand bed once agitated by the drill pipe due to a lower settling velocity.

When tested with water in a horizontal annulus, smaller cuttings have a higher volumetric concentration than larger cuttings, hence are more difficult to transport. However, this is not always true when tested under other conditions.

As shown in Figure 7, 0.45 mm sand has a slightly lower concentration than 1.4 mm cuttings at 70 degree hole angle under all three water flow rates. Though the difference is not that obvious, it happens at every drill pipe rotational speed tested. When PAC fluid is used, the smaller cuttings concentration is much lower than the larger cuttings concentration, both in horizontal and 70 degree annuli. The concentration difference between these two cuttings is greater in a highly inclined well than in a horizontal well, as shown in Figure 8. The same tendency remains for all the drill pipe rotational speeds tested. For example, 0.45 mm sand concentration is about 10% * higher than 1.4 mm cuttings at 70 degree hole angle with 40 rpm drill pipe rotational speed (Figure 8).

Figures 7 and 8 also show how hole angle affects the volumetric concentration of two different cuttings at different flow rates using different drilling fluids. As for 0.45 mm sand, the concentration in a horizontal well is slightly higher than that in a highly inclined well under almost all flow rates and all drill pipe rotational speeds, both for water and PAC. As a contrast, the concentration for 1.4 mm cuttings in a horizontal well is slightly lower that in a highly inclined well under almost all the flow rates and all the drill pipe rotational speeds, both for water and PAC.

In comparison with water, PAC has positive effects on reducing volumetric concentration of both 0.45 mm and 1.4 mm cuttings. However, the effects are greatly dependent on cuttings size. The cuttings concentration with PAC is much lower than with water for 0.45 mm sand, as shown in Figure 9. The same trend remains for both horizontal and highly inclined wells. With the increase of drill pipe rotation, the concentration difference between two fluids is even bigger. As for 1.4 mm cuttings, the concentration with PAC is only slightly lower than with water (Figure 10), both in horizontal and highly inclined wells. Increasing drill pipe rotational speed does not make bigger difference.

The extent to which the drill pipe rotation helps cuttings transport depends on the cuttings size and the type of drilling fluid. Figure 11 shows that pipe rotation has positive effects on reducing the volumetric concentration of both 0.45 mm and 1.4 mm cuttings at each flow rate tested. However, the three dotted lines for 0.45 mm sand are much steeper than the three solid lines for 1.4 mm cuttings. This corresponds to the previous

observation that smaller cuttings benefit more from drill pipe rotation than larger cuttings do. Comparing the pipe rotation effects under different drilling fluids indicates that pipe rotation with PAC has more positive effects than with water on 0.45 mm sand. It makes no apparent difference between PAC and water for 1.4 mm cuttings.

Effects on Equilibrium Cuttings Bed Height

Equilibrium bed height is the stationary bed height measured at steady state flow conditions. It does not account for the cuttings in suspension. Figure 17 illustrates how to measure equilibrium bed height when pipe rotation is present. Every bed height shown in the figures attached in the Appendix is converted to a dimensionless bed height, which is defined as the real bed height divided by the hole diameter.

As shown in Figure 12, the bed heights with PAC are lower than those with water for 0.45 mm sand at each flow rate and pipe rotational speed. However, PAC is not that helpful in reducing bed heights of 1.4 mm cuttings, though the general tendency is that bed heights with PAC are marginally lower than with water (Figure 13). This is consistent with the above observations on cuttings concentration.

The twelve lines involving thirty six experimental data points in Figure 12 and 13 show an interesting relationship between the equilibrium bed height and flow rate. The bed height almost linearly decreases with an increasing flow rate within the range of flow rate tested, regardless of pipe rotational speed, testing fluid or cuttings size. This relationship is employed in the following correlations for bed heights.

The cuttings size effects on bed heights at different water flow rates and pipe rotational speeds are plotted in Figure 14. Cuttings size has no apparent influence on bed heights when drill pipe rotational speed is less than 40 rpm. The bed heights increase with cuttings diameter only at higher flow rate when pipe rotation reaches 80 rpm.

Figure 15 indicates the effects of pipe rotational speeds for three different cuttings at three different water flow rates. The nine cases represented by the nine lines exhibit a common point. An increase of pipe rotational speed from zero to 40 rpm significantly reduces bed heights. Further increasing pipe rotation, however, only slightly reduces bed heights. The bed height under 200 gpm flow rate with 40rpm pipe rotation is approximately equivalent to that under 400 gpm without pipe rotation. Comparing this with previous observations on cuttings concentration (Figure 11) finds that pipe rotation within 40 rpm is more helpful in reducing bed height than in reducing cuttings concentration. When tested with PAC, the nine lines become steeper, which indicates that drill pipe rotation is more effective in reducing bed heights if PAC is the drilling fluid.

* The concentration difference here and in the following parts is calculated by directly subtracting two concentrations, it is not the relative difference.

Correlations for Cuttings Concentration and Bed Heights

Correlations are developed to predict annular cuttings volumetric concentration and equilibrium bed heights based on the experimental data. In order to account for the effects of the five operational variables, namely, liquid flow rate, cuttings size, hole angle, fluid type and drill pipe rotational speed, the following ten variables are used for dimensional analysis. The unit of each variable in terms of the three basic dimensions is also listed below.

No.	Variables \ Dimensions	M	L	T
1	C_v (Cuttings Volumetric Concentration)	0	0	0
2	D (Wellbore Diameter)	0	1	0
3	d (Drill Pipe Diameter)	0	1	0
4	V_{sl} (Superficial Liquid Velocity)	0	1	-1
5	d_p (Cuttings Diameter)	0	1	0
6	θ (Hole Angle)	0	0	0
7	Ω (Drill Pipe Rotational Speed)	0	0	-1
8	K (Fluid Consistency Index)	1	-1	n-2
9	ρ_f (Fluid Density)	1	-3	0
10	g (Gravitational Acceleration)	0	1	-2

Seven dimensionless variables are obtained according to the Buckingham Pi theorem.

$$\pi_1 = C_v , \tag{27}$$

$$\pi_2 = \frac{V_{sl}}{\sqrt{g(D-d)}} = F_r , \tag{28}$$

$$\pi_3 = \frac{\rho_f (\Omega d)^{2-n} (D-d)^n}{4K} = T_a , \tag{29}$$

$$\pi_4 = \frac{d_p}{D-d} = R_{dp}, \tag{30}$$

$$\pi_5 = \theta, \tag{31}$$

$$\pi_6 = \frac{\rho_f V_{sl}^{2-n}(D-d)^n}{8^{n-1}K} = R_{esl}, \tag{32}$$

$$\pi_7 = \frac{d}{D} = R_d, \tag{33}$$

where R_{esl} is the superficial Reynolds number, T_a is the Taylor number defined here, F_r is the superficial Froude number, R_d is the ratio of the drill pipe diameter to the wellbore diameter, and R_{dp} is the ratio of cuttings diameter to the annular hydraulic diameter. Since the influence of different R_d is not studied here, the last dimensionless variable π_7 is not included in the correlation.

Experimental results show very different behaviors in cuttings transport with water and PAC. Correlations for water and PAC have to be developed separately because one model is not able to accommodate both fluids. The effects of flow rate are reflected both in R_{esl} and F_r. Since K in R_{esl} does not affect the regression modeling, it is not necessary to use both R_{esl} and F_r in the regression. Considering the linear relationship between bed heights and flow rate which is proportional to F_r, F_r is selected as an important variable in the regression. The relationship between these variables is expressed as,

$$C_v = f(F_r, Ta, \theta, R_{dp}). \tag{34}$$

Similarly, replacing cuttings volumetric concentration, Cv, with bed height, h, in the above table yields another seven dimensionless variables, six of which are the same as before (from π2 to π7). The one accounting for the equilibrium bed height is $\frac{h}{D}$. Eliminating π6 and π7 as before, the relationship between these variables is expressed as,

$$\frac{h}{D} = f(F_r, Ta, \theta, R_{dp}). \tag{35}$$

The following general equation for cuttings concentration is selected based on the graphical effects of the four operational variables, namely, flow rate, pipe rotation, hole angle and cuttings size,

$$C_v = kF_r^{b_1}\theta^{b_2}R_{dp}^{b_3}\tanh(1+b_4Ta). \tag{36}$$

The correlation based on all the experimental data points with water is,

$$C_v = 22.9F_r^{-0.716}\theta^{0.15}R_{dp}^{-0.105}\tanh(1-9.7\times10^{-7}Ta). \tag{37}$$

The correlation based on all the experimental data with PAC for 0.45 mm sand is (d_p is eliminated in the correlations for PAC because regression involving d_p does not give satisfied correlations),

$$C_v = 259 F_r^{-1.05} \theta^{0.689} \tanh(1 - 2\times 10^{-5} Ta) . \tag{38}$$

The correlation based on all the experimental data with PAC for 1.4 mm sand is,

$$C_v = 28.7 F_r^{-0.651} \theta^{-0.179} \tanh(1 - 9.09\times 10^{-6} Ta) . \tag{39}$$

Since hole angle has only minor effects on equilibrium bed height, the following general equation for bed heights is selected based on the graphical effects of the three operational variables, namely, flow rate, pipe rotation and cuttings size,

$$\frac{h}{D} = k(b_1 + b_2 F_r)(1 + b_3 Ta)^{b_4} R_{dp}^{\ b_5} . \tag{40}$$

The correlation of bed height for water is,

$$\frac{h}{D} = 0.88(1.15 - 0.407 F_r)(1 + 1.866\times 10^{-5} Ta)^{0.326} R_{dp}^{\ 0.006} . \tag{41}$$

The correlation of bed height for PAC is,

$$\frac{h}{D} = 1.13(1.51 - 0.631 F_r)(1 + 2.565\times 10^{-4} Ta)^{0.325} R_{dp}^{\ 0.088} . \tag{42}$$

Predictions using the above five correlations for cuttings concentration and bed heights show a good agreement with experimental data. An example of the comparison between predicted values and experimental data is shown in Figure 16. Bed height obtained from Eq. (41) and Eq. (42), when pipe rotation is not present, can be used as an input for the mechanistic model for CRV.

Conclusions

(1) Experiments with 0.45mm and 1.4mm cuttings were completed on TUDRP LPAT flow loop;

(2) Smaller cuttings have a higher concentration than larger cuttings in a horizontal annulus when tested with water;

(3) Smaller cuttings have a lower concentration than larger cuttings in both horizontal and 70 degree hole angle annuli when tested with 0.25 lb/bbl PAC;

(4) Smaller cuttings concentration in a horizontal annulus is higher than that in a 70 degree hole angle annulus, while larger cuttings concentration exhibits an opposite trend;

(5) Drill pipe rotation is more helpful in reducing smaller cuttings concentration than in reducing larger cuttings concentration;

(6) Compared with water, 0.25 lb/bbl polymer decreases smaller cuttings concentration and bed height by 5-10%;

(7) Equilibrium bed height linearly decreases with the increase of flow rate within the range of flow rate tested.

References

1. Parker, D.J., "An Experimental Study of the Effects of Hole Washout and Cutting Size on Annular Hole Cleaning in Highly Deviated Wells", U. of Tulsa, Master's thesis, 1987.
2. Alain A. Gavignet, Ian J. Sobey, "Model Aids Cuttings Transport Prediction", SPE 15417, September 1989, JPT, Page 916-921.
3. Thor Inge F. Larsen, "A Study of the Critical Fluid Velocity in Cuttings Transport for Inclined Wellbores", U. of Tulsa, Master's thesis, 1990.
4. J.T. Ford et al., "Experimental Investigation of Drilled Cuttings Transport in Inclined Boreholes", SPE 20421, The 65th SPE Annual Technical Conference & Exhibition, New Orieans, LA, 23-26 September, 1990.
5. J.T. Ford, J.M. Peden, M.B. Oyeneyin, "Comprehensive Experimental Investigation of Drilled Cuttings Transport in Inclined Wells Including the Effects of Rotation and Eccentricity", SPE 20925, Hague, Netherlands, 22-24, October, 1990.
6. T.R. Sifferman and T.E. Becker, SPE Mobile R&D Corp., "Hole Cleaning in Full-Scale Inclined Wellbores", SPE 20422, The 65th SPE Annual Technical Conference & Exhibition, New Orieans, LA, 23-26 September, 1990.
7. Adel A. Bassal, "The Effect of Drillpipe Rotation on Cuttings Transport in Inclined Wellbores", U. of Tulsa, Mater's thesis, 1995.
8. A.L. Martins, et al. "Optimizing Cuttings Circulation In Horizontal Well Drilling", SPE 35341, International Petroleum Conference & Exhibition of Mexico, Villahermosa, Mexico, 5-7 March, 1996.
9. Q. Doan, SM Farouq, M. Oguztoreli Ali, A.E. George, "Sand Transport in a Horizontal Well: A Numerical Study", SPE 37568, Intl. Thermal Operations and Heavy Oil Symposium, Bakersfield, California, 10-12 February, 1997.
10. S. Walker and J. Li, "The effect of particle size, fluid rheology and pipe eccentricity on cuttings transport", SPE 60755, 2000 SPE/ICoTA Coiled Tubing Roundtable, Huston, TX, 5-6 April, 2000.

11. Ramadan M. Ahmed, "Mathematical Modeling and Experimental Investigation on Solids and Cuttings Transport", Norwegian University of Science and Technology, PhD dissertation, June 2001.
12. Gailani, J. Z., Jin, L., McNeil, J., and Lick, W., "Effects of Bentonite Clay on Sediment Erosion Rates", DOER Technical Notes Collection (ERDC TN-DOER-N9), 2001, U.S. Army Engineer Research and Development Center, Vicksburg, MS.
13. M.B. Oyeneyin and A.T. Faga, "Formation-Grain-Size Prediction Whilst Drilling--A Key Factor in Intelligent Sand Control Completions", SPE 56626, SPE Annual Technical Conference & Exhibition, Huston, TX, 3-6 October, 1999.
14. Theo G. M. van de Ven, Pulp and Paper Research Institute of Canada, Dept. of Chemistry, McGill University, Canada, "Colloidal Hydrodynamics", ISBN 0127107703, Academic Press, 1989.
15. Paul C. Hiemenz, "Principles of Colloid and Surface Chemistry", 2nd ed., rev. and expanded, ISBN 0824774760, Marcel Dekker, Inc. New York and Basel, 1986.
16. G.A. Kallio and M.W. Reeks, "A Numerical Simulation of Particle Deposition in Turbulent Boundary Layers", International Journal of Multiphase Flow, Vol.15, No. 3, pp. 433-446, 1989.
17. R. Mei, "An Approximate Expression for The Shear Lift Force on a Spherical Particle at Finite Reynolds number", Journal of Multiphase Flow, Vol. 18, No. 1, pp. 145-147, 1992.
18. R.K. Clark and K.L. Bickham, "A Mechanistic Model for Cuttings Transport", SPE28306, the SPE 69th Annual Technical Conference and Exhibition, New Orleans, LA, U.S.A., 25-28 September 1994.
19. Clift, R., Grace, J.R., and Weber, M.E., "Bubbles, Drops and Particles", Academic Press, New York, 1978.
20. Liang, S.C., Hong, T. and Fan, L.S., "Effect of Particle Arrangement on The Drag Force of a Particle", International Journal of Multiphase Flow (1996), Vol. 22, P285-306.
21. Saffman, P.G. "The Lift on Small Sphere in a Slow Shear Flow", Journal of Fluid Mechanics, Vol.22, pp. 385-400, 1965.
22. Ralph K. Iler, "The Colloid Chemistry of Silica and Silicates", P130-133, Cornell University Press, Ithaca, New York, 1995.
23. Bourgoyne, A.T., Millheim, K.K., Chenvert, M.E., and Young, F.S., "Applied Drilling Engineering", SPE Text book, Richardson (1991).
24. R. Byron Bird, Warren E. Stewart, Edwin N. Lightfoot, "Transport phenomena", New York, Wiley, 1960.

25. Schlichting, Hermann, “Boundary Layer Theory”, Translated by J. Kestin, New York McGraw-Hill 1955.
26. Morton M. Denn, “Process Fluid Mechanics”, P61-62, ISBN 0-13-723163-6, Englewood Cliffs, N.J. Prentice-Hall c1980.
27. F.M. Leslie and R.I. Tanner, “The Slow of a Visco-Elastic Liquid Past a Sphere”, Quart. Journ. Mech. and Applied Math., Vol. XIV, pt. 1, 1961.
28. Melvin L. Wasserman and John C. Slattery, “Upper and Lower Bounds on the Drag Coefficient of a Sphere in a Power-Model Liquid”, A.I. Ch. E. Journal, Vol. 10, No. 3, pp. 383-388, 1964.
29. Y.I. Cho and J.P. Hartnett, “Drag Coefficients of a Slowly Moving Sphere in Non-Newtonian Fluids”, Journal of Non-Newtonian Fluid Mechanics, Vol. 12, pp. 243-247, 1983.
30. Gu Dazhi and R.I. Tanner, “The Drag on a Sphere in a Power-Law Fluid”, Journal of Non-Newtonian Fluid Mechanics, Vol. 17 pp. 1-12, 1985.
31. D.I. Graham and T.E.R. Jones, “Settling and Transport of Spherical Particles in Power-Law Fluids at Finite Reynolds Number”, Journal of Non-Newtonian Fluid Mechanics, Vol. 54, pp. 465-488, 1994.
32. Byoichi Kurose and Satoru Komori, “Drag and Lift on a Rotating Sphere in a Linear Shear Flow”, Journal of Fluid Mechanics, Vol. 384, pp. 183-206, 1999.
33. David S. Dandy and Harry A. Dwyer, “A Sphere in Shear Flow at Finite Reynolds Number: Effect of Shear on particle Lift, Drag, and Heat Transfer”, Journal of Fluid Mechanics, Vol. 216, pp. 381-410, 1990.
34. D.W. Dodge and A.B. Metzner, “Turbulent Flow of Non-Newtonian Systems”, A.I. Ch. E. Journal, Vol. 5, No. 2, pp. 189-204, 1958.
35. T. Reed and A. Pilehvari, “A New Model for Laminar, Transitional, and Turbulent Flow of Drilling Muds”, SPE 25456, Production Operations Symposium held in Oklahoma City, OK, USA, March 21-23, 1993.
36. A.B. Yu, C.L. Feng, R.P. Zou and R.Y. Yang, “On the Relationship Between Porosity and Interparticle Forces”, Powder Technology, Vol. 130, pp. 20-76, 2003.
37. Muhammad Ali Qureshi, “Experimental Study on Effective Hole Cleaning Using a Mechanical Cleaning Device”, U. of Tulsa, Master’s thesis, 2004.

Appendix

Figures referred to in the text section

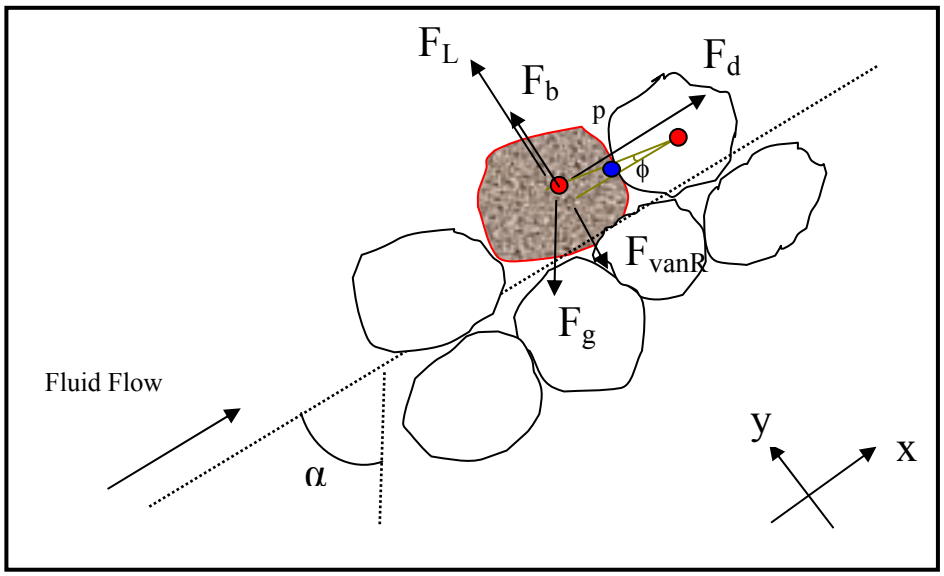

Figure 1 Forces Applied On A Small Protruding Particle On The Surface of a Cuttings Bed

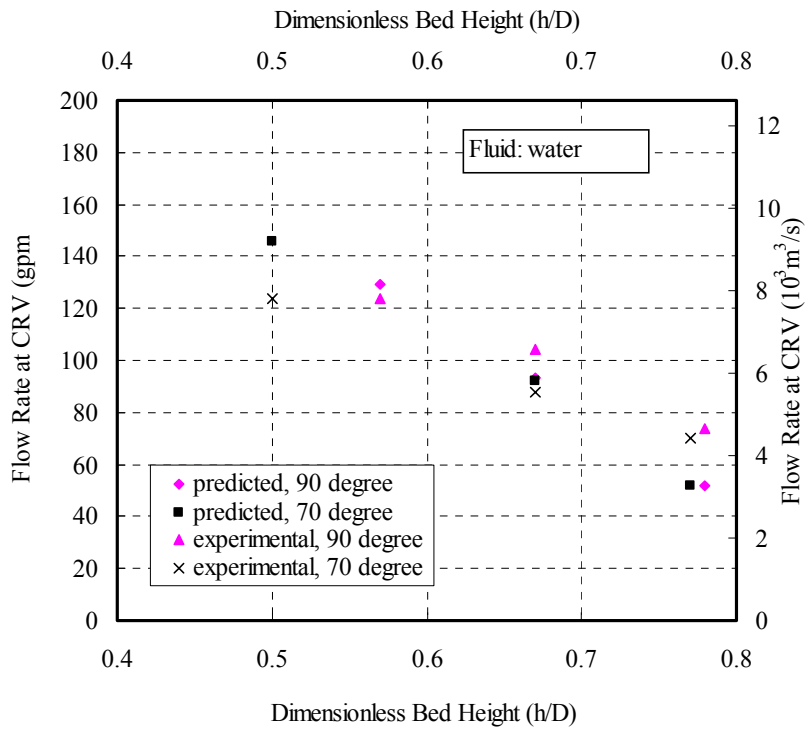

Figure 2 Comparison of Flow Rate at CRV between Mechanistic Modeling and Experimental Results Using Water and 0.45 mm sand

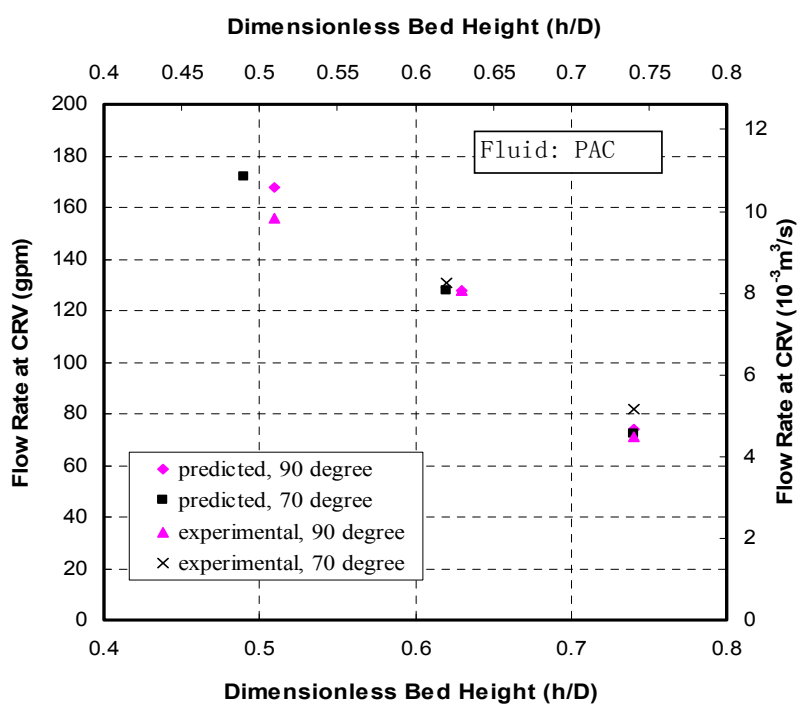

Figure 3 Comparison of Flow Rate at CRV between Mechanistic Modeling and Experimental Results Using PAC and 0.45 mm sand

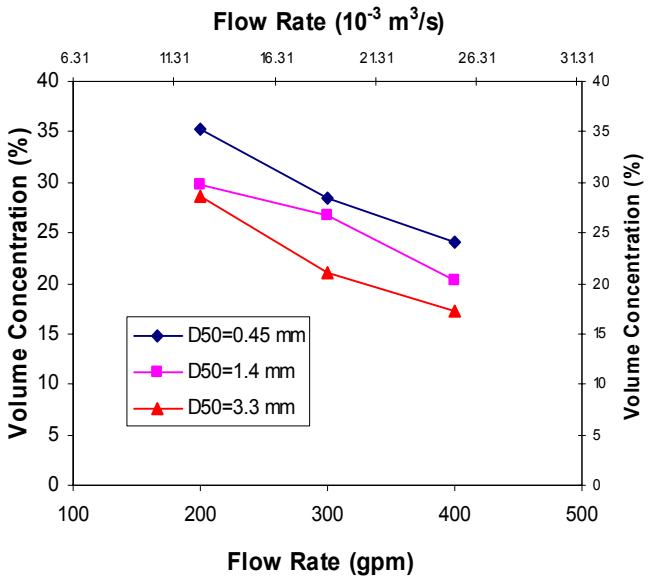

Figure 4 Annular Cuttings Volume Concentration vs. Water Flow Rate for Three Different Cuttings (No pipe rotation, 90^0, data of 3.3mm cuttings is from Muhammad Ali Qureshi [37])

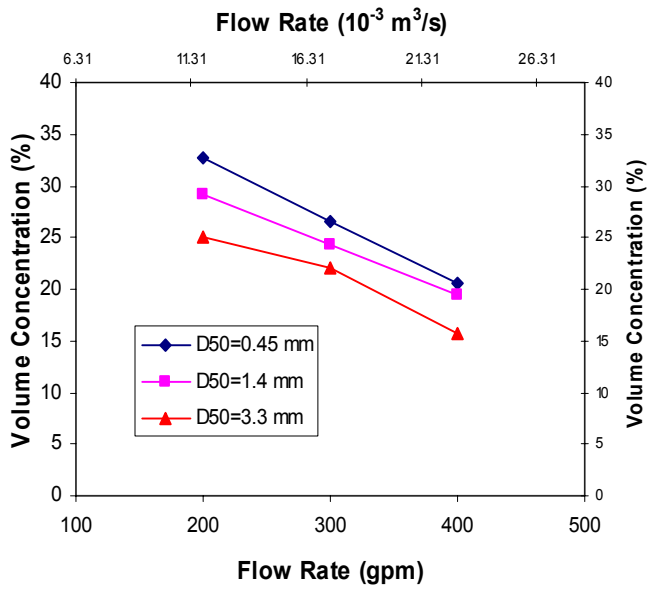

Figure 5 Annular Cuttings Volume Concentration vs. Flow Rate for Three Different Cuttings (40 rpm, 90^0, water, data of 3.3mm cuttings is from Muhammad Ali Qureshi [37])

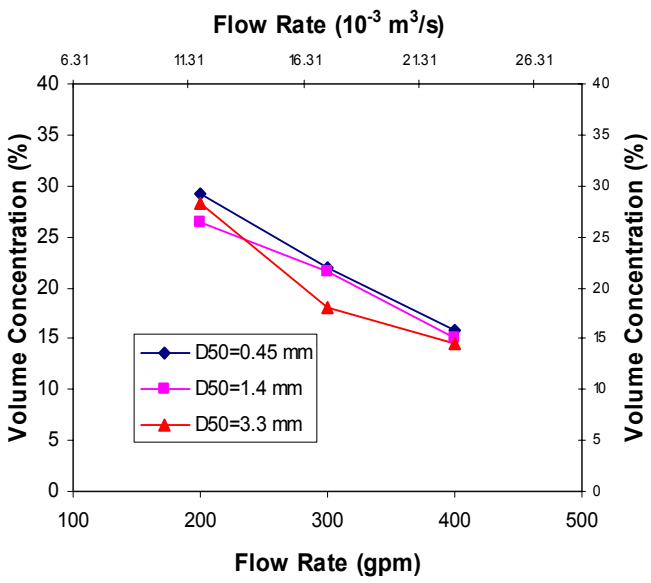

Figure 6 Annular Cuttings Volume Concentration vs. Flow Rate for Three Different Cuttings (80 rpm, 90^0, water, data of 3.3mm cuttings is from Muhammad Ali Qureshi [37])

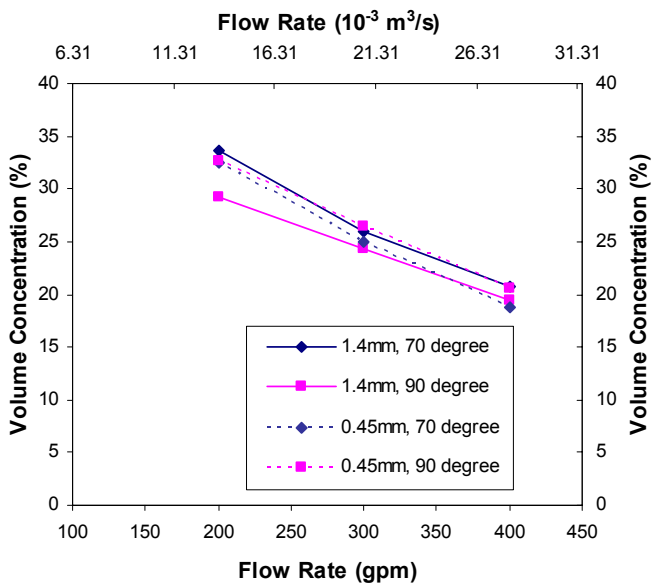

Figure 7 Annular Cuttings Volume Concentration vs. Flow Rate with 40 rpm Pipe Rotation at Different Hole Angles **(water)**

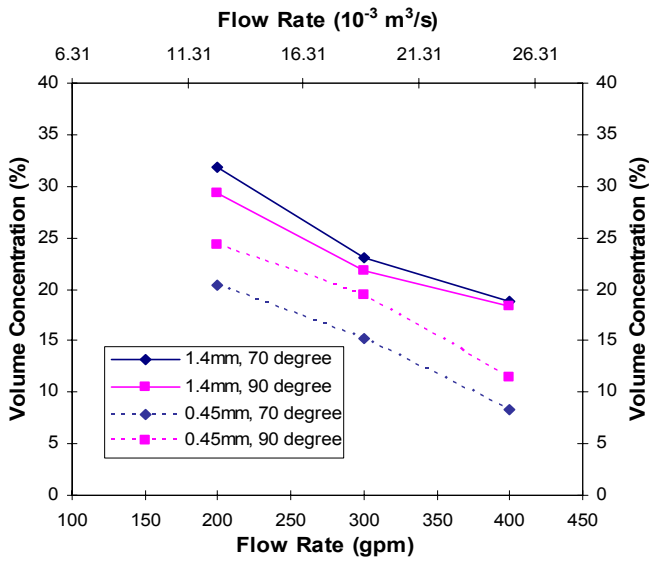

Figure 8 Annular Cuttings Volume Concentration vs. Flow Rate with 40 rpm Pipe Rotation at Different Hole Angles (**PAC**)

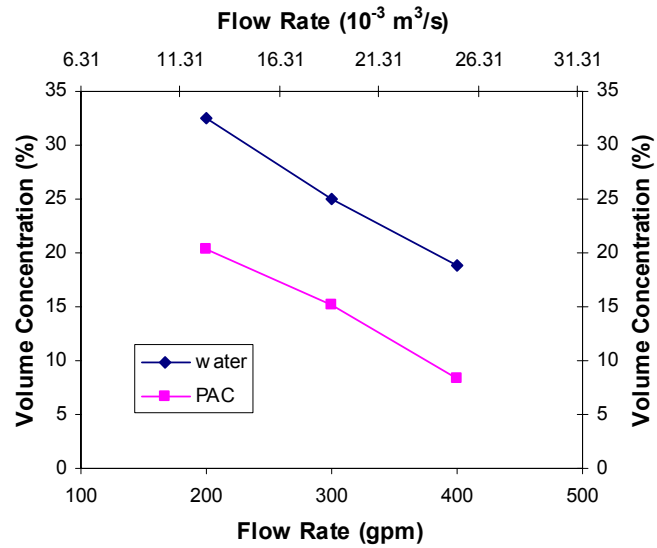

Figure 9 Annular Cuttings Volume Concentration vs. Flow Rate with 40 rpm Pipe Rotation at 70 degree (**0.45mm** sand)

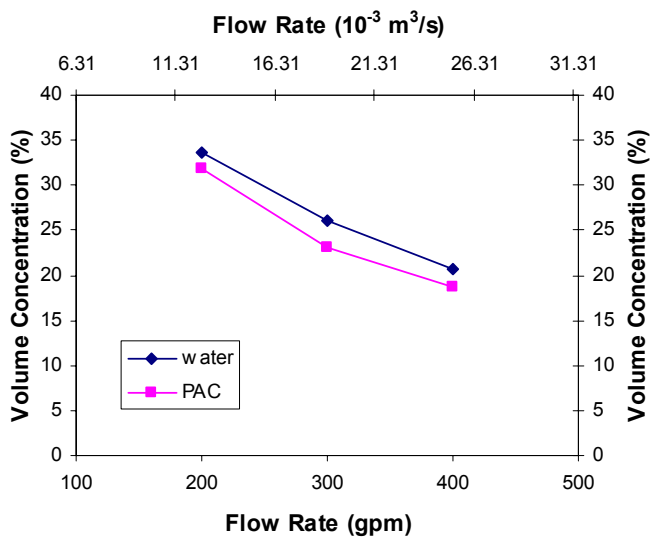

Figure 10 Annular Cuttings Volume Concentration vs. Flow Rate with 40 rpm Pipe Rotation at 70 degree (**1.4mm** sand)

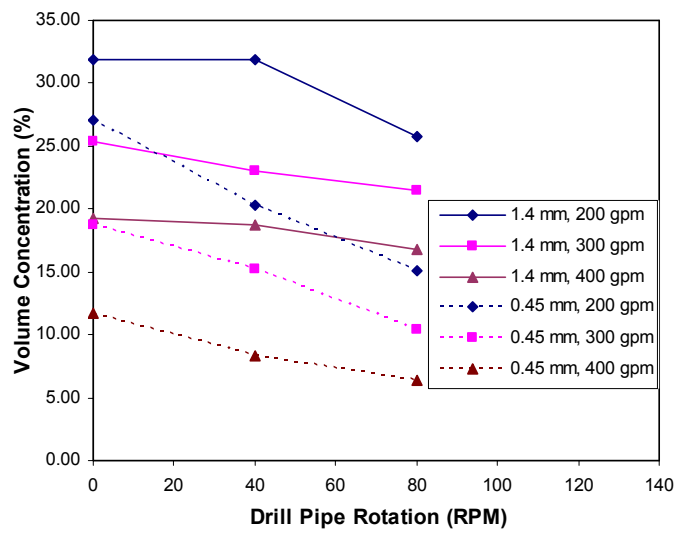

Figure 11 Annular Cuttings Volume Concentration vs. Drill Pipe Rotational Speed at 70 degree (**PAC**)

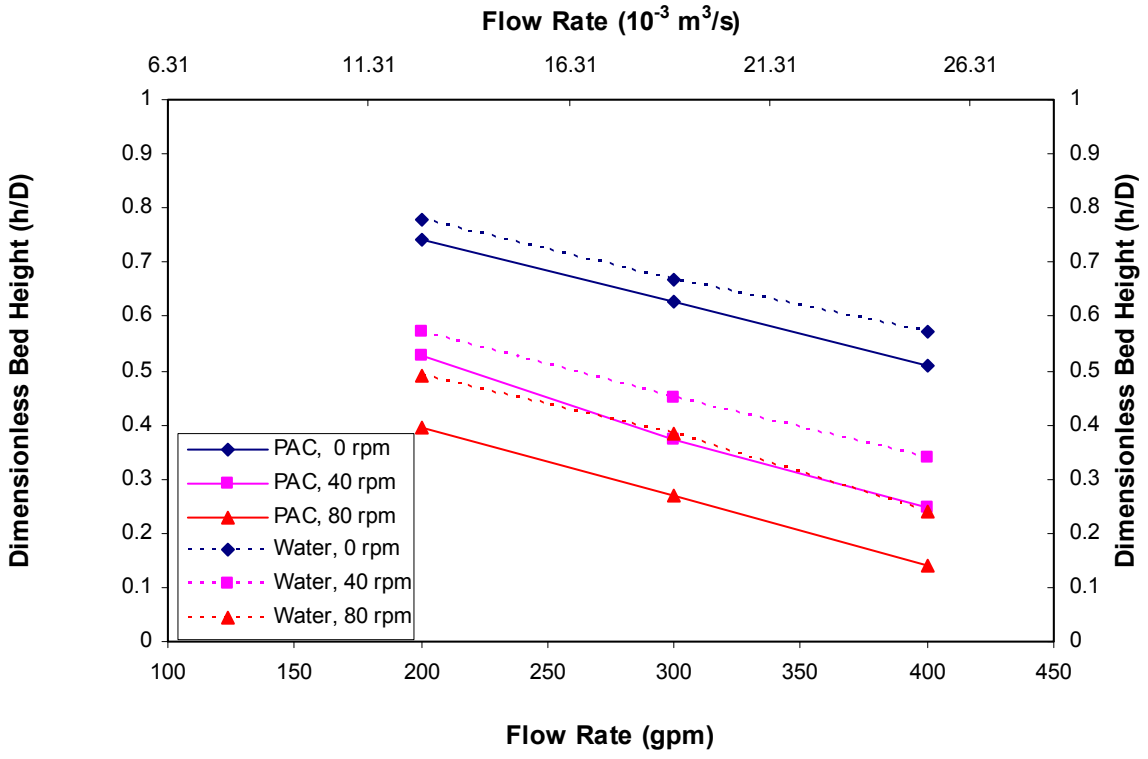

Figure 12 Dimensionless Sand Bed Height vs. Flow Rate (**0.45mm** sand, 90 degree)

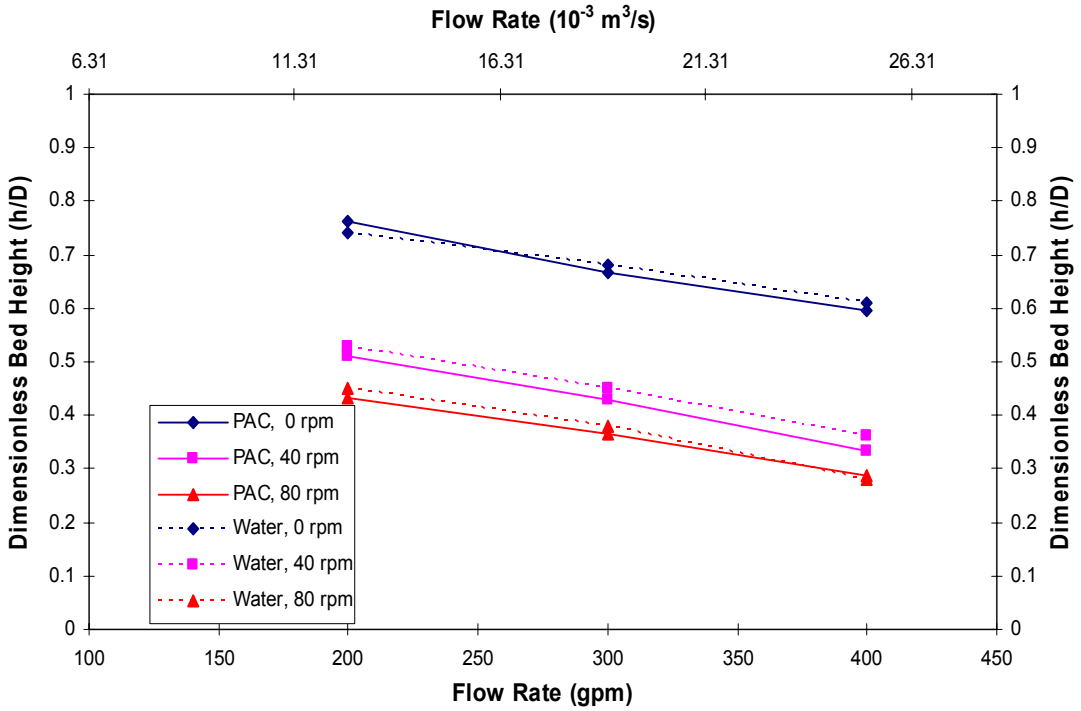

Figure 13 Dimensionless Sand Bed Height vs. Flow Rate (**1.4mm** sand, 90 degree)

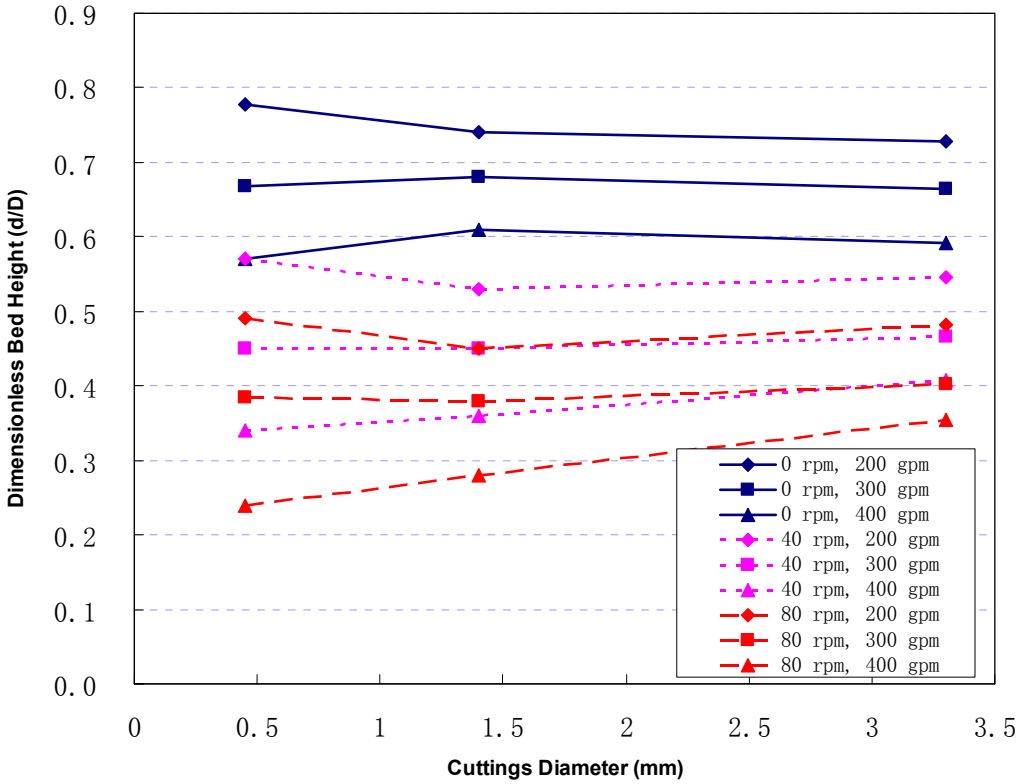

Figure 14 Dimensionless Sand Bed Height vs. Cuttings Diameter (**water, 90 degree**)

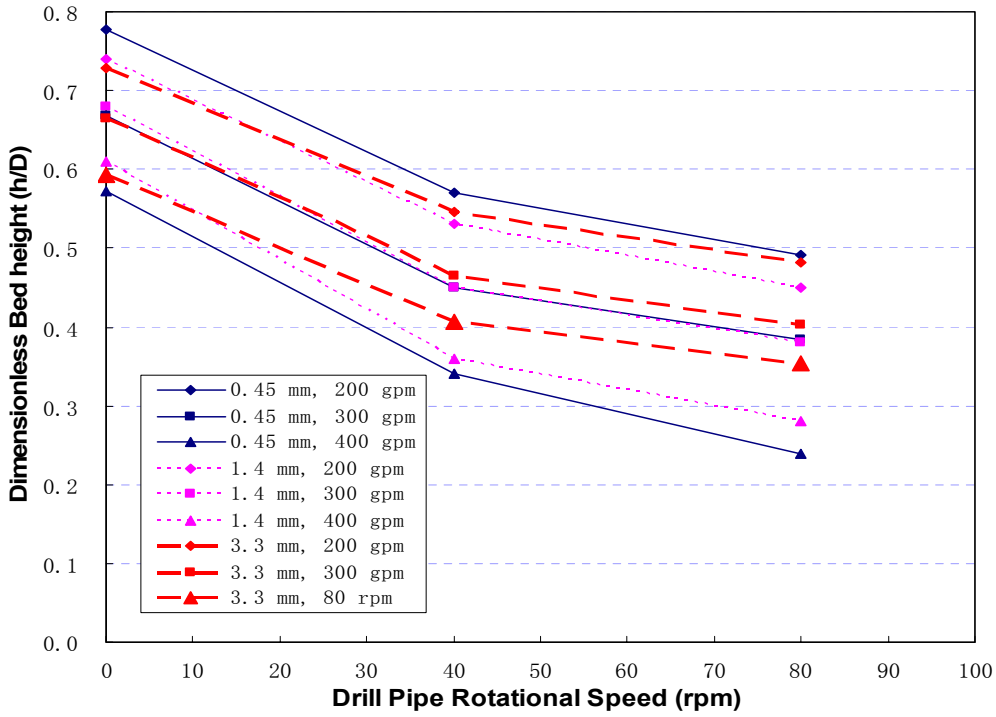

Figure 15 Dimensionless Sand Bed Height vs. Pipe Rotational Speed (**water, 90 degree**)

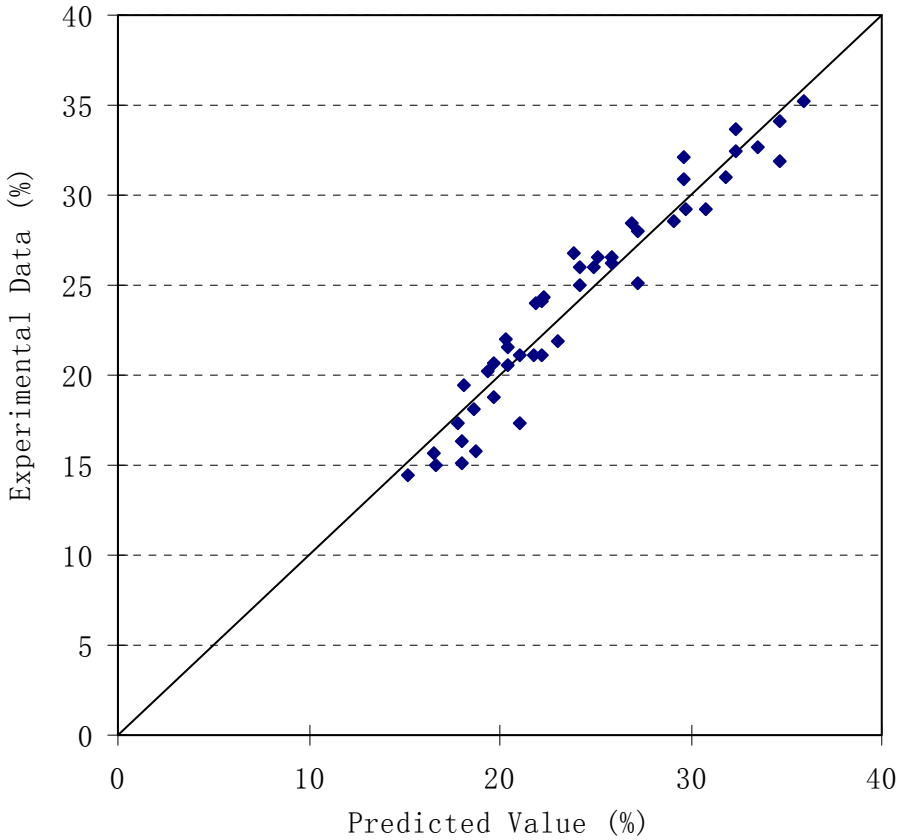

Figure 16 Comparison of predicted cuttings concentration from correlations with experimental data (water)

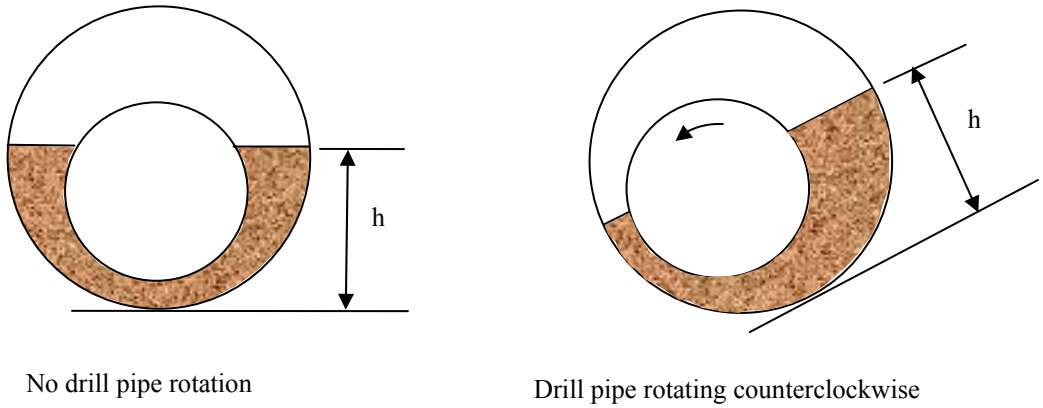

Figure 17 Equilibrium Bed Height Measurement

The Effect of Tool Joints on ECD While Drilling with Polymeric Fluids

Sarita Simoes

The Effect of Tool Joints on ECD While Drilling with Polymeric Fluids

INVESTIGATOR: Sarita Queiroz Simões

OBJECTIVE:

- To study the pressure losses in a concentric and eccentric annulus due to the presence of tool joints for a Power Law polymeric fluid flow with different geometries of tool joints using Computational Fluid Dynamics
- To develop a hydraulic model to predict the pressure losses in an annulus due to the presence of tool joints

PRESENT WORK:

- Development of the hydraulic model
- Development of VBA based simulator in an EXCEL interface to simulate real cases of wellbore obtaining pressure drop information for the system
- Conduction of 70% of the simulations proposed

APPROACH:

- To conduct an extensive review of related literature
- To carry out CFD simulations of polymeric drilling fluids flow in an annulus with the presence of tool joints
- To develop a hydraulic model to predict the fluid pressure losses in an annulus with the presence of tool joints

DELIVERABLES:

- Theoretical results and analysis of the influence of the tool joints on ECD for a polymeric fluid flow in an annulus
- Development of a hydraulic model to predict the fluid pressure losses in the studied system
- Development of a simulator to calculate ECD for a wellbore
- Semi-annual Advisory Board Meetings, Reports and a Final Report

THE UNIVERSITY of TULSA

The University of Tulsa
Drilling Research Projects

TUDRP

The Effect of Tool Joints on ECD While Drilling with Polymeric Fluids (Progress Report)

Sarita Queiroz Simões, The University of Tulsa, Drilling Research Projects

This report is prepared for TUDRP Advisory Board Meeting, May, 23-24, 2005, Tulsa-Oklahoma.

Investigator

Chemical Engineer, graduated from the Federal University of Rio de Janeiro, Rio de Janeiro, Brazil, in August 2003. She did an internship at the Research Center of Petrobras for one year working at the Well Engineering Technology Department. Currently she is enrolled in the M. S. program in Petroleum Engineering at the University of Tulsa.

Abstract

This report presents the status of the project. The results of some simulations are discussed here regarding the effect of eccentricity and tool joints. A dimensional analysis of the studied system is presented and also a TOOL JOINT simulator. Some concepts related to Computational Fluid Dynamics (CFD) are also presented here.

Project Status

Table 1: Project Status

Literature Review	90 %
CFD Software Training	95 %
Analytical Models	75 %
Simulations	70 %

Background

In recent years there has been an increase in drilling more ultra-deep and deepwater wells with high abnormal pressures. This is a trend that is likely to continue. One of the major challenges in ultra-deep and deepwater drilling is to maintain downhole pressures within the narrow window between the pore pressure and fracture gradient. Since the size of this operating window dictates the maximum ECD (Equivalent Circulating Density) that the well can tolerate, there is a need for careful control and prediction of ECD (Bern e*t al*, 2003).

ECD is governed by the hydrostatic head of the mud column and the frictional pressure loss in the annulus. Therefore, it is influenced by many factors including well and drillstring geometry, local drilling fluid rheology, and flow rate (Baranthol *et al*, 1995). The downhole pressure of a circulating fluid is the sum of its hydrostatic head (a function of mud density and cuttings loading) and frictional loss (a function of mud rheology, mud density, annular geometry, and flow rate) (Bern *at al*, 2004). Thus, in order to determine the ECD there is a need to calculate the friction pressure losses in the annulus.

Problem Statement

Wellbore pressure management is a critical part of normal drilling practices where static and dynamic fluid pressures are used to contain formation pressures and to assure wellbore stability. Excessive fluid pressure can create problems including reduced operating margins between the fracture and pore pressures and, in some cases, lost circulation (Bern e*t al*, 2003).

Reliable prediction of annular pressure losses is therefore needed in order to successfully adjust the whole set of drilling parameters and, for that, it is important to consider the presence of tool joints. This study will consider the use of polymeric drilling fluids, which are currently the most used fluids in the industry.

Objective

The objective of the study is to study the pressure losses in an annulus due to the presence of tool joints. The system to be investigated will consist of a Power Law fluid flow, with different annular geometries, with and without the presence of tool joints, for concentric and eccentric pipe without rotation.

Approach

In attempting to study this system one important tool available is Computational Fluid Dynamics (CFD), a well established technique used to investigate and optimize fluid flow in different applications. CFD is often used in conjunction with, as well as an alternative to, experimental testing. In some instances it can quickly and economically produce a large amount of information and is particularly attractive when conditions are difficult to reproduce experimentally (for example, high pressure). Most laminar and turbulent flows can be accurately simulated by a properly set-up CFD (Hycalog, 1997).

This study will be carried out using a commercial CFD software package called Fluent®. The system will consist of a non-rotating concentric and eccentric drill pipes, with tool joints, in a wellbore.

Computational Fluid Dynamics (CFD)

CFD is a tool used to simulate the behavior of systems involving fluid flow, heat transfer, and other related physical processes. A solution is obtained by solving conservation equations for momentum, mass, and heat transfer. Those equations are solved in their discrete form by an iterative method for different boundary conditions. The commercial software used in this project (Fluent®), uses the finite volume method for the numerical simulation. In this technique, the region of interest is divided into sub-regions, called control volumes (cells), and the conservation equations are discretized and solved iteratively for each control volume, obtaining as a result an approximate value for each variable within specific points of the domain.

In order to conduct the CFD analysis some main steps have to be followed:

- **Define the geometry:** the domain in which the governing equations will be solved and the solution obtained;
- **Generate the Grid:** finite volumes or cells;
- **Define the fluid domain:** create fluid regions (fluid, solids, conducting solid, porous media); assign fluid properties (viscosity, thermal conductivity, specific heat, density, etc); select the fluid models (turbulence models, compressibility, buoyancy, two-phase flow, etc);
- **Define the boundary conditions:** needed in all external surfaces of the geometry;
- **Solve the governing equations:** set the flow solver options ; iteratively solve the governing equations as a batch process; obtain convergence;

- **Examine results:** either in numerical or graphical format.

Simulation Matrix

The simulation matrix is shown in Table 2. The geometries were chosen to cover the most practical cases.

Table 2: Simulation Matrix

				Tool Joint			
Mud Type	**Fluid Flow Rate (GPM)**	**Number of Tool Joints**	**Drill Pipe Size and Style**	**Outside Diam. of Pin and Box (in)**	**Inside Diam. of Pin (in)**	**Combined Length of Pin and Box (in)**	**Wellbore Diameter (in)**
Water	75	0	2 3/8 EU-X	3 3/8	1 3/4	15	5 1/2
HEC	150	1					
Xanthan Gum	225						
Water	150	0	4 1/2 IEU-G	6 1/4	3	17	8 1/2
HEC	300	1					
Xanthan Gum	450						
Water	300	0	5 1/2 IEU-X	7	4	17	12 1/4
HEC	600	1					
Xanthan Gum	900						

For each of the geometries, three different drill pipes eccentricities (0, 0.5 and 1) and two different convergence/divergence tool joints angles (35 and 90 degrees for convergence and 18 or 90 degrees for divergence) will be simulated. The total number of simulations will be 243.

The geometries were numerated in order to have an organized set of data. Figure 1 shows a schematic view of the geometries. A summary of the simulated geometries up to now is shown in Table 3.

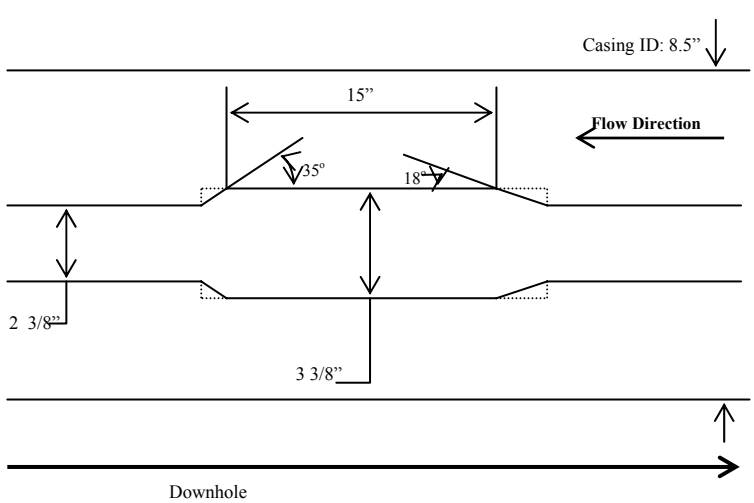

Figure 1: Schematic View of One of the Simulated Geometries

Table 3: Simulations Finished

Geometry	Pipe (in)	Wellbore (in)	Number of Tool Joints	Convergence Angle (degrees)	Divergence Angle (degrees)	Eccentricity
G1	2 3/8	5 1/2	0	0	0	0
G2	2 3/8	5 1/2	0	0	0	0.5
G3	2 3/8	5 1/2	0	0	0	1
G4	2 3/8	5 1/2	1	90	90	0
G5	2 3/8	5 1/2	1	90	90	0.5
G10	5 1/2	12 1/4	0	0	0	0
G11	5 1/2	12 1/4	0	0	0	0.5
G12	5 1/2	12 1/4	0	0	0	1
G13	5 1/2	12 1/4	1	90	90	0
G14	5 1/2	12 1/4	1	90	90	0.5
G19	4 1/2	8 1/2	0	0	0	0
G20	4 1/2	8 1/2	0	0	0	0.5
G21	4 1/2	8 1/2	0	0	0	1
G22	4 1/2	8 1/2	1	90	90	0
G28	2 3/8	5 /12	1	18	35	0
G31	5 1/2	12 1/4	1	18	35	0
G34	5 1/2	12 1/4	1	18	35	0

For each of the geometries simulated three different fluids and flow rates were used. Therefore, for each of the geometries nine simulations were conducted.

The fluid used for the simulations were water and two polymeric fluids. The rheology data (obtained from Andre Leibsohn Martins/Petrobras) for the polymeric fluids is presented in Table 4.

Table 4: Rheology Data

XC 4 LB/BBL		**HEC 3 LB/BBL**	
K ($Pa.s^n$, $lb.s^n/100ft^2$)	3.82 (7.95e-2)	K ($Pa.s^n$, $lb.s^n/100ft^2$)	2.23 (4.64e-2)
n	0.19	n	0.43

K is a measure of the consistency of the fluid and n is a measure of the degree of non-Newtonian behavior.

The density of the polymeric fluids was considered to be the same as water (1000 kg/m^3).

All simulations conducted for the polymeric fluids modeled the flow using the Power Law model (equation 1), available on the commercial software.

$$\tau = K\dot{\gamma}^{n} \tag{1}$$

where τ is the shear stress and γ is the shear rate.

The simulations conducted for water were in turbulent regime. The flow was modeled using the κ-ε model. This model was chosen for its robustness, economy, and reasonable accuracy for a wide range of turbulent flows.

For the κ-ε model the turbulent viscosity (μ_T) is calculated using equation 2 (Fluent® Manual).

$$\mu_T = C_\mu \rho \frac{\kappa^2}{\varepsilon} \tag{2}$$

where C_μ is an empirical constant specified in the turbulence model (approximately 0.09), ρ is the density, κ is the turbulent kinetic energy and ε is the turbulent dissipation rate. The last two variables need to be estimated in order to initialize the flow in each simulation.

They were estimated using the following equations.

$$\kappa = \frac{3}{2}(vI)^2 \tag{3}$$

where v is the average velocity at the inlet and I is the turbulence intensity calculated by,

$$I = 0.16(\mathrm{Re}_{DH})^{-1/8} \tag{4}$$

and Re_{DH} is the Reynolds number calculated using the concept of the hydraulic diameter.

The turbulent dissipation rate can be estimated by,

$$\varepsilon = C_\mu^{3/4} \frac{\kappa^{3/2}}{l} \tag{5}$$

l being the turbulent length scale determined by,

$$l = 0.07 * D_H \tag{6}$$

The simulations conducted for the polymeric fluids were in laminar regime.

Results for some of these simulations are presented in the Results and Conclusions section.

Data Management

One of the big challenges of this project is to find a useful way to manage all the data obtained from the two hundred forty three simulations. One of the ways to do that is creating an interface, in this case using EXCEL, making use of computational code to access all the data and through numeric based

correlations (presented later in this report) obtained from the data using statistic software, output pressure losses results for a real case specified by the user.

A simulator, called TOOLJOINTS simulator, is under development using Visual Basic for Applications (VBA) language in an EXCEL interface. This simulator can be used to estimate the pressure loss in a wellbore including the effect of tool joints. The simulator is structured in areas explained in details as below.

- **Input Area (Front End)**

In this area the user is allowed to input all the data about the geometry of the wellbore, fluid and flow properties of the system. The geometry can consist of either one annular section or several annular sections with different dimensions composing a real directional wellbore. The user is also allowed to input the data in different unit systems. Schematic views of the wellbore are plotted for better visualization of the system simulated. Figure 2 shows the interface for the input area.

- **Database Area (hidden from user)**

In this area all the data related to the simulations is stored. This area contains the calculated dimensionless groups obtained from the dimensional analysis. Figure 3 shows the interface for the database area.

- **Correlation Area (hidden from user)**

In this area all the dimensionless groups are organized and the correlations for each and every region are stored. Figure 4 shows the interface for the correlation area.

- **Calculation Area (hidden from the user)**

In this area, initially the data input from the user in the Input Area is converted in SI units, then the dimensionless groups different from f (friction factor) are calculated using the input data. The friction pressure loss for each region is calculated from f, which is obtained from the correlations. This information is used to calculate the friction pressure loss for each annular section established by the user. The hydrostatic pressure, the total pressure drop and the ECD are also calculated for all sections to obtain the downhole pressure. Figure 5 shows the interface for the calculation area.

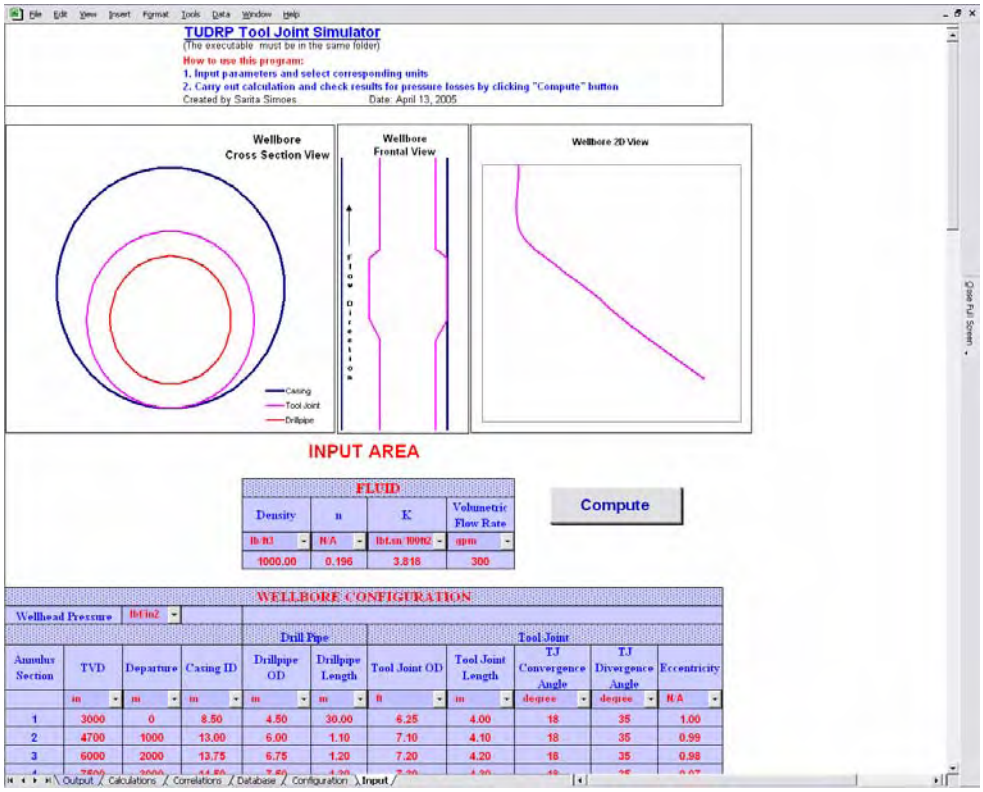

Figure 2: Input Area

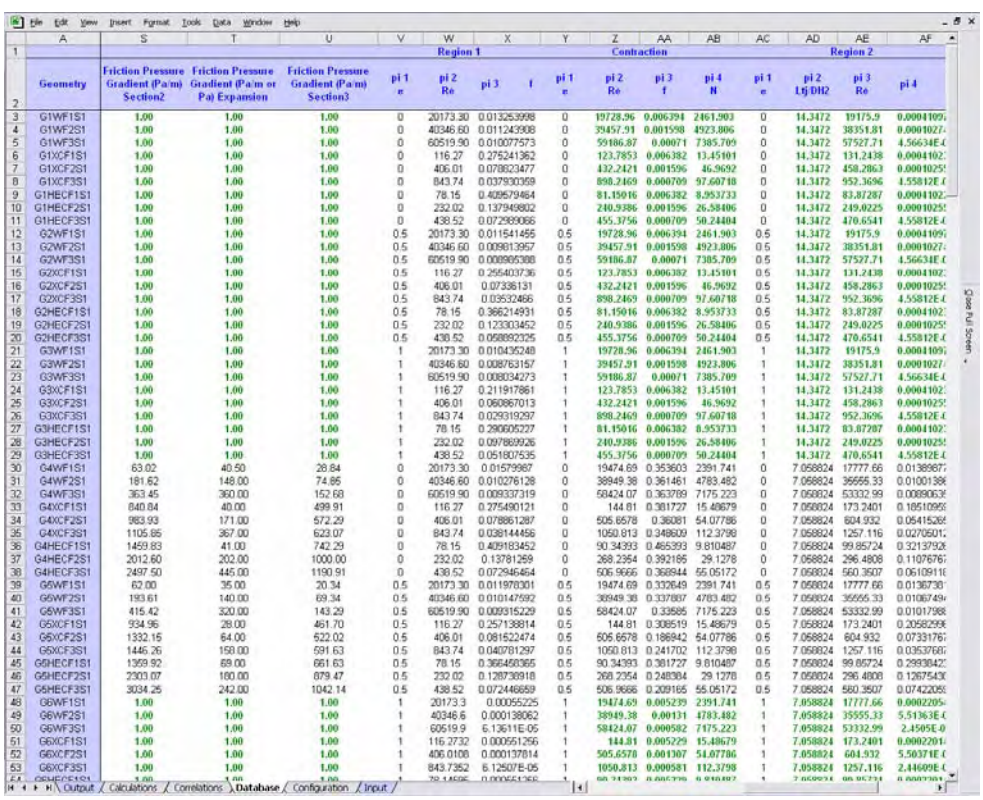

	A	S	T	U	V	W	X	Y	Z	AA	AB	AC	AD	AE	AF
1						Region 1			Contraction				Region 2		
2	Geometry	Friction Pressure Gradient (Pa/m) Section2	Friction Pressure Gradient (Pa/m or Pa) Expansion	Friction Pressure Gradient (Pa/m) Section3	pi 1 e	pi 2 Re	pi 3 f	pi 1 e	pi 2 Re	pi 3 f	pi 4 N	pi 1 e	pi 2 Ltj/DH2	pi 3 Re	pi 4
3	G1WF1S1	1.00	1.00	1.00	0	20173.30	0.013263998	0	19728.96	0.006394	2461.903	0	14.3472	19175.9	0.0004109
4	G1WF2S1	1.00	1.00	1.00	0	40346.60	0.011243908	0	39457.91	0.001598	4923.806	0	14.3472	38351.81	0.0001027
5	G1WF3S1	1.00	1.00	1.00	0	60519.90	0.010077573	0	59186.87	0.00071	7385.709	0	14.3472	57527.71	4.56634E-0
6	G1XCF1S1	1.00	1.00	1.00	0	116.27	0.275241362	0	123.7853	0.006382	13.45101	0	14.3472	131.2438	0.0004102
7	G1XCF2S1	1.00	1.00	1.00	0	406.01	0.078823477	0	432.2421	0.001596	46.9692	0	14.3472	458.2863	0.0001025
8	G1XCF3S1	1.00	1.00	1.00	0	843.74	0.037930359	0	898.2469	0.000709	97.60718	0	14.3472	952.3696	4.55812E-0
9	G1HECF1S1	1.00	1.00	1.00	0	78.15	0.409579464	0	81.15016	0.006382	8.953733	0	14.3472	83.87287	0.0004102
10	G1HECF2S1	1.00	1.00	1.00	0	232.02	0.137949802	0	240.9386	0.001596	26.58406	0	14.3472	249.0225	0.0001025
11	G1HECF3S1	1.00	1.00	1.00	0	438.52	0.072989066	0	455.3756	0.000709	50.24404	0	14.3472	470.6541	4.55812E-0
12	G2WF1S1	1.00	1.00	1.00	0.5	20173.30	0.011541455	0.5	19728.96	0.006394	2461.903	0.5	14.3472	19175.9	0.0004109
13	G2WF2S1	1.00	1.00	1.00	0.5	40346.60	0.009813957	0.5	39457.91	0.001598	4923.806	0.5	14.3472	38351.81	0.0001027
14	G2WF3S1	1.00	1.00	1.00	0.5	60519.90	0.008995388	0.5	59186.87	0.00071	7385.709	0.5	14.3472	57527.71	4.56634E-0
15	G2XCF1S1	1.00	1.00	1.00	0.5	116.27	0.255403736	0.5	123.7853	0.006382	13.45101	0.5	14.3472	131.2438	0.0004102
16	G2XCF2S1	1.00	1.00	1.00	0.5	406.01	0.07336131	0.5	432.2421	0.001596	46.9692	0.5	14.3472	458.2863	0.0001025
17	G2XCF3S1	1.00	1.00	1.00	0.5	843.74	0.03532466	0.5	898.2469	0.000709	97.60718	0.5	14.3472	952.3696	4.55812E-0
18	G2HECF1S1	1.00	1.00	1.00	0.5	78.15	0.366214931	0.5	81.15016	0.006382	8.953733	0.5	14.3472	83.87287	0.0004102
19	G2HECF2S1	1.00	1.00	1.00	0.5	232.02	0.123303452	0.5	240.9386	0.001596	26.58406	0.5	14.3472	249.0225	0.0001025
20	G2HECF3S1	1.00	1.00	1.00	0.5	438.52	0.058892325	0.5	455.3756	0.000709	50.24404	0.5	14.3472	470.6541	4.55812E-0
21	G3WF1S1	1.00	1.00	1.00	1	20173.30	0.010435248	1	19728.96	0.006394	2461.903	1	14.3472	19175.9	0.0004109
22	G3WF2S1	1.00	1.00	1.00	1	40346.60	0.008763157	1	39457.91	0.001598	4923.806	1	14.3472	38351.81	0.0001027
23	G3WF3S1	1.00	1.00	1.00	1	60519.90	0.008034273	1	59186.87	0.00071	7385.709	1	14.3472	57527.71	4.56634E-0
24	G3XCF1S1	1.00	1.00	1.00	1	116.27	0.211917861	1	123.7853	0.006382	13.45101	1	14.3472	131.2438	0.0004102
25	G3XCF2S1	1.00	1.00	1.00	1	406.01	0.060867013	1	432.2421	0.001596	46.9692	1	14.3472	458.2863	0.0001025
26	G3XCF3S1	1.00	1.00	1.00	1	843.74	0.029319297	1	898.2469	0.000709	97.60718	1	14.3472	952.3696	4.55812E-0
27	G3HECF1S1	1.00	1.00	1.00	1	78.15	0.290605227	1	81.15016	0.006382	8.953733	1	14.3472	83.87287	0.0004102
28	G3HECF2S1	1.00	1.00	1.00	1	232.02	0.097869926	1	240.9386	0.001596	26.58406	1	14.3472	249.0225	0.0001025
29	G3HECF3S1	1.00	1.00	1.00	1	438.52	0.051807535	1	455.3756	0.000709	50.24404	1	14.3472	470.6541	4.55812E-0
30	G4WF1S1	63.02	40.50	26.84	0	20173.30	0.01579987	0	19474.69	0.353603	2391.741	0	7.058824	17777.66	0.0138987
31	G4WF2S1	181.62	148.00	74.85	0	40346.60	0.010276128	0	38949.38	0.361461	4783.482	0	7.058824	35555.33	0.0100138
32	G4WF3S1	363.45	360.00	152.68	0	60519.90	0.009337319	0	58424.07	0.363789	7175.223	0	7.058824	53332.99	0.0089063
33	G4XCF1S1	840.84	40.00	499.91	0	116.27	0.275490121	0	144.81	0.381727	15.48679	0	7.058824	173.2401	0.1851095
34	G4XCF2S1	983.93	171.00	572.29	0	406.01	0.078861287	0	505.6578	0.36081	54.07786	0	7.058824	604.932	0.0541526
35	G4XCF3S1	1105.85	367.00	623.07	0	843.74	0.038144456	0	1050.813	0.348609	112.3798	0	7.058824	1257.116	0.0270501
36	G4HECF1S1	1459.83	41.00	742.29	0	78.15	0.409183452	0	90.34393	0.465393	9.810487	0	7.058824	99.85724	0.3213792
37	G4HECF2S1	2012.60	202.00	1000.00	0	232.02	0.13781269	0	268.2354	0.392185	29.1278	0	7.058824	296.4808	0.1107676
38	G4HECF3S1	2497.50	445.00	1190.91	0	438.52	0.072946464	0	506.9666	0.368944	55.05172	0	7.058824	560.3507	0.0610911
39	G5WF1S1	62.00	35.00	20.34	0.5	20173.30	0.011978301	0.5	19474.69	0.332649	2391.741	0.5	7.058824	17777.66	0.0136730
40	G5WF2S1	193.61	140.00	69.34	0.5	40346.60	0.010147592	0.5	38949.38	0.337887	4783.482	0.5	7.058824	35555.33	0.0106749
41	G5WF3S1	415.42	320.00	143.29	0.5	60519.90	0.009315229	0.5	58424.07	0.33585	7175.223	0.5	7.058824	53332.99	0.0101798
42	G5XCF1S1	934.96	28.00	461.70	0.5	116.27	0.257138814	0.5	144.81	0.308519	15.48679	0.5	7.058824	173.2401	0.2058299
43	G5XCF2S1	1332.15	64.00	522.02	0.5	406.01	0.081522474	0.5	505.6578	0.186942	54.07786	0.5	7.058824	604.932	0.0733176
44	G5XCF3S1	1446.26	150.00	591.63	0.5	843.74	0.040781297	0.5	1050.813	0.241702	112.3798	0.5	7.058824	1257.116	0.0353766
45	G5HECF1S1	1359.92	69.00	661.63	0.5	78.15	0.366450365	0.5	90.34393	0.381727	9.810487	0.5	7.058824	99.85724	0.2993642
46	G5HECF2S1	2303.07	180.00	879.47	0.5	232.02	0.128736918	0.5	268.2354	0.248384	29.1278	0.5	7.058824	296.4808	0.1267543
47	G5HECF3S1	3034.25	242.00	1042.14	0.5	438.52	0.072446659	0.5	506.9666	0.209165	55.05172	0.5	7.058824	560.3507	0.0742205
48	G6WF1S1	1.00	1.00	1.00	1	20173.3	0.00055225	1	19474.69	0.005239	2391.741	1	7.058824	17777.66	0.0002205
49	G6WF2S1	1.00	1.00	1.00	1	40346.6	0.000138062	1	38949.38	0.00131	4783.482	1	7.058824	35555.33	5.51363E-0
50	G6WF3S1	1.00	1.00	1.00	1	60519.9	6.13611E-05	1	58424.07	0.000582	7175.223	1	7.058824	53332.99	2.4505E-0
51	G6XCF1S1	1.00	1.00	1.00	1	116.2732	0.000551256	1	144.81	0.005229	15.48679	1	7.058824	173.2401	0.0002201
52	G6XCF2S1	1.00	1.00	1.00	1	406.0108	0.000137814	1	505.6578	0.001307	54.07786	1	7.058824	604.932	5.50371E-0
53	G6XCF3S1	1.00	1.00	1.00	1	843.7352	6.12507E-05	1	1050.813	0.000581	112.3798	1	7.058824	1257.116	2.44609E-0

Output / Calculations / Correlations / Database / Configuration / Input

Figure 3: Database Area

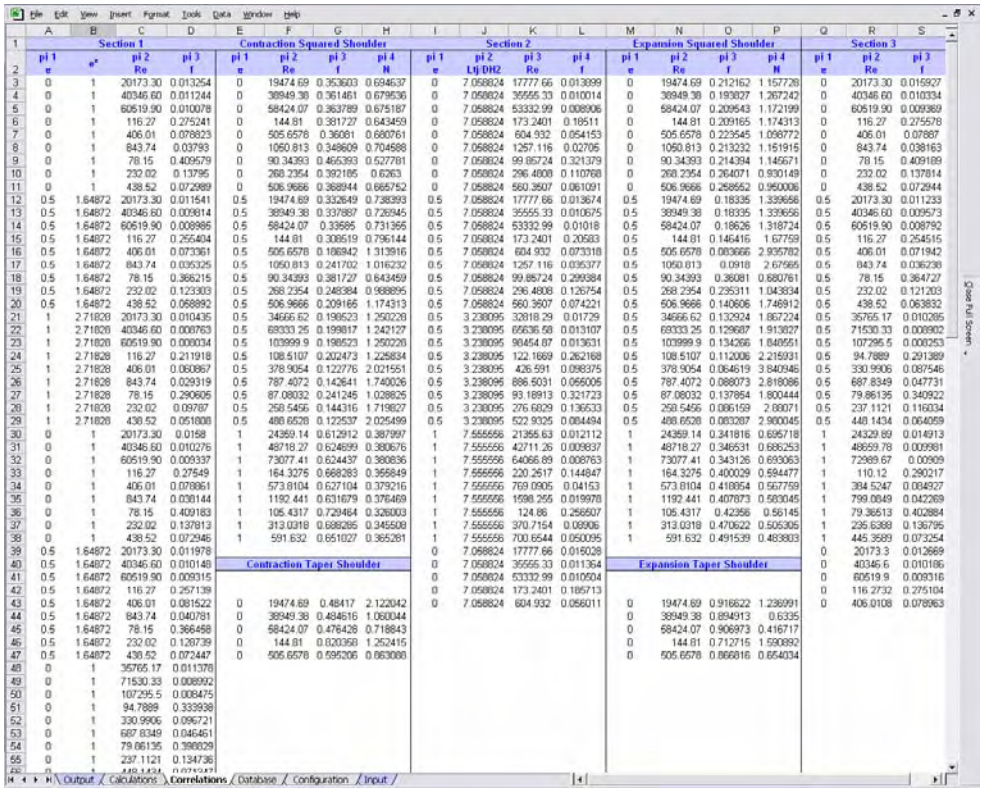

	A	B	C	D	E	F	G	H	I	J	K	L	M	N	O	P	Q	R	S
1	Section 1				Contraction Squared Shoulder				Section 2				Expansion Squared Shoulder				Section 3		
2	pi 1	e*	pi 2	pi 3	pi 1	pi 2	pi 3	pi 4	pi 1	pi 2	pi 3	pi 4	pi 1	pi 2	pi 3	pi 4	pi 1	pi 2	pi 3
	e		Re	f	e	Re	f	N	e	Ltj/DH2	Re	f	e	Re	f	N	e	Re	f
3	0	1	20173.30	0.013254	0	19474.69	0.353603	0.694637	0	7.058824	17777.66	0.013099	0	19474.69	0.212162	1.157726	0	20173.30	0.015927
4	0	1	40346.60	0.011244	0	38949.38	0.361461	0.679536	0	7.058824	35555.33	0.010014	0	38949.38	0.193027	1.267242	0	40346.60	0.010334
5	0	1	60519.90	0.010078	0	58424.07	0.363789	0.675187	0	7.058824	53332.99	0.008906	0	58424.07	0.209543	1.172199	0	60519.90	0.009369
6	0	1	116.27	0.275241	0	144.81	0.381727	0.643459	0	7.058824	173.2401	0.18511	0	144.81	0.209165	1.174313	0	116.27	0.275578
7	0	1	406.01	0.078823	0	505.6578	0.36081	0.680761	0	7.058824	604.932	0.054153	0	505.6578	0.223545	1.098772	0	406.01	0.07887
8	0	1	843.74	0.03793	0	1050.813	0.348609	0.704588	0	7.058824	1257.116	0.02706	0	1050.813	0.213232	1.151915	0	843.74	0.038163
9	0	1	78.15	0.409579	0	90.34393	0.465393	0.527781	0	7.058824	99.85724	0.321379	0	90.34393	0.214394	1.145671	0	78.15	0.409189
10	0	1	232.02	0.13795	0	268.2354	0.392185	0.6263	0	7.058824	296.4808	0.110768	0	268.2354	0.264071	0.930149	0	232.02	0.137814
11	0	1	438.52	0.072989	0	506.9666	0.388944	0.665752	0	7.058824	560.3507	0.061091	0	506.9666	0.258552	0.950006	0	438.52	0.072944
12	0.5	1.64872	20173.30	0.011541	0.5	19474.69	0.332649	0.738393	0.5	7.058824	17777.66	0.013674	0.5	19474.69	0.18335	1.339656	0.5	20173.30	0.011233
13	0.5	1.64872	40346.60	0.009814	0.5	38949.38	0.337887	0.726945	0.5	7.058824	35555.33	0.010675	0.5	38949.38	0.18335	1.339656	0.5	40346.60	0.009573
14	0.5	1.64872	60519.90	0.008985	0.5	58424.07	0.33585	0.731365	0.5	7.058824	53332.99	0.01018	0.5	58424.07	0.18626	1.318724	0.5	60519.90	0.008792
15	0.5	1.64872	116.27	0.255404	0.5	144.81	0.308519	0.796144	0.5	7.058824	173.2401	0.20583	0.5	144.81	0.146416	1.67759	0.5	116.27	0.254515
16	0.5	1.64872	406.01	0.073361	0.5	505.6578	0.186942	1.313916	0.5	7.058824	604.932	0.073318	0.5	505.6578	0.083666	2.935782	0.5	406.01	0.071942
17	0.5	1.64872	843.74	0.035325	0.5	1050.813	0.241702	1.016232	0.5	7.058824	1257.116	0.035377	0.5	1050.813	0.0918	2.67565	0.5	843.74	0.036238
18	0.5	1.64872	78.15	0.366215	0.5	90.34393	0.381727	0.643459	0.5	7.058824	99.85724	0.299384	0.5	90.34393	0.36081	0.680761	0.5	78.15	0.364727
19	0.5	1.64872	232.02	0.123303	0.5	268.2354	0.248384	0.988895	0.5	7.058824	296.4808	0.126754	0.5	268.2354	0.235311	1.043834	0.5	232.02	0.121203
20	0.5	1.64872	438.52	0.068892	0.5	506.9666	0.209165	1.174313	0.5	7.058824	560.3507	0.074221	0.5	506.9666	0.140606	1.746912	0.5	438.52	0.063832
21	1	2.71828	20173.30	0.010435	0.5	34666.62	0.198523	1.250228	0.5	3.238095	32818.29	0.01729	0.5	34666.62	0.132924	1.867224	0.5	35765.17	0.010285
22	1	2.71828	40346.60	0.008763	0.5	68333.25	0.199817	1.242127	0.5	3.238095	65636.58	0.013107	0.5	68333.25	0.129687	1.913027	0.5	71530.33	0.008902
23	1	2.71828	60519.90	0.008034	0.5	103999.9	0.198523	1.250228	0.5	3.238095	98454.87	0.013631	0.5	103999.9	0.134266	1.849551	0.5	107295.5	0.000253
24	1	2.71828	116.27	0.211918	0.5	108.5107	0.202473	1.225834	0.5	3.238095	122.1669	0.262168	0.5	108.5107	0.112006	2.215931	0.5	94.7889	0.291389
25	1	2.71828	406.01	0.060867	0.5	378.9054	0.122776	2.021551	0.5	3.238095	426.591	0.098375	0.5	378.9054	0.064619	3.840946	0.5	330.9906	0.087546
26	1	2.71828	843.74	0.029319	0.5	787.4072	0.142641	1.740026	0.5	3.238095	886.5031	0.066006	0.5	787.4072	0.088073	2.818086	0.5	687.8349	0.047731
27	1	2.71828	78.15	0.290605	0.5	87.08032	0.241245	1.028825	0.5	3.238095	93.18913	0.321723	0.5	87.08032	0.137864	1.800444	0.5	79.86135	0.340922
28	1	2.71828	232.02	0.09787	0.5	258.5456	0.144316	1.719827	0.5	3.238095	276.6829	0.136533	0.5	258.5456	0.086159	2.88071	0.5	237.1121	0.116034
29	1	2.71828	438.52	0.051808	0.5	488.6528	0.122537	2.025499	0.5	3.238095	522.9325	0.084494	0.5	488.6528	0.083287	2.960045	0.5	448.1434	0.064059
30	0	1	20173.30	0.0158	1	24359.14	0.612912	0.387997	1	7.555556	21355.63	0.012112	1	24359.14	0.341816	0.695718	1	24329.89	0.014913
31	0	1	40346.60	0.010276	1	48718.27	0.624699	0.380676	1	7.555556	42711.26	0.009837	1	48718.27	0.346531	0.686253	1	48659.78	0.009981
32	0	1	60519.90	0.009337	1	73077.41	0.624437	0.380836	1	7.555556	64066.89	0.008763	1	73077.41	0.343126	0.693063	1	72989.67	0.00909
33	0	1	116.27	0.27549	1	164.3275	0.668283	0.356849	1	7.555556	220.2617	0.144847	1	164.3275	0.400029	0.594477	1	110.12	0.290217
34	0	1	406.01	0.078861	1	573.8104	0.627104	0.379216	1	7.555556	769.0905	0.04153	1	573.8104	0.418854	0.567759	1	384.5247	0.084927
35	0	1	843.74	0.038144	1	1192.441	0.631679	0.376469	1	7.555556	1598.255	0.019978	1	1192.441	0.407873	0.563045	1	799.0849	0.042269
36	0	1	78.15	0.409183	1	105.4317	0.729464	0.326003	1	7.555556	124.86	0.258607	1	105.4317	0.42356	0.56145	1	79.36513	0.402884
37	0	1	232.02	0.137813	1	313.0318	0.688265	0.345508	1	7.555556	370.7154	0.08906	1	313.0318	0.470622	0.505305	1	235.6388	0.136795
38	0	1	438.52	0.072946	1	591.632	0.651027	0.365281	1	7.555556	700.6544	0.050095	1	591.632	0.491539	0.483803	1	445.3589	0.073254
39	0.5	1.64872	20173.30	0.011978					0	7.058824	17777.66	0.015028					0	20173.3	0.012669
40	0.5	1.64872	40346.60	0.010148	Contraction Taper Shoulder				0	7.058824	35555.33	0.011364	Expansion Taper Shoulder				0	40346.6	0.010186
41	0.5	1.64872	60519.90	0.009315					0	7.058824	53332.99	0.010504					0	60519.9	0.009316
42	0.5	1.64872	116.27	0.257139					0	7.058824	173.2401	0.185713					0	116.2732	0.275104
43	0.5	1.64872	406.01	0.081522	0	19474.69	0.48417	2.122042	0	7.058824	604.932	0.056011	0	19474.69	0.916622	1.236991	0	406.0108	0.078963
44	0.5	1.64872	843.74	0.040781	0	38949.38	0.484616	1.060044					0	38949.38	0.894913	0.6335			
45	0.5	1.64872	78.15	0.366458	0	58424.07	0.476428	0.718843					0	58424.07	0.906973	0.416717			
46	0.5	1.64872	232.02	0.128739	0	144.81	0.820358	1.252415					0	144.81	0.712715	1.590892			
47	0.5	1.64872	438.52	0.072447	0	505.6578	0.595206	0.863088					0	505.6578	0.866816	0.654034			
48	0	1	35765.17	0.011376															
49	0	1	71530.33	0.008992															
50	0	1	107295.5	0.008475															
51	0	1	94.7889	0.333938															
52	0	1	330.9906	0.096721															
53	0	1	687.8349	0.046461															
54	0	1	79.86135	0.398829															
55	0	1	237.1121	0.134736															

Figure 4: Correlation Area

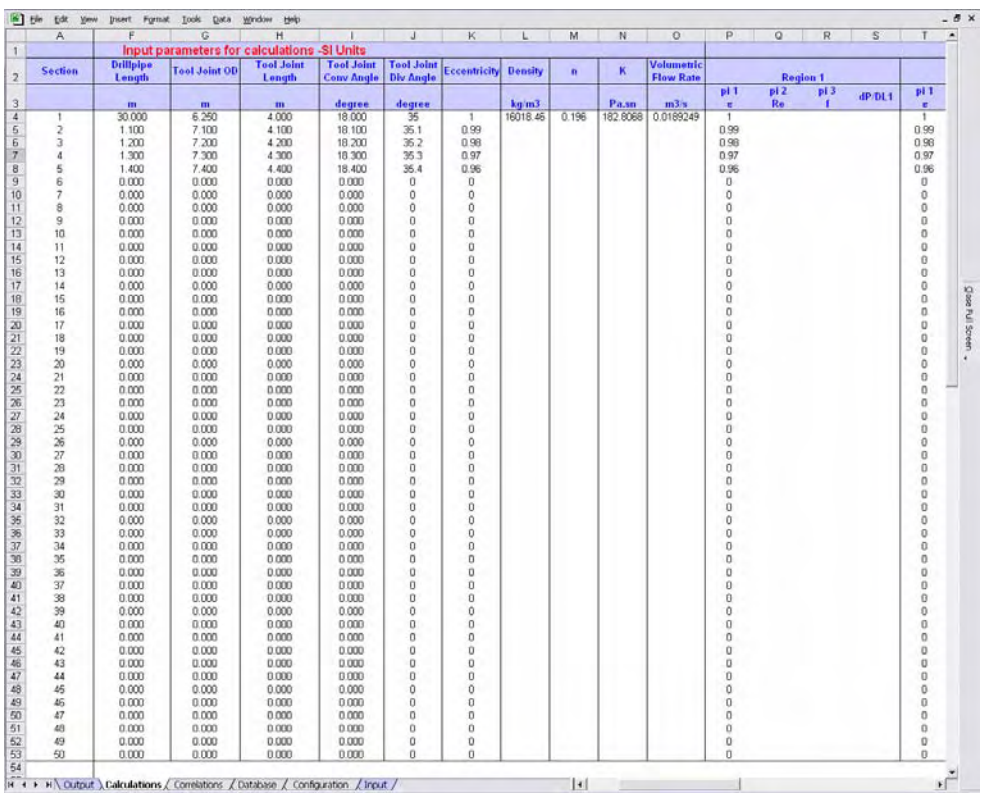

	A	F	G	H	I	J	K	L	M	N	O	P	Q	R	S	T
1		Input parameters for calculations -SI Units														
2	Section	Drillpipe Length	Tool Joint OD	Tool Joint Length	Tool Joint Conv Angle	Tool Joint Div Angle	Eccentricity	Density	n	K	Volumetric Flow Rate	Region 1				
3		m	m	m	degree	degree		kg/m3		Pa.sn	m3/s	pi 1 e	pi 2 Re	pi 3 f	dP/DL1	pi 1 e
4	1	30.000	6.250	4.000	18.000	35	1	16018.46	0.196	182.8068	0.0189249	1				1
5	2	1.100	7.100	4.100	18.100	35.1	0.99					0.99				0.99
6	3	1.200	7.200	4.200	18.200	35.2	0.98					0.98				0.98
7	4	1.300	7.300	4.300	18.300	35.3	0.97					0.97				0.97
8	5	1.400	7.400	4.400	18.400	35.4	0.96					0.96				0.96
9	6	0.000	0.000	0.000	0.000	0	0					0				0
10	7	0.000	0.000	0.000	0.000	0	0					0				0
11	8	0.000	0.000	0.000	0.000	0	0					0				0
12	9	0.000	0.000	0.000	0.000	0	0					0				0
13	10	0.000	0.000	0.000	0.000	0	0					0				0
14	11	0.000	0.000	0.000	0.000	0	0					0				0
15	12	0.000	0.000	0.000	0.000	0	0					0				0
16	13	0.000	0.000	0.000	0.000	0	0					0				0
17	14	0.000	0.000	0.000	0.000	0	0					0				0
18	15	0.000	0.000	0.000	0.000	0	0					0				0
19	16	0.000	0.000	0.000	0.000	0	0					0				0
20	17	0.000	0.000	0.000	0.000	0	0					0				0
21	18	0.000	0.000	0.000	0.000	0	0					0				0
22	19	0.000	0.000	0.000	0.000	0	0					0				0
23	20	0.000	0.000	0.000	0.000	0	0					0				0
24	21	0.000	0.000	0.000	0.000	0	0					0				0
25	22	0.000	0.000	0.000	0.000	0	0					0				0
26	23	0.000	0.000	0.000	0.000	0	0					0				0
27	24	0.000	0.000	0.000	0.000	0	0					0				0
28	25	0.000	0.000	0.000	0.000	0	0					0				0
29	26	0.000	0.000	0.000	0.000	0	0					0				0
30	27	0.000	0.000	0.000	0.000	0	0					0				0
31	28	0.000	0.000	0.000	0.000	0	0					0				0
32	29	0.000	0.000	0.000	0.000	0	0					0				0
33	30	0.000	0.000	0.000	0.000	0	0					0				0
34	31	0.000	0.000	0.000	0.000	0	0					0				0
35	32	0.000	0.000	0.000	0.000	0	0					0				0
36	33	0.000	0.000	0.000	0.000	0	0					0				0
37	34	0.000	0.000	0.000	0.000	0	0					0				0
38	35	0.000	0.000	0.000	0.000	0	0					0				0
39	36	0.000	0.000	0.000	0.000	0	0					0				0
40	37	0.000	0.000	0.000	0.000	0	0					0				0
41	38	0.000	0.000	0.000	0.000	0	0					0				0
42	39	0.000	0.000	0.000	0.000	0	0					0				0
43	40	0.000	0.000	0.000	0.000	0	0					0				0
44	41	0.000	0.000	0.000	0.000	0	0					0				0
45	42	0.000	0.000	0.000	0.000	0	0					0				0
46	43	0.000	0.000	0.000	0.000	0	0					0				0
47	44	0.000	0.000	0.000	0.000	0	0					0				0
48	45	0.000	0.000	0.000	0.000	0	0					0				0
49	46	0.000	0.000	0.000	0.000	0	0					0				0
50	47	0.000	0.000	0.000	0.000	0	0					0				0
51	48	0.000	0.000	0.000	0.000	0	0					0				0
52	49	0.000	0.000	0.000	0.000	0	0					0				0
53	50	0.000	0.000	0.000	0.000	0	0					0				0

Figure 5: Calculation Area

- **Output Area (Front End)**

In this area the obtained data from the calculations is displayed to the user. The user will be able to see plots of pressure along the wellbore and also detailed information about friction pressure drop, hydrostatic pressure, total pressure and ECD for every section of the wellbore. Graphs with the output data are presented in order to better illustrate the results obtained.

Figure 6 shows the interface for the output area.

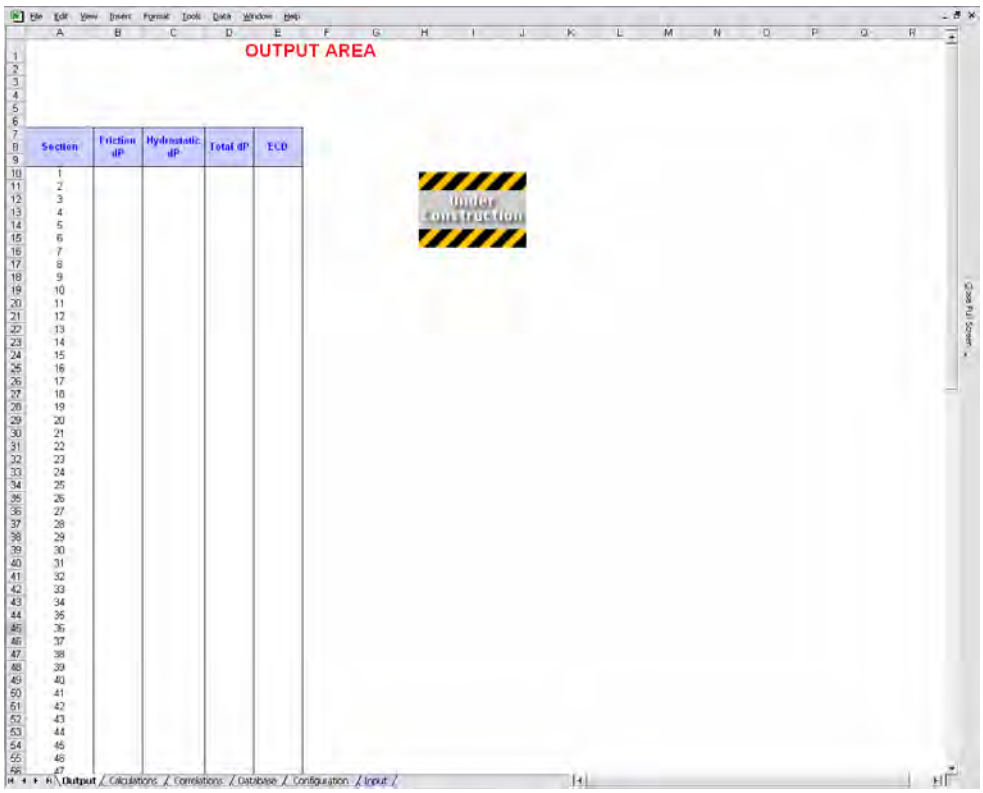

Figure 6: Output Area

With this simulator it will be possible to obtain values of ECD when using different fluids, different flow rates and different geometries of tool joints in a real wellbore, which will aid in the design of the well.

Dimensional Analysis

In order to conduct a dimensional analysis for the system, it was divided in five regions. The reason for adopting this procedure was that a dimensional analysis for the entire system would not reduce the

number of variables significantly. The five regions are presented in Figure 7. Table 5 presents all the relevant variables of the system.

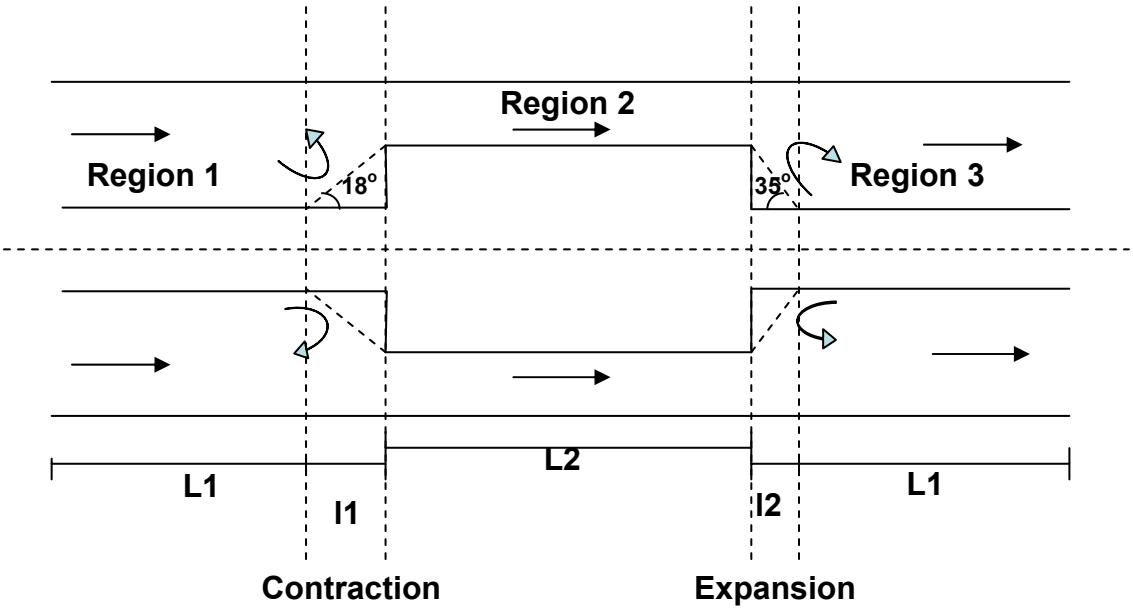

Figure 7: Regions Used in the Dimensional Analysis

Region 1

Region 1 consists of the annulus between the casing and the drillpipe at the entrance region of the system. The relevant variables to model this section are: effective diameter (D_{eff1}), eccentricity (ε), density of the fluid (ρ), flow behavior index (n), consistency index (K), velocity (v_1) and friction pressure gradient $\left(\Delta P / \Delta L\big|_1\right)$. After the dimensional analysis the following dimensionless groups were obtained.

$$group1 = \varepsilon \tag{7}$$

$$group2 = \mathrm{Re} = \frac{D_{eff1}^{n} v_1^{2-n} \rho}{K 8^{n-1}} \tag{8}$$

$$group3 = f_1 = \frac{D_{H1} \Delta P / \Delta L\big|_1}{\rho v_1^2} \tag{9}$$

D_{H1} is defined as:

$$D_{H1} = ID_{cas} - OD_{pipe} \tag{10}$$

D_{eff1} and v_1 are defined in the analysis of the contraction region for tool joints with squared shoulders.

The groups obtained for this section are correlated in a way that the friction factor obtained, f, is a function of the Reynolds number and eccentricity.

At this point the data available from the simulations for this section was enough to try to obtain correlations. First the data was divided into laminar and turbulent case and then the correlations were obtained using STATISTICA.

For laminar case the groups are correlated by,

$$f = 28.85547 e^{-0.306533\varepsilon} \mathrm{Re}^{-0.974629} \tag{11}$$

with R=0.997.

For turbulent case the groups are correlated by,

$$f = 0.153594 e^{-0.219428\varepsilon} \mathrm{Re}^{-0.246635} \tag{12}$$

with R=0.87.

For the other regions the correlations were not obtained since at this point the available data from the simulations is not enough to find reasonable results.

Contraction

The contraction region was modeled separately for the two different types of tool joints.

- **Tool Joints with Squared Shoulder**

This region consists of an annulus section with the presence of a sudden contraction. The relevant variables to model this section are: casing internal diameter (ID_{cas}), drillpipe outer diameter (OD_{pipe}), tool joint outer diameter (OD_{tj}), effective diameters (D_{eff1}, D_{eff2}, D_{eff}), hydraulic diameters (D_{H1}, D_{H2}, D_H), tool joint convergence angle (β), eccentricity (ε), density (ρ), flow behavior index (n), consistency index (K),

velocities (v_1, v_2, v), contraction friction pressure loss (ΔP_{cont}). After the dimensional analysis the following dimensionless groups were obtained.

$$group1 = \varepsilon \tag{13}$$

$$group2 = \mathrm{Re} = \frac{D_{eff}^{n} v^{2-n} \rho}{K 8^{n-1}} \tag{14}$$

$$group3 = f_c = \frac{\Delta P_{cont}}{\rho v^2} \tag{15}$$

$$group4 = N = \frac{\rho Q (v_2 - v_1)}{K \left(\frac{3n+1}{4n}\right)^n \left(\frac{8v}{D_{eff}}\right)^n A_c} \tag{16}$$

Where D_{eff}, v and A_c are defined as:

$$D_{eff} = \frac{D_{eff1} + D_{eff2}}{2} \tag{17}$$

$$v = \frac{v_1 + v_2}{2} \tag{18}$$

$$A_c = \frac{\pi}{4}\left(OD_{tj}^2 - OD_{pipe}^2\right) \tag{19}$$

D_{eff1} and D_{eff2} are calculated by the following procedure:

$$Y = 0.37 n^{-0.14} \tag{20}$$

$$Z = 1 - \left[1 - \left(\frac{D_i}{D_o}\right)^Y\right]^{1/Y} \tag{21}$$

D_i is the ODpipe and D_o the ID_{cas} when calculating $D_{eff1;}$ and D_i is the OD_{tj} and D_o the ID_{cas} when calculating D_{eff2}.

$$G = \frac{\left(1 + \frac{Z}{2}\right)\left[(3 - Z)n + 1\right]}{n(4 - Z)} \tag{22}$$

$$D_{eff} = \frac{D_H}{G} \tag{23}$$

where D_{H1} is defined as in equation (10) and D_{H2} is defined similarly as:

$$D_{H2} = ID_{cas} - OD_{tj} \tag{24}$$

and v_1 and v_2 are calculated by:

$$v_1 = \frac{4Q}{\pi\left(ID_{cas}^2 - OD_{pipe}^2\right)} \tag{25}$$

$$v_2 = \frac{4Q}{\pi\left(ID_{cas}^2 - OD_{tj}^2\right)} \tag{26}$$

The groups obtained for this section are correlated in a way that the friction factor obtained, f, is a function of the Reynolds number, eccentricity, and a third group that accounts for the acceleration happening in this region.

- **Tool Joints with Taper Shoulder**

This region consists of an annulus section with the presence of a gradual contraction. The relevant variables to model this section are: casing internal diameter (ID_{cas}), drillpipe outer diameter (OD_{pipe}), tool joint outer diameter (OD_{tj}), effective diameters (D_{eff1}, D_{eff2}, D_{eff}), hydraulic diameters (D_{H1}, D_{H2}, D_H), tool joint convergence angle (β), contraction region length (l_1), eccentricity (ε), density (ρ), flow behavior index (n), consistency index (K), velocities (v_1, v_2, v), contraction friction pressure gradient ($\Delta P/\Delta L_{cont}$). After the dimensional analysis the following dimensionless groups were obtained.

$$group1 = \varepsilon \tag{27}$$

$$group2 = \mathrm{Re} = \frac{D_{eff}^n v^{2-n} \rho}{K 8^{n-1}} \tag{28}$$

$$group3 = f_c = \frac{D_H \left.\frac{\Delta P}{\Delta L}\right|_{cont}}{\rho v^2} \tag{29}$$

$$group4 = N = \frac{\rho l_1}{K\left(\frac{3n+1}{4n}\right)^n \left(\frac{8v}{D_{eff}}\right)^n} \left[\frac{Q\left(2D_{H1}\tan\beta - l_1 \tan^2\beta\right)}{\pi\left(D_{H1}^2 - D_{H1} l_1 \tan\beta + \frac{l_1^2}{4}\tan^2\beta\right)^2} \right] \tag{30}$$

D_{eff}, v and D_{H1} are calculated as defined before and D_H is defined by:

$$D_H = \frac{D_{H1} + D_{H2}}{2} \tag{31}$$

The groups obtained for this section are correlated in a way that the friction factor obtained, f, is a function of the Reynolds number, eccentricity, and a third group that accounts for the acceleration happening in this region.

Region 2

Region 2 consists of the annulus between the casing and the tool joint. The relevant variables to model this section are: effective diameter (D_{eff2}), tool joint length (L_{tj}), eccentricity (ε), density of the fluid (ρ), flow behavior index (n), consistency index (K), velocity (v_2) and friction pressure gradient $\left(\Delta P / \left.\Delta L\right|_2\right)$. After the dimensional analysis the following dimensionless groups were obtained.

$$group1 = \varepsilon \tag{32}$$

$$group2 = \frac{L_{tj}}{D_{H2}} \tag{33}$$

$$group3 = \mathrm{Re} = \frac{D_{eff2}^n v_2^{2-n} \rho}{K 8^{n-1}} \tag{34}$$

$$group4 = f_1 = \frac{D_{H2} \left.\Delta P / \Delta L\right|_2}{\rho v_2^2} \tag{35}$$

D_{H1}, D_{eff2} and v_2 are calculated as defined in equations (10), (23) and (26).

The groups obtained for this section are correlated in a way that the friction factor obtained, f, is a function of the Reynolds number, eccentricity, and a third group that includes the tool joint length.

Expansion

The expansion region was modeled separately for the two different types of tool joints.

- **Tool Joints with Squared Shoulder**

This region consists of an annulus section with the presence of a sudden expansion. The relevant variables to model this section are: casing internal diameter (ID_{cas}), drillpipe outer diameter (OD_{pipe}), tool joint outer diameter (OD_{tj}), effective diameters (D_{eff2}, D_{eff3}, D_{eff}), hydraulic diameters (D_{H2}, D_{H3}, D_H), tool joint divergence angle (θ), eccentricity (ε), density (ρ), flow behavior index (n), consistency index (K), velocities (v_2, v_3, v), contraction friction pressure loss (ΔP_{exp}). After the dimensional analysis the following dimensionless groups were obtained.

$$group1 = \varepsilon \tag{36}$$

$$group2 = \mathrm{Re} = \frac{D_{eff}^{n} v^{2-n} \rho}{K 8^{n-1}} \tag{37}$$

$$group3 = f_c = \frac{\Delta P_{\exp}}{\rho v^2} \tag{38}$$

$$group4 = \frac{\rho Q (v_3 - v_2)}{K \left(\frac{3n+1}{4n} \right)^n \left(\frac{8v}{D_{eff}} \right)^n A_e} \tag{39}$$

Where D_{eff}, v and A_c are defined as:

$$D_{eff} = \frac{D_{eff\,2} + D_{eff\,3}}{2} \tag{40}$$

$$v = \frac{v_2 + v_3}{2} \tag{41}$$

$$A_e = \frac{\pi}{4}\left(OD_{tj}^2 - OD_{pipe}^2\right) \tag{42}$$

The effective diameters and velocities are calculated in a similar manner as done it was before for D_{eff1}, D_{eff2}, v_1 and v_2.

The groups obtained for this section are correlated in a way that the friction factor obtained, f, is a function of the Reynolds number, eccentricity, and a third group that accounts for the deceleration happening in this region.

- **Tool Joints with Taper Shoulder**

This region consists of an annulus section with the presence of a gradual expansion. The relevant variables to model this section are: casing internal diameter (ID_{cas}), drillpipe outer diameter (OD_{pipe}), tool joint outer diameter (OD_{tj}), effective diameters (D_{eff2}, D_{eff3}, D_{eff}), hydraulic diameters (D_{H2}, D_{H3}, D_H), tool joint divergence angle (θ), expansion region length (l_2), eccentricity (ε), density (ρ), flow behavior index (n), consistency index (K), velocities (v_2, v_3, v), contraction friction pressure gradient ($\Delta P/\Delta L_{exp}$). After the dimensional analysis the following dimensionless groups were obtained.

$$group1 = \varepsilon \tag{43}$$

$$group2 = \mathrm{Re} = \frac{D_{eff}^n v^{2-n} \rho}{K 8^{n-1}} \tag{44}$$

$$group3 = f_c = \frac{D_H \left.\frac{\Delta P}{\Delta L}\right|_{\exp}}{\rho v^2} \tag{45}$$

$$group4 = N = \frac{\rho l_2}{K\left(\frac{3n+1}{4n}\right)^n \left(\frac{8v}{D_{eff}}\right)^n} \left[\frac{Q\left(2D_{H3}\tan\theta - l_2 \tan^2\theta\right)}{\pi\left(D_{H3}^2 - D_{H3} l_2 \tan\theta + \frac{l_2^2}{4}\tan^2\theta\right)^2} \right] \tag{46}$$

D_{eff}, v and D_{H3} are calculated as defined before and D_H is defined by:

$$D_H = \frac{D_{H2} + D_{H3}}{2} \tag{47}$$

The groups obtained for this section are correlated in a way that the friction factor obtained, f, is a function of the Reynolds number, eccentricity, and a third group that accounts for the deceleration happening in this region.

Region 3

Region 3 consists of the annulus between the casing and the drillpipe at the exit of the system. The relevant variables to model this section are: effective diameter (D_{eff3}), eccentricity (ε), density of the fluid (ρ), flow behavior index (n), consistency index (K), velocity (v_3) and friction pressure gradient $\left(\Delta P / \Delta L\big|_3\right)$. After the dimensional analysis the following dimensionless groups were obtained.

$$group1 = \varepsilon \tag{48}$$

$$group2 = \mathrm{Re} = \frac{D_{eff3}^{n} v_3^{2-n} \rho}{K 8^{n-1}} \tag{49}$$

$$group3 = f_1 = \frac{D_{H3} \Delta P / \Delta L\big|_3}{\rho v_3^2} \tag{50}$$

D_{H3} is defined as:

$$D_{H3} = ID_{cas} - OD_{pipe} \tag{51}$$

The correlations for the contraction region, region 2, expansion region and region 3 are going to be obtained when all the simulations are complete.

The groups obtained for this section are correlated in a way that the friction factor obtained, f, is a function of the Reynolds number and eccentricity.

Table 5: Variables

Quantity	Symbol	Dimensions
asing ID	ID_{cas}	L
Drillpipe OD	OD_D	L
Tool Joint OD	OD_{TJ}	L
Hydraulic Diameter	D_{H1}, D_{H2}, D_{H3}, D_H	L
Effective Diameter	D_{eff1}, D_{eff2}, D_{eff3}, D_{eff}	L
Tool Joint Convergence Angle	β	None
Tool Joint Divergence Angle	θ	None
Contraction Region Length	l_1	L
Expansion Region Length	l_2	L
Eccentricity	ε	None
Density	ρ	ML^{-3}
Flow Behavior Index	n	None
Consistency Index	K	$ML^{-1}T^{n-2}$
Velocity	v_1,v_2, v_3, v	LT^{-1}
Friction Pressure Gradient/Region1	$\Delta P/\Delta L_1$	$ML^{-2}T^{-2}$
Contraction Friction Pressure Gradient	$\Delta P/\Delta L_{cont}$	$ML^{-2}T^{-2}$
Contraction Friction Pressure Loss	ΔP_{cont}	$ML^{-1}T^{-2}$
Friction Pressure Gradient/Region2	$\Delta P/\Delta L_2$	$ML^{-2}T^{-2}$
Expansion Friction Pressure Gradient	$\Delta P/\Delta L_{exp}$	$ML^{-2}T^{-2}$
Expansion Friction Pressure Loss	ΔP_{exp}	$ML^{-1}T^{-2}$
Friction Pressure Gradient/Region3	$\Delta P/\Delta L_3$	$ML^{-2}T^{-2}$

Results and Conclusions

At this moment any final conclusion can be made since there is approximately 30% of the total number of simulations to be run.

Some results and concluding remarks are presented here for the simulations completed up to now.

Figure 8 shows that, for water (turbulent flow) in the geometry with a 2 3/8 drillpipe and 5 1/2 wellbore without tool joints, the pressure gradient decreases with increase in eccentricity.

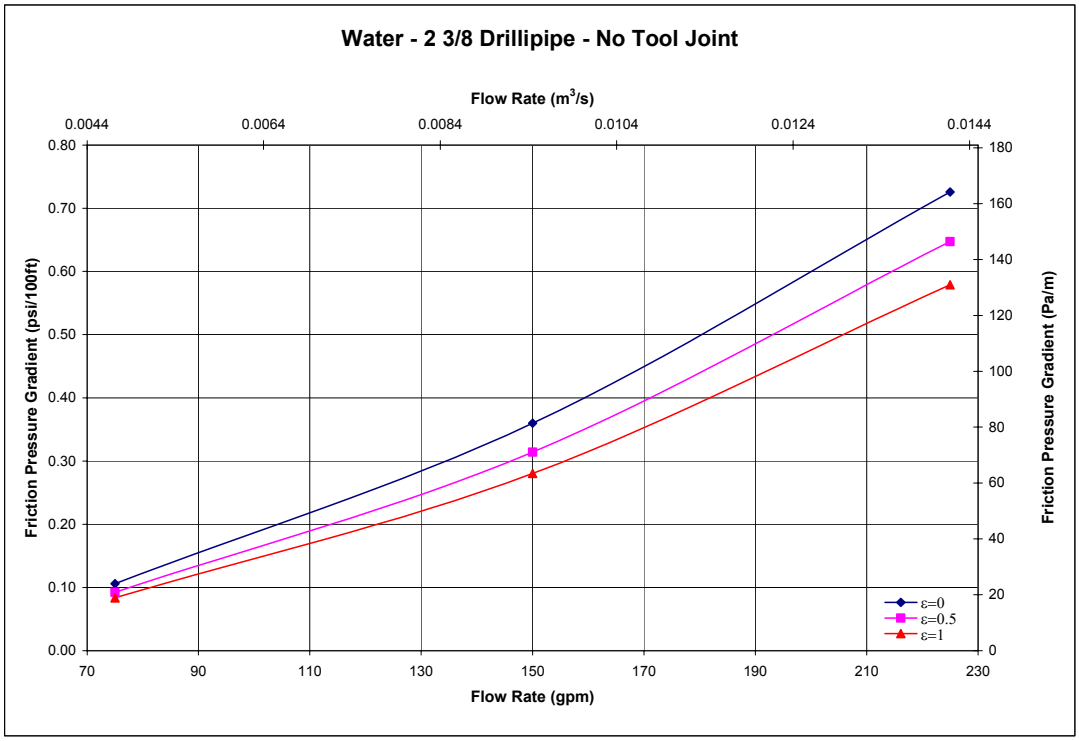

Figure 8: 2 3/8 Drillpipe - Water - Effect of eccentricity. No Tool Joints

The same behavior was observed for the simulations run for non Newtonian fluids. Figure 9 illustrates the effect of eccentricity in the same geometry as presented in Figure 8 except for one of the polymeric fluids (XC) in laminar flow.

Observing Figure 8 and 9 it can be seen that the effect of eccentricity is more pronounced for the non-Newtonian fluid.

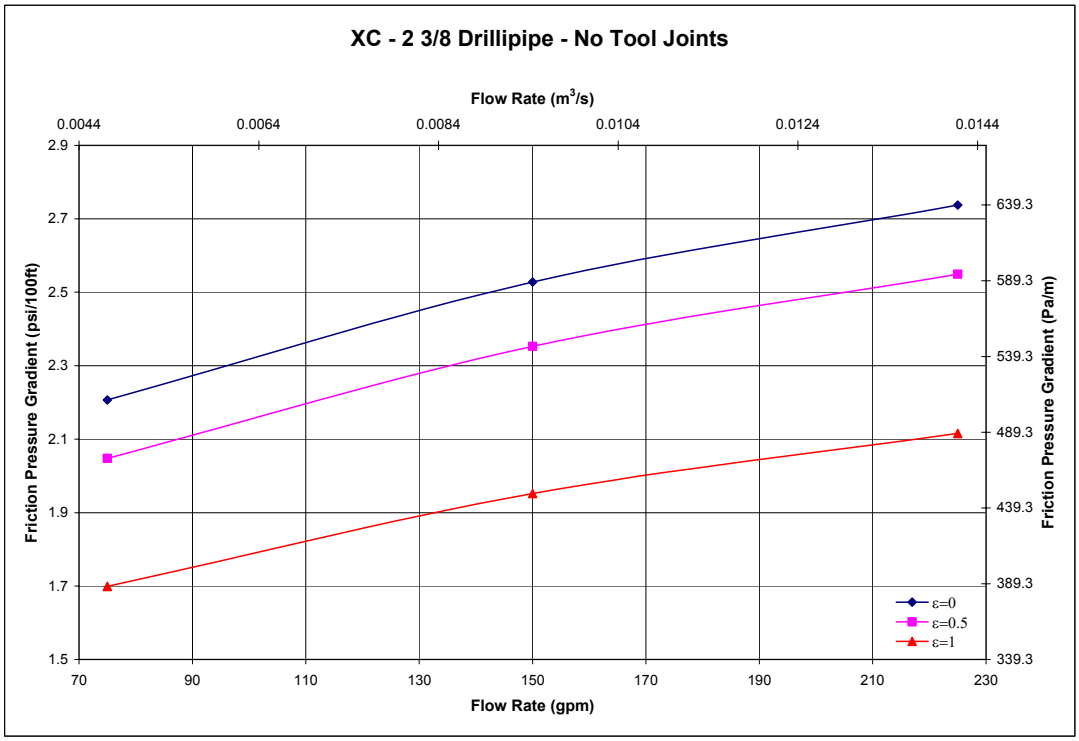

Figure 9: 2 3/8 Drillpipe - XC - Effect of eccentricity. No Tool Joints

The decrease in pressure gradient with increase in eccentricity was also observed for the geometries with the squared shoulder tool joints. Figures 10 and 11 illustrate this.

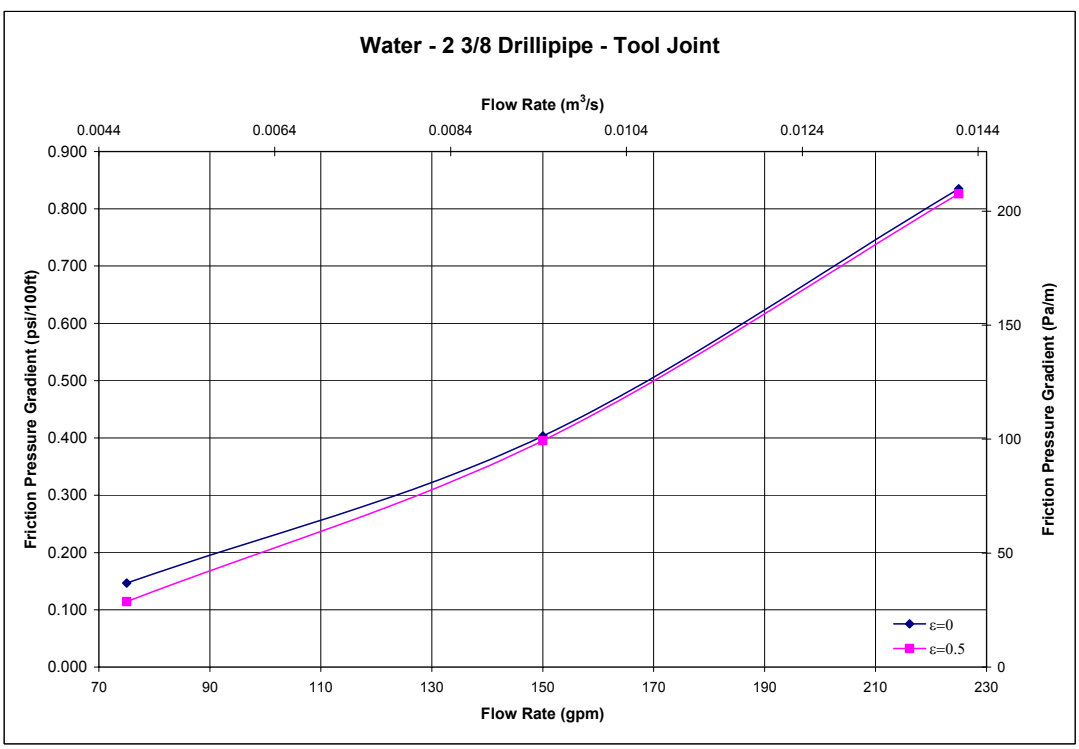

Figure 10: 2 3/8 Drillpipe - Water - Effect of eccentricity. Tool Joints

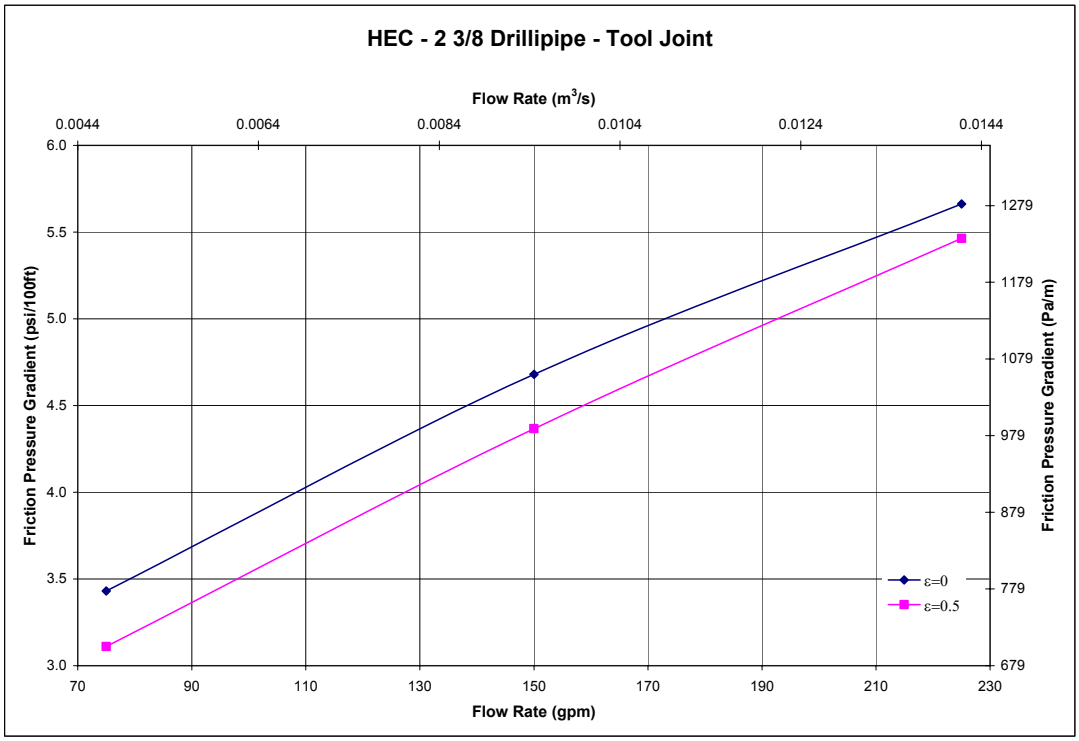

Figure 11: 2 3/8 Drillpipe - HEC - Effect of eccentricity. Tool Joints

The same type of behavior was observed for the two other annular configurations.

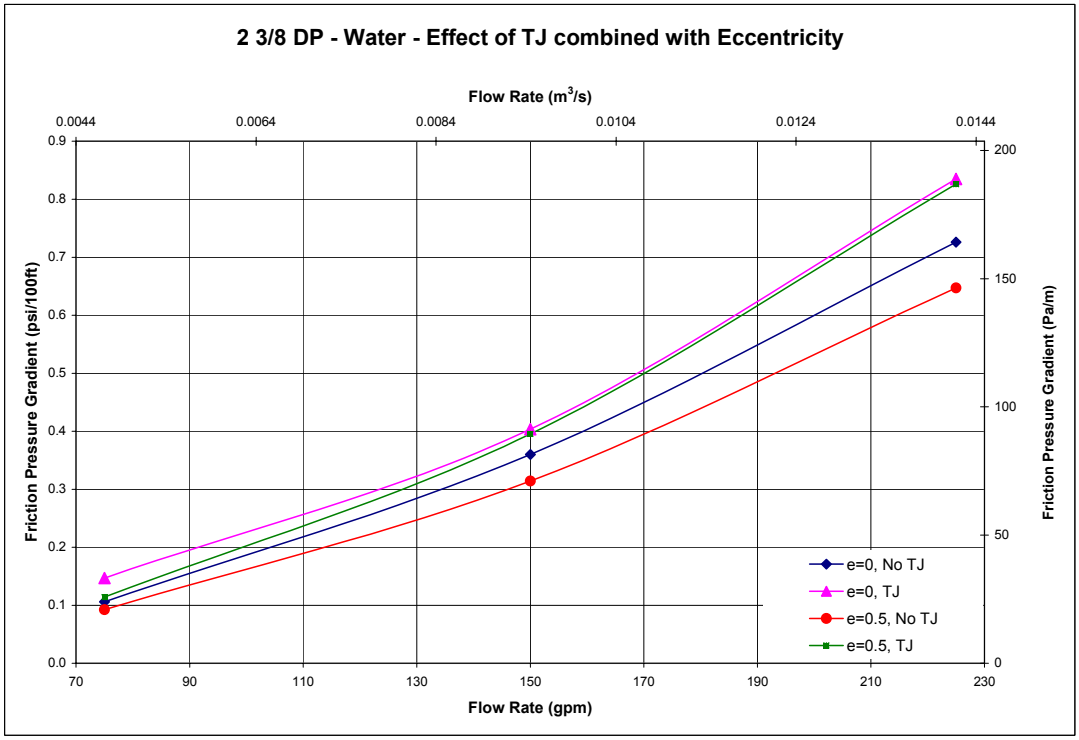

Figure 12: 2 3/8 Drillpipe – Water- Effect of Squared Tool Joint combined with Tool Joint

Figure 12 compares, for the geometry with a 2 3/8 drillpipe in a 5 1/2 wellbore, the effect of tool joints combined with eccentricity. The graph shows that for water in the presence of tool joints the effect of eccentricity is smaller compared to the geometry without tool joints. The graph also shows that for zero eccentricity the effect of the tool joints (approximated 12%) is smaller when compared with the 0.5 eccentricity geometry (approximated 21%).

At this point any conclusions are made about the taper tool joints due to limited available data.

After all the simulations are complete final conclusions will be made regarding the effect of different fluids, different flow rates, different convergence and divergence tool joint angles for three wellbore configurations.

Proposed Time Line – Future Work

The proposed time line for completing this study is showed in Table 6.

Table 6: Proposed Time Line

	2003	2004			2005	
	Fall	Spring	Summer	Fall	Spring	Summer
Literature Review						**5%**
CFD Software training						**5%**
Simulations						**30%**
Modeling						**25%**
Analysis of the results of the simulations						**30%**
Final Report						**70%**

Deliverables

1. Theoretical results and analysis of the influence of the tool joints on ECD for a polymeric fluid flow in an annulus;
2. Development of a hydraulic model to predict the fluid pressure losses in the studied system;

3. Development of a simulator to calculate ECD for a wellbore;
4. Semi-annual Advisory Board Meetings Reports and a Final Report.

References

1. Bern, P. A., Hosie, D., Bansal, R. K., Stewrt, D., Lee, B., "A New Downhole Tool for ECD Reduction", Paper SPE 81642 presented at IADC/SPE Underbalanced Technology Conference an Exhibition held in Houston (25-26 March 2003).
2. Bern, P. A., Armagost, W. K., Bansal, R. K., "Managed Pressure Drilling with the ECD Reduction Tool", Paper SPE 89737 Annual Technical Conference and Exhibition, Houston, Texas, 26-29 September 2004.
3. Baranthol, C., Alfenore, J., Cotterill, M.D., Poux-Guillaume, G., "Determination of Hydrostatic Pressure an Dynamic ECD by Computer Models and Field Measurements on the Directional HPHT Well 22130C-13", Paper SPE 29430 presented at IADC/SPE Drilling Conference held in Amsterdam (28 february-2 March 1995).
4. Cartalos, U., Dupuis, D., "An Analysis Accounting for the Combined Effect of Drillstring Rotation and Eccentricity on pressure Losses in Slimhole Drilling", Paper SPE 25769 presented at IADC/SPE Drilling Conference held in Amsterdam 23-25 February 1993.
5. API Standard RP 7G.
6. Davison, J. M., Clary, S., Saasen, A., Allouche, M., Bodin, D. and Nguyen, V-A.: "Rheology of Various Drilling Fluid Systems Under Deepwater Drilling Conditions and the Importance of Accurate Predictions of Downhole Fluid Hydraulics", Paper SPE 56632, Annual Technical Conference and Exhibition, Houston, Texas, 3-6 October 1999.
7. Silva, M. A. and Shah, S. N.: "Friction Pressure Correlations of Newtonian and Non-Newtonian Fluids through Concentric and Eccentric Annuli", Paper SPE 60720, SPE/ICoTA Coiled Tubing Roundtable, Houston, Texas, 5-6 April 2000.
8. Hycalog, G. R. W., Barton, N. A. and Loughborough U., G. K. H.: "Usind New Computational Fluid Dynamics Techniques to Improve PDC Bit Performance", Paper SPE 37580, SPE/IADC Drilling Conference, Amsterdam, The Netherlands, 4-6 March 1997.
9. Jeong, Y., Shah, S., "Analysis of Tool Joint Effects for Accurate Friction Pressure Loss Calculations", Paper SPE 87182, IADC/SPE Drilling Conference, Dallas, Texas, 2-4 March 2004.

Mathematical Modeling of Transient Wellbore Trajectory for Complex BHA

Mohammad Oyarhossein

Mathematical Modeling of Transient Wellbore Trajectory for Complex BHA

INVESTIGATOR: Mohammad Oyarhossein

INTRODUCTION:
The concept of wellbore deviation is becoming a very important issue with the increase in application of directional drilling. In the 1950s, A. Lubinski and H. B. Woods (1953) proposed their pioneering theory in the area of deviation control. In their theory, they suggested that formation characterization should be taken into account as we deal with anisotropic formation. After that, S. Miska extended their work by suggesting the concept of Bit Anisotropic Index (BAI). It is believed that as we drill with anisotropic bits, the effects of bit anisotropy should be considered too. Our work will use the Transfer Matrix theory for the static condition calculation (complex BHA) and develop a mathematical model to predict the Transient Trajectory in anisotropic system.

In the first ABM report, the concept of Transfer Matrix was developed. Also, the mathematical model for the drill collars (field matrixes) was discussed. In the second ABM report, stabilizers were modeled and some of the results were covered. Also, the direction of the BHA as a result of the side force and weight on bit (WOB) was discussed. In this report, bent subs will be added to the system. In addition, we will discuss the Drilling Ahead model.

OBJECTIVES:
- Develop a method (based upon the concept of Transfer Matrix) to determine the static equilibrium configuration for complex BHA (multi-elements, stabilizers and bent subs) in a straight 2D wellbores
- Develop a mathematical model to predict the Transient Trajectory of a wellbore for an anisotropic drilling conditions

APPROACH:
As in the case of more complex BHA including stabilizers and bent subs, the Transfer Matrix approach is applied for this research. The concept of transfer matrix method is to dissect a complex BHA and to analyze the behavior of each component separately. For each component, analytical differential equation can be derived. From these equations, the stated variables of the component: displacement, deflection, moment and internal shear force of the component can be developed into a “Behavior” or “Transfer Matrix”.

.

DELIVERABLES:
- Develop a mathematical model that can be used for a static complex BHA configuration and the factors affecting the transient trajectory predictions
- Computer code to predict the transient trajectory for complex BHA
- Final Report

TUDRP

Mathematical Modeling of Transient Wellbore Trajectory for Complex BHA

Mohammad Oyarhossein, The University of Tulsa, Drilling Research Projects

This report is prepared for TUDRP Advisory Board Meeting, May 23 - 24, 2005, Tulsa-Oklahoma.

Abstract

The main goal of this research is to predict the length and the shape of a wellbore (rate of inclination change) between two subsequent equilibrium drilling conditions, which is called the "Transient Trajectory". This study will help us to have a better understanding of the factors affecting well trajectory, bit selection, BHA (Bottom Hole Assembly) design, and formation characterization for directional drilling purposes under isotropic and anisotropic drilling conditions.

The BHA mechanical equilibrium conditions and therefore, the resultant force and tilt angle at the bit, are based on the theory of elastic beams and the concept of Transfer Matrix. In this report, governing equations to calculate the side force and tilt angle (for complex BHA in 2D) are developed. Then, the effects on BHA parameters on the side force and final equilibrium angle will be discussed.

Project Status

Literature Review	95%
Mathematical Modeling of BHA	100%
Numerical Modeling	85%
Programming	65%
Thesis Writing	30%

Objectives

The objectives of this study are:

- Develop a method (based upon the concept of Transfer Matrix) to determine the static equilibrium configuration for complex BHA (multi-elements, stabilizers and bent subs) in a straight 2D wellbores;
- Develop a mathematical model to predict the Transient Trajectory of a wellbore for an anisotropic drilling conditions

Literature Review

With the increase in application of directional drilling, the concept of wellbore deviation is becoming increasingly important. In the 1950s, A. Lubinski and H. B. Woods (1953) proposed their pioneering theory in the area of deviation control. In their theory, they suggested that formation characterization should be taken into account as we drill with anisotropic formation. After that, Miska extended their work by suggesting the concept of Bit Anisotropic Index (BAI). It is believed that as we drill with anisotropic bits, the effects of bit anisotropy should be considered too. Our work will use the Transfer Matrix theory for the static condition calculation (complex BHA) and develop a mathematical model to predict the Transient Trajectory in anisotropic system.

Past Work

In the first ABM report, the concept of Transfer Matrix was developed. Also, the mathematical model for the drill collars (field matrixes) was discussed.

In the second ABM report, stabilizers were modeled and some of the results were covered. Also, the direction of the BHA as a result of the side force and weight on bit (WOB) was discussed. Here, in this report, bent subs will be included in the system. We will discuss the Drilling Ahead model, too.

Approach

Static Equilibrium Conditions:

Bent subs are commonly used to control the side force and the tilt. Bent subs can point upward to have a more building tendency or can point downward to increase the dropping tendency. If we have a bent sub in the system, multiplication of matrixes can be shown as explained in Appendix A. In a short notation, we can say:

$$\begin{pmatrix} c \\ 0 \\ 0 \\ h_l \\ 1 \end{pmatrix}_{x=LengthofTangency} = A \bullet \begin{pmatrix} 0 \\ y_0' \\ 0 \\ h_0 \\ 1 \end{pmatrix}_{x=0,atBit} + B \qquad \text{(Eq - 1)}$$

Where:

c : Dimensionless clearance at the length of tangency

A, B : $A = [a_{ij}]$ where $i, j = 1,2,...,5$ and $B = [b_{k1}]$ where $k = 1,2,3,..,5$

Having matrix A and matrix B, we are able to find a solution for the dimensionless side force at the bit (h_0) and other unknowns. The solution will be categorized as:

- There is NO contact point between the bit and the length of tangency:

$$h_0 = \frac{a_{25}a_{32} - a_{22}a_{35} + a_{32}b_{21} - a_{22}b_{31}}{\nabla} \qquad \text{(Eq - 2)}$$

$$y_0' = \frac{a_{24}a_{35} - a_{25}a_{34} + a_{24}b_{31} - a_{34}b_{21}}{\nabla} \qquad \text{(Eq - 3)}$$

Where:

$$\nabla = a_{22}a_{34} - a_{24}a_{32} \qquad \text{(Eq - 4)}$$

- There is a contact point between the bit and the length of tangency:

$$h_0 = \frac{a_{35}u_{12}^1 - a_{32}u_{15}^1 + u_{12}^1 b_{31} \pm a_{32}c_{st,1}}{\nabla} \qquad \text{(Eq - 5)}$$

$$y_0' = \frac{a_{34}u_{15}^1 - a_{35}u_{14}^1 - u_{14}^1 b_{31} \pm a_{34}c_{st,1}}{\nabla} \qquad \text{(Eq - 6)}$$

Where:

$$\nabla = a_{32}u_{14}^1 - a_{34}u_{12}^1 \qquad \text{(Eq - 7)}$$

u_{ij}^1 = The field matrix of the first element

Detailed derivation can be found in Appendix B. Also, some results can be found in Appendix C.

Direction Tendency under Isotropic Condition:

The direction tendency can be categorized in the four sub categories:

A) Isotropic condition:

If we have an isotropic system, the direction tendency can be simply expressed as:

$$\Phi = \alpha + ArcTan\left(\frac{H_o}{WOB}\right) \qquad \text{(Eq - 8)}$$

B) Isotropic Bit, Anisotropic Formation:

In an isotropic formation, the direction of the BHA can be calculated as:

$$\psi = \gamma - ArcTan[(1 - FAI) \bullet Tan(\gamma - \Phi)] \qquad \text{(Eq - 9)}$$

C) Isotropic Formation, Anisotropic Bit:

In the cases that we have just the anisotropic bit and formation is isotropic, one can calculate the direction tendency as:

$$\delta = \alpha + \beta - ArcTan[(1 - BAI) \bullet Tan[\alpha + \beta - \Phi]] \qquad \text{(Eq - 10)}$$

D) Anisotropic Formation, Anisotropic Bit:

If we have anisotropic bit and anisotropic formation (dual anisotropy), the following equations were suggested by Suchato[9] in 1985:

$$\alpha_N = ArcTan[\frac{ASin\psi + Sin\delta}{ACos\psi + Cos\delta}] \qquad \text{(Eq - 11)}$$

$$A = \frac{K_D}{B_B}\sqrt{\frac{1-(2-FAI)Sin^2(\gamma-\Phi)}{1-(1-BSI)^2 Sin^2(\alpha+\beta-\Phi)}} \qquad \text{(Eq - 12)}$$

In equation (12), the ratio $\frac{K_D}{B_B}$ is required to determine the direction of drilling in dual anisotropic cases. Since no correlation has been developed to calculate that ratio, an empirical experiment (case study) is needed.

In the above equations:

$\alpha =$ Inclination angle, deg

ψ = Direction of drilling anisotropic formation, deg.

δ = Direction of drilling anisotropic bit condition, deg.

γ = Formation dip angel, deg.

Φ = Drilling direction in isotropic condition, deg.

FAI = Formation Anisotropy Index

BAI = Bit Anisotropy Index

Drilling Ahead:

Recently, Henky Chan[2] found a new approach to predict transient trajectory. He calculated the static mechanical behavior of the BHA. To link the static state to the dynamic situation, he applied the Drill Ahead model (dynamic model) which is based on the rate of penetration (ROP) as a function of resultant force.

$$ROP = \frac{dF}{dt} = C.\text{Resultant Force}^{k} \qquad \text{(Eq - 13)}$$

As the BHA drills ahead, modification of the BHA's boundary conditions is required; however, the elastic bending equation of the drill string can be kept unchanged if the coordinate reference frame is also continuously changing according to the movement of the BHA as it is shown in Fig.1.

$$yposition_{end} = r_N + (l_N - \frac{F}{m_2}) \bullet Tan(\alpha_{N-1} - \alpha_N) \qquad \text{(Eq - 14)}$$

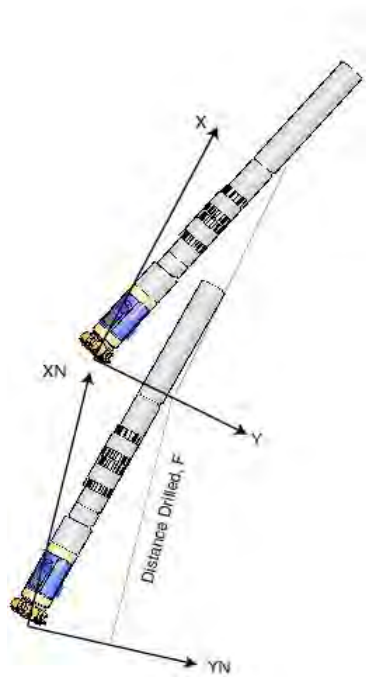

Fig. 1: Drill Ahead Model

Preliminary Results:

Some simulations were done using Drill Ahead model. The effects of WOB, inclination angle and drill collars OD on the side force and the final equilibrium angle were studied. The results can be found in Appendix D.

Increasing WOB will increase the distance when we reach to a point that the side force will be zero. In our cases, we stopped the simulations when we think the first stabilizer may not touch the wellbore. Also, increasing WOB will decrease the dropping tendency at the bit where the axial load increase. In addition, it is believed that increasing WOB will result in a greater final equilibrium angle in an isotropic system (Fig. D – 2 and Fig. D – 3).

It can be predicted that increasing the initial inclination angle will increase the dropping tendency as well as the distance (Fig. D – 4). However, it seems that it does not have a noticeable effect on the final equilibrium angle (Fig. D – 5)

In Fig. D – 6, the effect of drill collars size on the side force is shown. Increasing the OD size will increase the dropping tendency but does not have a great effect on the distance. In addition, as shown in Fig. D – 7, increasing the OD size will not affect the final equilibrium angle either.

In Fig. D – 1, the original case was simulated in order to predict the trajectory of a wellbore. As we drill ahead, the inclination angle decreases and will result in an increase of the side force. The effects of the first stabilizer and the inclination angle were studied in Fig. D – 8 and Fig. D – 9, too. For small inclination angle, there may be a chance for the stabilizers not touch the wellbore (the side force at the stabilizers decreasing as Fig. D – 9). Furthermore, for a constant inclination angle, the more distance from the bit, will result in a more dropping tendency. On the other hand, the first stabilizer's side force increase and the second stabilizer's side force remain almost constant.

Deliverables

- Develop a mathematical model that can be used for a static complex BHA configuration and the factors affecting the transient trajectory predictions;
- Computer code to predict the transient trajectory for complex BHA;
- Final Report

Nomenclature

h_0 = The dimensionless side force at the bit
y'_0 = The dimensionless slope at the bit
$yposition_{end}$ = Deflection at the length of tangency
l = Tangency length
r = Dimensionless radial clearance at the length of tangency
m_1, m_2, m_3 = Dimensionless factors
FAI = Formation Anisotropy Index
BAI = Bit Anisotropy Index
U = The Transfer Matrix for each element
P = The Point Transfer Matrix for each stabilizer

Greek Letters

α = Inclination angle, deg
ψ = Direction of drilling anisotropic formation, deg.
δ = Direction of drilling anisotropic bit condition, deg.
γ = Formation dip angel, deg.
Φ = Drilling direction in isotropic condition, deg.
∇ = Constant
$\beta_i^2 = \frac{w_i}{e_i}$

Subscripts

i = Indicator

References

1. Callas, N. P., "Predicting borehole Trajectories", Oil & Gas Journal, Aug. 24, 1981.
2. Chan, Henky: "Mathematical Modeling of Transient Well Bore Trajectory for Simple BHA" Master's Thesis, University of Tulsa, 2001..
3. Ho, H. S., "Prediction of Drilling Trajectory in Directional Wells Via a New Rock Bit Interaction Model", SPE 16658.
4. Larson, P.A. and J. J. Azar: "Three-Dimensional, Quasi-Static, Drill Ahead BHA Model for Well Bore Trajectory Prediction and Control" SPE 23530, 1991.
5. Lubinski, A.: "Developments in Petroleum Engineering", 1987, Vol. 1
6. Murpey C. E and Cheatham, J. B.: "Hole Deviation and Drill String Behavior" SPE 1259
7. Neubert, M. and Heising, G., "Advanced Trajectory Simulation of Directional Wellbores".
8. Pikey, Walyer D. and Pilkey, Orrin H., "Mechanics of Solid", ROBERT E. KRIEGER PUBLISHING COMPANY, 1986
9. Suchato, P., "Description of the Initial Part of Transient Borehole Trajectory Behavior in Two-Dimensions", Master's thesis, University of New Mexico, 1985.

Appendix A – Modeling Approach, Matrix Formulation

As mentioned, the "Transfer Matrix" Method links the initial condition to the boundary condition. Since we are modeling a complex BHA, let us model a system of elements that includies: drilling collars, stabilizers and bent subs. considering our notation where we use "U Matrix" for the "Field Matrix" and "P Matrix" as a "Point Matrix", we can write:

$$\begin{pmatrix} c \\ 0 \\ 0 \\ h_l \\ 1 \end{pmatrix}_{x=l} = U_i \left\{ \begin{array}{l} P_{i-1}U_{i-1}P_{i-2}U_{i-2}\cdots U_2P_1U_1 \begin{pmatrix} 0 \\ y_0' \\ 0 \\ h_0 \\ 1 \end{pmatrix}_{x=0} + P_{i-1}U_{i-1}P_{i-2}U_{i-2}\cdots P_2U_2P_1 \begin{pmatrix} 0 \\ \hat{s}_1 \\ 0 \\ 0 \\ 0 \end{pmatrix} \\ + P_{i-1}U_{i-1}\cdots P_3U_3P_2 \begin{pmatrix} 0 \\ \hat{s}_2 \\ 0 \\ 0 \\ 0 \end{pmatrix} + \cdots + P_{i-1}U_{i-1}P_{i-2} \begin{pmatrix} 0 \\ \hat{s}_{i-2} \\ 0 \\ 0 \\ 0 \end{pmatrix} + P_{i-1} \begin{pmatrix} 0 \\ \hat{s}_{i-1} \\ 0 \\ 0 \\ 0 \end{pmatrix} \end{array} \right\} \qquad (A-1)$$

Where:

c : Dimensionless clearance at the length of tangency

$\hat{s}_i$: Dimensionless bent sub angle

Note that:

a) Usually at the bent sub we have a contact point. This has been taken care of when we introduced both a point matrix and the vector at the bent sub.

b) We have proved the same equation when we have multi element and multi stabilizers (contact point without bent subs).

c) If there is a contact point between the stabilizers, program will exit.

Appendix B - Calculating the dimensionless Side Force and Tilt Angle in the Complex System

In order to be able to calculate the dimensionless Side Force at the bit and Tilt Angle at the bit, first let us review the matrix formulation for the Complex System:

$$\begin{pmatrix} c \\ 0 \\ 0 \\ h_l \\ 1 \end{pmatrix}_{x=l} = U_i \left\{ \begin{array}{l} P_{i-1}U_{i-1}P_{i-2}U_{i-2}\cdots U_2P_1U_1 \begin{pmatrix} 0 \\ y_0' \\ 0 \\ h_0 \\ 1 \end{pmatrix}_{x=0} + P_{i-1}U_{i-1}P_{i-2}U_{i-2}\cdots P_2U_2P_1 \begin{pmatrix} 0 \\ \hat{s}_1 \\ 0 \\ 0 \\ 0 \end{pmatrix} \\ + P_{i-1}U_{i-1}\cdots P_3U_3P_2 \begin{pmatrix} 0 \\ \hat{s}_2 \\ 0 \\ 0 \\ 0 \end{pmatrix} + \cdots + P_{i-1}U_{i-1}P_{i-2} \begin{pmatrix} 0 \\ \hat{s}_{i-2} \\ 0 \\ 0 \\ 0 \end{pmatrix} + P_{i-1} \begin{pmatrix} 0 \\ \hat{s}_{i-1} \\ 0 \\ 0 \\ 0 \end{pmatrix} \end{array} \right\} \qquad \text{(B – 1)}$$

In another notation, if we define:

$$A = U_iP_{i-1}U_{i-1}P_{i-2}U_{i-2}\cdots U_2P_1U_1 \qquad \text{(B – 2)}$$

And;

$$B = U_i \left\{ \begin{array}{l} P_{i-1}U_{i-1}P_{i-2}U_{i-2}\cdots P_2U_2P_1 \begin{pmatrix} 0 \\ \hat{s}_1 \\ 0 \\ 0 \\ 0 \end{pmatrix} + P_{i-1}U_{i-1}\cdots P_3U_3P_2 \begin{pmatrix} 0 \\ \hat{s}_2 \\ 0 \\ 0 \\ 0 \end{pmatrix} \\ + \cdots + P_{i-1}U_{i-1}P_{i-2} \begin{pmatrix} 0 \\ \hat{s}_{i-2} \\ 0 \\ 0 \\ 0 \end{pmatrix} + P_{i-1} \begin{pmatrix} 0 \\ \hat{s}_{i-1} \\ 0 \\ 0 \\ 0 \end{pmatrix} \end{array} \right\} \qquad \text{(B – 3)}$$

Then, we can write Equation (B – 1) as:

$$\begin{pmatrix} c \\ 0 \\ 0 \\ h_l \\ 1 \end{pmatrix}_{x=LengthofTangency} = A \bullet \begin{pmatrix} 0 \\ y_0' \\ 0 \\ h_0 \\ 1 \end{pmatrix}_{x=0,atBit} + B \qquad (B-4)$$

Where:

c : Dimensionless clearance at the length of tangency

$\hat{s}_i$: Dimensionless bent sub angle

A, B : $A = [a_{ij}]$ where $i, j = 1,5$ and $B = [b_{k1}]$ where $k = 1,5$

U_i : Field Transfer Matrix for each element

Now as we guess the length of the last element, matrix A and B are known. Consequently, to be able to calculate the side force at tilt angle at the bit, there can be two possible cases that should be considered:

Case 1: "No Contact Point"

Case 2: "There is a Stabilizer" which contacts the wellbore at the end of the first element

Generally, in the both cases, all the boundary conditions must be satisfied. On other words, the following equation first should meet the boundary for each case and then solved for the dimensionless side force and the tilt angle at the bit.

$$\begin{pmatrix} c \\ 0 \\ 0 \\ h_l \\ 1 \end{pmatrix}_{End} = \begin{bmatrix} a_{11} & a_{12} & a_{13} & a_{14} & a_{15} \\ a_{21} & a_{22} & a_{23} & a_{24} & a_{25} \\ a_{31} & a_{32} & a_{33} & a_{34} & a_{35} \\ a_{41} & a_{42} & a_{43} & a_{44} & a_{45} \\ a_{52} & a_{52} & a_{53} & a_{54} & a_{55} \end{bmatrix} \begin{pmatrix} 0 \\ y_0' \\ 0 \\ h_0 \\ 1 \end{pmatrix}_{Initial} + \begin{pmatrix} b_1 \\ b_2 \\ b_3 \\ b_4 \\ b_5 \end{pmatrix} \qquad (B-5)$$

Case 1: "No Contact Point"

In this case, there is no known boundary right after the first element – neither a contacting stabilizer nor a bent sub. Therefore, using equation (B – 5), we can write:

$$y'_{x=l} = a_{21}y_0 + a_{22}y'_0 + a_{23}\left(e_{i-1}y''_0\right) + a_{24}h_0 + a_{25} + b_{21} = 0 \qquad \text{(B – 6a)}$$

$$y''_{x=l} = a_{31}y_0 + a_{32}y'_0 + a_{33}\left(e_{i-1}y''_0\right) + a_{34}h_0 + a_{35} + b_{31} = 0 \qquad \text{(B – 6b)}$$

Or in a simpler form:

$$y'_{x=l} = a_{22}y'_0 + a_{24}h_0 + a_{25} + b_{21} = 0 \qquad \text{(B – 7a)}$$

$$y''_{x=l} = a_{32}y'_0 + a_{34}h_0 + a_{35} + b_{31} = 0 \qquad \text{(B – 7a)}$$

Solving equations (B – 7) for h_0 and y'_0 yields:

$$h_0 = \frac{a_{25}a_{32} - a_{22}a_{35} + a_{32}b_{21} - a_{22}b_{31}}{\nabla} \qquad \text{(B - 8)}$$

$$y'_0 = \frac{a_{24}a_{35} - a_{25}a_{34} + a_{24}b_{31} - a_{34}b_{21}}{\nabla} \qquad \text{(B – 9)}$$

Where:

$$\nabla = a_{22}a_{34} - a_{24}a_{32} \qquad \text{(B – 10)}$$

Note that if the guess value for the length of the last element (in order to calculate the tangency length) is true, the following equation must be satisfied:

$$a_{12}y'_0 + a_{14}h_0 + a_{15} + b_{11} - c_l = 0 \qquad \text{(B – 11)}$$

Case 2: "There is a Stabilizer" which contacts the wellbore at the end of the first element

The procedure in this section is essentially the same as the previous one. Note that the stabilizer at the end of the first element is not a floating type, but it can touch either an upper or lower part of the wellbore. Using the equation (B – 5) we can have:

$$y_{x=a_1} = u_{11}^1 y_0 + u_{12}^1 y_0' + u_{13}^1 \left(e_{i-1} y_0''\right) + u_{14}^1 h_0 + u_{15}^1 = \pm c_{st,1} \qquad \text{(B – 12a)}$$

$$y_{x=l}'' = a_{31} y_0 + a_{32} y_0' + a_{33} \left(e_{i-1} y_0''\right) + a_{34} h_0 + a_{35} + b_{31} = 0 \qquad \text{(B – 12b)}$$

Or in a simpler form:

$$y_{x=a_1} = u_{12}^1 y_0' + u_{14}^1 h_0 + u_{15}^1 = \pm c_{st,1} \qquad \text{(B – 13a)}$$

$$y_{x=l}'' = a_{32} y_0' + a_{34} h_0 + a_{35} + b_{31} = 0 \qquad \text{(B – 13b)}$$

Solving equations (B – 14) for h_0 and y_0' yields:

$$h_0 = \frac{a_{35} u_{12}^1 - a_{32} u_{15}^1 + u_{12}^1 b_{31} \pm a_{32} c_{st,1}}{\nabla} \qquad \text{(B - 14)}$$

$$y_0' = \frac{a_{34} u_{15}^1 - a_{35} u_{14}^1 - u_{14}^1 b_{31} \pm a_{34} c_{st,1}}{\nabla} \qquad \text{(B – 15)}$$

Where:

$$\nabla = a_{32} u_{14}^1 - a_{34} u_{12}^1 \qquad \text{(B – 16)}$$

u_{ij}^1 = The field matrix of the first element

Note that if the guess value for the length of the last element (in order to calculate the tangency length) is true, the following equation must be satisfied:

$$a_{12} y_0' + a_{14} h_0 + a_{15} + b_{21} - c_l = 0 \qquad \text{(B – 17)}$$

Appendix C - Results : Static condition

Table C - 1: General Wellbore Data

NUMBER OF ELEMENTS:	7
Hole Diameter:	12.25 inch.
Inclination angle:	45.00 degree
Weight on the Bit:	30000 Pounds
Mud Density:	10.00 Pounds/Gallon

Table C - 2: BHA Data

Element	OD	ID	Length	Density	Stabilizer OD	Bent Sub
Unit	(in)	(in)	(ft)	(lb/ft)	(in)	(deg)
1	7.750	5.957	3.60	137.15	12.125	0.00
2	7.750	5.957	2.77	137.15	7.750	0.00
3	7.750	5.957	3.33	137.15	7.750	+1.00
4	7.750	5.957	14.34	137.15	7.750	0.00
5	8.000	2.812	17.50	148.98	12.187	0.00
6	8.000	2.812	35.00	148.98	12.187	0.00
7	8.000	2.812	---	148.98	8.00	0.00

Table C - 3: Results

Tangency Length:	120.85 Feet
Side Force at the bit:	9964.4 Pounds
Tilt Angle:	0.031 Degree
Side Force at the stabilizer (1):	-12737.7 Pounds
Side Force at the stabilizer (2):	-1705.1 Pounds
Side Force at the stabilizer (3):	-4585.4 Pounds

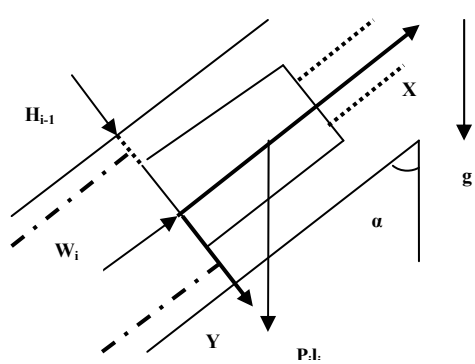

Fig. C - 1: System of Coordinate

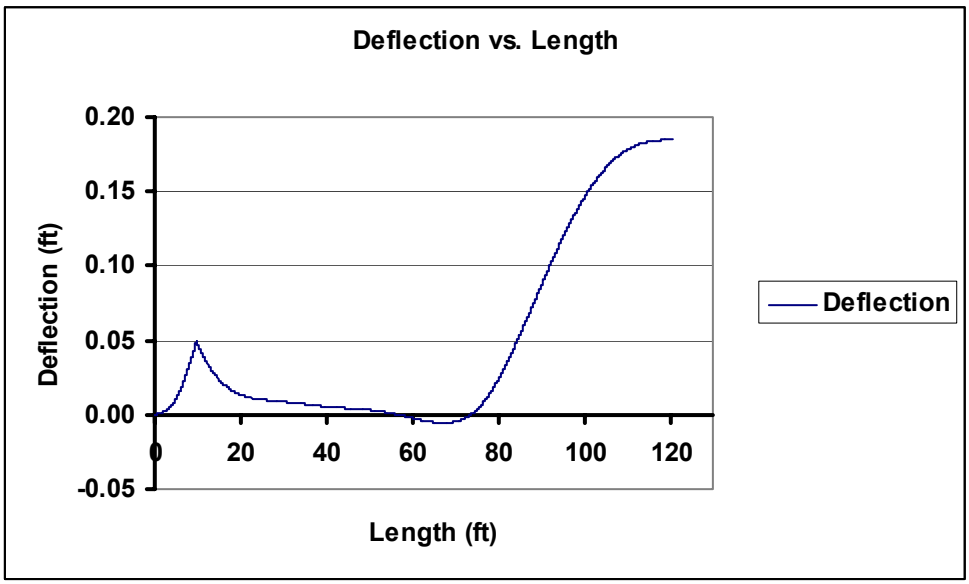

Fig. C – 2: Deflection vs. Length

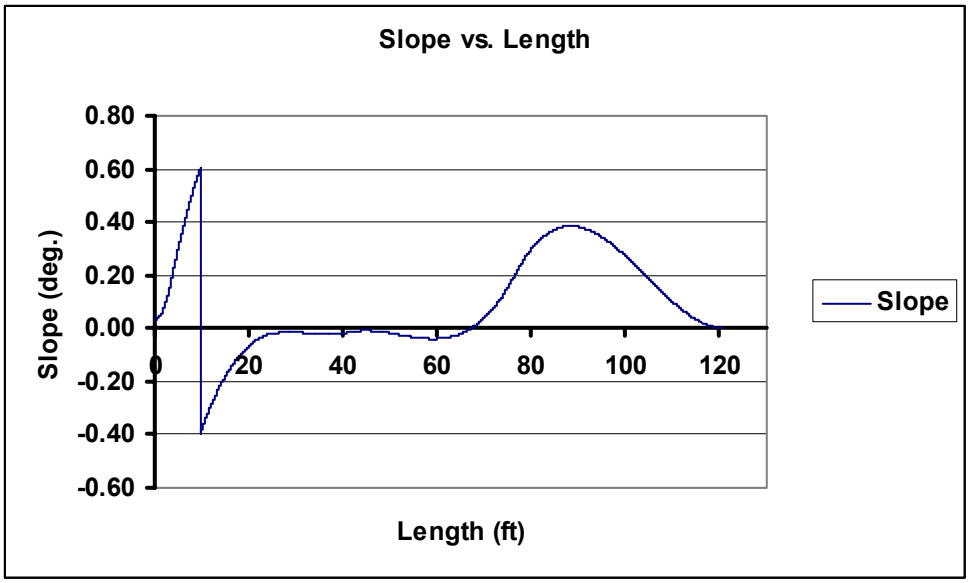

Fig. C – 3: slope vs. Length

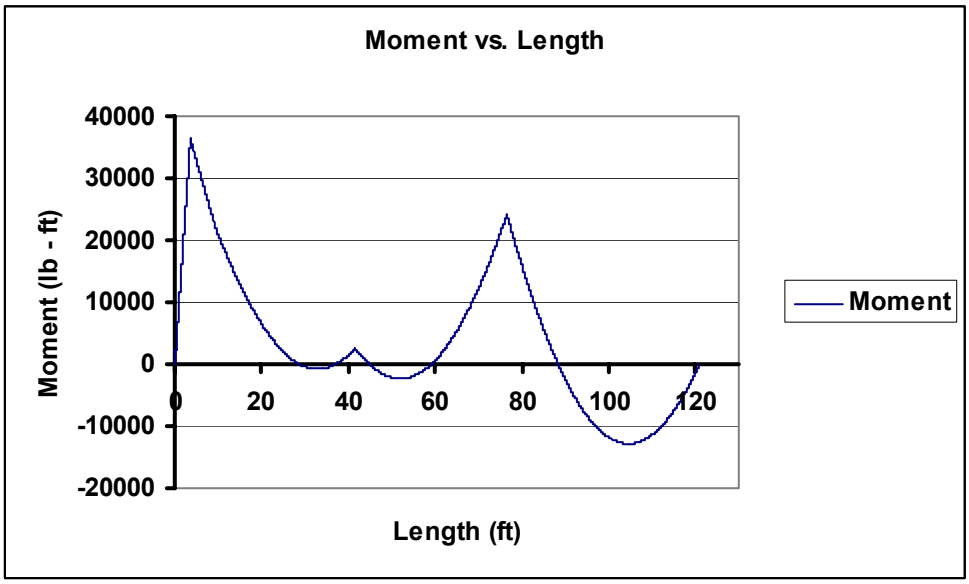

Fig. C – 4: Moment vs. Length

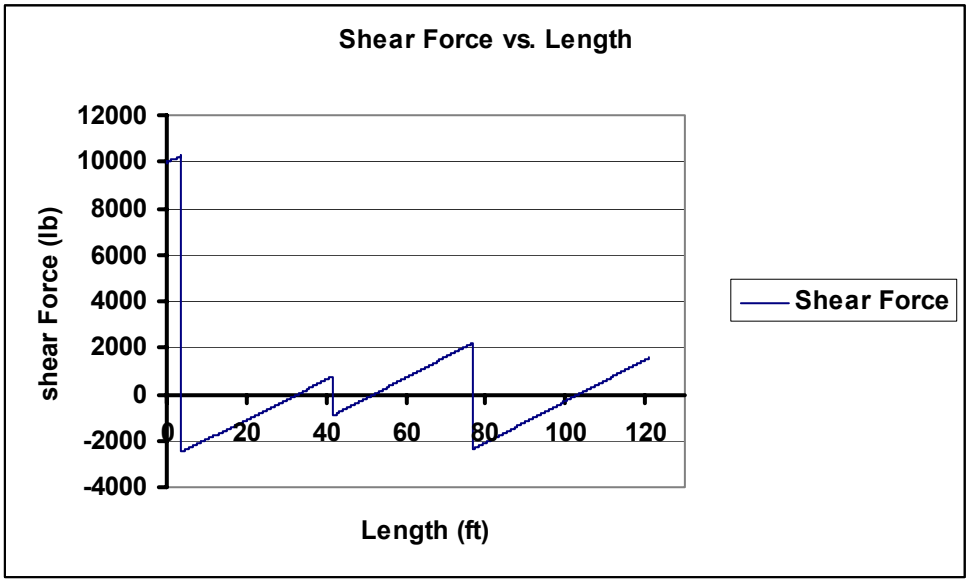

Fig. C – 5: Shear Force vs. Length

Appendix D – Results: Drilling Ahead

Table C - 1: General Wellbore Data

Number of elements:	3
Hole Diameter:	8.50 inch.
Inclination angle:	45.00 degree
Weight on the Bit:	30000 Pounds
Mud Density:	10.00 Pounds/Gallon

Table C - 2: BHA Data

Element	OD	ID	Length	Density	Stabilizer OD	Bent Sub
Unit	(in)	(in)	(ft)	(lb/ft)	(in)	(deg)
1	6.25	2.25	15.00	90.30	8.375	0.00
2	6.25	2.25	30.00	90.30	8.438	0.00
3	6.25	2.25	---	90.30	6.25	0.00

Table C - 3: Results

Tangency Length:	78.40 Feet
Side Force at the bit:	-315 Pounds
Tilt Angle:	0.038 Degree
Side Force at the stabilizer (1):	1056.9 Pounds
Side Force at the stabilizer (2):	2148.2 Pounds

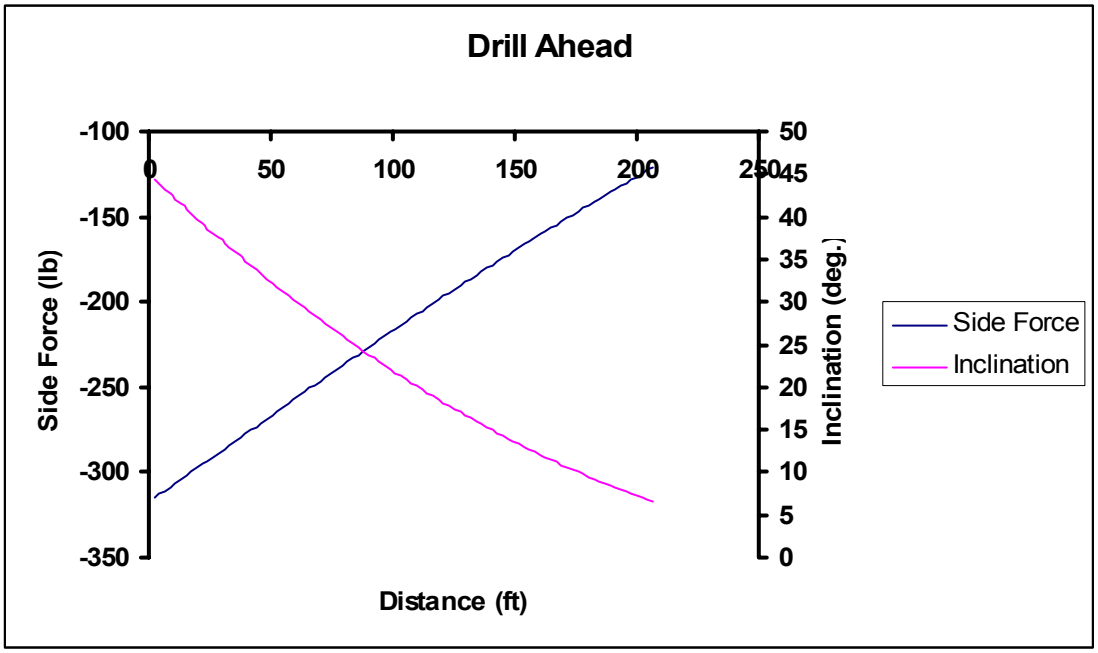

Fig. D – 1: Drill Ahead for original case

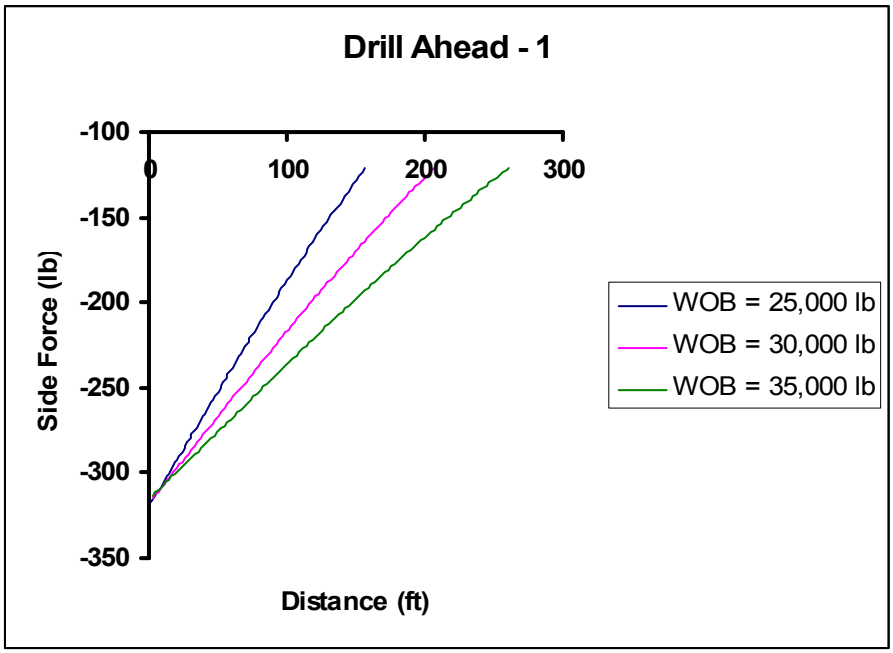

Fig. D – 2: Effects of WOB on Side Force

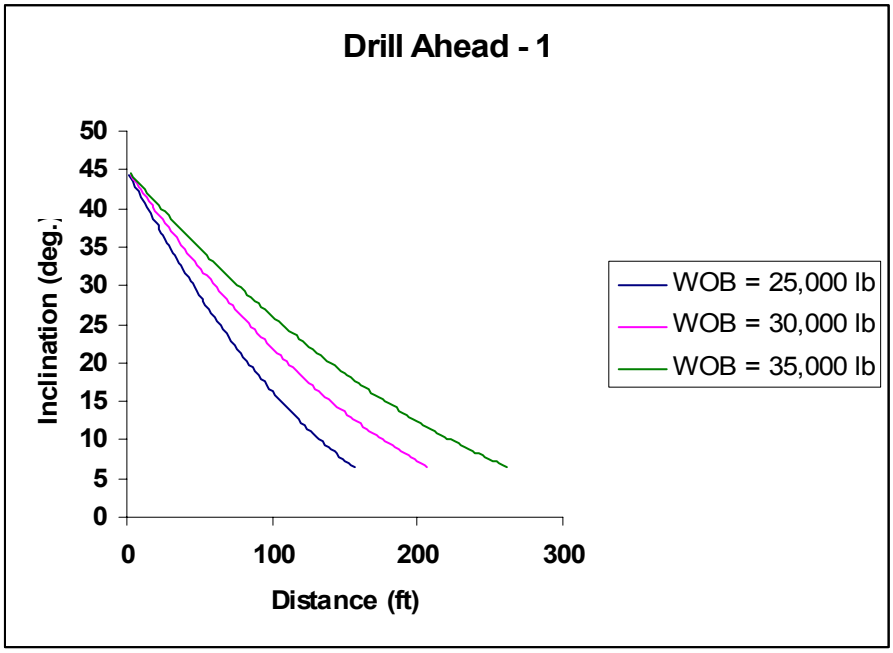

Fig. D – 3: Effects of WOB on Final Equilibrium Angle

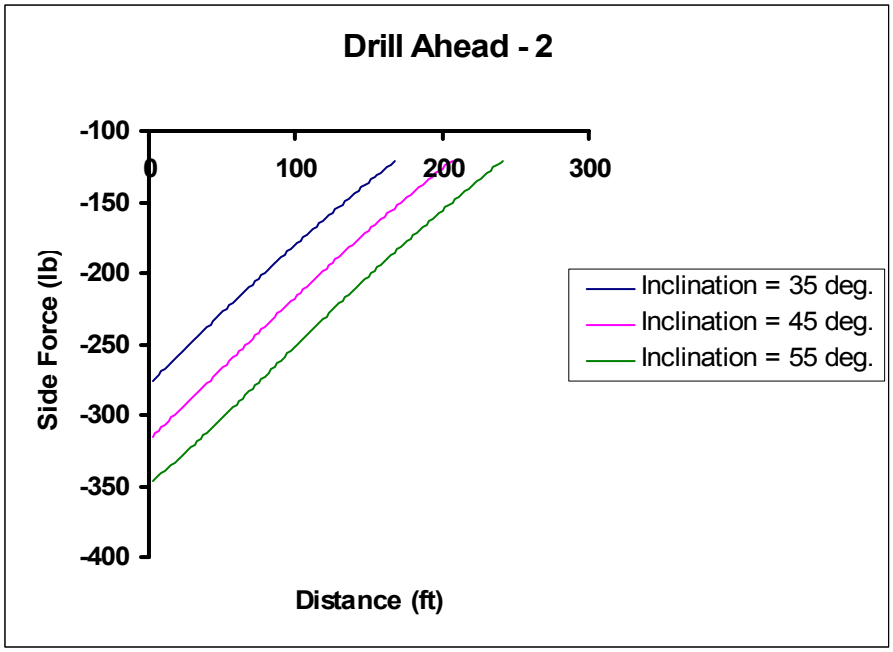

Fig. D – 4: Effects of Inclination angle on Side Force

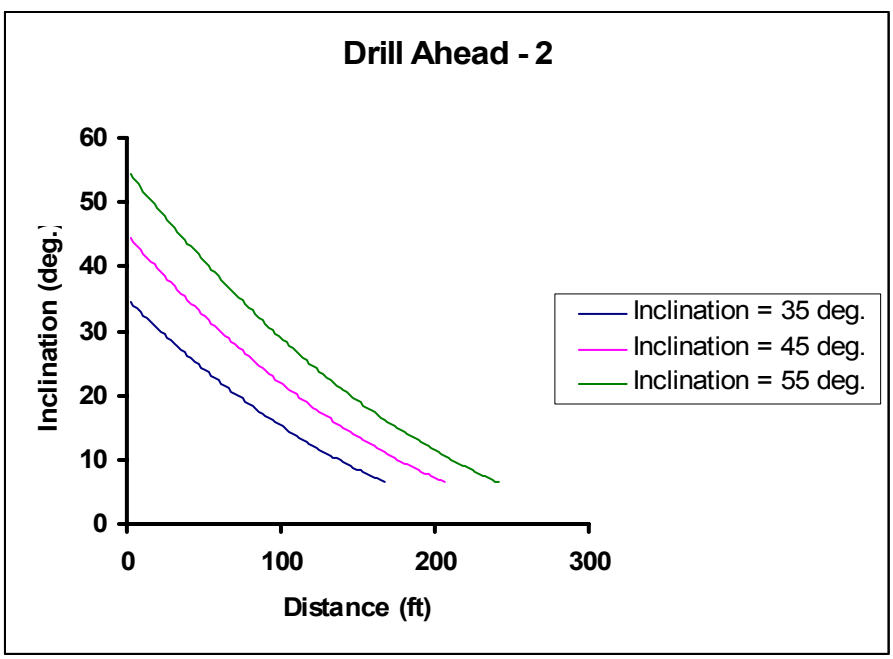

Fig. D – 5: Effects of Inclination angle on Final Equilibrium Angle

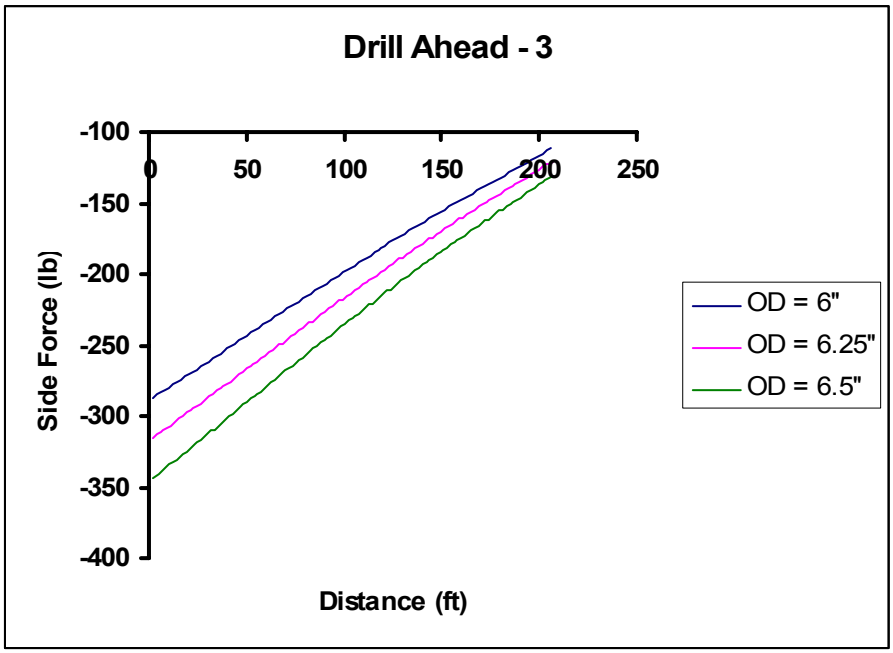

Fig. D – 6: Effects of Drill Collar Size on Side Force

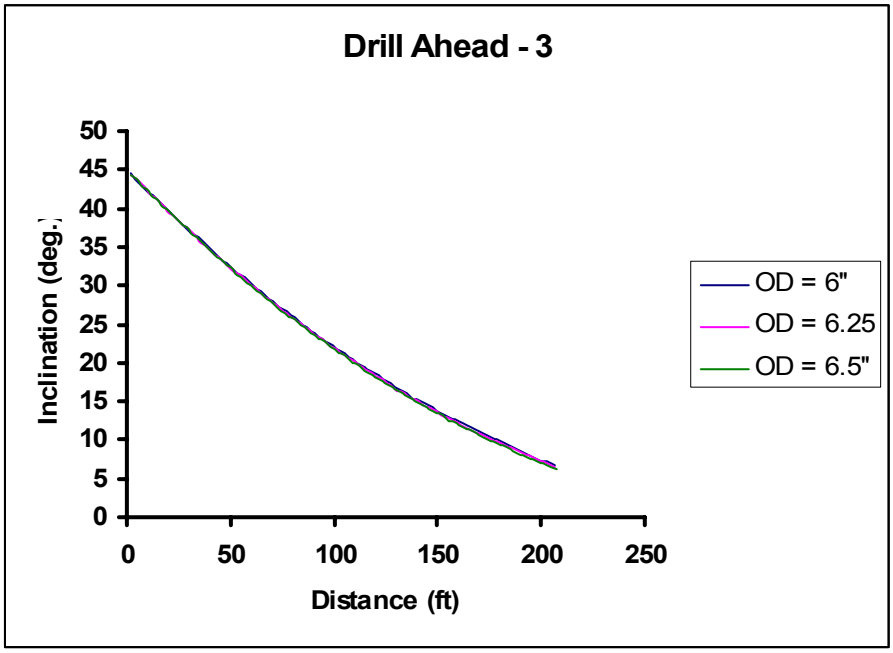

Fig. D – 7: Effects of Drill Collar Size on Final Equilibrium Angle

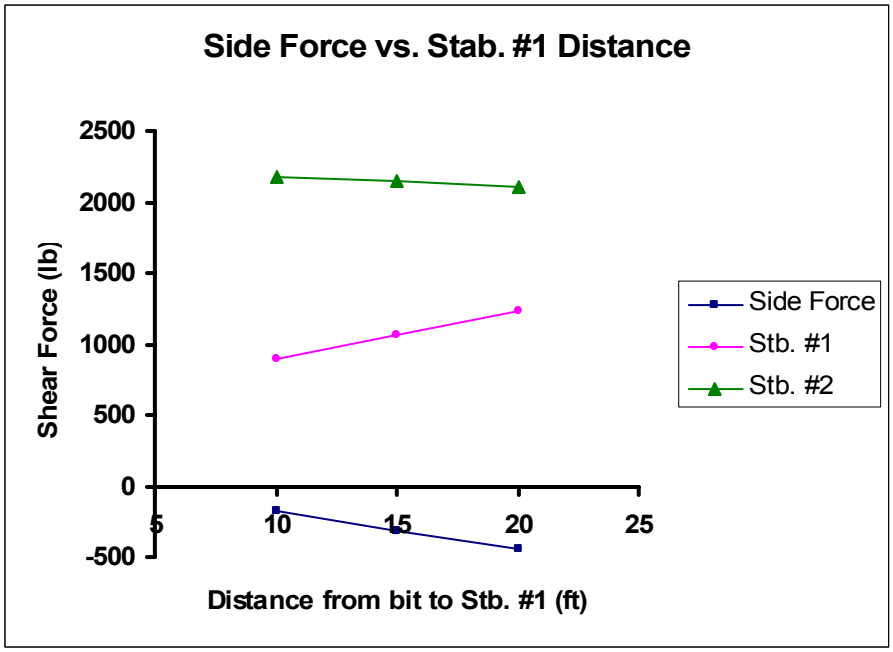

Fig. D – 8: Effects of Stb. #1 Position on the Side Forces

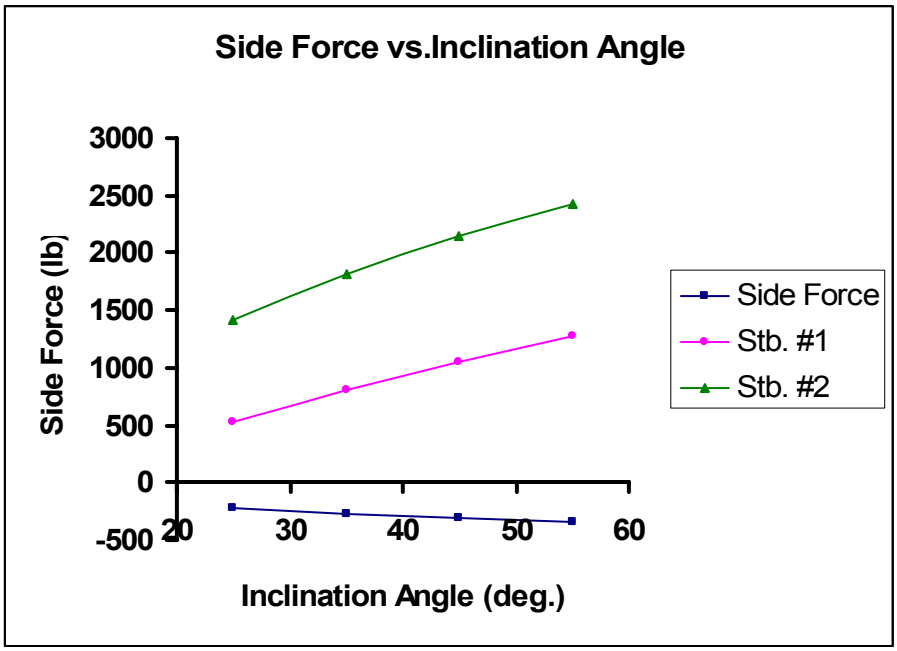

Fig. D – 9: Effects of Inclination Angle on the Side Forces

Study on Effective Hole Cleaning Using “Sweeps” in Horizontal Wellbores

Sandeep Valluri

Study on Effective Hole Cleaning Using "Sweeps" in Horizontal Wellbores

INVESTIGATOR: Sandeep Valluri

SPONSOR: TUDRP

OBJECTIVE:

- Experimental and theoretical study of the influence of drilling parameters combinations on cuttings bed removal using "viscous sweeps".

SCOPE OF WORK:

- Viscous sweeps;
- Testing variables: annular flow velocity, fluid type, fluid rheology, and drill pipe rotary speed;
- Mechanistic model for the "bed erosion" process.

DELIVERABLES:

- The experimental database which can be used to better understand the effect of rheology of fluids on sweep efficiency.
- Mechanistic model for the "bed erosion" process.
- Semi-annual Advisory Board Meeting (ABM) reports and the Final Report.

PROJECT TIME TABLE:

	2004			2005		
	Spring	Summer	Fall	Spring	Summer	Fall
Literature Review						
Literature Review & Modeling						
Experiments						
Model Verification						
Final Report						

THE UNIVERSITY of TULSA

TUDRP

The University of Tulsa
Drilling Research Projects

Study on Effective Hole Cleaning Using "Sweeps" in Horizontal Wellbores"

(Progress Report)

Sandeep Valluri, University of Tulsa, Drilling Research Projects,
Masters of Science, Oil & Natural Gas Engineering, A&M, Kingsville, B.E. Chemical Engineering DSCE, India.

This report is prepared for TUDRP Advisory Board Meeting, May, 2005, Tulsa, Oklahoma

---

Abstract:

This is the second report being presented for this project. This report presents experimental results obtained from the tests conducted on the Low Pressure Ambient Temperature flow loop as well as preliminary test results from a new proposed test matrix. Based on results from preliminary tests, subsequent "sweep" tests were conducted according to a modified Test Matrix. A detailed analysis of the experimental data obtained is presented. The effect of parameters such as, rheology, flow rate & drill pipe rotation on volume cutting concentration removed, bed heights and pressure drop are presented. The theoretical modeling related to the "fluid-fluid" displacement is under progress. However after the comments and suggestions received from the member companies, the focus of this report will be the results from the "sweep" tests.

Project Status

Literature Review	85%	
Flow Loop Training	L.P.A.T. (*)	E.P.E.T. (**)
	100 %	15%
Modeling	40%	
Experiments	L.P.A.T. (*)	E.P.E.T. (**)
	100%	0%

(*) L.P.A.T. (low pressure ambient temperature loop), (**) E.P.E.T. (Elevated Pressure Elevated Temperature loop)

Introduction:

This project focuses on the particular technique termed as "sweeps", in which circulation of specific fluids specially formulated to remove the cuttings beds, are periodically necessary. In vertical and near vertical wells these fluids are devised to add to the lifting of the cuttings to the surface. In "deviated" wells they are designed to add to the shear forces on the top layer of the cuttings bed, thus adding to the "erosion" of the cuttings bed.

Problem Statement:

Poor cuttings transport in deviated and extended reach wells has warranted the need for novel techniques to clean the wellbore of the cuttings bed that has been formed by the deposition of cuttings that are generally fine and smaller sized cuttings. Drilling fluid "sweeps" are used in order to clean the borehole from cuttings that are not removed by ordinary drilling fluid circulation. There has been a lack of certainty as to the sweep type selection in the field. In addition there is not much information pertaining to use of the "sweeps", a sign that this particular area of research has not received its due attention. Therefore a rigorous experimental and theoretical analysis of the "sweeps" to quantify the "efficiency" of the drilling fluid "sweeps" needs to be performed.

Generally in practice the sweep fluids are injected in addition to the drilling mud that is already present in the well-bore. The sweep fluid "displaces" the base fluid out of the drill-pipe as well as the well-bore while contributing to the bed erosion process. The stability of the interface between the base fluid and the sweep fluid is of concern. The stability of the interface may have some influence on the efficiency of sweep as it may affect the rheology of the sweep fluid due to mixing etc. Various models [1], [2], [3], [4] allow a careful investigation of individual effects of various parameters that effect the displacement efficiency. The major parameters that effect the displacement are the fluid rheology, fluid density & the fluid yield stress.

Past Work:

Preliminary "sweep" tests were conducted on the LPAT flow loop. Before the preliminary tests could be conducted, fluid characterization was performed for the following reasons:

1) To design fluids with a mixture of appropriate quantities of PAC (Poly-anionic Cellulose) & XCD (Xanthum Gum), and to obtain the required rheological properties, with focus on the yield points in the range of 20, 30 & 40 Lb/100ft^2.

2) To study the effect of temperature on the rheology of the designed fluids.

The initial test matrix required flow rates of the sweep of 100, 200 & 300 gpm. The results from these tests indicated that the 100gpm sweep tests were ineffective and would not aid in drawing any tangible conclusions from the "sweep" tests. The test matrix was modified to incorporate sweep tests with higher flow rates. The preliminary tests were designed to quantify the sweep efficiency based on the volume of the sweep.

Experimental Section:

The appendix contains Figure 1 showing the schematic diagram of the current flow loop with the modifications made to incorporate the "Sweeps". The experimental section of the LPAT flow loop is 90 ft long and consists of an 8-in. inner diameter transparent casing with 4.5 in. outer diameter drill pipe. The drill pipe can be rotated up to 120 rpm (revolution per minute R.P.M.). A 75 H.P. centrifugal pump (maximum tested capacity is 650 g.p.m.) is used to pump fluid into the flow loop. The cuttings are injected at the inlet of the annular test section where they merge with the test section.

As mentioned earlier, the test matrix needed to be modified to incorporate higher flow rates of the "sweep". The higher flow rates would require high volumes of the "sweep" fluid and we did not have the required facilities to run these high volume sweeps. Thus the "sweep efficiency" will be quantified based on time rather than volume. All the sweep tests have been designed for two minute sweeps in the test section, irrespective of the flow rate. Based on this design the modified test matrix is as follows:

Fluid Type	**Flow rate G.P.M. (m^3/s)**	**Drill Pipe Rotation (RPM)**	**Rate of Penetration (ft/hr)**	**Bed Height**	**Test Time (mins)**
Fluid A (PAC+XCD Yield 20 Lb/100 ft^2)	200 (0.0126)	0,50,100	30-50	40-50% of Annulus	2
Fluid B (PAC+XCD Yield 30 Lb/100 ft^2)	300 (0.0189)	0,50,100	30-50	40-50% of Annulus	2
Fluid C (PAC+XCD Yield 40 Lb/100 ft^2)					
Fluid D (Water)	400 (0.0252)	0,50,100	30-50	40-50% of Annulus	2

LPAT Test Procedure

A standard procedure is followed for conducting the experiments, the steps of which are provided below. For any successful run, it is necessary that steady-state conditions be reached in the test section before data acquisition can be initiated.

1. The test fluid is prepared, by adding the required amount of both PAC (Poly-anionic Cellulose) and XCD (Xanthum Gum) to water in the primary tank indicated by 2 in Figure1.
2. Prime the centrifugal pump if the primary tank indicated by 2 in Figure1 is emptied and filled with a new fluid.
3. Once the fluid is prepared, measure the rheology of the fluid and then transfer this fluid to the secondary tanks indicated by 3, by switching the valves indicated by 7 with the help of the centrifugal pump.
4. Check the rheology of the fluid again after the fluid has been transferred to the secondary tanks to ensure that the fluid has maintained the desired rheologic properties.
5. Clean the primary tank with water, to ensure there is no contamination of the base fluid, i.e. water with polymer. Fill the primary tank with water to begin tests.
6. Start LabView® on the computer terminal (create a new file for every experiment run).
7. Open up the main mud valve at least 30%.
8. Start the mud pump to establish flow rate of water through the test section indicated by 1.
9. Once a steady flow rate has been established and circulation of the drilling fluid has been ensured, start the cuttings injection auger indicated by 9, from both the LabView® interface as well as the control panel switch.
10. Adjust the valve lever on the injection tank indicated by 5, to establish a steady ROP (cuttings injection). At this time, cuttings will start falling into the flow stream and will be pushed into the test section by the auger.
11. Start the shale-shaker indicated by 4 from the control panel.
12. Carefully observe the dP-12 and dP-13 plots on the LabView® interface. These curves will increase at first and then level off when a steady state has been achieved. At the same time, observe the ROP plot on the interface. The ROP plot should remain steady around an average value during a run. The average value will be the effective cuttings injection rate

during the experiment and can be changed by altering the valve position on the injection tank or changing the auger speed.

13. Close the hold-up valve, to isolate the test section, and divert the flow into the bypass line indicated by 8, by opening the bypass line valve. Cuttings will be trapped inside the test-section by doing so. The weight of these cuttings must now be determined.
14. Close the cuttings injection valve and turn off the injection auger from both the control panel as well as the LabView® interface. This will stop further injection of cuttings into the test section. Stop the centrifugal pump.
15. Close the main water inlet and open the secondary mud tank valve.
16. Start the centrifugal pump and allow the "sweep" fluid to run in through the by-pass line.
17. Once the desired flow rate is obtained, open the hold-up valve and close the by-pass valve, allowing the fluid to "sweep" the test section. Note down the start time of the test. The end time of the test is two minutes after the start time.
18. Start pipe rotation if required by the test.
19. Continue data logging. A complete data sheet is provided in the appendix for reference. This data sheet contains the records maintained in addition to the ones kept using the LabView® interface.
20. As soon as the "sweep" is complete, open the by-pass valve and close the hold-up valve simultaneously. Turn off the centrifugal pump and stop pipe rotation.
21. Switch the valves again from the secondary tanks to the primary tank and start the centrifugal pump to clean the by-pass and test section with water.
22. Increase the flow rate in order to clean the bypass line and the hoses. This step is also called the 'first flush'.
23. If required, start drill-pipe rotation from the control panel switch. Adjust the drill-pipe rotational speed with the knob on the control panel and read the current rpm from the display.
24. When the weight of the collection tank becomes steady, open the hold-up valve while simultaneously closing the bypass line valve. This step is termed the 'second flush'. Note the collection tank weight prior to opening the hold-up valve in this step.

25. When the test section has been flushed completely and all the cuttings are removed note the collection tank weight. The difference between the collection tank weights before and after the second flush gives the weight of the cuttings inside the test section at a steady state. This cuttings' weight is used for computations and analysis in the later part of the report.
26. Proceed to shut off the mud pump and the shale-shaker.
27. On the LabView® interface, press 'STOP' to save and close the data file.

Sweep Test Results:

Thirty six sweep tests in all were performed on the LPAT flow loop. The effect of different drilling parameters, i.e. the fluid rheology, drill pipe rotation and flow rate on cuttings removal is discussed in this section.

The analysis of the data obtained appears to indicate that it is not sufficient to focus on one drilling parameter, i.e. the rheology of the fluid alone to clean the wellbore. Tests clearly show that, a proper combination of these drilling parameters is required for efficient hole cleaning. All the figures mentioned in this section are found in the appendix.

Effect of Rheology:

Three different fluids with yield points of 20, 30 & 40 lb/100ft^2 were prepared to study the effect of rheology on the bed erosion and cutting removal process. In "deviated" wells the sweeps are designed to add to the shear forces on the top layer of the cuttings bed, thus adding to the "erosion" of the cuttings bed. But tests indicate that it is not sufficient to only increase the viscosity of the sweep to efficiently "erode" the cuttings bed. Figure 3 shows the plot of dimensionless bed height, before and after sweeps, for water and fluids with yield points of 20, 30 & 40 lb/100ft^2 at 400 gpm, without any drill pipe rotation. Dimensionless bed height is defined as the ratio between the calculated bed height and the inner diameter of the casing. This figure clearly shows that change of rheology alone from 20 to 40 lb/100ft^2 has almost no effect on the "erosion" process. This is also indicated by Figure 14, the cutting volume concentration removed, for water and fluids with yield points of 20, 30 & 40 lb/100ft^2 at 300 gpm and 0 rpm. Figures 3 & 14 also show that water appears to have the most reduction in bed height and most cuttings removed. A comparison of the flow conditions, as shown in the table, for the fluids shows that the viscous fluids are in laminar flow as compared to water which is in turbulent flow. We will thus discuss the effect of flow rate next.

Effect of Flow Rate:

Figure 2 is a plot of dimensionless bed height for fluid with yield point of 20 Lb/100ft^2 at flow rates of 200 300 & 400 gpm. The figure shows that increase of the flow rate from 200 to 400 gpm does not have any noticeable effect on the bed height. This is also indicated by Figure 12, plot of volume concentration removed, for fluid with yield point of 30 Lb/100ft^2 at flow rates of 200 300 & 400 gpm without any drill pipe rotation. But in comparison when we look at Figure 4, i.e. plot of dimensionless bed height for water at flow rates of 200 300 & 400 gpm, there is a large difference in bed heights. This is also indicated by Figure 10, plot of volume concentration removed, for water at flow rates of 200 300 & 400 gpm without any drill pipe rotation. The difference may again be explained by looking at the flow conditions. Table 2 presented in the appendix, shows that the viscous fluids are in laminar flow as compared to water which is in turbulent flow. This has also been observed by J.M. Peden et. Al. [5], who observed that transition from turbulent to laminar flow, resulted in an inconsistent relationship between the fluid viscosity and MTV (Minimum Transport Velocity). The concept of MTV presumes that a hole can be efficiently cleaned by either maintaining cuttings rolling or in suspension, if the annular velocity is equal or greater than a minimum transport velocity for that operational condition. In the case of the viscous fluid the circulating fluid appears to take the path of least resistance and simply flow over the cuttings bed, i.e. the space between the cuttings bed and the casing.

Closer observation of Figure 4 shows the problem with using water as the sweep fluid. Although water appears to be very efficient in cleaning the test section, the figure indicated that, the bed is completely removed at one end of the section i.e. the inlet end, but higher as it moves towards the outlet end of the section. This gives an early indication of an uneven cleaning of the wellbore while using water as the sweep fluid. For a further analysis we look at the effect of drill pipe rotation on the bed erosion process.

Effect of drill pipe rotation:

It has been shown [6] that drill pipe rotation has a significant effect on hole cleaning during directional drilling. All the tests that incorporate drill pipe rotation showed that it has a considerable effect on cutting removal. This is indicated by Figure 16, plot of dimensionless bed height for fluid with yield point of 30 Lb/100ft^2, with drill pipe rotational speeds of 0, 50, 100 rpm and a flow rate of 300 gpm, Figure 5, plot of dimensionless bed height for water, at drill pipe rotational speeds of 0, 50, 100 rpm and a flow rate of 300 gpm, Figure 12, plot of volume concentration removed for fluid with yield point of 30 Lb/100ft^2, with drill pipe rotational speeds of 0, 50, 100 rpm and a flow rate of 300 gpm and Figure 11,

plot of volume concentration removed for water, with drill pipe rotational speeds of 0, 50, 100 rpm and a flow rate of 300 gpm The next step is to study the effect of the different parameters on cuttings removal in relation to each other. Figure 7, plot of dimensionless bed height for fluid with yield point of 30 Lb/100ft^2 at flow rates of 200 300 & 400 gpm and drill pipe rotation speed of 50rpm, shows the positive effect the comparatively low rotational speed has on the bed erosion process. This plot shows that, under the influence of drill pipe rotation, the increase of flow rate of the viscous fluid improves cuttings removal. This is also indicated by Figure 6, plot of dimensionless bed height for water at flow rates of 200 300 & 400 gpm and drill pipe rotational speed of 50rpm. The drill pipe rotation agitates the cuttings and helps lift them into the stream of the sweep fluid, thus facilitating the cuttings removal.

In the presence of drill pipe rotation, we study Figure 15, plot of volume of cuttings concentration removed, for water and fluids with yield points of 20, 30, 40 Lb/100ft^2, flow rate of 300 gpm and rotational speed of 50 rpm. In this figure we see that an increase in the yield point has a positive effect on the cuttings removal. This is also indicated by Figure 8, plot of dimensionless bed height for water and fluids with yield point of 20, 30 and 40 Lb/100ft^2, with drill pipe rotational speed of 50 rpm and a flow rate of 300 gpm.

The uneven cutting removal when the sweep fluid is water may also be seen more clearly under the influence of drill pipe rotation. For this, we study Figure 9, plot of dimensionless bed heights in the lower end with, water & fluid with yield points of 20, 30 and 40 Lb/100ft^2, with flow rate pf 300 gpm and rotational speed of 50 rpm. We see that when the fluid is water, the bed height tends to be higher than the bed before the sweep test, on the lower side of the test section.

Effect of different parameters on differential pressure:

To study the effect of different parameters on pressure we study figures 17 & 18, plots of measured differential pressure versus time (duration of the sweep, two minutes). Measured differential pressure reflects the frictional pressure drop along the test section. Figure 17 is a plot of differential pressure versus time for water with different drill pipe rotational speeds of 0, 50 & 100 rpm at 300 gpm. As depicted in the figure, the pressure drop generally decreases with increase in pipe rotation. This is because the higher pipe rotation results in less cuttings concentration in the test section and thus a larger flow area. At 50 rpm, the pressure decrease due to cuttings removal appears to be compensated by the increase in pressure due to the turbulence caused by drill pipe rotation. But at 100 rpm, the pressure decrease is quite noticeable. The same can be seen in figure 18, differential pressure versus time for fluid with yield point of 30 Lb/100ft^2 with drill pipe rotational speeds of 0, 50 & 100 rpm and flow rate of 300 gpm.

Proposed New Test Matrix for LPAT flow loop:

To get a better understanding of the effect of the different parameters, the following test matrix is proposed. These tests will also be conducted on the LPAT flow loop. The test matrix is presented:

Fluid Type	Flow rate G.P.M. (m^3/s)	Drill Pipe Rotation (RPM)	Rate of Penetration (ft/hr)	Bed Height	Test Time (mins)
Fluid A (Low Viscosity)	200 (0.0126)	0,50,100	30-50	40-50% of Annulus	2
Fluid B (Low Viscosity)	300 (0.0189)	0,50,100	30-50	40-50% of Annulus	2
Fluid C (Weighted sweep?)	400 (0.0252)	0,50,100	30-50	40-50% of Annulus	2

The test procedure for these tests will be as follows:

LPAT Test Procedure for proposed test matrix:

The test procedure will be changed slightly for the test with the Low viscosity fluid. The procedure will be changed in the following ways:

1. We will use water as the "base fluid" to generate the initial cuttings bed.
2. We also propose to use a high viscosity fluid as the "base fluid" to generate the initial cuttings bed to perform tests.
3. Cuttings under study would be in the range of $1/4^{th}$ to $1/8^{th}$ inch gravel.
4. We propose to use a cuttings bed height in the range of 40-50% of pipe for all tests.
5. Once the initial bed has been generated, the "weighted sweep fluid" will be injected at flow rates in the range of 200, 300 & 400 gpm.
6. We propose to use varying pipe rotations, in the range of 0, 50, 100 rpm.
7. An estimate of the "efficiency" of the "sweeps" will then be determined based on the in-situ cuttings concentration.

Preliminary Test results:

Four tests have been completed from the new test matrix. The tests were conducted by first building the cuttings bed by using a base fluid of relatively high viscosity fluid. The sweep fluids used were water and a fluid with relatively low viscosity. The rheological parameters for the fluids are as follows:

Fluid	n	K (lbfs^n/100ft^2)
Base Fluid (1.5 lb/bbl PAC)	0.69	0.46
Low viscosity fluid (0.5 lb/bbl)	0.72	0.21

Table1: Rheological parameters of fluids:

Figure 19 shows a dimensionless bed height for bed built with high viscosity fluid and using "sweeps" of water and low viscosity fluid, without any drill pipe rotation. This figure gives an early indication that, even in the absence of drill pipe rotation, the low viscosity fluid has a considerable effect on cuttings removal and thus the dimensionless bed height. Data analysis for these tests is still in progress and will be presented in the next report.

PROJECT TIME TABLE:

	2004			2005		
	Spring	Summer	Fall	Spring	Summer	Fall
Literature Review						
Literature Review & Modeling						
Experiments						
Model Verification						
Final Report						

Future Work:

1. Experimental data from "viscous sweep" tests from the LPAT & EPET flow loops.
2. Mechanistic and regression models

References:

1) Raymond W. Flumerfelt, "Laminar displacement of Non-Newtonian fluid in parallel plate narrow gap annular geometries." S.P.E. 4486, April 1975.
2) Robert M. Beirute, and Raymond W. Flumerfelt, "Mechanics of the displacement process of drilling muds by cement slurries using an accurate rheological model." S.P.E. 5801, 1977.
3) D. Nguyen and S.S. Rahman, "A mathematical model for laminar displacement of one Non-Newtonian fluid by another in horizontal concentric annuli." Chem. Eng. Comm. 2000.
4) Ahmadi Tehrani, John Ferguson and S.H. Bitttleson, "Laminar displacement in annuli: A combined experimental and theoretical study." S.P.E. 24569.
5) J.M. Peden, J.T. Ford and M.B. Oyeneyin, Heriot-Watt U, "Comprehensive Experimental Investigation of Drilled Cutting Transport in Inclined Wells Including the Effects of Rotation and Eccentricity." S.P.E. 20925.
6) R. Alfredo Sanchez and J.J. Azar, U. of Tulsa, A.A. Bassal and A.L. Martins, "Effect of Drill pipe Rotation on Hole Cleaning During Directional-Well Drilling." S.P.E. Journal 4 (2), June 1999.

APPENDIX:

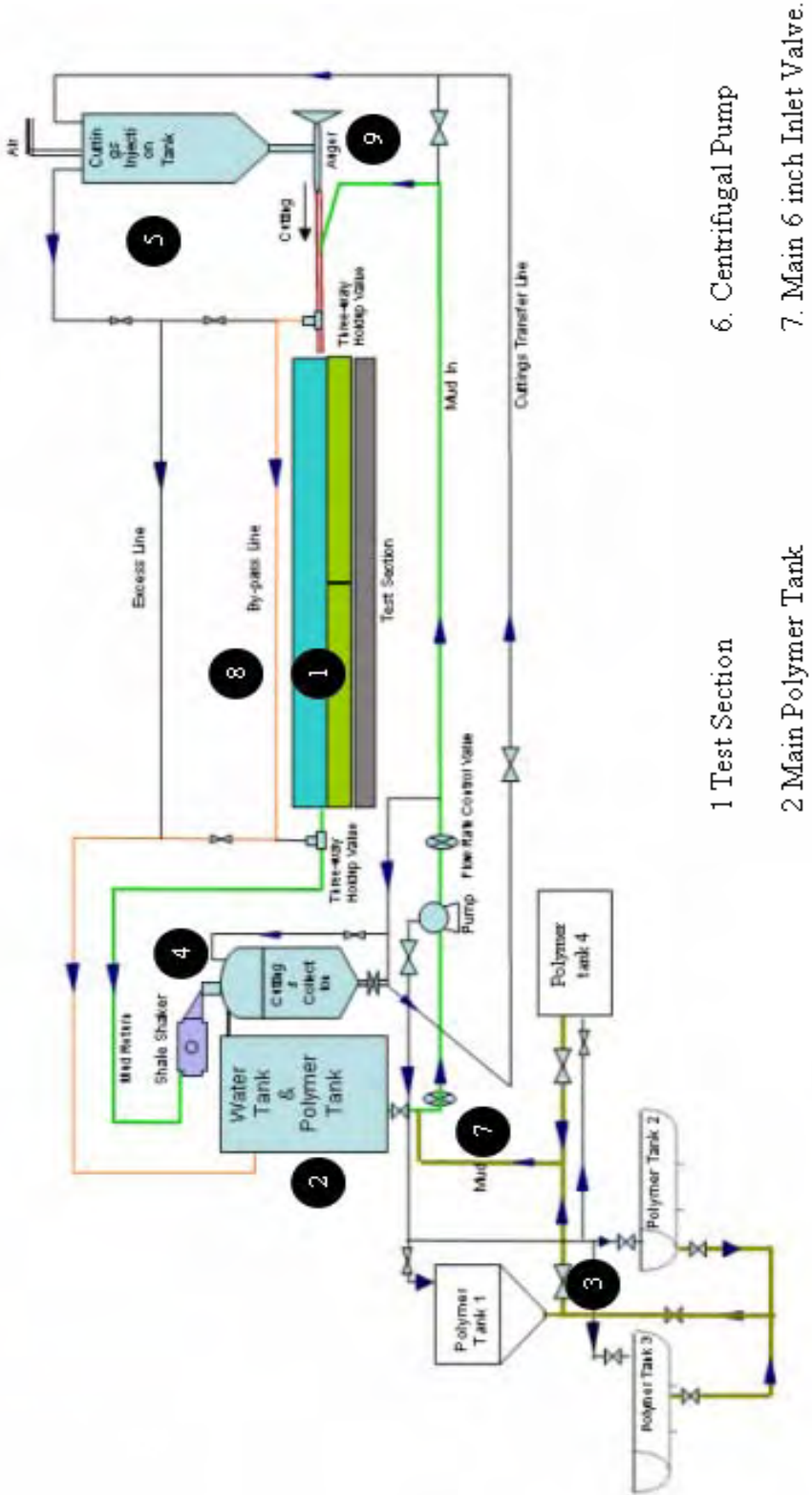

1 Test Section
2 Main Polymer Tank
3 Secondary Tanks
4 Cuttings Collection Tank
5 Cuttings Injection Tank
6. Centrifugal Pump
7. Main 6 inch Inlet Valve.
8. By-Pass Line
9. Auger

Figure 1. Schematic diagram of flow loop

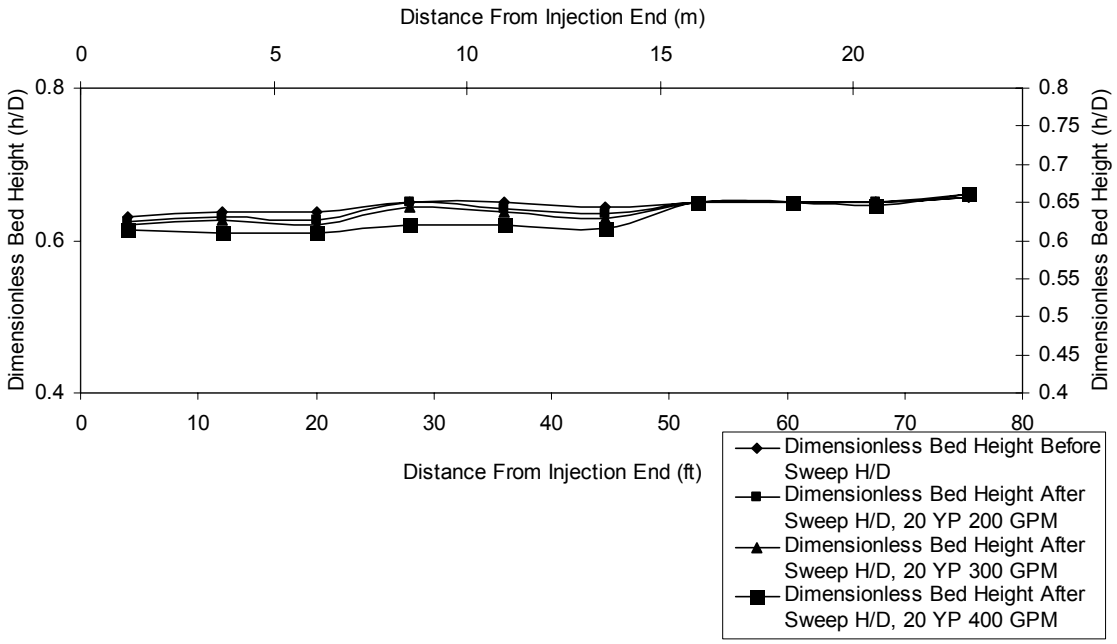

Figure 2: Dimensionless bed height for fluid with yield point of 20 Lb/100ft^2 at flow rates of 200 300 & 400 gpm.

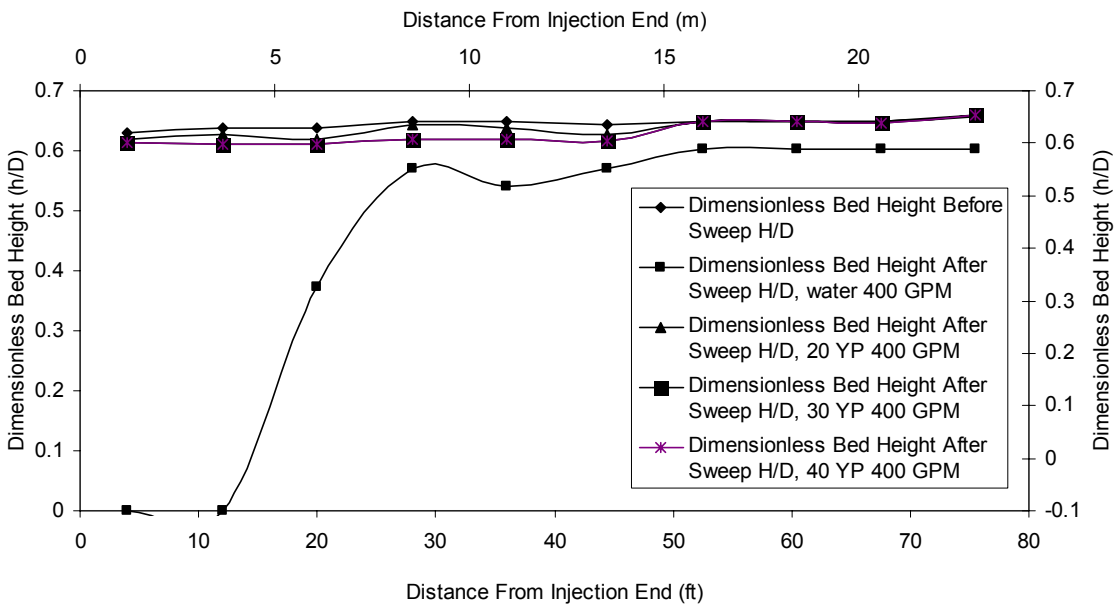

Figure 3: Dimensionless bed height, before and after sweeps, for water and fluids with yield points of 20, 30 & 40 lb/100ft^2 at 400 gpm, without any drill pipe rotation.

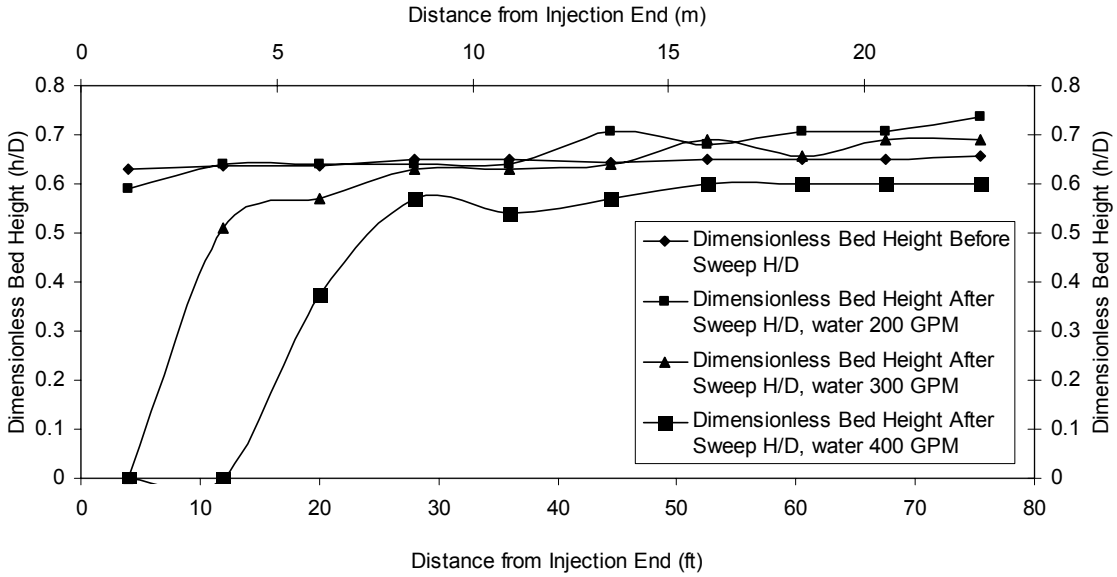

Figure 4: Dimensionless bed height for water at flow rates of 200 300 & 400 gpm

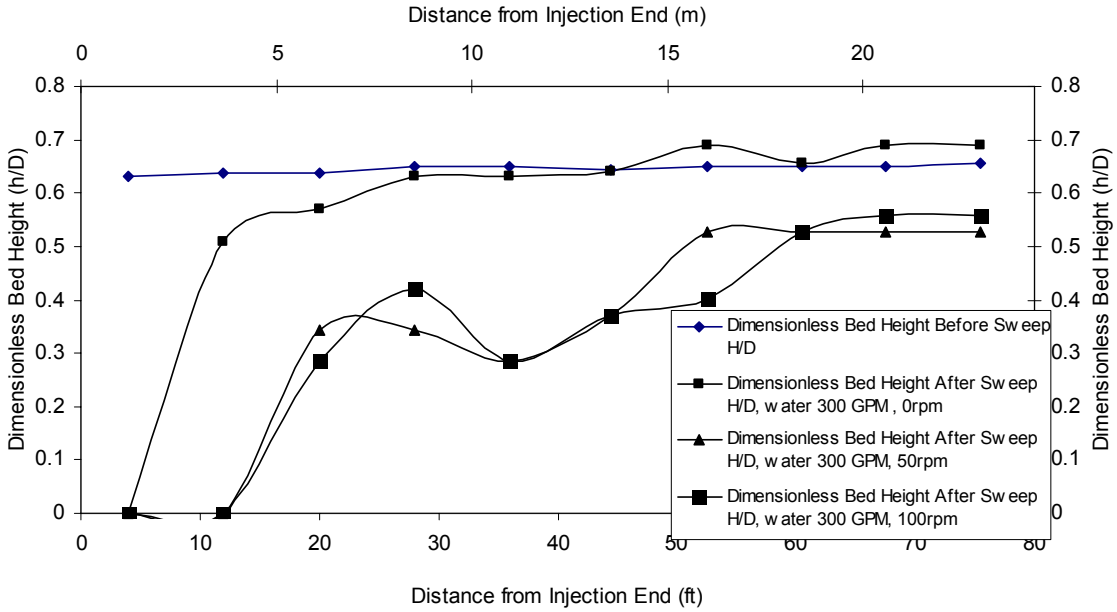

Figure 5: Dimensionless bed height comparison of water drill pipe rotational speeds of 0, 50, 100 rpm at 300 gpm.

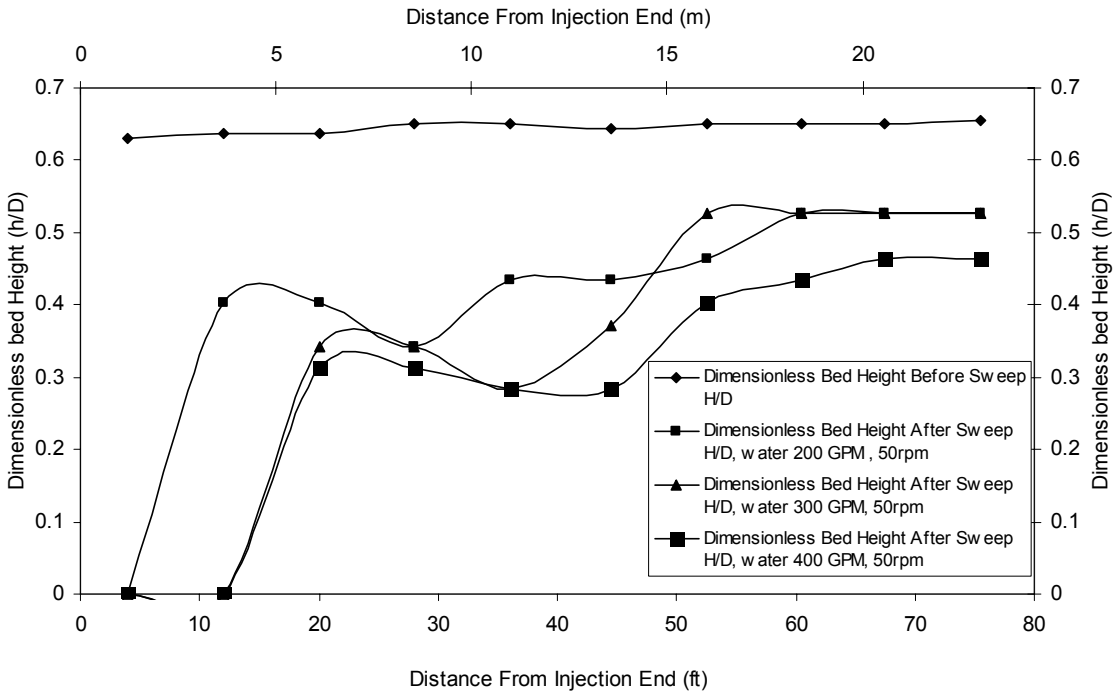

Figure 6: Dimensionless bed height comparison of water with flow rates of 200, 300, and 400 gpm, 50rpm.

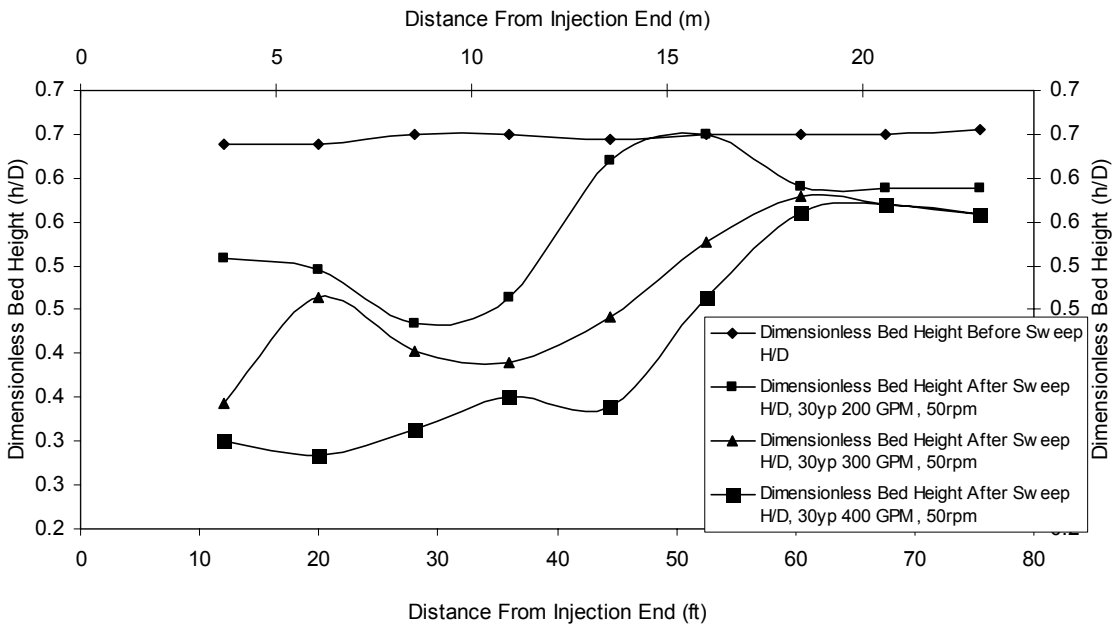

Figure 7: Dimensionless bed height comparison of fluid with yield point of 30 lb/100ft^2 with flow rates of 200, 300, and 400 gpm, 50rpm

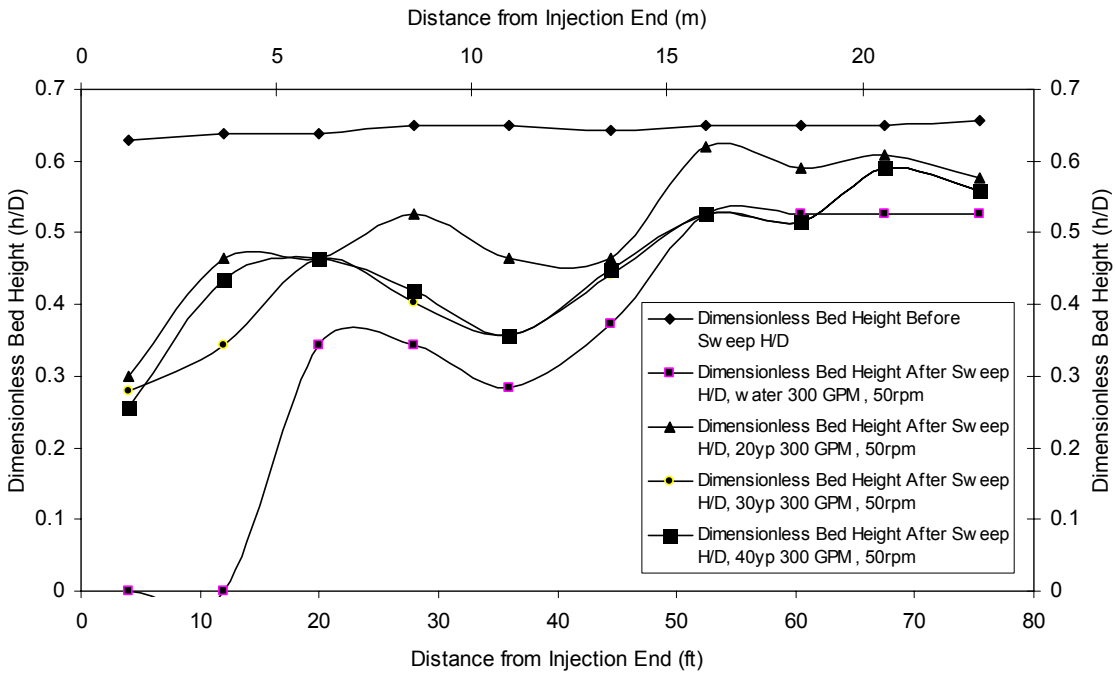

Figure 8: Dimensionless bed height comparison of water and fluids with yield points of 20, 30, 40 lb/100ft^2 with 50 rpm & 300 gpm.

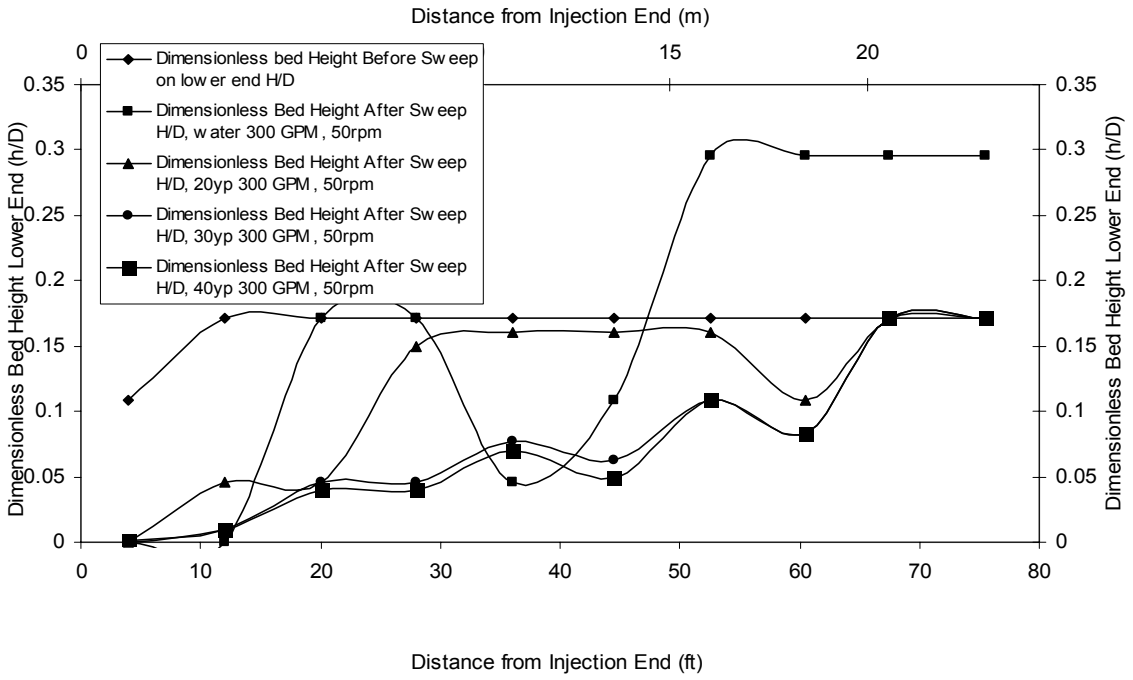

Figure 9: Dimensionless bed height comparison of bed heights in the lower end with, water & 20 yp, 30 yp, 40 yp fluid, 300 gpm & 50 rpm.

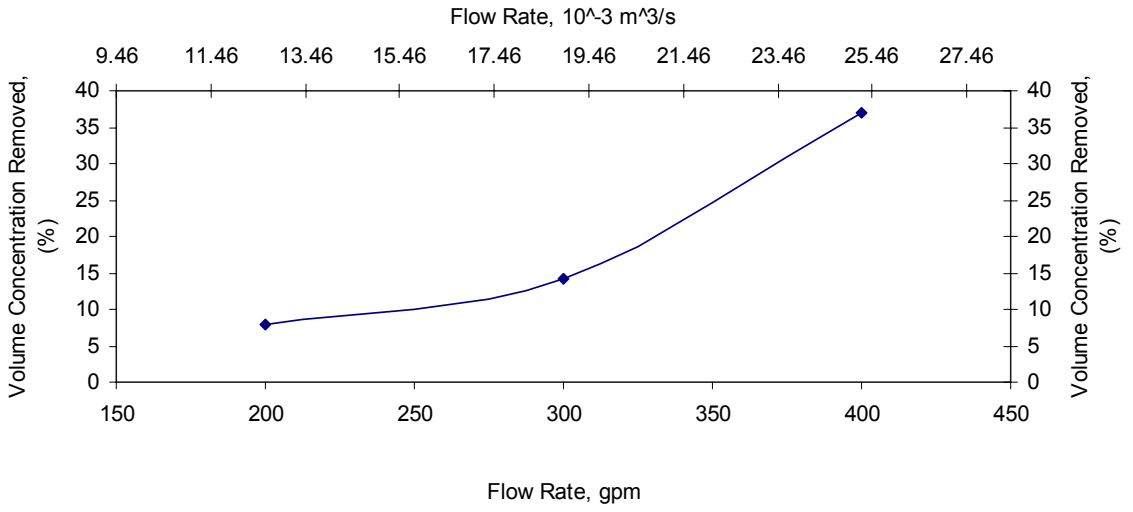

Figure 10: Volume Concentration removed comparison of 200, 300 & 400 gpm water 0 rpm

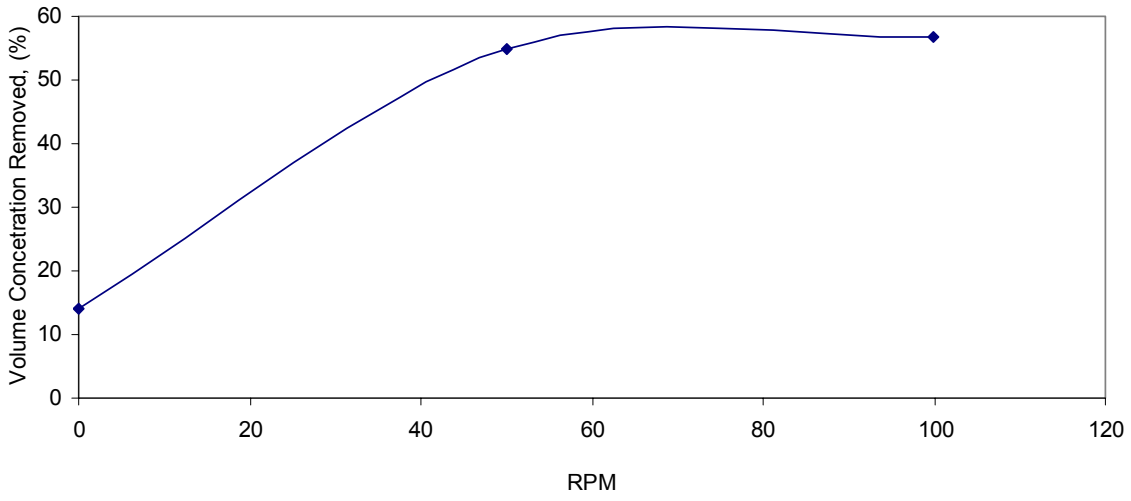

Figure 11: Volume concentration removed comparison of 300 gpm water 0, 50, 100 rpm.

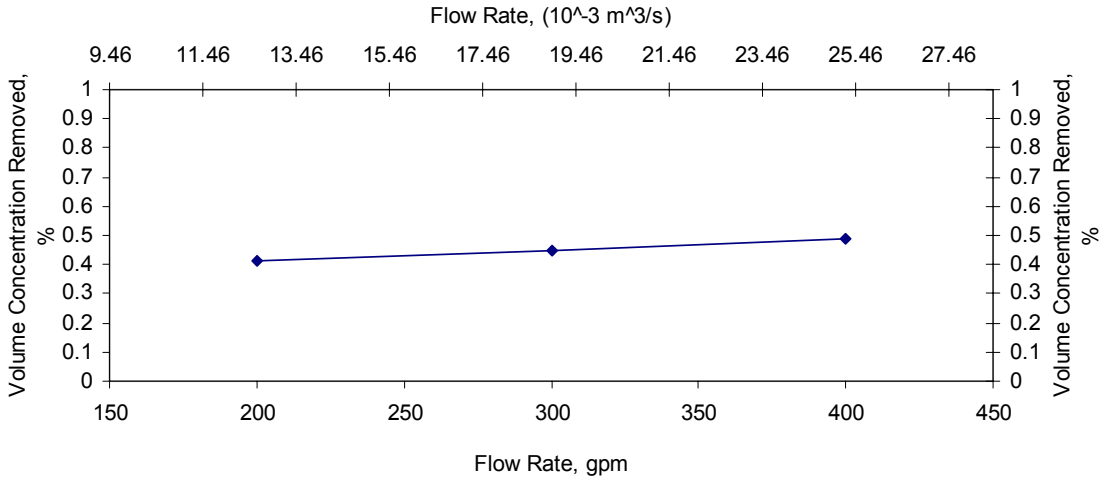

Figure 12: Volume concentration removed comparison of 200, 300 & 400 gpm, for fluid with yield point of 30 lb/100ft^2, 0 rpm.

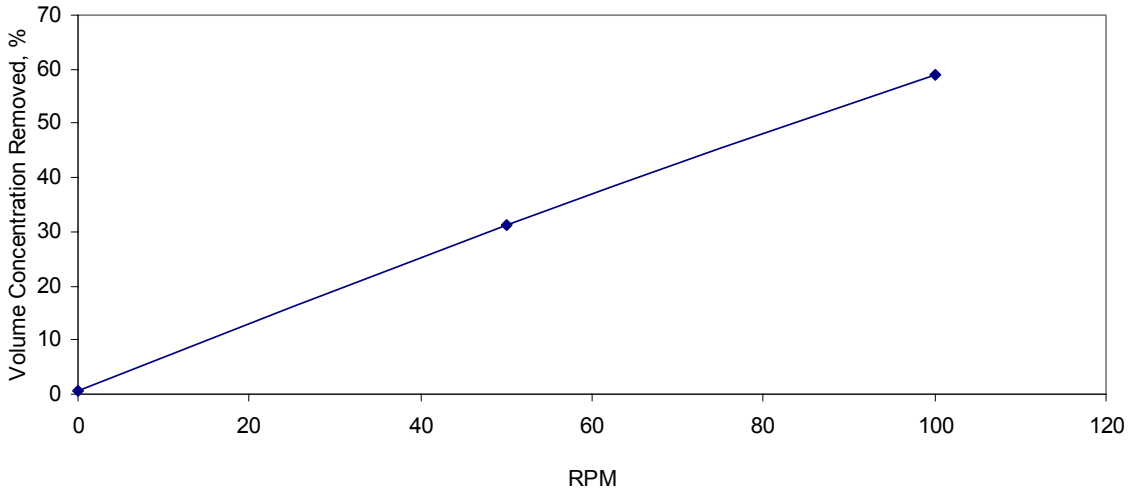

Figure 13: Volume concentration removed comparison of 300 gpm for fluid with yield point of 30 lb/100ft^2, 0, 50, 100 rpm

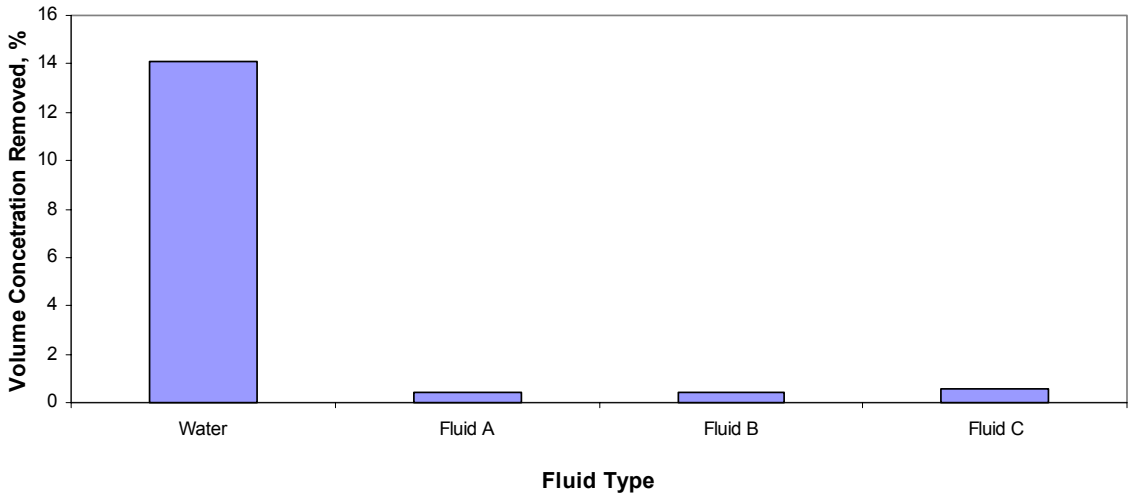

Figure 14: Volume concentration removed comparison of 300 gpm water & fluid with yield points of 20, 30, 40 lb/100ft^2 & 0 rpm

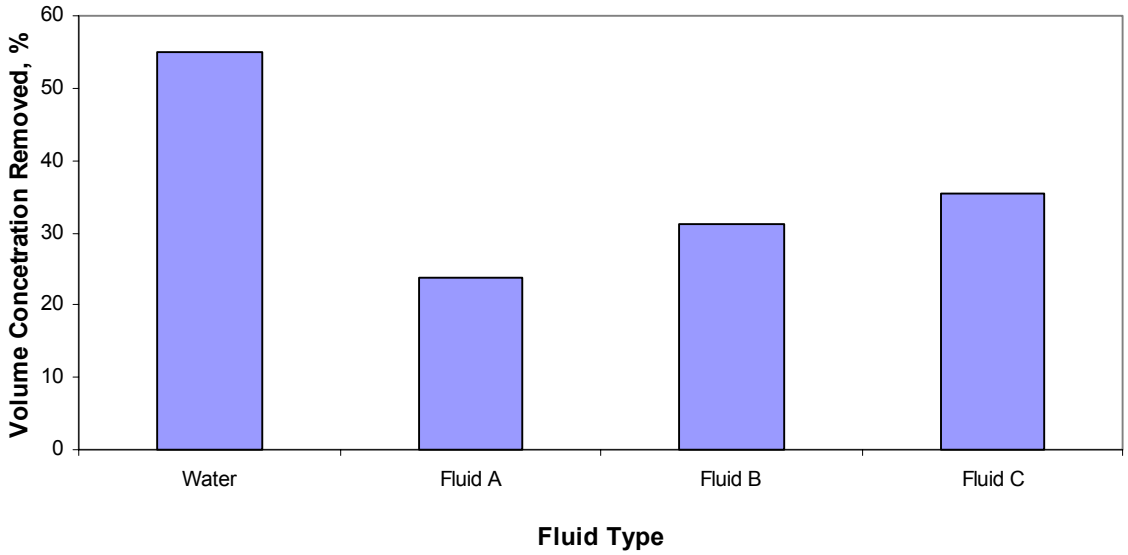

Figure 15: Volume concentration removed comparison of 300 gpm water and fluid with yield points of 20, 30, 40 lb/100ft^2, 50 rpm

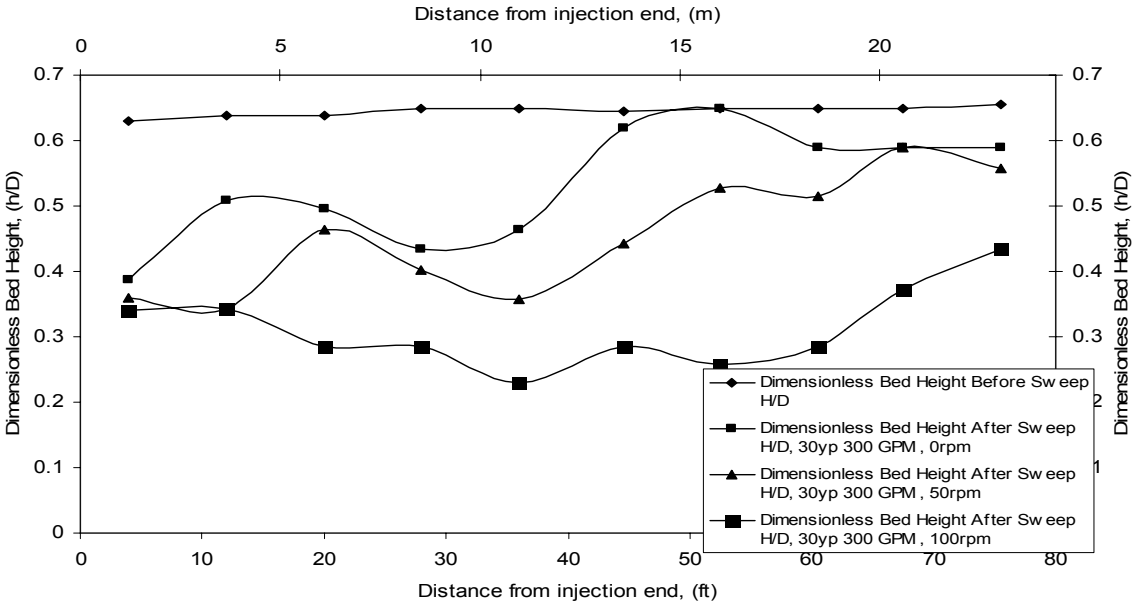

Figure 16: Dimensionless bed height comparison of fluid with yield point of 30 Lb/100ft^2 drill pipe rotational speeds of 0, 50, 100 rpm at 300 gpm.

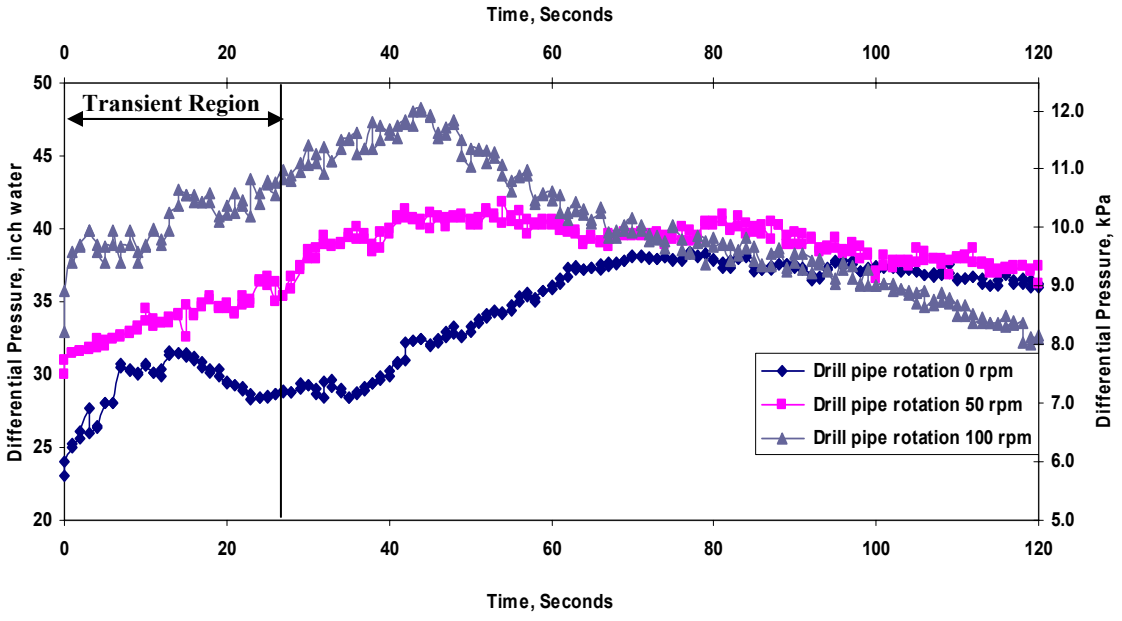

Figure 17: Differential Pressure versus time for water with different drill pipe rotational speeds of 0, 50 & 100 rpm at 300 gpm.

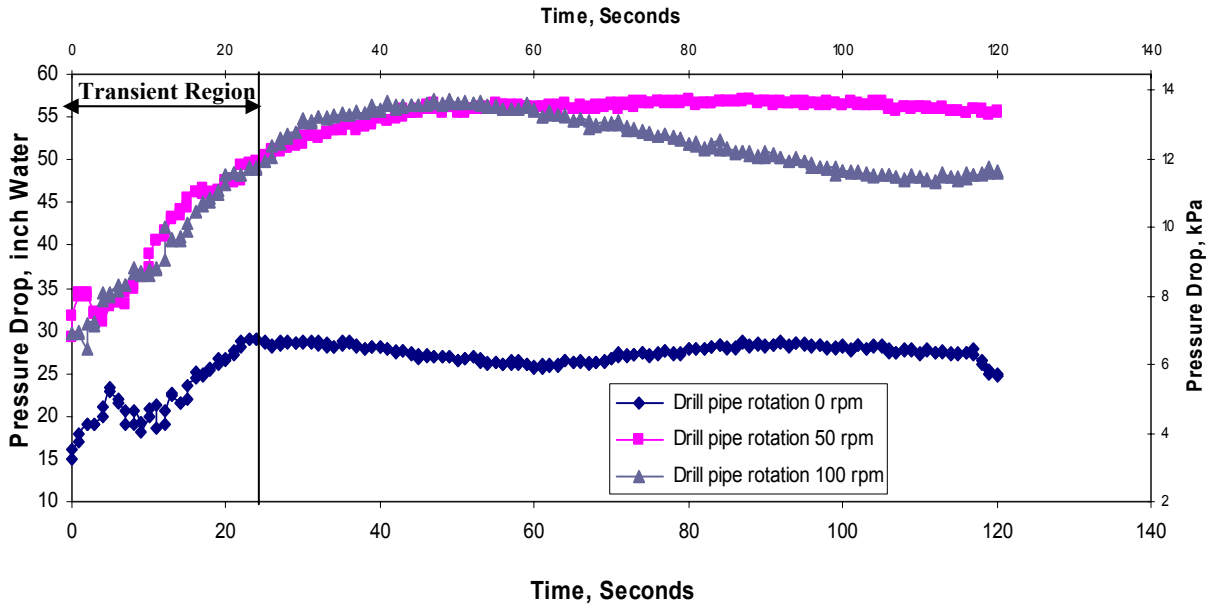

Figure 18: Differential Pressure versus time for fluid with yield point of 30 Lb/100ft^2 with drill pipe rotational speeds of 0, 50 & 100 rpm and flow rate of 300 gpm.

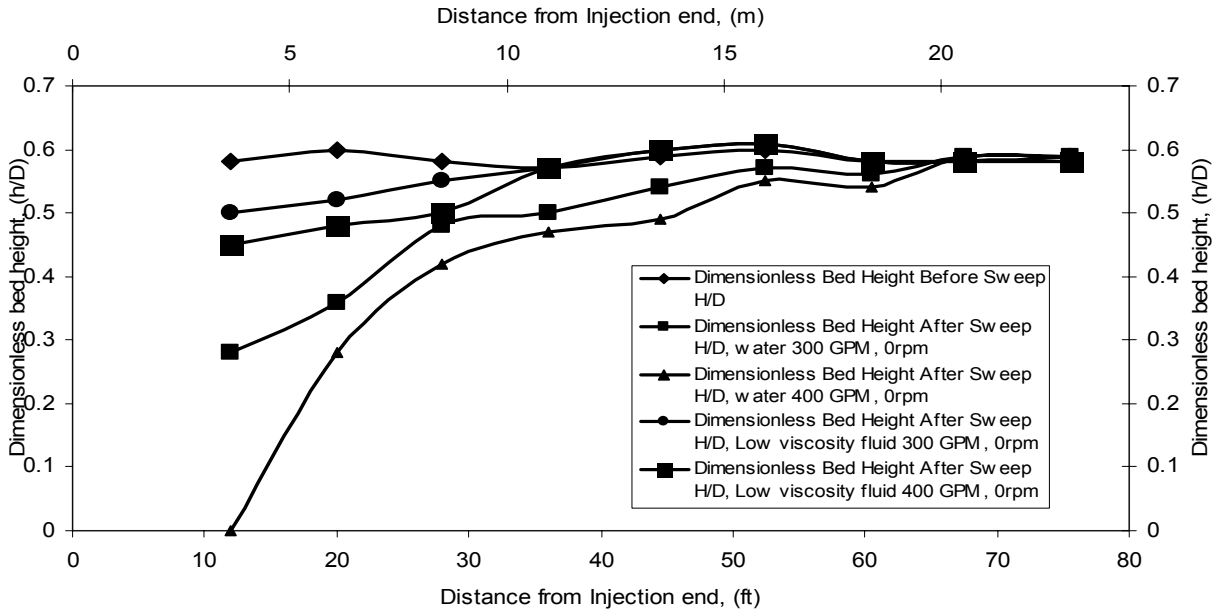

Figure 19: Dimensionless bed height for bed built with high viscosity fluid and using "sweeps" of water and low viscosity fluid.

Fluid	Flow Rate (Gpm)	Reynolds Number(Nre)	Fluid	Flow Rate (Gpm)	Reynolds Number(Nre)
Fluid A (20 Lb/100ft^2)	200	173.9	**Fluid A (40 Lb/100ft^2)**	300	216.3
Fluid A (30 Lb/100ft^2)	200	120.9	**Fluid D (Water)**	300	58208.1
Fluid A (40 Lb/100ft^2)	200	102.7	**Fluid A (20 Lb/100ft^2)**	400	571.5
Fluid D (Water)	200	38805.4	**Fluid A (30 Lb/100ft^2)**	400	408.6
Fluid A (20 Lb/100ft^2)	300	349.8	**Fluid A (40 Lb/100ft^2)**	400	365.1
Fluid A (30 Lb/100ft^2)	300	247.4	**Fluid D (Water)**	400	77610.8

Table2: Reynolds Number for different fluids at different flow rates.

Study on Effective Hole Cleaning Using "Sweeps" in Horizontal Well-bores

Test No: **Test Date:** **Conducted by: Sandeep Valluri**

Fluid Type _____ **Flow Rate (gpm)** _____ **Drill Pipe RPM** _____

ROP _____ **Bed Height(% of pipe)** _____

Test time **Start Time** _____ **Stop Time (Start Time+2mins)** _____

Differential Pressure before Cuttings Injection (inch of water)

With water **DP 1-3** _____ **DP 1-2** _____

With pipe rotation **DP 1-3** _____ **DP 1-2** _____

Cuttings Injection & Collection Tank Weights (lbs)

Before Injection **Collection** _____ **Injection** _____

At First holdup **Collection** _____ **Injection** _____
(After bed is formed)

Sample Data sheet

At Second holdup **Collection** _____ **Injection** _____
(After "Sweep")

After flush **Collection** _____ **Injection** _____
(Flush including by-pass)

Differential Pressure during sweep(inch of water)

With Fluid **DP 1-3** _____ **DP 1-2** _____

Bed Height Before & After Sweep

Reference Point	1	2	3	4	5	6	7	8	9	10
Distance	75.5	67.5	60.5	52.5	44.5	36	28	20	12	4
Side1(cm)										
Side2(cm)										
Height(cm)										

Reference Point	1	2	3	4	5	6	7	8	9	10
Distance	75.5	67.5	60.5	52.5	44.5	36	28	20	12	4
Side1(cm)										
Side2(cm)										
Height(cm)										

Other Observations or Notes:

Study of Cuttings Transport with Foam under Elevated Pressure and Elevated Temperature Conditions

Zhu Chen

Study of Cuttings Transport with Foam under Elevated Pressure and Elevated Temperature Conditions

INVESTIGATOR: Zhu Chen

INTRODUCTION:

The use of foams as drilling fluids has experienced a large growth in underbalanced drilling operations. Nevertheless, foam is a compressible, dynamically unstable non-Newtonian fluid with complex structures. There is a need to better characterize foam rheology.

Meanwhile, when foam is used to drill horizontal wells, since foam is a light-density fluid with high viscosity, it is still not well understood the efficiency of foam to carry cuttings out of the horizontal wellbore. No study has been conducted under simulated Downhole conditions. Therefore, this study will focus on cuttings transport with foam in horizontal configurations at Elevated Pressure and Elevated Temperature conditions. This study will help to better design foam drilling and clean-out operations.

OBJECTIVES:

1. Experimental investigation of foam rheology in pipes and annulus under ETEP conditions;
2. Experimentally determine and numerically predict volumetric requirements for effective cuttings transport with foam in horizontal wellbores without pipe rotation;
3. Develop a mechanistic cuttings-transport computer simulator;
4. Verify the computer simulator via comparisons with experimental data.

APPROACH:

1. Use both Advanced Cuttings Transport Facility (ACTF) and Foam Generator/Viscometer to study foam rheology;
2. Carry out experiments of cuttings transport with foam at EPET using ACTF;
3. Modeling cuttings transport with foam and developing a computer simulator.

PROJECT STATUS:

Foam rheology with both ACTF and Foam Generator/Viscometer has been completed; 85% of experiments of cuttings transport with foam under EPET conditions have been completed, the tests were carried out at temperatures from 80 to 170°F, and test pressure were from 100 to 400psig.

FUTURE WORK:

To complete cuttings transport with foam tests at EPET, and to develop a mechanistic model and computer program for pressure drop and cuttings concentration prediction.

DELIVERABLES:

1. Semi-annual Advisory Board Meeting progress reports;
2. Final project report;
3. Experimental data from cuttings transport and foam rheology studies at EPET conditions;
4. Mechanistic simulator of foam flow behavior and cuttings transport with foam.

Study of Cuttings Transport with Foam under Elevated Pressure and Elevated Temperature Conditions

Zhu Chen, The University of Tulsa, Drilling Research Projects

This report is prepared for TUDRP Advisory Board Meeting, May 23-24, 2005, Tulsa-Oklahoma.

1. Introduction

The major objectives of this project are: 1) to experimentally investigate foam rheology in pipes and annulus under ETEP conditions; 2) to experimentally determine and numerically predict volumetric requirements for effective cuttings transport with foam in horizontal wellbores, initially without pipe rotation; 3) to develop a mechanistic cuttings-transport computational tool; and 4) verification of the computational tool for cuttings transport with foam prediction via comparisons with experimental data from the ACTF Flow Loop.

The following tasks have been undertaken in the past half a year:

- Polymer-based (HEC) foam rheology tests using a rotational viscometer (Foam Generator/ Viscometer)
- Data processing of foam rheology tests using Pipe Viscometer (ACTF)
- Foam hydraulic simulator for annular foam flow simulation
- Cuttings Transport with Foam tests at EPET conditions

2. Project Status

		2002	2003			2004			2005	Status
		Fall	Spring	Summer	Fall	Spring	Summer	Fall	Spring	
Literature Review	Foam Rheology									95%
	Cuttings Transport with Foam									95%
Laboratory Tests	Weatherford Foam Properties Evaluation Tests									100%
	Foam Rheology Tests With Foam Generator/Viscometer									100%
ACTF Flow Loop tests	Foam Rheology Tests									90%
	Cuttings Transport With Foam Tests									85%
Theoretical Modeling	Mechanistic Model Development									60%
	Computer Simulator									30%

3. Foam Rheology Characterization

To study cuttings transport efficiency of foam, the rheology of foam needs to be well characterized and understood, because it is one of the key parameters that affects cuttings transport. However, foam rheology is very complex, it can be affected by foam quality (V_{gas}/V_{foam}), liquid phase rheology, foam generation method, temperature and pressure, wall slip, etc. Therefore, a sizeable effort has been spent to characterize the rheology of foam using both pipe viscometer (ACTF) and rotational viscometer (Foam Generator/Viscometer).

Three parts will be covered in this section, which are: i) Results of foam rheology measurements using ACTF pipe viscometer. The experiments were done during fall, 2004, but detailed data analysis is presented here; ii) Results of foam rheology measurements using rotational viscometer (Foam Generator/Viscometer); iii) Comparisons of foam rheology measurements using the two different viscometers (pipe viscometer versus rotational viscometer).

3.1 Foam Rheology Measurements using ACTF

The Advanced Cuttings Transport Flow Loop (developed under the auspices of ACTS-JIP) of the University of Tulsa was utilized for this foam rheology experimental study. Details of ACTS Flow Loop and test procedure for foam rheology tests can be found in the previous ABM reports. Foam rheology tests were conducted during 2004 to study foam rheological properties with varying foam qualities and polymer concentrations. Liquid hydroxylethylcellulose (HEC) solutions with different polymer concentrations (0%, 0.25% and 0.5%) were used as the liquid phase. For all the tests, a commercial surfactant (KLEAN-FOAM) was injected at 1% v/v liquid flow rate. Three foam qualities (70%, 80% and 90%) were considered. Test pressure and temperature were maintained at 100 psig and 80°F. For each test, gas and liquid flow rates were predetermined to maintain in-situ foam velocities of approximately 1 ft/s, 2 ft/s, 3ft/s and 4 ft/s. Under steady-state conditions, static pressure, temperature and frictional pressure drop were measured and recorded.

HEC Polymer-based Fluid Rheology. Before conducting foam rheology experiments, liquid HEC polymer was mixed with water at desired liquid phase concentrations (0.25% and 0.5% v/v) in the 100-bbl tank. Then rheology of the liquid phase was measured with a rotational viscometer. Power Law rheological parameters were obtained for two different polymer fluids, which were shown in Table 3.1.1. Results show that the liquid phase consistency index "K_L" decreases significantly as polymer concentration decreases while the flow behavior index "n_L" decreases very little with the decrease in polymer concentration.

Table 3.1.1 Rheology of Polymer Fluids Using Chan 35 Viscometer

Formulation	Reading						Power Law Model
	θ (600)	θ (300)	θ (200)	θ (100)	θ (6)	θ (3)	
0.25% Liquid HEC Polymer Fluid	8	4.1	3.2	1.6	0.2	0.1	$\tau = 0.0143\ \gamma^{0.806}$
0.5% Liquid HEC Polymer Fluid	13.5	7.5	5	3	0.3	0.2	$\tau = 0.0255\ \gamma^{0.799}$

Foam rheology tests were carried out at static pressure 100 psig and temperature 80°F. Plots of wall shear stress versus observed nominal Newtonian wall shear rate are presented in previous report, but for the sake of reference, a sample plot for 70% quality foams is presented in Fig. 3.1.1. In the plot, there are nine curves, representing three polymer concentrations in three different pipes (2”, 3” and 4” pipes). The plots clearly show that polymer does affect foam rheology. Significant rheological variations exist between aqueous foams and polymer-based foams. More viscous foams can be generated with higher polymer concentration. In addition, the effect of wall slip can be observed from the plots. Three distinct flow curves are observed for the 2”, 3” and 4” pipe sections for the same foam.

Foam Rheology without Considering Wall Slip. When non-slip boundary conditions are assumed, theoretically, foam rheology can be determined with only one single-size pipe viscometer at different flow rates, and rheology is independent of pipe diameter. Alternatively, experimental data of wall shear stress versus observed wall shear rate in the 2”, 3” and 4” pipes should fall in a single curve. For Power Law fluid, the generalized consistency index, K’, and flow behavior index, N, are constant and can be obtained from the flow curve plot. Also, the consistency index, K can be obtained from:

$$n = N = \frac{d\ln(\tau_W)}{d\ln(8v/D)}, \quad K = K'\left(\frac{4N}{3N+1}\right)^N$$

Figure 3.1.2 shows an example of the single flow curve on logarithmic scale for 80% quality foam with 0.25% polymer concentration. A Power Law rheological model best fit the experimental data of all foams used in this investigation. It is found that for a given foam quality, an increase in polymer concentration results in only a small change in foam flow behavior index, and this is probably because the polymer concentration (or liquid phase apparent viscosity) is low. For the sake of simplicity, foam flow behavior index is considered constant for a given foam quality. A summary of the results is given in Table 3.1.2. It can be found that with an increase in polymer concentration, foam consistency index, K_F, increases. As foam quality increases, the flow behavior index, n_F, decreases.

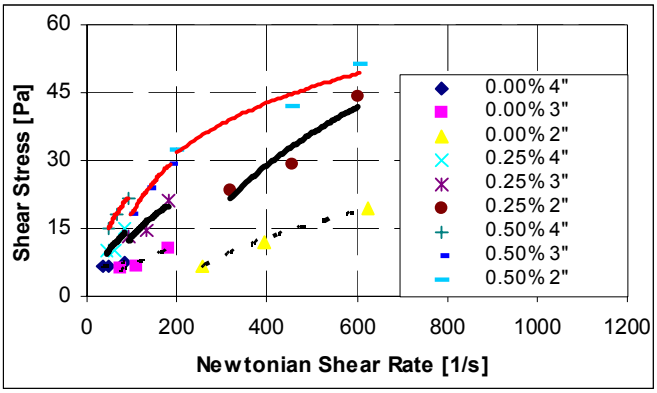

Fig. 3.1.1 Wall Shear Stress versus Observed Nominal Newtonian Shear Rate (Γ= 70%, Polymer Conc. = 0, 0.25%, 0.5%)

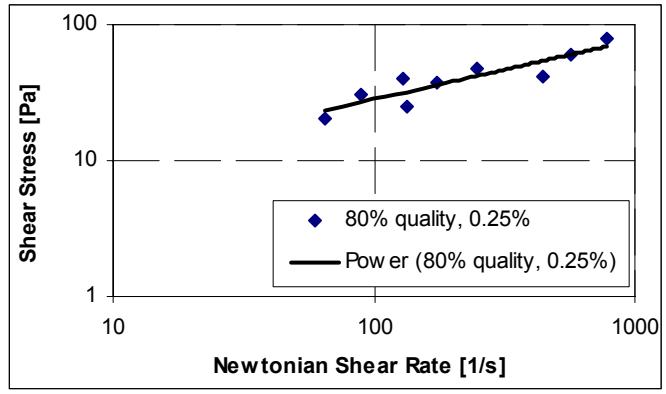

Fig. 3.1.2 Wall Shear Stress versus Observed Nominal Newtonian Shear Rate (Γ= 80%, Polymer Conc.= 0.25%)

Table 3.1.2 Foam Rheological Parameters without Considering Wall Slip

Foam Type	n_F	K' (Pa.s^n)	K_F (Pa.s^n)
70% Aqueous Foam	0.45	0.94	0.835
70% 0.25% Polymer Foam	0.45	2.46	2.185
70% 0.5% Polymer Foam	0.45	3.86	3.429
80% Aqueous Foam	0.40	2.23	1.959
80% 0.25% Polymer Foam	0.40	4.81	4.235
80% 0.5% Polymer Foam	0.40	7.85	6.911
90% Aqueous Foam	0.36	4.26	3.732
90% 0.25% Polymer Foam	0.36	7.98	6.991
90% 0.5% Polymer Foam	0.36	10.94	9.584

Foam Rheological Parameters Correlation. Having studied various parameters that affect polymer based foam rheology; correlations have been developed to predict rheology of these foams for practical field applications. A method used in the field of Colloid Science and Suspension Rheology[2] has been adopted here for foam rheology predictions. Accordingly, the foam consistency index "K_F" is correlated to the liquid phase apparent viscosity and foam quality by:

$$\frac{K_F}{\mu_L} = e^{a\cdot\Gamma^2 + b\cdot\Gamma + c} \quad ; \quad n = -0.45\Gamma + 0.7633$$

Where "a", "b" and "c" are functions of liquid phase apparent viscosity, μ_L, which is evaluated at 300 s^{-1}. The unit of μ_L is presented in cP. "a", "b" and "c" are given by:

$$a = (-0.533\mu_L^2 + 3.6735\mu_L - 13.546)$$
$$b = (0.8926\mu_L^2 - 6.5877\mu_L + 29.966)$$
$$c = (-0.3435\mu_L^2 + 2.5273\mu_L - 14.218)$$

Here the apparent viscosity is chosen instead of the liquid consistency index "K_L" because liquid consistency index is strongly interrelated with the flow behavior index. In other words, the viscosity of the polymer base liquid can be better characterized by the apparent viscosity at shear rate of 300 s^{-1}. Therefore, in this study, foam consistency index "K_F" is correlated with foam quality and liquid phase apparent viscosity.

This correlations agree with rheology measurement in this study. To assess the applicability of these correlations for other applications, comparisons are made between predictions and published data by Khade et al.[1]. Table 3.1.3 compares measured apparent viscosity (γ = 511 s^{-1}) of guar foam (guar concentration of 20 lb/Mgal, Γ = 70% and 80%) at different temperatures by using the proposed correlations.

Table 3.1.3 Predicted Foam Apparent Viscosity (γ=511 s^{-1}) Vs. Measurements from a Previous Study[1] (Guar Conc. = 20lb/Mgal, or 2.4 kg/m^3)

Quality		70%		80%	
T (°F)	$\mu_{L,300}$ (cP)	Measured (cP)	Predicted (cP)	Measured (cP)	Predicted (cP)
100	9.22	80.3	101.7	179.2	218.1
125	8.04	73.5	82.3	154.7	165.7
150	6.74	57.5	67.8	128.3	131.3
175	4.99	38.9	54.5	103.6	105.4
200	5.40	39.5	57.2	92	110.1

It can be seen that the predictions are in good agreement with the measured data. This justifies the applicability of the model. The proposed correlation is valid when the apparent liquid phase viscosity at 300 s^{-1} is between 1 and 8.1 cP.

This correlation gives good rheological parameter prediction when foam quality is within 70% to 90%, and liquid phase apparent viscosity is between 1 to 8.1cP. If we have to estimate K_F, n_F values for foams with quality higher than 90% or lower than 70%, it is recommend to correlate K_F, n_F only with foam quality based on the measurement from Table 3.1.2 for three foams separately, and don't include liquid phase apparent viscosity in the correlations. Therefore, for aqueous foam, 0.25% and 0.5% HEC polymer foams, K_F can be correlated with foam quality, Γ, as:

$$\frac{K_{F,aqueous}}{1} = e^{-10.47\cdot\Gamma^2+24.27\cdot\Gamma-12.03}; \quad \frac{K_{F,0.25\%}}{4.7} = e^{-8.09\cdot\Gamma^2+18.77\cdot\Gamma-9.95}; \quad \frac{K_{F,0.5\%}}{8.1} = e^{18.78\cdot\Gamma^2+35.19\cdot\Gamma-16.29}.$$

3.2 Rheology of Polymer Foams with Rotational Viscometer (Foam Generator/Viscometer)

Foam rheology experiments were also conducted using a Foam Generator and Viscometer Apparatus and Process (Fig. 3.2.1). This process utilizes a flow-through Couette viscometer with original smooth cup-rotor assembly and with two sets of roughened cup-rotor assemblies. This apparatus generates foam with controllable properties and allows the foam to flow through a modified Couette-type rotational viscometer. The flow rate is regulated so that rheology of the foam is determined under constant foam quality, pressure and temperature. A visualization cell coupled to an image acquisition device permits structure characterization of the foam in parallel with the rheological measurements. Besides the original smooth cup-rotor assembly, the two sets of cup-rotor assemblies (Table 3.2.1) with different wall roughnesses were used to investigate the effect of wall slip on foam rheology measurements.

Table 3.2.1 Surface Roughnesses of Cup-Rotor Assemblies

		Average Roughness [μm]	Standard Deviation of Roughness [μm]
Smooth Cup-Rotor Assembly	Cup	3.1	3.7
	Rotor	2.0	2.4
Less Roughened Cup-Rotor Assembly #1	Cup	13.0	15.6
	Rotor	38.0	45.5
More Roughened Cup-Rotor Assembly #2	Cup	21.0	25.6
	Rotor	44.0	50.0

The equipment has been described in detail in previous ABM reports, and it is basically unchanged since last ABM. The only difference is the installation of an electronic scale that used to measure the foam flow rate through the viscometer. It is important to allow enough flow through the viscometer to minimize the effects of foam drainage and axial flow on rheology measurements.

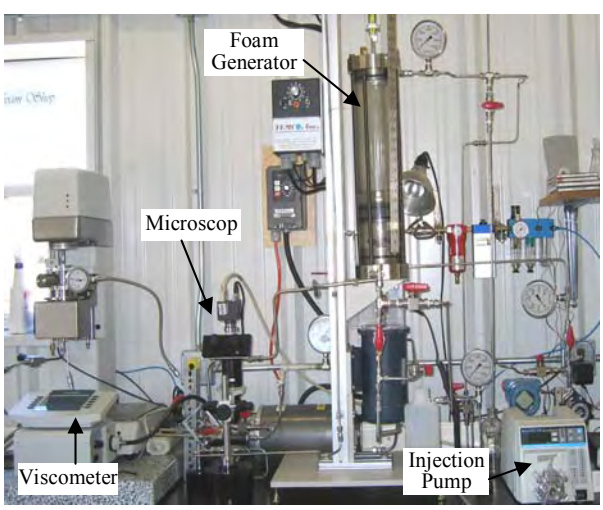

Fig. 3.2.1 Foam Generator/ Viscometer

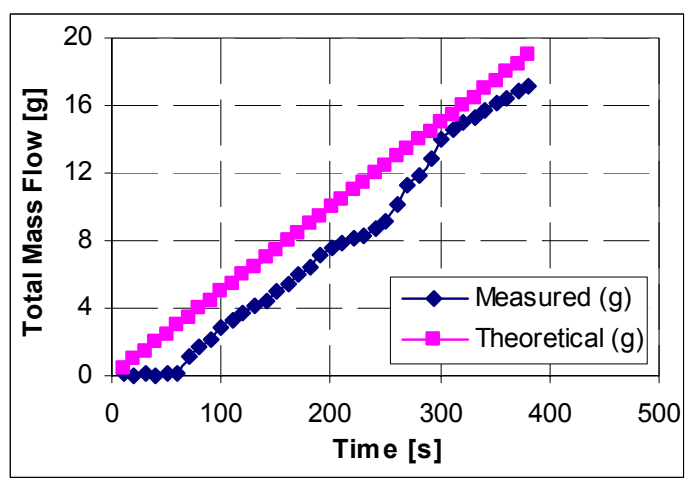

Fig. 3.2.2 Total Mass Flow Through The Viscometer Versus Time for an 80% Quality 0.25% Polymer Foam

The appropriate foam flow rate through the viscometer was determined to be 15 mL/min. This corresponds to a mass flow rate of 15*(1-Γ) g/min. Figure 3.2.2 shows a sample data (80% quality, 0.25% polymer foam measured with roughened cup-rotor assembly #2) of the total mass of foam flowing through the viscometer versus time. Two curves, which represent the theoretical and measured total mass flows, are plotted on the same set of axes. Foam rheology measurement with the viscometer starts when the two curves become approximately parallel by adjusting the needle valve position. For this particular test, the actual foam mass flow rate was maintained at approximately 3 g/min (i.e. 15 mL/min).

Test Matrix. A test matrix for the rheology experiments is presented in Table 3.2.2. Test temperature and pressure were maintained at 25°C and 25 psig. HEC polymer concentration varied from 0.25% to 0.5%. Three foam qualities (70%, 80% and 90%) were tested. Surfactant concentration was 1% by volume.

Table 3.2.2 Test Matrix for Foam Rheology Experiments

	Test Set #1	**Test Set #2**	**Test Set #3**
Measurement Assembly	Smooth Assembly	Less Roughened Assembly #1	More Roughened Assembly #2
Foam Formulation	Air + water + surfactant (1% v/v Weatherford KLEAN-FOAM)+ polymer (Weatherford KLEAN-VISH)		
Polymer concentration	0, 0.25%, 0.5%	0, 0.25%, 0.5%	0, 0.25%, 0.5%
Foam Quality	70%, 80%, 90%	70%, 80%, 90%	70%, 80%, 90%
T (°C)	25	25	25
P (psig)	25	25	25

Base Fluid Rheology. Two concentrations (0.25% and 0.5% v/v) of HEC polymer fluids were prepared, and the rheology of the liquid phase was the same as it was given in Table 3.1.2.

Foam Rheology Measurements. Polymer-based foam rheology was measured using both smooth and roughened cup-rotor assemblies. Measured shear stress readings were corrected using calibration curves for each shear rate. Figures 3.2.3 and 3.2.4 show rheologies of 70%, 80% and 90% quality foams (0.25% and 0.5% polymer concentration, respectively) using the smooth cup-rotor assembly. The foams behave like shear thinning fluids and measured shear stresses increase with foam quality. This means foam apparent viscosity increases with foam quality. Similarly, with the increase of polymer concentration from 0.25% to 0.5%, measured shear stresses increase. This means foam apparent viscosity increases with polymer concentration. A Power-Law rheological model was used to fit the measured data.

Measurements obtained using smooth and roughened cup-rotor assemblies can be used to examine wall slip

phenomena and provide improved rheological measurements. Foam rheology measurements obtained with the roughened cup-rotor assembly #1 are presented in Figs. 3.2.5 and 3.2.6. These plots show that at a given shear rate, the shear stresses measured with the roughened cup-rotor assemblies are higher than those measured with the smooth assembly. This can be explained by the wall slip since the cup-rotor assemblies differ only in their surface roughnesses. Experiments were also performed using a more roughened assembly (assembly #2). Figures 3.2.7 and 3.2.8 show flow curves obtained using cup-rotor assembly #2. Again, results show that at a given shear rate, the shear stresses measured with the roughened cup-rotor assemblies are higher than those measured with the smooth assembly.

For low foam quality (70%), it seems that the measured shear stress with cup-rotor assembly #2 is the highest. This means that the more roughened cup-rotor assembly is effective in minimizing the wall slip at low foam qualities. Cup-rotor assembly #2 has wider and deeper grooves, which make it possible to contain more liquid in the grooves. Nonetheless, the differences between the measured stresses are not significant for low quality foams.

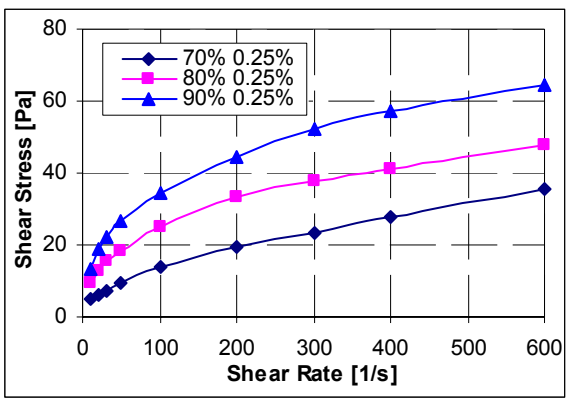

Fig. 3.2.3 Polymer Foam (0.25%) Rheology Measured Using Smooth Cup-Rotor Assembly

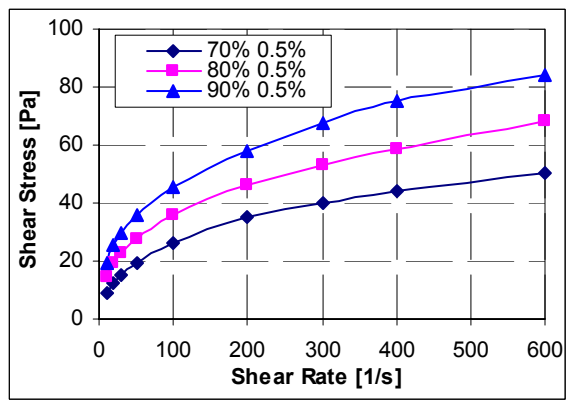

Fig. 3.2.4 Polymer Foam (0.5%) Rheology Measured Using Smooth Cup-Rotor Assembly

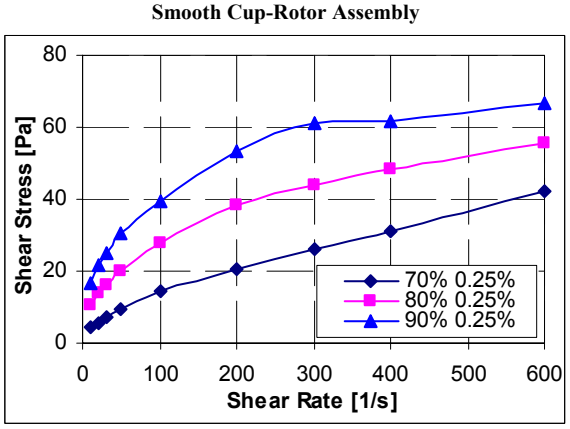

Fig. 3.2.5 Polymer Foam (0.25%) Rheology Measured Using Less Roughened Cup-Rotor Assembly # 1

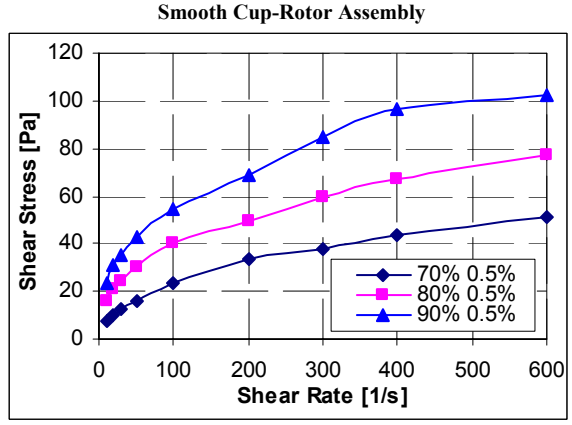

Fig. 3.2.6 Polymer Foam (0.5%) Rheology Measured Using Less Roughened Cup-Rotor Assembly # 1

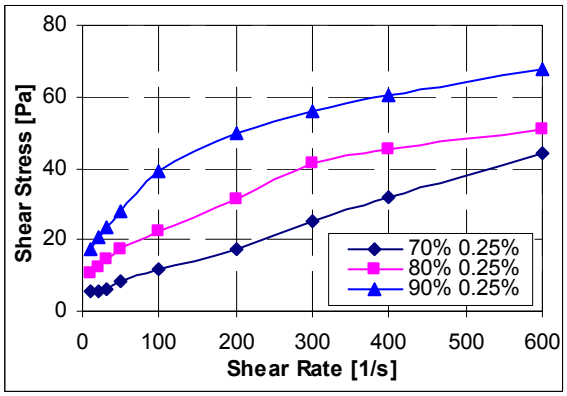

Fig. 3.2.7 Polymer Foam (0.25%) Rheology Measured Using More Roughened Cup-Rotor Assembly #2

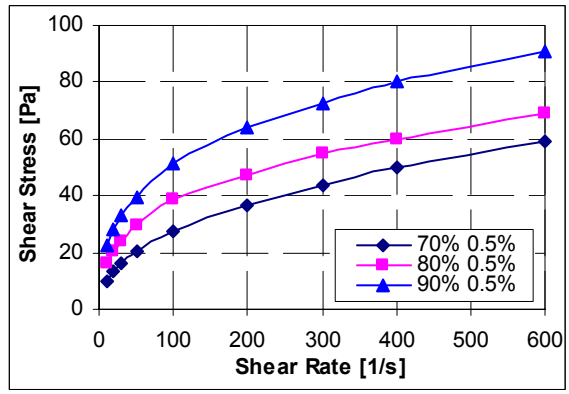

Fig. 3.2.8 Polymer Foam (0.5%) Rheology Measured Using More Roughened Cup-Rotor Assembly #2

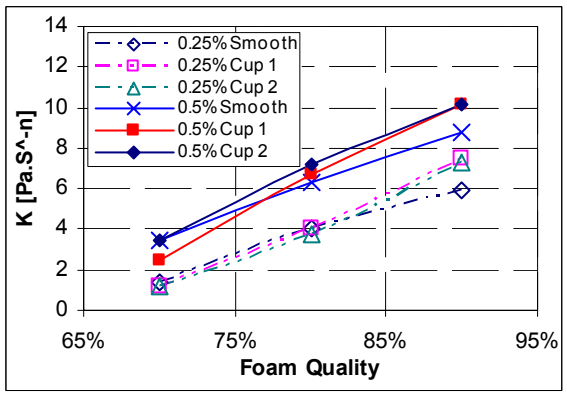

Fig. 3.2.9 Flow Consistency Index Versus Foam Quality, Polymer Concentrations and Cup-Rotor Assemblies

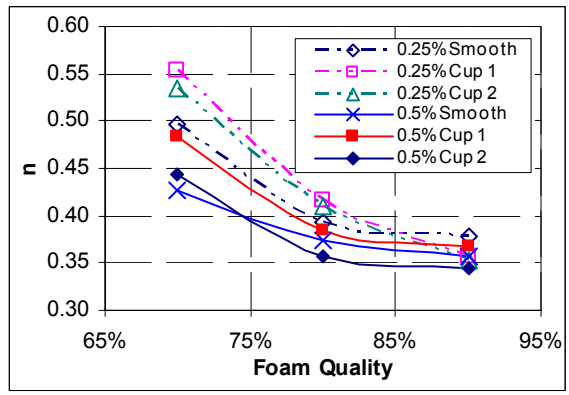

Fig. 3.2.10 Flow Behavior Index Versus Foam Quality, Polymer Concentrations and Cup-Rotor Assemblies

Careful examination of flow curves for 80% and 90% quality foams indicates that the shear stresses measured using cup-rotor assembly #1 are higher than those obtained using assembly #2. This is possibly because of the differences in the liquid slip layer thickness. For higher quality foams (80% and 90%), the slip layer is relatively thin. Even the shallow grooves of cup-rotor assembly #1 are sufficient to enclose the thin liquid films. The groove width of the cup-rotor assembly #1 is only 254μm (0.01 inch), which is much smaller than the groove width of assembly #2 (635μm or 0.025 inch). As a result, assembly #1 has more protrusions per contact area than assembly #2. The greater the number of protrusions, the more effectively they can immobilize foams on the surfaces and thus reduce wall slip.

Flow curves of foams with different qualities and polymer concentrations that were measured with different cup-rotor assemblies were further processed. All flow curves were fitted with Power-Law rheological models. Figures 3.2.9 and 3.2.10 present the flow consistency index, K, and flow behavior index, n, values. It can be seen from the plots that: i) for foams with the same polymer concentration but measured with different cup-rotor assemblies, although differences in foam rheological parameters K and n are observed, these values are still scattered around a single curve; ii) as polymer concentration changes from 0.25% to 0.5%, K and n values

change dramatically, which means that polymer concentrations play a more pronounced role in rheology than wall slip; iii) as foam quality changes, significant changes in K and n values are observed and these variations are also more pronounced than wall slip effect; iv) for a given polymer concentration, the consistency index increases as the foam quality increases while n decreases as foam quality increases.

Results indicate that for low quality foams (70-80%), the flow behavior index, n, is sensitive to polymer concentration and foam quality. However, for high quality foams (80-90%), n is less sensitive to polymer concentration and foam quality.

Results of this study show that surface roughness reduces wall slip and improves polymer-based foam rheology measurements. The measured shear stress difference using different cup-rotor assemblies is mostly within 30%. However, as foam quality increases from 70% to 90%, the measured shear stress increases more than 100%. Also, if we compare the present results with previous study on foam without polymer, we can find that as polymer concentration changes from 0 to 0.5%, the measured shear stress increases significantly. Based on the foam rheology measurements obtained from different cup-rotor assemblies, it can be concluded that wall slip does affect foam rheology measurements. However, foam quality and liquid phase rheology are more important in determining the bulk foam rheology.

Bubble Characterization Results. Bubble size analysis was performed from photographs of the foams. The mean and standard deviation of bubble size distribution were determined, taking into consideration the magnification. Figure 3.2.11 shows images of 0.25% polymer based foams with 70%, 80% and 90% qualities.

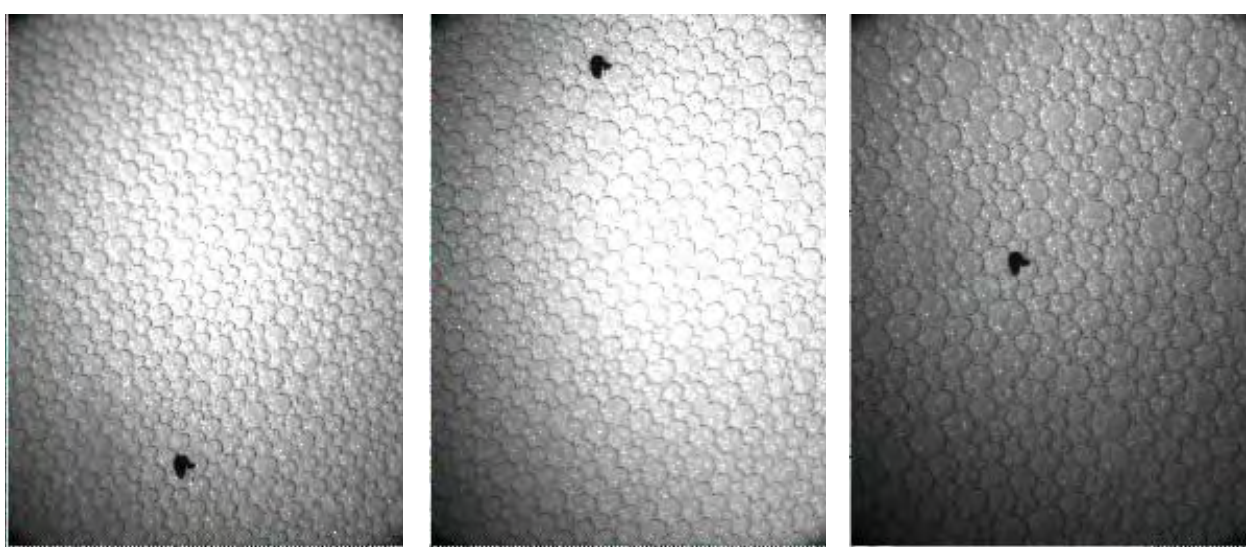

Fig. 3.2.11 Sample of 0.25% Polymer Foam Pictures (Left: Γ=70%; Middle: 80%; Right: Γ=90%)

A summary of bubble size analysis for 70%, 80% and 90% quality foams with 0.25% and 0.5% polymer

concentrations is presented in Table 3.2.3. Bubble size distributions of the foam samples are shown in Fig. 3.2.12. The results indicate that, as foam quality increases from 70% to 90%, the mean bubble size of the foam increases and the circularity of foam bubbles decreases. The shape of 90% quality foam is close to hexagonal. The mean bubble size increases is due to the requirement for an adequate amount of liquid present for smaller bubbles. If high quality foams generate smaller bubbles, a greater volume of liquid will be required to form the liquid film. However, for high quality foams the amount of liquid is limited, and thus the formation of small bubbles is hindered. From Fig. 3.2.12, it appears that as polymer concentration changes from 0.25% to 0.5%, as long as foam quality is the same, mean bubble size and size distribution remain very close.

Table 3.2.3 Summary of Bubble Size Analysis

Foam Type	70% 0.25%	80% 0.25%	90% 0.25%	70% 0.5%	80% 0.5%	90% 0.5%
Mean bubble Size [μm]	57.7	82.9	98.7	70.7	82.2	93.9
Std. Dev. [μm]	28.3	28.0	36.5	18.5	28.6	29.6

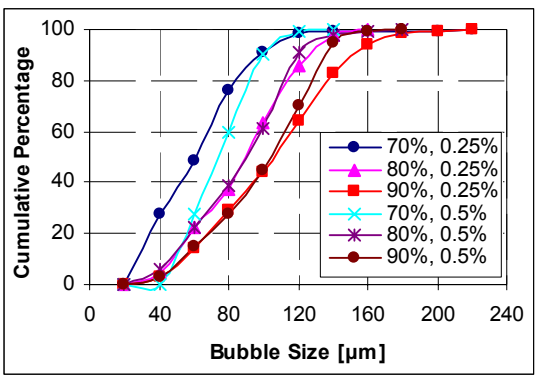

Fig. 3.2.12 Cumulative Bubble Size Distribution for 70%, 80% and 90% Quality Foams

From the results of the foam viscometer measurements, we can find that: i) Foam rheology measured with smooth and roughened cup-rotor assemblies indicates that wall slip effect does exist; ii) When foam rheology is measured with the smooth cup-rotor assembly, lower K values and higher n values are obtained; iii) By using the roughened cup-rotor assemblies, wall slip can be suppressed; thus, better foam rheology measurement can be obtained with Couette-type viscometers that have roughened cup-rotor assemblies; iv) Besides foam quality, foam rheology is affected by the liquid phase rheology. The higher the concentration of viscosifying polymer, the higher the apparent viscosity of foam; v) It is possible to increase the foam apparent viscosity either by increasing foam quality, or by adding polymers in the liquid phase. This offers more choices in controlling foam rheology during foam drilling operations.

3.3 Comparisons of Foam Rheology Measurements using ACTF vs. Rotational Viscometer

Both aqueous and polymer-based foam have been studied, using ACTF pipe viscometer and flow-through rotational viscometer (Foam Generator/Viscometer, FGV). Basically, the same polymer HEC, same surfactant KLEAN-FOAM with 1% v/v used. Also, foam quality and test temperatures are the same. The only difference is test pressure. According to a previous study done at TUDRP by Lourenco[3], test pressure does not affect foam rheology much. Therefore, we tried to compare the apparent viscosity of foam measured with two different apparatuses. In such a way, we can check whether the Foam Generator/Viscometer provide accurate foam rheology measurements.

Figures 3.3.1 to 3.3.11 show the apparent viscosity of 70%, 80% and 90% quality foams, it can be found that the measurements for 70%, 80% quality foams are nearly the same. For 90% foams, the apparent viscosity obtained using Foam Generator/Viscometer is lower than that measured with pipe viscometer (ACTF). This is probably due to the design of the propeller at the bottom of the Foam Generator Clinder. Currently, a 3-inch propeller is used and it may not be powerful enough to mix 90% quality high-viscosity foam and obtain a homogenous foam. More study on why apparent viscosity of 90% foam is lower is needed.

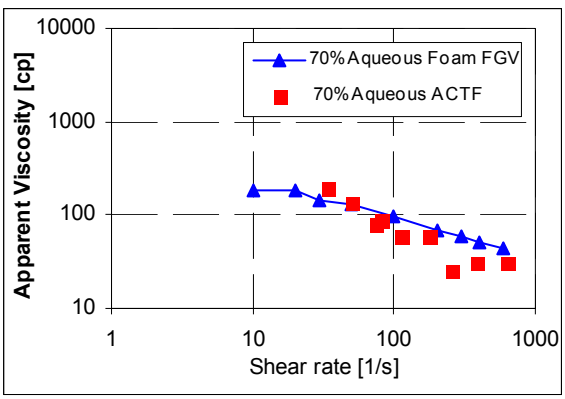

Fig. 3.3.1 Apparent Viscosity of 70% Aqueous Foam Measured with ACTF and FGV

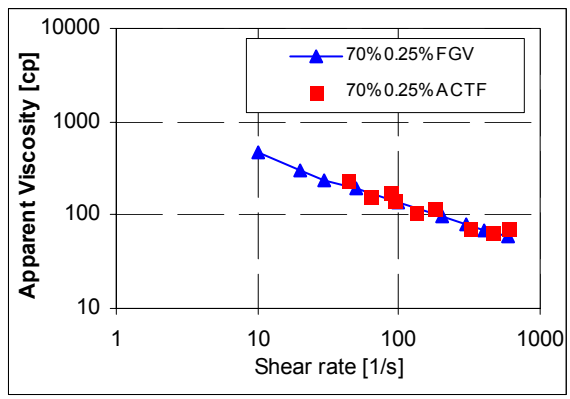

Fig. 3.3.2 Apparent Viscosity of 70% 0.25% Foam Measured with ACTF and FGV

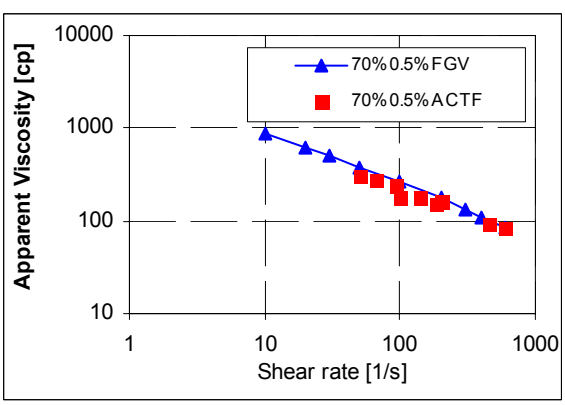

Fig. 3.3.3 Apparent Viscosity of 70% 0.5% Foam Measured with ACTF and FGV

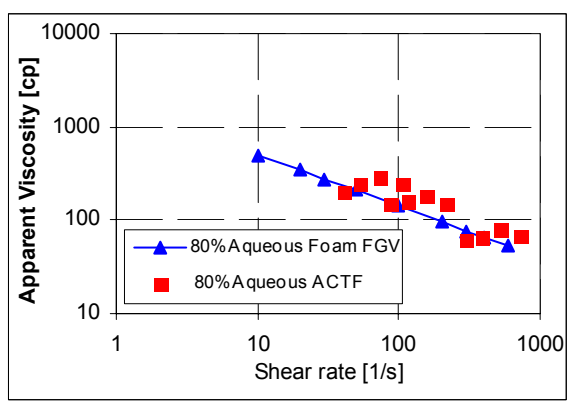

Fig. 3.3.4 Apparent Viscosity of 80% Aqueous Foam Measured with ACTF and FGV

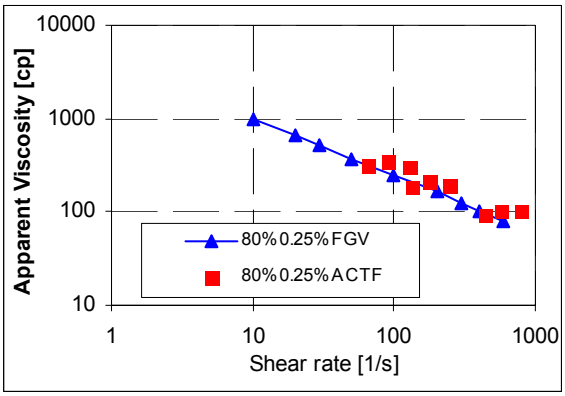

Fig. 3.3.5 Apparent Viscosity of 80% 0.25% Foam Measured with ACTF and FGV

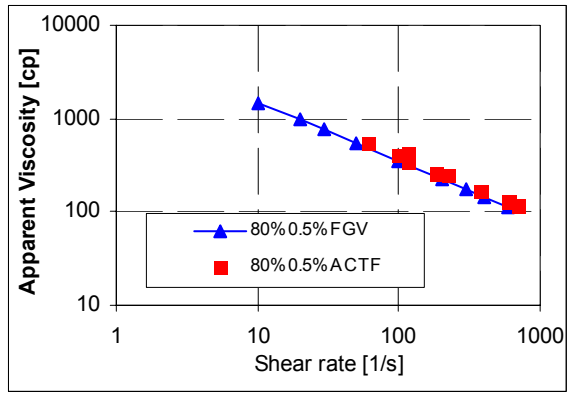

Fig. 3.3.6 Apparent Viscosity of 80% 0.5% Foam Measured with ACTF and FGV

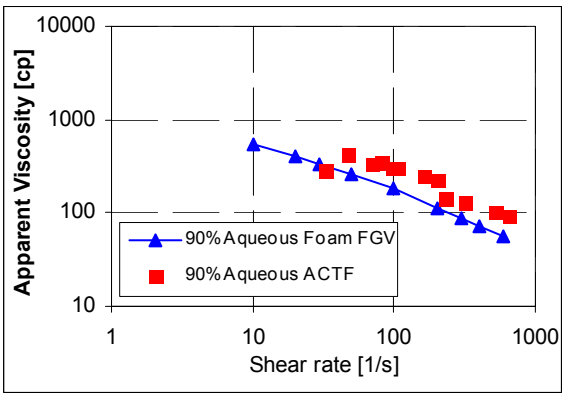

Fig. 3.3.7 Apparent Viscosity of 90% Aqueous Foam Measured with ACTF and FGV

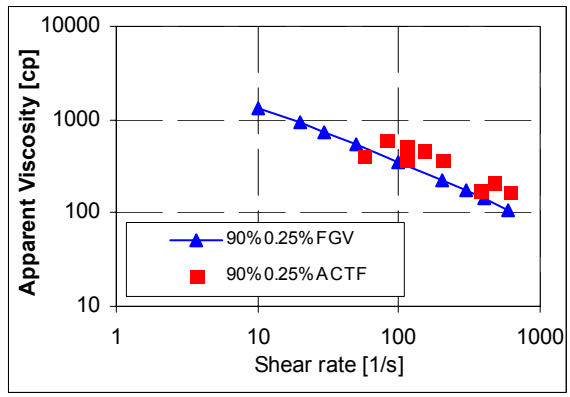

Fig. 3.3.8 Apparent Viscosity of 90% 0.25% Foam Measured with ACTF and FGV

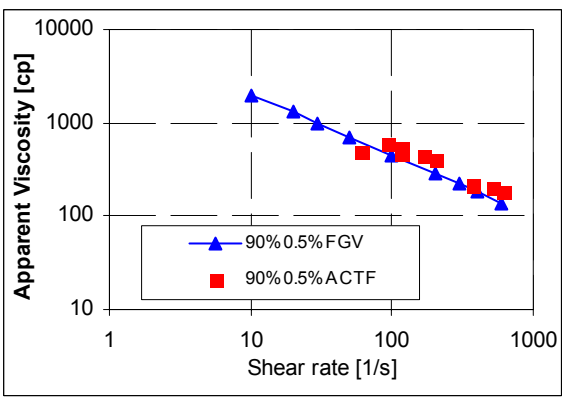

Fig. 3.3.11 Apparent Viscosity of 90% 0.5% Foam Measured with ACTF and FGV

Based on current experimental results, the Foam Generator/Viscometer can be used to measure foam rheology with desired accuracy. This is very useful since measuring foam rheology using a large-scale pipe viscometer like ACTF can be very costly.

4. Simulation of Polymer Effect on Hydraulics of Foam Drilling Operations

Previous results indicate that polymer does affect apparent viscosity of foam. The higher the polymer

concentration, the higher the apparent viscosity of foams. Also, foam quality changes along the wellbore, which also affects foam apparent viscosity. To quantitatively compare hydraulics of foam drilling using aqueous foam and polymer-based foam, a foam hydraulic program using Visual Basic has been written and this program can be used to analyze different scenarios during foam drilling operations. Especially, it can be used to evaluate how much and to what extent polymer will affect foam rheology and, in turn, affect hydraulics of foam drilling operations.

A simplified foam hydraulics program has been developed for annular foam flow with given liquid and air injection rate, and back pressure. This program can be used to calculate the pressure profile, foam flow velocity, foam quality, foam apparent viscosity, frictional pressure gradient, hydrostatic pressure gradient and total pressure gradient in the annulus. This calculation of air volume is based on ideal gas Equation of State assuming Z factor is equal to 1. Calculation procedure starts from the top of the exit with given back pressure, foam quality.

we will use the rheological parameters correlations that have been developed for the three different foams (aqueous foam, 0.25% polymer foam and 0.5% polymer foam). In such a way, we can investigate how foam rheology affects bottom hole pressure and pressure gradient, etc.

Figure 4.1 shows the schematic annulus. In this program: i) since the calculation started from the top of the annulus downward, only pressure drop in the annulus is calculated; ii) for the sake of simplicity, only drilling pipe with the same diameter is considered, and the wellbore diameter is also constant. The following sequences of calculations were used in order to simulate the foam behavior along the annulus:

1. Based on Q_{liquid}, Q_{air}, backpressure, calculate foam quality and foam velocity at the top of the wellbore;
2. Assume a pressure increment of 10 psia. Therefore, P1=P2+10;
3. Calculate average foam density between point 1 and point 2;
4. Calculate foam velocity at point 2;
5. Calculate average wall shear stress for the segment between point 1 and point 2, for foam with Power Law rheological model, when it flows in annular space:

$$\frac{12v_f}{D_o - D_i} = \frac{\tau_w^{\frac{1}{n}}}{K^{\frac{1}{n}}} \times \left(\frac{3n}{1+2n}\right)$$

Note: K, n values are changing with depth, and they are functions of liquid phase viscosity μ_L and foam quality, Γ. For each kind of foam, K, n can be correlated with foam quality.

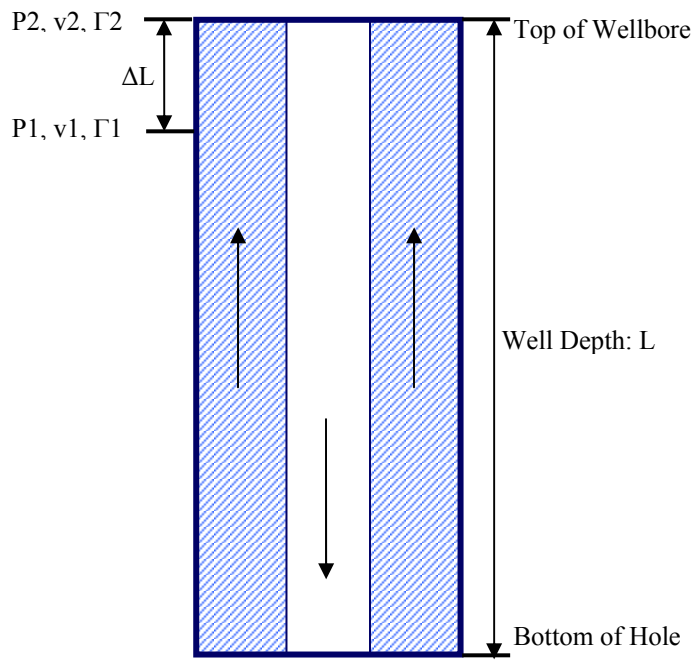

Fig. 4.1 Simplified Schematic of a Wellbore

6. Calculate frictional pressure drop and Reynolds number:

$$Re = \frac{12\rho_F \cdot v_f^{\,2}}{\tau_w}$$

$$\frac{dP}{dL} = \frac{2 \cdot f \cdot \rho_f \cdot v_f^{\,2}}{Do - Di}$$

If flow is turbulent (Re > 2100), calculate friction factor, f, and then based on f, calculate true τ_w

$$\frac{1}{\sqrt{f}} = \frac{4}{n^{0.75}} \times \log\left(Re \cdot f^{1-\frac{n}{2}} \right) - \frac{0.4}{n^{1.2}}$$

If flow is laminar (Re < 2100), accept τ_w obtained in step 5

$$\frac{dP}{dL} = \frac{4 \times \tau_w}{Do - Di}$$

7. Calculate the length of segment ΔL:

$$\Delta L = \frac{\left[(P_1 - P_2) + \beta \frac{\dot{m}_f}{A} (v_1 - v_2) \right] D_H}{4\tau_w + \rho_f \, g \, D_H \mathrm{Cos}(\alpha)}$$

8. Calculate temperature at point 2;
9. Go to step 3 and repeat calculations to obtain the desired accuracy of calculating length of segment ΔL;

10. This process is done until the summation of each calculated ΔL reaches the bottom of the wellbore.

The input data used in this simulation is given in Table 4. The input value can be changed in the simulator. In this case study, these values were selected to guarantee that foam quality in the annulus is between 55% to 97%. Please note that liquid injection rate is 40 gpm and gas injection rate is 1200 SCFM; these parameters have been used in some practical foam drilling operations.

Table 4. Input Data For Foam Hydraulics Simulation

Liquid Density (Kg/m^3)	$\rho_L = 1000$	Gas Molecular Weight (lbm/lbmol)	Mg = 28.9
Liquid Flow Rate (GPM)	$Q_L = 40$	Gas Flow Rate (SCFM)	$Q_g = 1200$
Hole Size (inches)	$D_{hole} = 8.5$	Depth (ft)	L = 10000
Pipe O.D. (inches)	Do = 5	Temperature Gradient (°F/100ft)	$\Delta T = 1.5$
Surface Temperature (°F)	Ts = 80	Surface Back Pressure (psig)	Ps = 100

Figures 4.2 to 4.9 show the simulation results using three different foams (aqueous foam, 0.25% and 0.5% HEC polymer foams) under the same drilling conditions. Pressure profile, foam density profile, foam flow velocity profile, foam quality profile, frictional pressure gradient, hydrostatic pressure gradient, total pressure gradient, ratio of hydrostatic/friction versus depth are shown.

For the same operating conditions, when polymers are added (from 0 to 0.5%), bottom hole pressure increases from 1165 psi to 1894 psi, foam density increases from 247 kg/m3 to 429 kg/m3, foam flow velocity decreases from 0.51 m/s to 0.31 m/s, foam quality decreases from 71.5% to 55% and total pressure gradient is also greatly increased because of polymer effect.

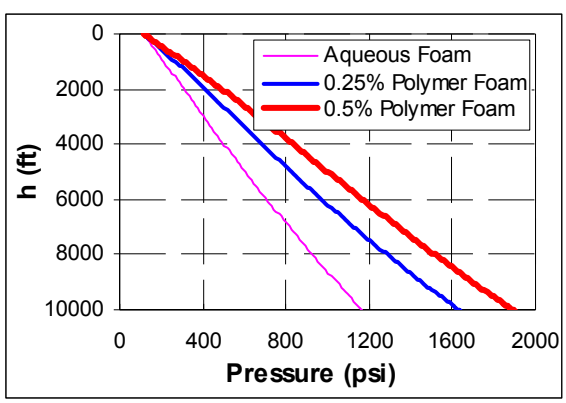

Fig. 4.2 Pressure vs. Depth

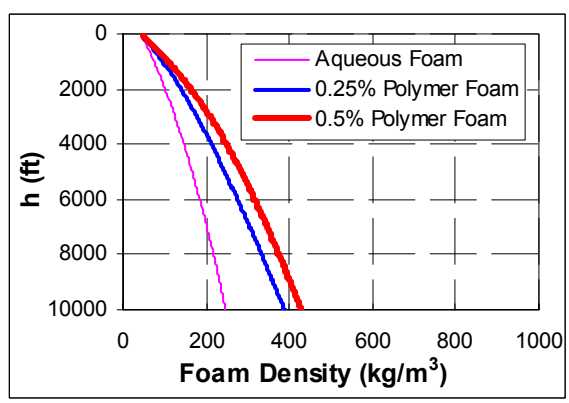

Fig. 4.3 Foam Density vs. Depth

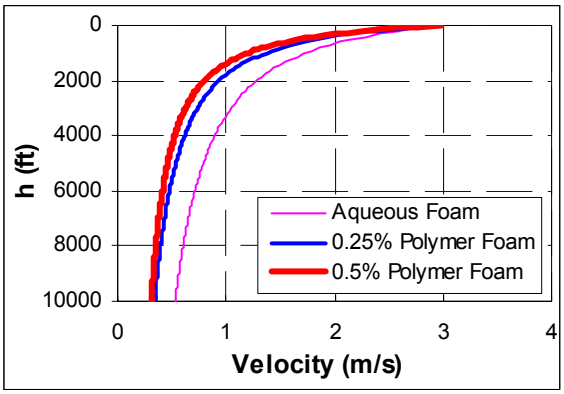

Fig. 4.4 Foam Velocity vs. Depth

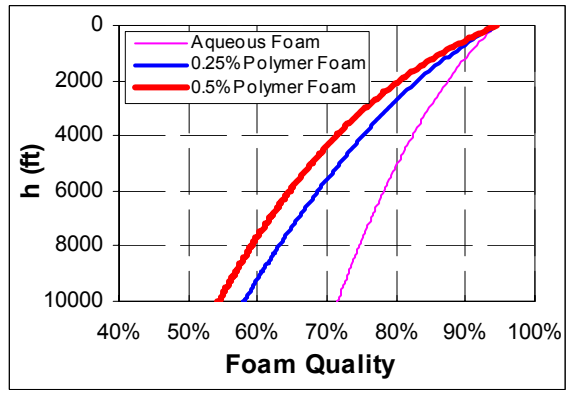

Fig. 4.5 Foam Quality vs. Depth

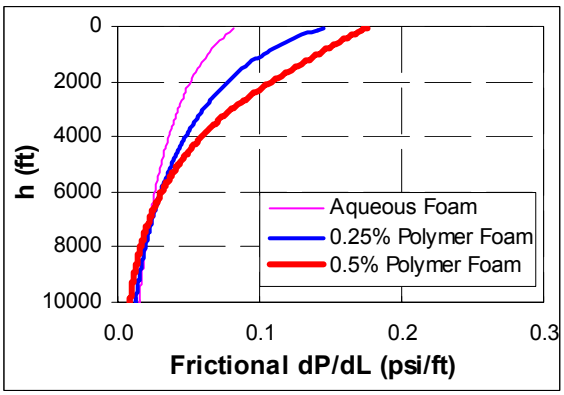

Fig. 4.6 Frictional dP/dL vs. Depth

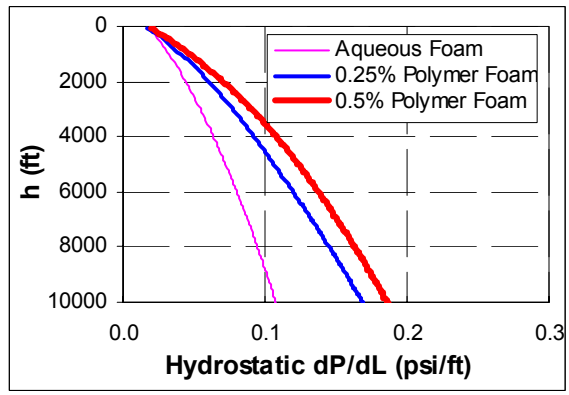

Fig. 4.7 Hydrostatic dP/dL vs. Depth

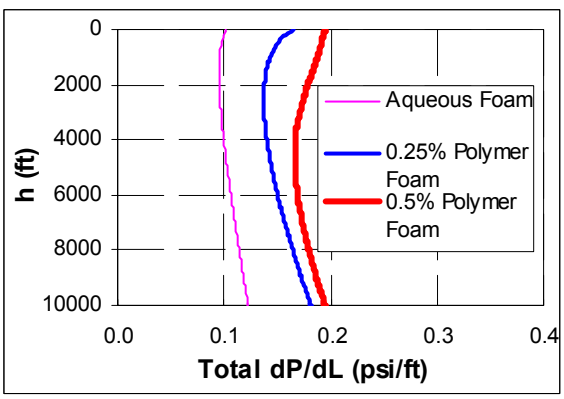

Fig. 4.8 Total dP/dL vs. Depth

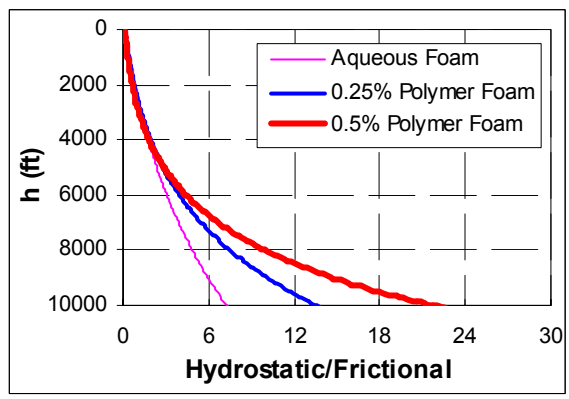

Fig. 4.9 Hydrostatic/Frictional vs. Depth

A careful look at the frictional pressure gradient, hydrostatic pressure gradient and total pressure gradient reveals that at the top of the wellbore, because of high foam flow velocity and foam quality, the flow is friction-dominated and the hydrostatic pressure gradient is not significant. However, at deeper depths of the wellbore (around 5000-6000 ft in this case), the frictional pressure gradient component decreases and it does not affect total pressure drop much. The hydrostatic pressure drop component dominates the pressure drop in the deeper part of the wellbore. From the total pressure gradient plot, we can observe that as polymer concentration

increases, the length of the friction-dominated region (from the top of the wellbore downward) increases. Below the friction-dominated region is the hydrostatic-dominated region. It can be also found that as polymer concentration increases, the total pressure gradient increases, which results in a higher bottom hole pressure.

5. ACTF Experiments on Cuttings Transport with Foam

5.1 Test Facility

Cuttings Transport with foam tests were performed with the ACTF Flow Loop. The test section is an annulus with 5.76” ID casing and 3.5” OD drill pipe. It is 73 ft (22 m) in length, in a horizontal configuration and the drillpipe was not rotated. Two view ports allow observation of flow characteristics in the test section. Two nuclear densitometers are used to measure foam and foam-cuttings mixture densities. A new stator was installed during this period, and the new stator has proven to be effective to deliver desired amount of air at EPET conditions.

5.2 Test Matrix

The main objectives for cuttings transport with foam tests are to study the effect of polymer additives, foam quality, foam flow velocity, temperature and pressure on cuttings transport efficiency with foam.

Based on equipment capability, chemicals quantities (surfactant, breaker and polymer quantities), and time frame, a test matrix is designed given in the table below. Eight groups of tests were conducted during experimental investigation of cuttings transport. Test pressure was varied from 100 psig to 400 psig, and test temperature was changed from 80 °F to 170°F.

Table 5.1 Test Matrix for Cuttings Transport with Foam Experiments

	Description	Pressure (psig)	Temperature (°F)	Number of Tests
Group #1	Low Pressure, Low Temperature Polymer Effect Tests	100	80	10
Group #2	Low Pressure, Low Temperature Baseline Tests	100	80	10 (1 test left)
Group #3	Low Pressure, Medium Temperature Tests	100	120	5
Group #4	Low Pressure, Elevated Temperature Tests	100	160	3
Group #5	Medium Pressure, Low Temperature Tests	250	80	5
Group #6	Elevated Pressure, Low Temperature Tests	400	80	3
Group #7	Medium Pressure, Medium Temperature Tests	250	120	3 (1 test left)
Group #8	Elevate Pressure, Elevated Temperature Tests	400	170	3

Tests of foam quality, foam flow velocity, and polymer effect on cuttings transport at low pressure and low

temperature conditions (Test Group #1, #2) have been studied before last ABM, detailed results can be found in the Nov. 2004 ABM report.

Tests during this period of time focused on temperature and pressure effects on cuttings transport with foam. To study temperature and pressure effect on cuttings transport with foam, with consideration of all the parameters (P, T, foam quality, foam flow velocity), the number of tests needed to run is huge (at least 80 tests in total). Also, it is impossible to run some of the tests. For example, test of 90% quality foam with velocity of 6ft/s at 400 psig and 80°F requires air flow rate of 1004 SCFM. The present maximum gas flow rate is 515 SCFM (the maximum range of the air flow meter). This gas flow rate allows us to test at maximum 3 ft/s for 90% quality foam at 400 psig and 80°F.

At low pressure and low temperature conditions (100psig and 80°F), experiments were designed to find the "critical" velocity at which all the cuttings are suspended in the foam. However, to evaluate cutting transport efficiency at higher pressure/temperature conditions, tests were designed not to find the "critical" velocity, but to run foam cuttings tests with the same foam quality and velocity under varying pressure and temperature conditions. Thus, based on the steady-state cuttings concentrations in the horizontal test annular section, the effects of pressure and temperature on cuttings transport efficiency using foams can be evaluated. Tables 5.2 to 5.7 show test matrix for test Group #3 to #8.

Table 5.2 Test Matrix for Cuttings Transport Test Group #3

Quality	Velocity (ft/s)	Pressure (psig)	Temperature (°F)
90%	3	100	120
90%	4	100	120
90%	5	100	120
80%	3	100	120
70%	3	100	120

Table 5.3 Test Matrix for Cuttings Transport Test Group #4

Quality	Velocity (ft/s)	Pressure (psig)	Temperature (°F)
90%	3	100	160
90%	4	100	160
90%	5	100	160

Table 5.4 Test Matrix for Cuttings Transport Test Group #5

Quality	Velocity (ft/s)	Pressure (psig)	Temperature (°F)
80%	2	250	80
80%	3	250	80
80%	4	250	80
90%	3	250	80
70%	3	250	80

Table 5.5 Test Matrix for Cuttings Transport Test Group #6

Quality	Velocity (ft/s)	Pressure (psig)	Temperature (°F)
90%	3	400	80
80%	3	400	80
70%	3	400	80

Table 5.6 Test Matrix for Cuttings Transport Test Group #7

Quality	Velocity (ft/s)	Pressure (psig)	Temperature (°F)
90%	3	250	120
80%	3	250	120
70%	3	250	120

Table 5.7 Test Matrix for Cuttings Transport Test Group #8

Quality	Velocity (ft/s)	Pressure (psig)	Temperature (°F)
90%	3	400	170
80%	3	400	170
70%	3	400	170

5.3 Test Results and Discussions

The Effect of Temperature on Cuttings Transport. Figure 5.3.1 compares the cuttings concentration in the annulus versus temperature for 90% quality foams at 80°F and 120°F. Figure 5.3.2 compares the cuttings concentration versus foam quality for foams flowing at 3 ft/s at 80°F and 120°F. Both plots indicate that as temperature changes from 80°F to 120°F , cuttings concentration does not change much.

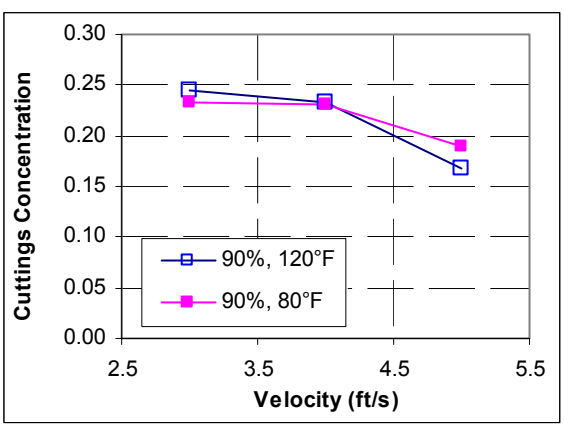

Fig. 5.3.1 Cuttings Concentration vs. Flow Velocity (Γ = 90%; T = 80, 120°F)

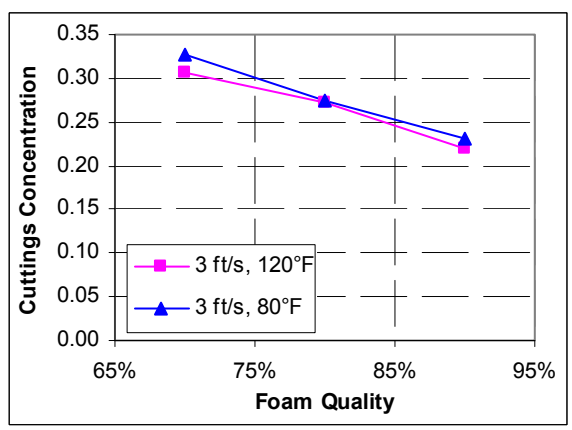

Fig. 5.3.2 Cuttings Concentration vs. Foam Quality (v = 3 ft/s; T = 80, 120°F)

Figure 5.3.3 compares the cuttings concentration versus foam flow velocity at 80°F and 160°F for 90%

quality foams. When temperature is increased from 80°F to 160°F, the cuttings concentrations at flow velocity of 3 ft/s, 4 ft/s and 5 ft/s increase by 2.8%, 5.7% and 2.2% respectively. Examination of differential pressure drop in annulus indicates that as temperature increases, the differential pressure drop decreases by about 30% (Fig. 5.3.4). Nevertheless, despite the slight increase in cuttings concentration, this change may not substantially impact the cutting transport efficiency for practical foam drilling operation.

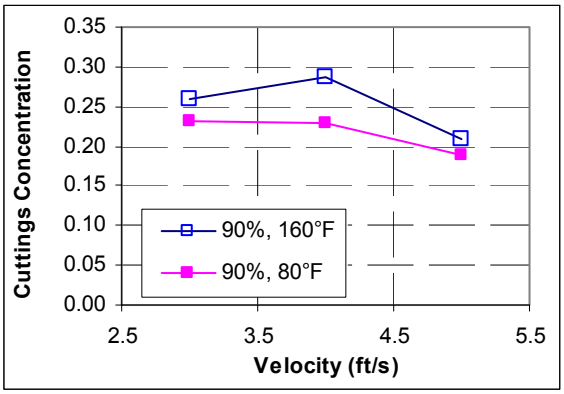

Fig. 5.3.3 Cuttings Concentration vs. Flow Velocity (Γ = 90%; T = 80, 160°F)

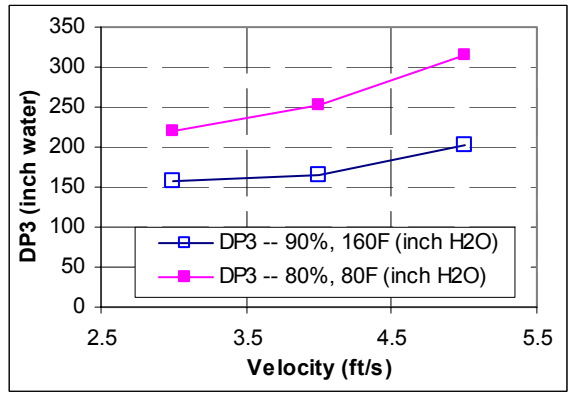

Fig. 5.3.4 Differential Pressure in the Annulus vs. Flow Velocity (Γ = 80%, 90%; T = 80 , 160°F)

The Effect of Pressure on Cuttings Transport. Figure 5.3.5 compares the cuttings concentration versus foam flow velocity for 80% quality foams at pressures of 100 and 250psig. No obvious change of cuttings concentration was observed. Figure 5.3.6 compares the cuttings concentration versus foam quality at pressures of 100 and 250psig for foams flowing at 3 ft/s. it seems that as pressure increases, there is a slightly decrease of cuttings concentration in the annulus.

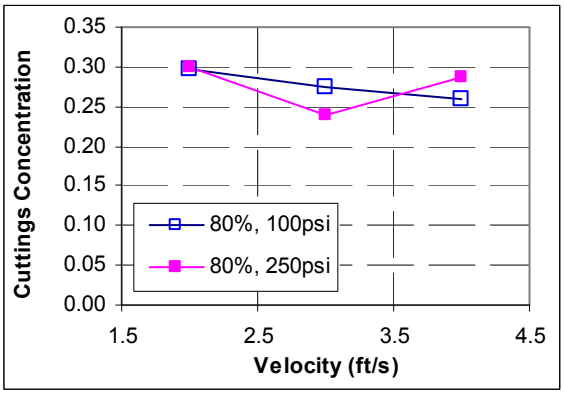

Fig. 5.3.5 Cuttings Concentration vs. Flow Velocity (Γ = 80%; P = 100, 250psig)

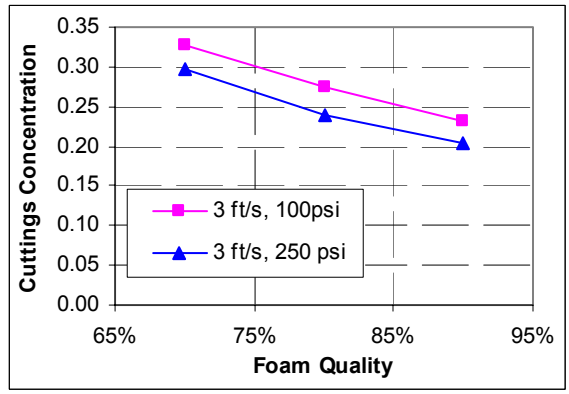

Fig. 5.3.6 Cuttings Concentration vs. Foam Quality (v = 3 ft/s; P = 100, 250psig)

Figure 5.3.7 compares the cuttings concentration versus foam quality for foams at 100psi and 400psig

flowing at 3 ft/s. It seems that there is a decrease in cuttings concentration in the annulus at the higher pressure. Due to the small number of experiments under high pressure conditions, it is premature to draw conclusions. More experience is needed in controlling the tests at higher pressure conditions. From the experiments, we observed that at higher pressure conditions, the cuttings bed becomes less stable. Because of the compressibility of air, pressure surges can cause the foam to expand and move very rapidly. This would be expected to help cuttings removal.

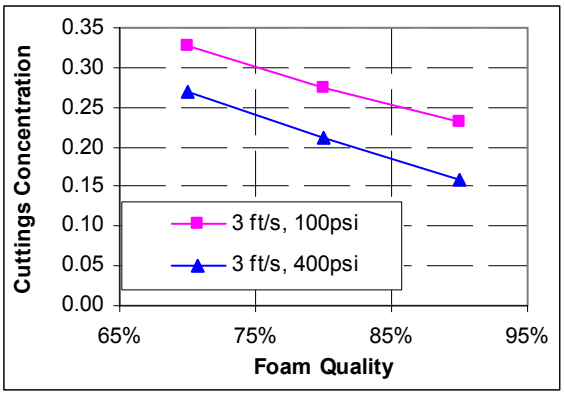

Fig. 5.3.7 Cuttings Concentration vs. Foam Quality (v = 3ft/s; P = 100, 400 psig)

The Combined Effect of Pressure and Temperature on Cuttings Transport. Figure 5.3.8 shows the cuttings concentration versus foam quality for foams flowing at 3 ft/s. This plot illustrates that as both temperature and pressure increase (temperature from 80°F to 120°F, pressure from 100 to 250psig), cuttings transport efficiency does not change significantly. Figure 5.3.9 compares cuttings concentration versus foam

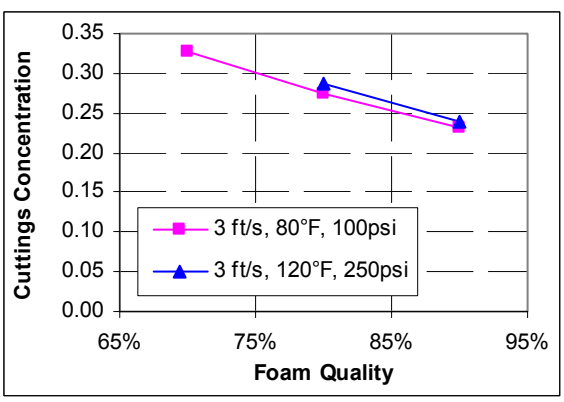

Fig. 5.3.8 Cuttings Concentration vs. Both Pressure and Temperature Change for 80%, 90% Quality Foams Flowing at 3 ft/s

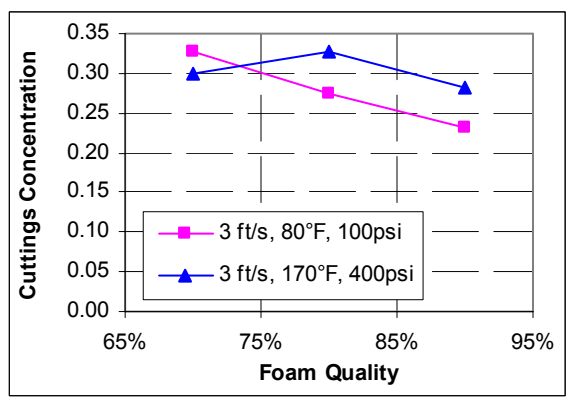

Fig. 5.3.9 Cuttings Concentration vs. Medium Pressure and Temperature for 70%, 80%, 90% Quality Foam Flowing at 3 ft/s

quality for foams flowing at 3 ft/s under LPAT and EPET conditions. It can be observed that as both

temperature and pressure increases (temperature from 80°F to 170°F, pressure from 100 to 400psig), cuttings concentrations slightly increase for 80% and 90% quality foams. But again, the change is still insignificant.

Based on the experimental results for all different combinations of pressure and temperature conditions, it can be found that at high temperature and/or high pressure conditions, there are slight changes in cuttings transport concentrations, but the changes are fairly limited. Basically, foam maintains its cuttings transport property quite well even under simulated downhole conditions. This is a very desirable property for foam.

Since foam is not that sensitive to pressure and temperature change, therefore, if time permitting, we will put more emphasis on cuttings transport with foam at higher velocities and low foam qualities, these tests will be done under low pressure and low temperature conditions.

6. Future Work

After this ABM, more work still needs to be done for this project, which includes:

1. Finish foam cuttings tests especially at higher velocity for low quality foams;
2. Conduct foam rheology tests under EPET conditions if time permitting;
3. Data processing and analysis;
4. Modeling of cuttings transport with foam.

7. References

1. Khade, S.D., Shah S.N.: "New Rheological Correlations for Guar Foam Fluids," SPE 80895, presented at the SPE Production and Operations Symposium held in Oklahoma City, Oklahoma (March 22-25, 2003).
2. Larson, R.G.: "The Structure and Rheology of Complex Fluids, " Oxford University Express. ISBN 0-19-512197-X (1998).
3. Lourenco, A.: "Study of Foam Flow under Simulated Downhole Conditions," M.S. Thesis, The University of Tulsa, Tulsa, Oklahoma (2002).

Continuing Foam Rheological Characterization Studies Using the Foam Generator and Viscometer Apparatus

Mark B. Pickell

Continuing Foam Rheological Characterization Studies Using the Foam generator and Viscometer Apparatus

---

Investigator: Mark B. Pickell, P.E.

Objective: An attempt has been made to conduct experiments with the Foam Generator and Viscometer Apparatus that would be reflective of pipe flow conditions in which volume equalized equations would be applicable.

Approach: A water / Weatherford surfactant / nitrogen gas foam was created at pressure, investigated, isothermally expanded to a lower pressure, and examined again.

Results: These experiments showed that, once Power Law volume equalized equations were applied, the data was segregated by the initial high pressure and the lower expanded pressure, rather than plotting along a single line as would have been expected.

Preliminary Conclusions: The preliminary conclusion is that the segregation could be a result of the equipment being used or an expected result because of differences between the initial high pressure foam and the lower expanded pressure foam. These differences being: pressure; quality; and/or possibly different rheological models (e.g. Power Law vrs. Bingham Plastic). Additional testing is required.

Continuing Foam Rheological Characterization Studies Using the Foam Generator and Viscometer Apparatus

Mark B. Pickell, P.E. The University of Tulsa Drilling Research Projects

This report is prepared for TUDRP Advisory Board Meeting, May 23-24, 2005, Tulsa . Oklahoma

---

Since our meeting last May, we have attempted to conduct experiments that would be reflective of pipe flow conditions in which volume equalized equations would be applicable. This work falls in line with prior investigations in that the purpose of the Foam Generator is to augment experiments conducted on the TUDRP flow loops by providing independent measurements and to provide a means for independent rheological research which will advance the consortia's ability to accurately predict down-hole phenomena.

Based on experimental investigation of polymer-based foams, Valko and Economides [1] presented principle of volume equalization to describe the rheology of foams. The technique uses the specific-volume expansion ratio, ε, as the additional parameter representing the phase composition of foam. This quantity is defined as the ratio of the liquid density to the foam density, which varies along the flow path because of the change in the pressure. The specific-volume expansion ratio at a given temperature and pressure is given by:

$$\varepsilon = \frac{\rho_L}{\rho_f},$$

The principle of volume equalization is derived from an invariance requirement. It assumes that for a straight duct flow of constant cross section, both compressible and incompressible flows posses the invariance property. This means that the loss of mechanical energy is proportional to the kinetic energy, in other words the Reynolds number is constant. A constitutive equation that provides the required invariance is called volume equalized. For instance, the volume equalized power law equation can be written as:

$$\frac{\tau}{\varepsilon} = K_{VE}\left(\frac{\gamma}{\varepsilon}\right)^n,$$

One of the advantages of this approach is that when the volume equalized wall shear stress is plotted against the volume equalized nominal Newtonian shear rate on a log-log scale, results in a straight line for a wide range of foam qualities and pressures.

Volume equalized equations have been shown to be useful in hydraulic calculations because they provide a means by which compressible fluids under varying conditions can be modeled using one set of parameters. Classically, the empirical data supporting the mathematical model has been obtained by using pipe rheometers. With the invention of the Foam Generator and Viscometer Apparatus an additional

means is available to collect data. The objective of these experiments is to take data obtained by using the Foam Generator / Viscometer, manipulate it using volume equalized equations, and determine if the results compare well with the anticipated analytical model.

For these experiments, a water / Weatherford surfactant / nitrogen gas foam was chosen. The approach was to create foam under pressure, investigate its properties, then isothermally expand that foam to a lower pressure, and investigate its properties again. The volume, quality, pressure, and temperature of the foam is known at the beginning and end of each investigation. When the foam is expanded to a lower pressure, the new volume, pressure, and temperature are measured, and the new quality is calculated. The obvious difference between the experiments cited by Valko and Economides and those discussed here is that theirs were conducted in a pipe rheometer and these have been done in a foam generator and viscometer. In a circulating pipe rheometer mass is conserved over the measured length and the density of the flow can be stated with certainty at any given point. The equivalence used here is Mass Ratio β defined as:

$$\beta = m_g / m_l$$

or, the ratio of the mass of the gas phase of the foam to the mass of the liquid phase.

Theoretically then, as long as the relative gas content of the foam is constant, the volume equalized power law model should plot as a single straight line on log-log coordinates.

The equipment is basically unchanged since the last ABM. The high-pressure foam generator cylinder has been installed as has an electronic scale currently being used as a measure of flow rate but the functionality of the apparatus is still the same.

Foam Generator and Viscometer Apparatus

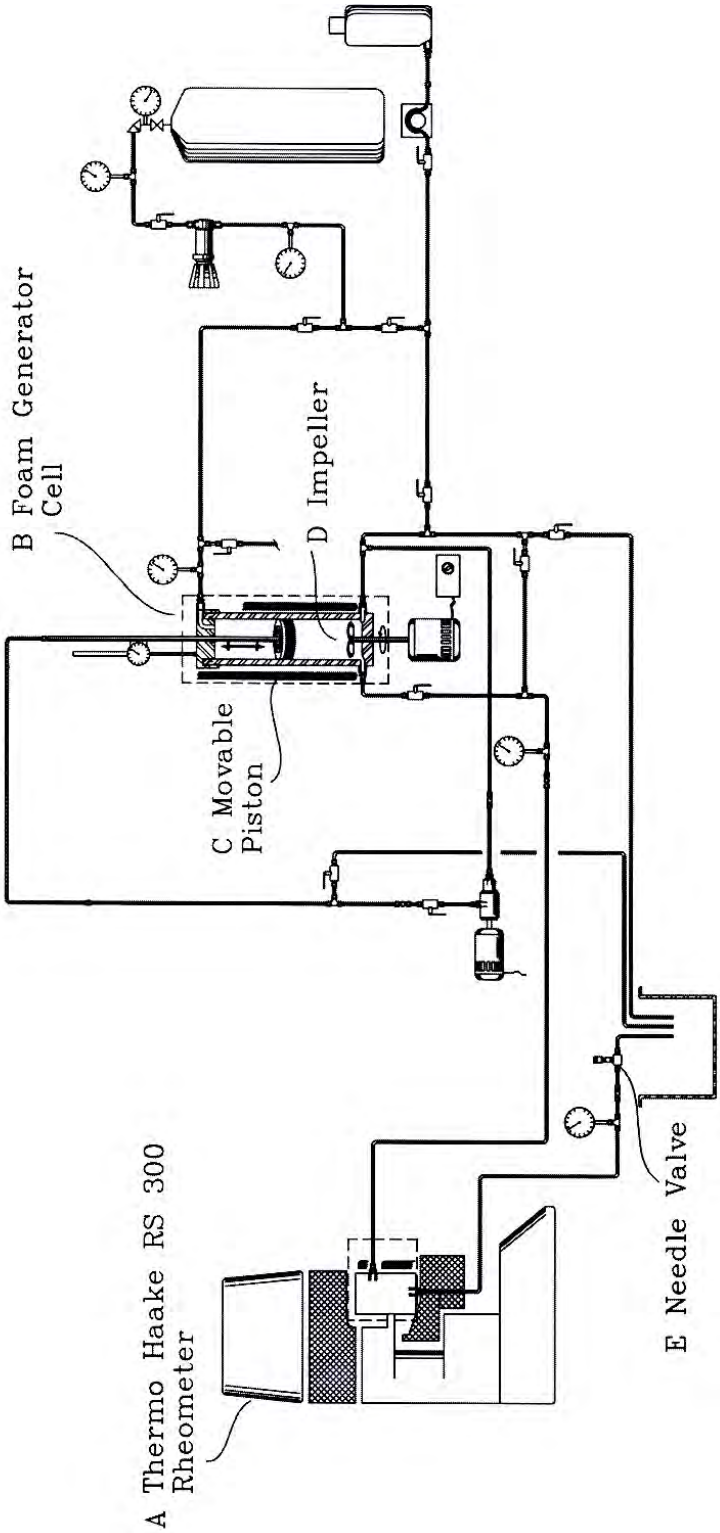
A Thermo Haake RS 300
Rheometer
B Foam Generator
Cell
C Movable
Piston
D Impeller
E Needle Valve

The first foam investigated was a .75 quality foam at 20 °C and 600 psig which was investigated, then expanded into a .83 quality foam at 20 °C and 400 psig, then investigated again. Plotting shear stress against shear rate the results predictably arranged themselves by pressure:

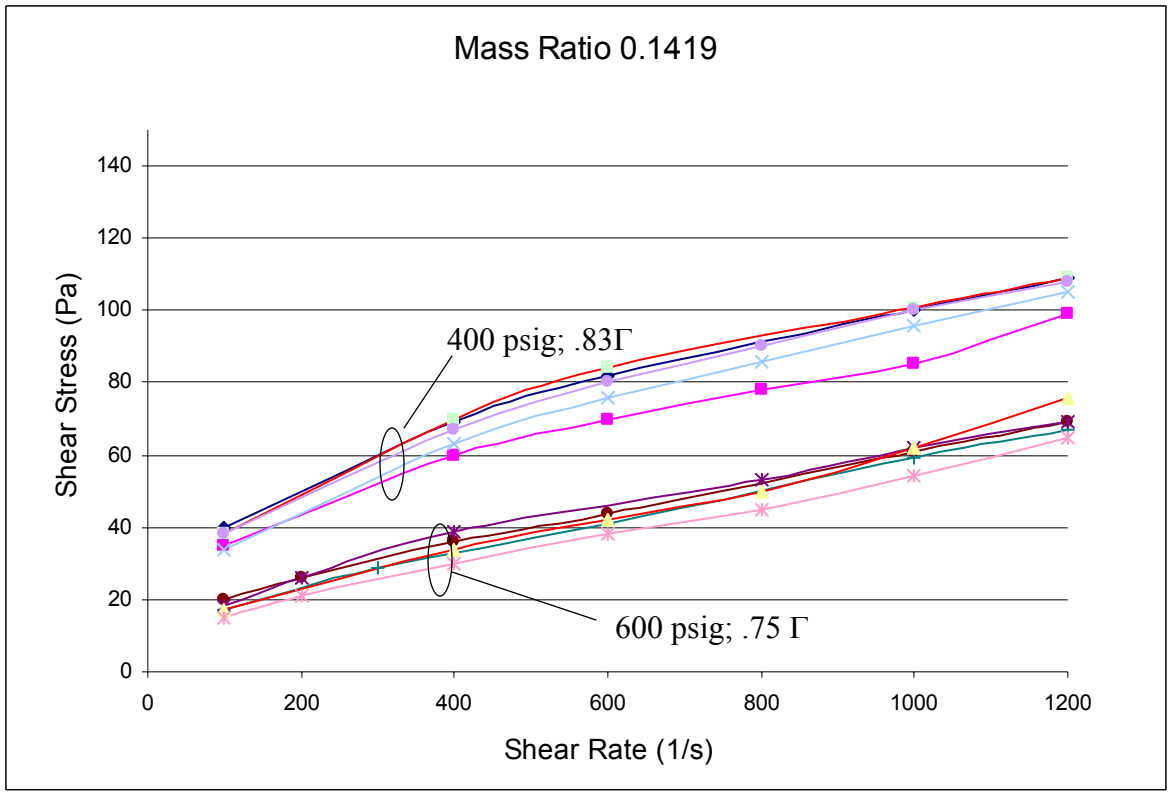

The same experiments, this time plotting apparent viscosity against shear rate, again, predictably the results group according to pressure:

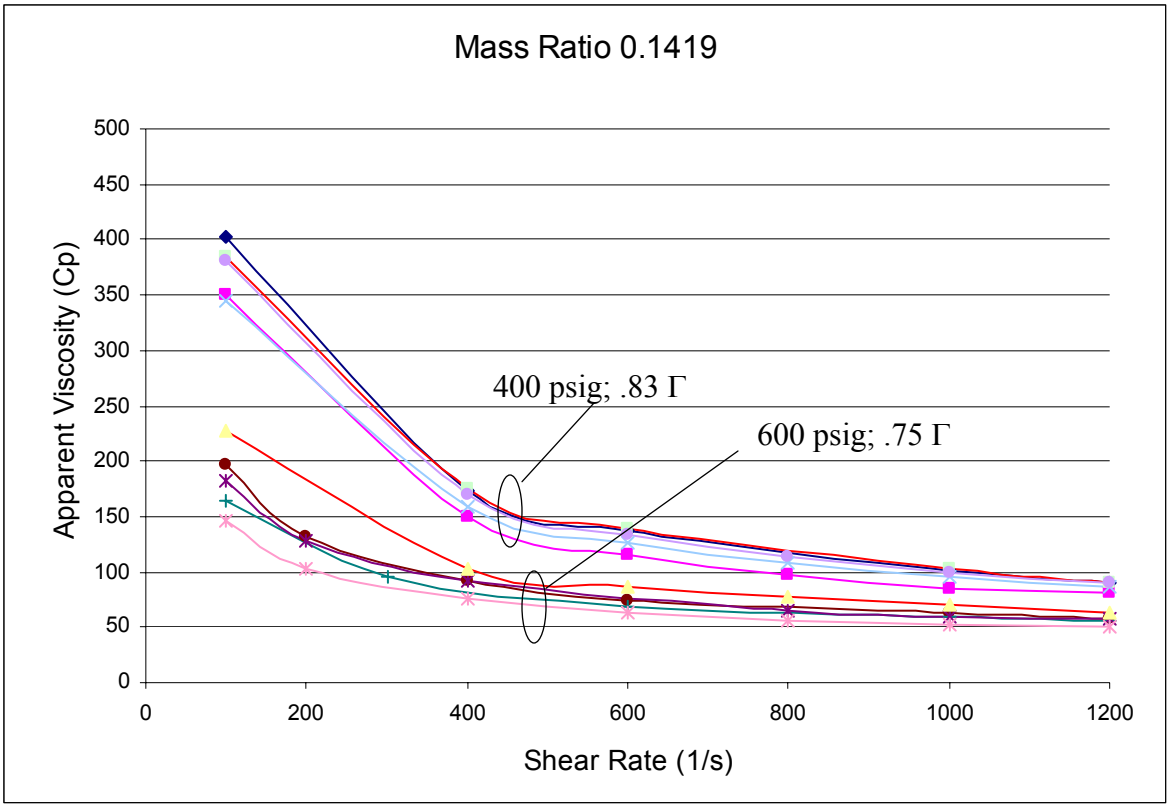

Applying volume equalized equations to this data:

				P_1						P_2	
Sample	V_1 Orig. Vol. ml	Orig. Meas. inches	Γ_1 Orig. Qual.	Orig. Press. psig	m_{g1} gm gas	m_{l1} gm water	β_1 mass ratio	ε_{s1} Orig. Exp. Ratio	End Meas. inches	Expanded Press. psig	Expanded Meas. inches
012705	1408.4	6	0.75	600	49.956	352.088	0.1419	3.6636747	3.4375	400	4.875
021005	1408.4	6	0.75	600	49.956	352.088	0.1419	3.6636747	2.5	400	3.6875
021105	1408.4	6	0.75	600	49.956	352.088	0.1419	3.6636747	2.125	400	3.25
021405	1408.4	6	0.75	600	49.956	352.088	0.1419	3.6636747	3.2813	400	4.5938
021405c	1081.3	4.5938	0.82	400	27.895	196.606	0.1419	5.0375373			
021505	1408.4	6	0.82	400	36.332	256.065	0.1419	5.0375373			
022105	1408.5	6	0.75	600	49.961	352.125	0.1419	3.6636747			

Expanded Vol. ml	V_2 New Vol. ml	Vol. N2 ml	m_{g2} gm gas	Vol. H20 ml	gm water	β_2 mass ratio	Γ_2 New Qual.	ε_{s2} New Exp. Ratio
1146.722	812.41977	609.3148	28.81768	203.1049	203.10494	0.1419	0.82	5.157174
870.5593	594.39651	445.7974	21.08409	148.5991	148.59913	0.1419	0.83	5.330158
768.8151	507.18721	380.3904	17.99065	126.7968	126.7968	0.1419	0.84	5.495699
1081.327	776.09419	582.0706	27.52916	194.0235	194.02355	0.1419	0.82	5.097603

We can now plot the volume equalized shear stress:

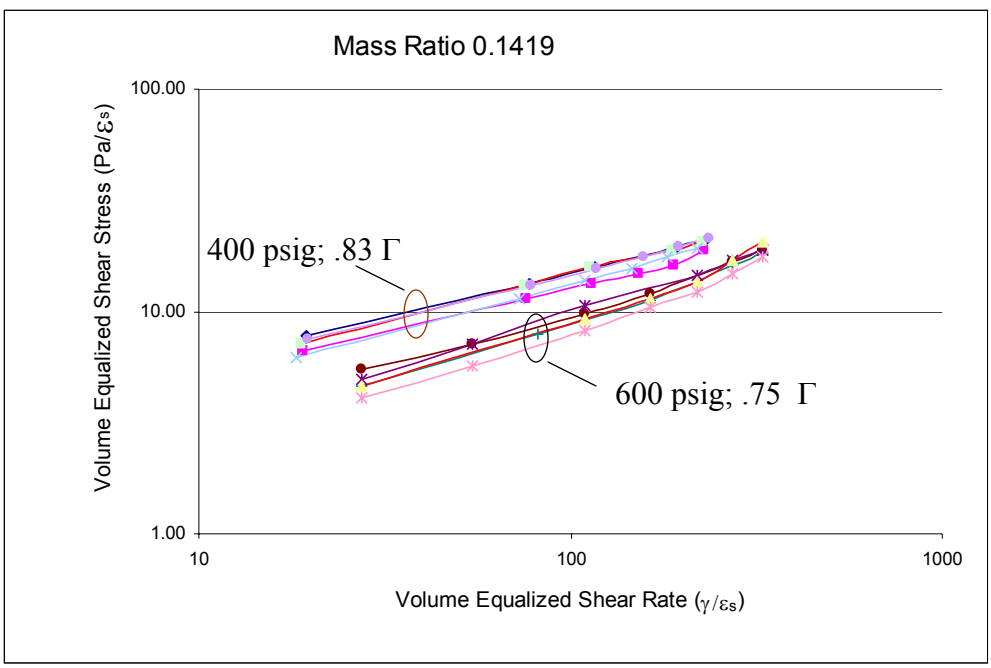

Most interesting is that the data is still segregated between the 400 psig and the 600 psig. The Volume Equalized plot did not come into a single line. For comparison the non-volume equalized data on a log-log plot clearly shows that the data has come together very considerably. Only by the scale of the plot can we see that the data has segregated.

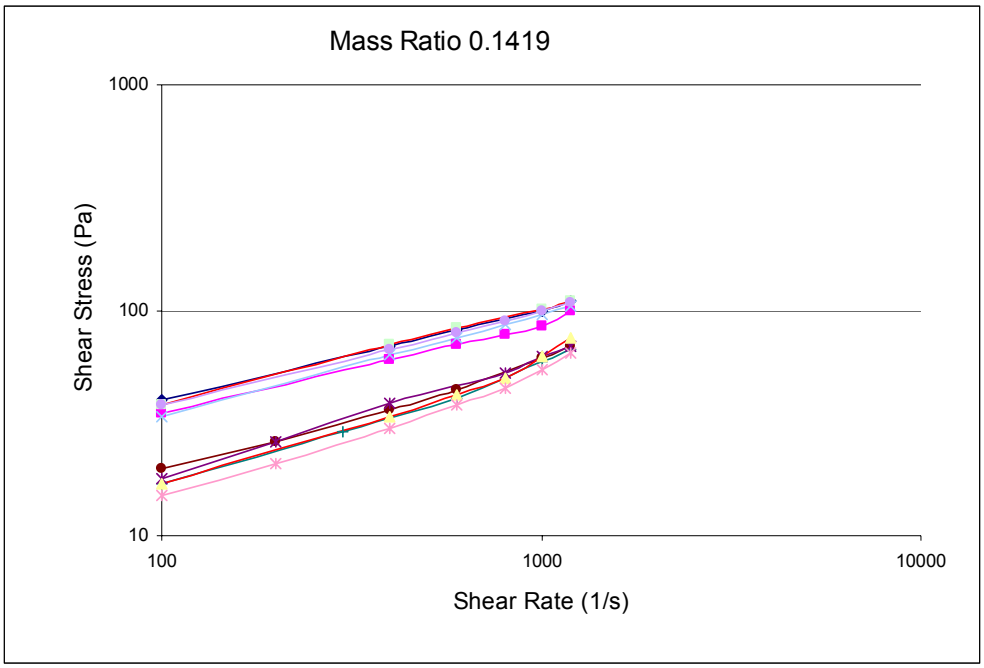

Looking at the data again, now on the same scale:

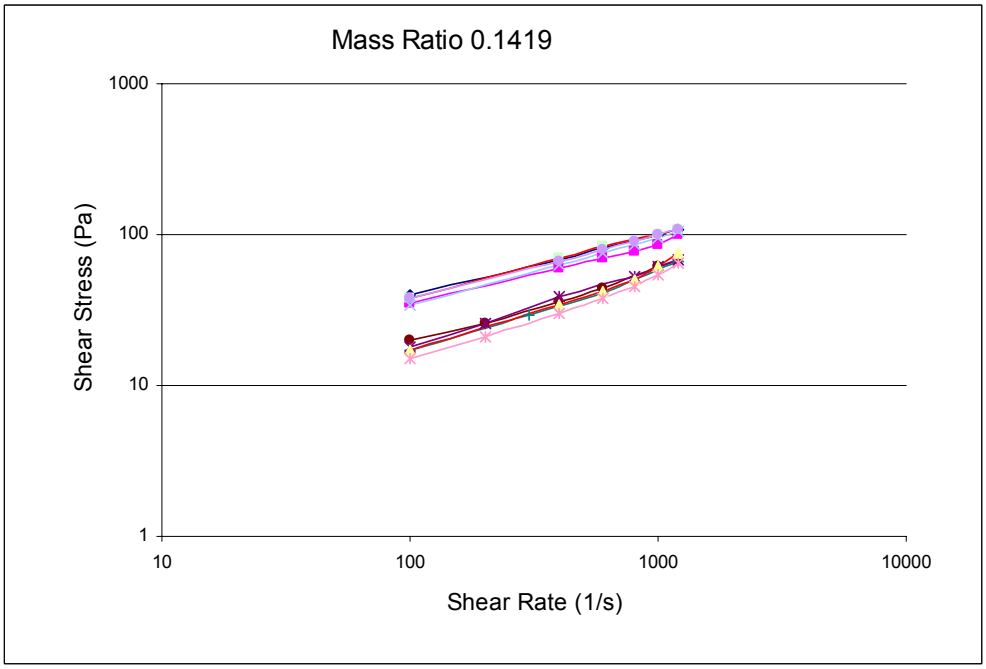

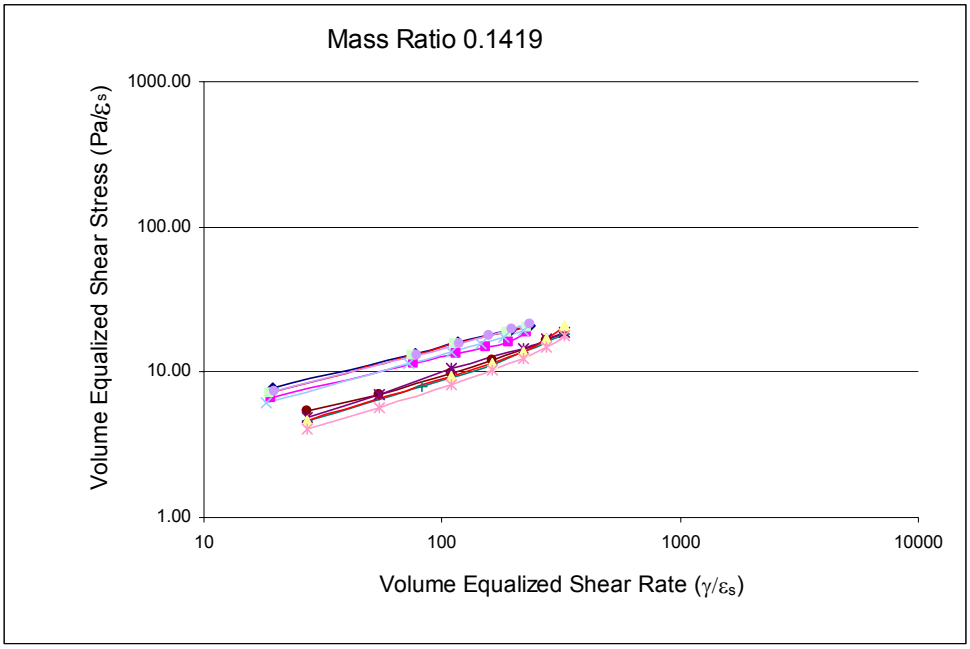

the span of data is narrowed by a factor of 10 by the application of the Volume Equalized Equations.

The calculated volume equalized K_{VE} and n:

Sample	Γ Quality	P psig	ε_s Expansion Ratio	n	K_{VE}
012705a	0.75	600	3.664	0.486	0.930
012705b	0.82	400	5.157	0.393	2.416
021005a	0.75	600	3.664	0.378	1.562
021005b	0.83	400	5.33	0.441	1.958
021105a	0.75	600	3.664	0.500	0.888
021105b	0.84	400	5.496	0.445	1.701
021405a	0.75	600	3.664	0.485	0.823
021405b	0.82	400	5.097	0.409	2.206
021505a	0.83	400	5.264	0.389	2.116
022105	0.75	600	3.664	0.530	0.850

Two additional Mass Flow Ratios were investigated albeit briefly. Graphs and calculations for those data points are shown in Appendix A:

A preliminary conclusion of these experiments could be that perhaps the precision and consistency of the Foam Generator and Viscometer Apparatus that is good enough as to allow us to see stratifications in the data that might, under some circumstances, go unnoticed as data scatter. Another conclusion could be that these experiments demonstrate a phenomenon between foam qualities less than 0.80 and foam qualities greater than 0.80. If a quality of 0.80 is indeed a boundary line across which different empirical results happen, then the majority of these experiments confirm that. Only with one test (mass ratio 0.1340 in Appendix A) was the initial foam and the expanded foam both on the same side of 0.80 quality (0.92 and 0.85). Interestingly, the volume equalized graph for that test did plot significantly as a single line.

Other conclusions might focus on pressure differences or the combination of quality and pressure such as a change in rheological models where .75 G @ 600 psig might be considered more alike with a Power Law fluid and .83 G @ 400 psig might be considered more alike with a Bingham Plastic.

As a preliminary investigation to see if the results from the Foam Generator and Viscometer Apparatus can be used in conjunction with volume equalized equations, the objectives were achieved.

In order to better sort out these observations, a full test matrix which would include several different qualities of foam, for example 0.60 to 0.95, and pressures from 30 psig to 800 psig, and temperatures from 68 ºF to180 ºF needs to be completed. These experiments have only investigated a single mass ratio and looked briefly at two others. This then, for the time being at least, is an oddity that warrants further investigation to see if this pattern continues under more varied conditions. If that proves to be the case then a mathematical explanation may be sought.

References:

1. “Volume Equalized Constitutive Equations for Foamed Polymer Solutions”, P. Valko and M.J. Economides, The Society of Rheology, Inc., 1992

APPENDIX A

Graphs and data on two additional mass flow ratios are provided below:

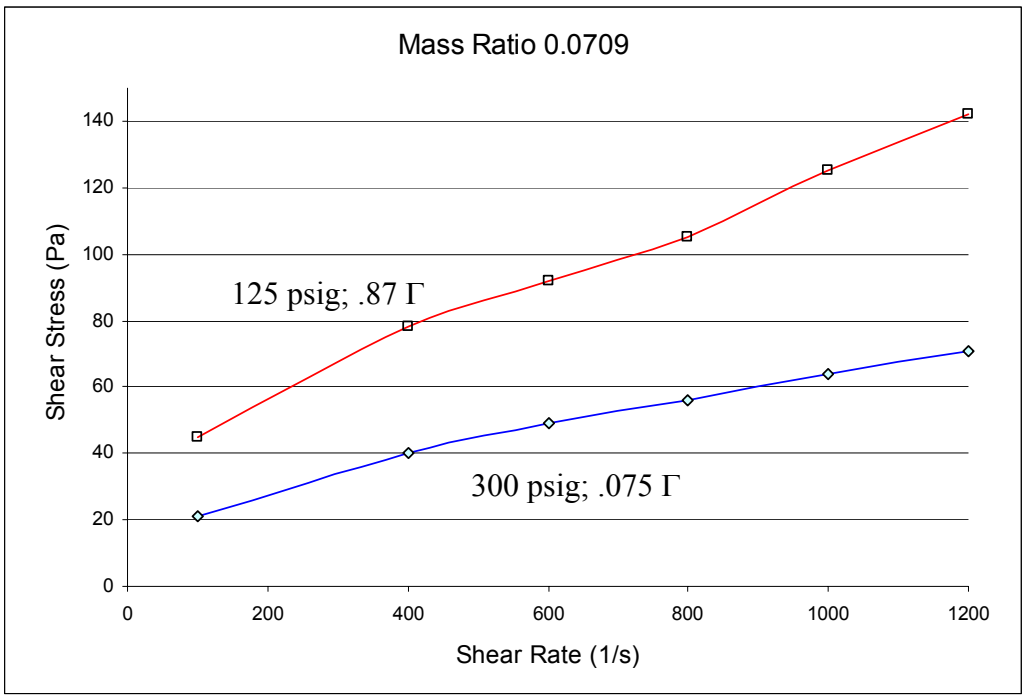

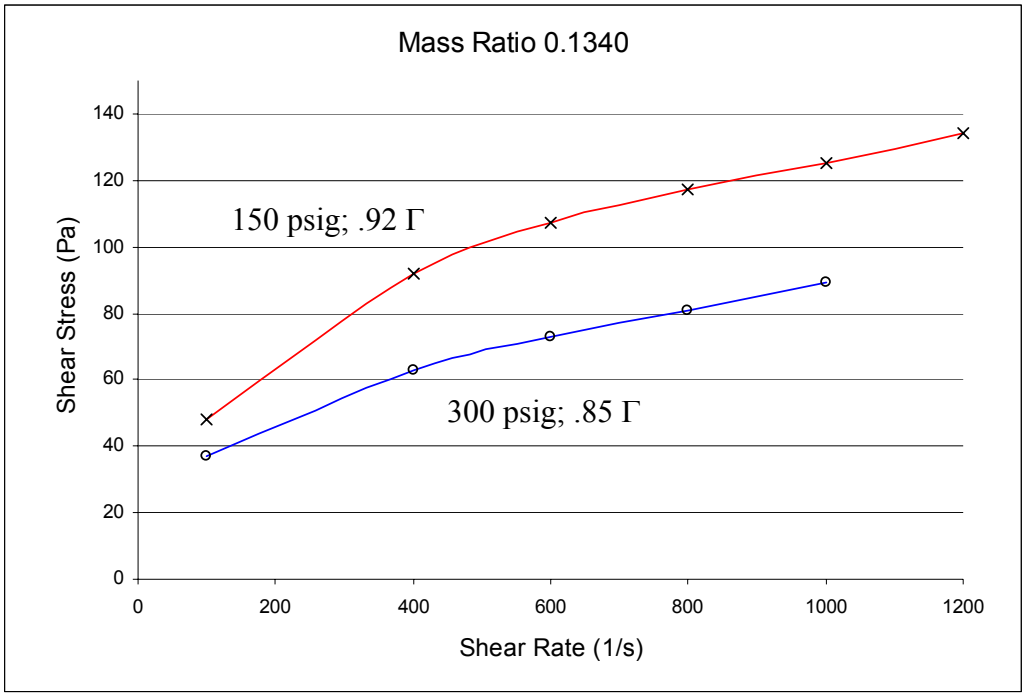
Mass Ratio 0.1340
Shear Stress (Pa)
Shear Rate (1/s)
150 psig; .92 Γ
300 psig; .85 Γ
0
20
40
60
80
100
120
140
0
200
400
600
800
1000
1200

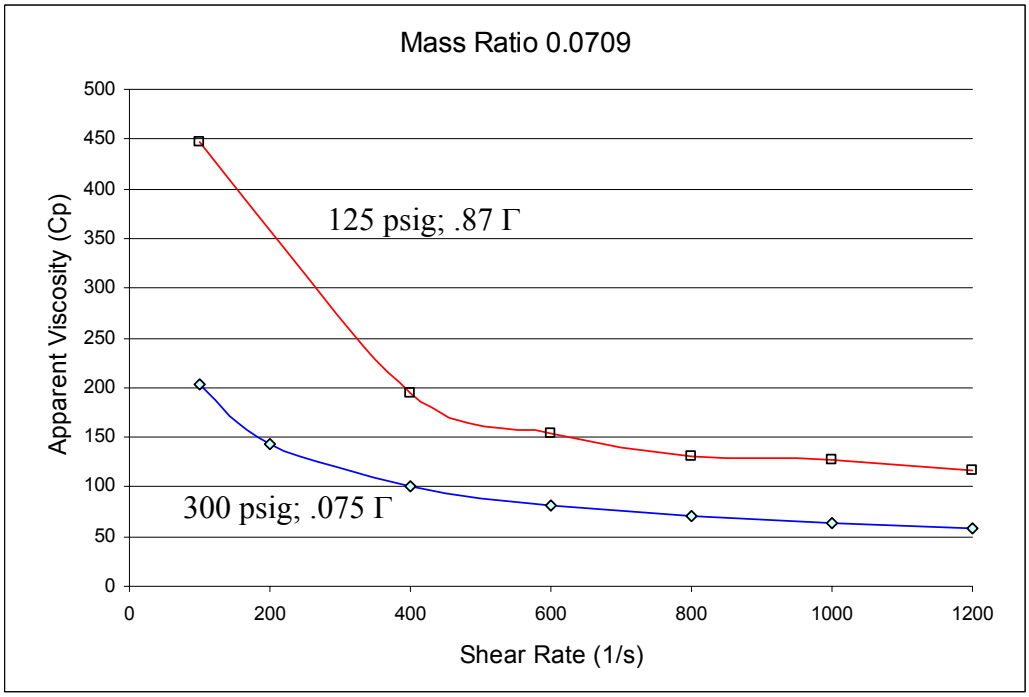
Mass Ratio 0.0709
Apparent Viscosity (Cp)
Shear Rate (1/s)
125 psig; .87 Γ
300 psig; .075 Γ
0
50
100
150
200
250
300
350
400
450
500
0
200
400
600
800
1000
1200

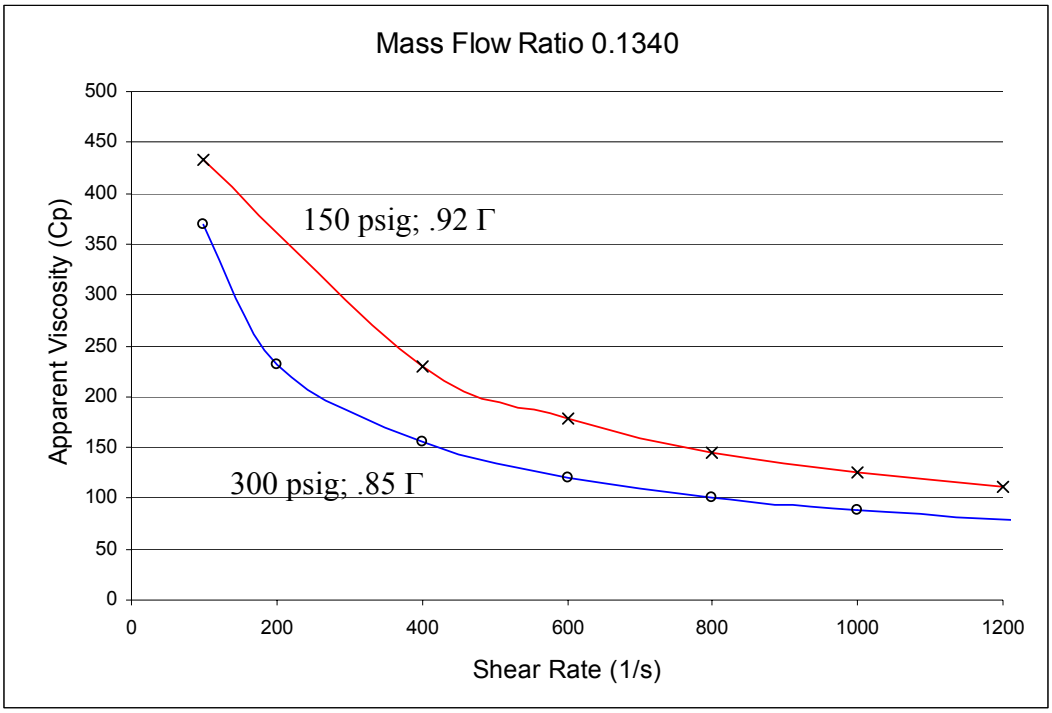
Mass Flow Ratio 0.1340
Apparent Viscosity (Cp)
500
450
400
350
300
250
200
150
100
50
0
0
200
400
600
800
1000
1200
Shear Rate (1/s)
150 psig; .92 Γ
300 psig; .85 Γ

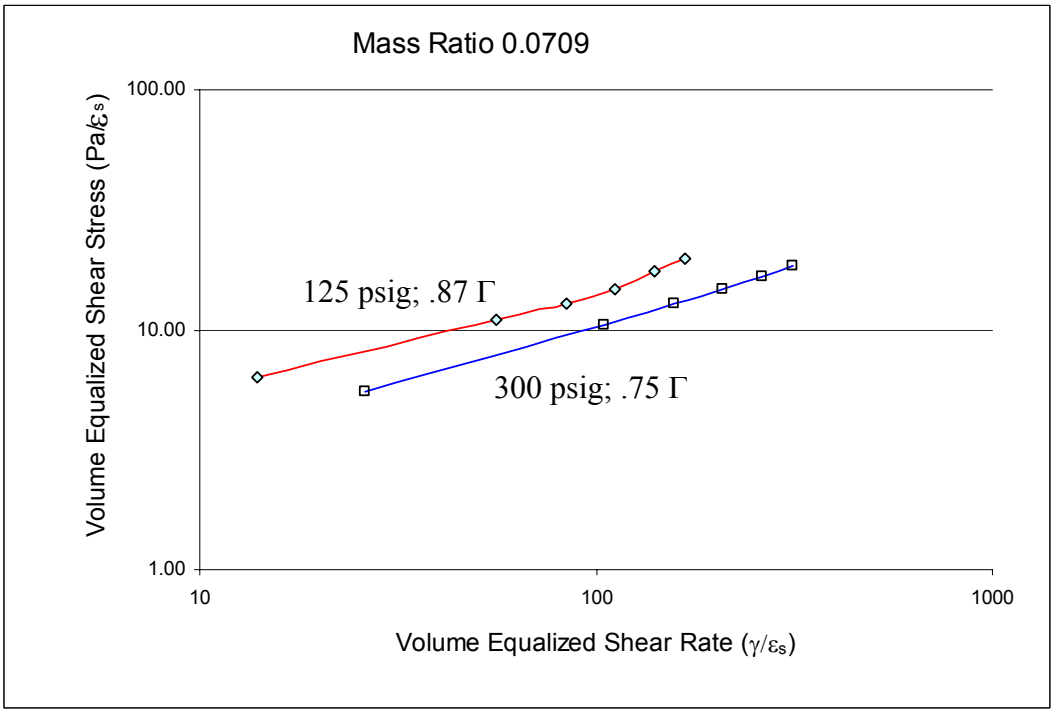
Mass Ratio 0.0709
Volume Equalized Shear Stress (Pa/εs)
100.00
10.00
1.00
10
100
1000
Volume Equalized Shear Rate (γ/εs)
125 psig; .87 Γ
300 psig; .75 Γ

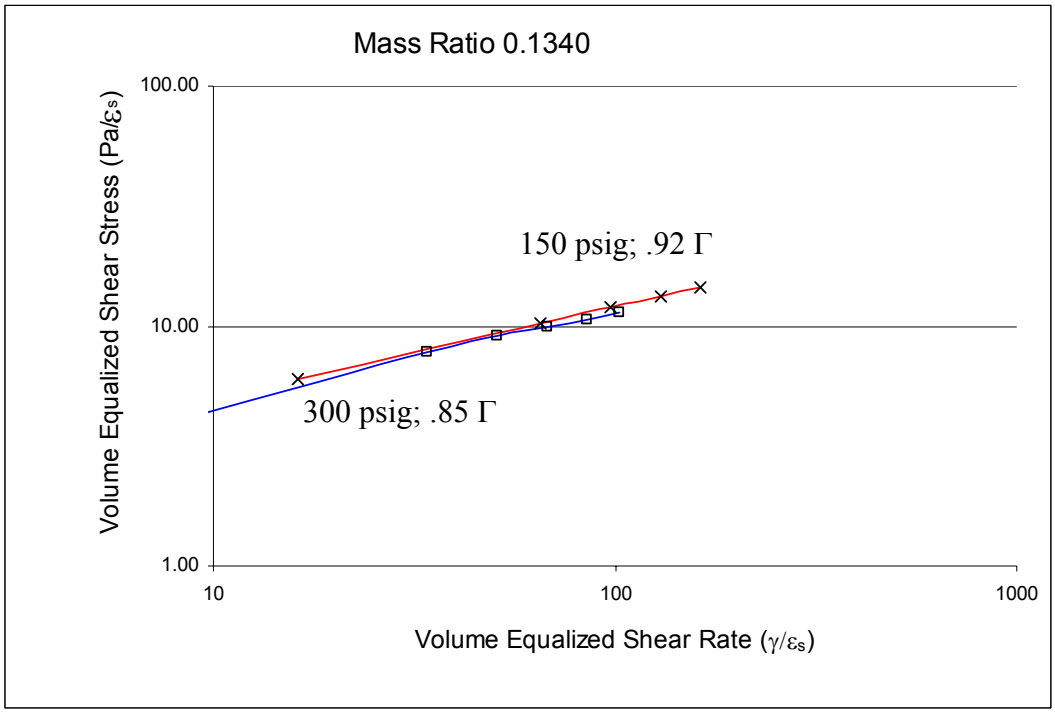

				P_1						P_2	
	v_1	Orig.	Γ_1	Orig.	m_{g1}	m_{l1}	β_1	ε_{s1}		Expanded	Expanded
	Orig. Vol.	Meas.	Orig.	Press.	gm	gm	mass	Orig.	End Meas.	Press.	Meas.
Sample	ml	inches	Qual.	psig	gas	water	ratio	Exp. Ratio	inches	psig	inches
021605	1408.4	6	0.75	300	24.978	352.088	0.0709	3.8244574	3.0625	125	5.75
021805	1408.5	6	0.85	300	28.312	211.275	0.134	6.1347811	2.9688	150	5.75

Expanded	v_2		m_{g2}			β_2	Γ_2	ε_{s2}
Vol.	New Vol.	Vol. N2	gm	Vol. H20	gm	mass		New
ml	ml	ml	gas	ml	water	ratio	New Qual.	Exp. Ratio
1350.21	725.21047	543.9078	12.86212	181.3026	181.30262	0.0709	0.87	7.153266
1350.21	703.56977	598.0343	14.14209	105.5355	105.53547	0.1340	0.92	11.73512

Sample	Γ	P	ε_s		
	Quality	psig	Expansion Ratio	n	K_{VE}
021605a	0.75	300	3.824	0.465	1.205
021605b	0.87	125	7.153	0.397	2.209
021805a	0.85	300	6.135	0.384	2.065
021805b	0.92	150	11.737	0.469	1.4979

An Experimental Study and Modeling of The Effect of Hydraulic Vibrations on Axial Force Transfer in Horizontal Wellbores

Elie Barakat

An Experimental Study and Modeling of the Effect of Hydraulic Vibrations on Axial Force Transfer in Horizontal Wellbores

INVESTIGATOR: Elie R. Barakat

INTRODUCTION:

Coiled tubing is an emerging technology and one of the fastest growing areas of oilfield drilling. Extending the reach is one of the main challenges for coiled tubing operators. Due to the inability to rotate coiled tubing, one of the main limitations is the poor axial force transfer and therefore inadequate weight on bit which in turn results in decreased rate of penetration and, as a consequence, increasing drilling cost per foot.

This paper presents an approach to reduce the problem of friction between coiled tubing and wellbores. The effect of hydraulic vibrations on this friction, induced by using a solenoid type valve, will be investigated. This valve interrupts the flow of water flowing inside the tube string which makes it vibrate.

Literature review of the problem showed that all formulas for buckling forces and force-pitch relation were derived under the assumptions of frictionless system and static conditions. There are no published papers that deal with dynamic systems that account for friction. The results of this study are useful for non rotating strings.

OBJECTIVES:

- The main purpose of this study is to perform experiments under controllable conditions in order to determine the effect of hydraulic vibrations on first, the buckling forces and second, the axial force transfer in horizontal wellbores. Variables such as the frequency f (Hz), the amplitude A (psi) of the pressure pulses, the water flow rate Q (gpm) and the axial loading force F (Lb) will be controlled and varied to study their effect in our experiments.
- Develop a corresponding mechanistic model or correlations.

APPROACH:

Extending the horizontal reach can be achieved by using hydraulic vibration and therefore introducing oscillations to the coiled tubing string. Thereby the effective friction factor between the coiled tubing and the wellbore will be reduced.

DELIVERABLES:

- Advisory board meeting progress and final report
- Experimental database and a regression model

EXPECTED COMPLETION DATE: May 2006

An Experimental Study and Modeling of the Effect of Hydraulic Vibrations on Axial Force Transfer in Horizontal Wellbores

Elie R. Barakat, The University of Tulsa Drilling Research Projects

This report is prepared for TUDRP Advisory Board Meeting, May 23-24, 2005, Tulsa-Oklahoma.

Investigator

Elie R. Barakat graduated from the American University of Beirut (AUB) with a Bachelor of Engineering in Mechanical Engineering in 2004. He is enrolled in the master's program at the University of Tulsa (TU) and has been working with TUDRP since February 2005.

Abstract

Coiled tubing is an emerging technology and one of the fastest growing areas of oilfield drilling. Extending the reach is one of the main challenges for coiled tubing operators. Owing to inability to rotate coiled tubing, one of the main limitations is the poor axial force transfer and therefore inadequate weight on bit which in turn results in decreased rate of penetration and, as a consequence, increasing drilling cost per foot.

This paper presents an approach to reduce the problem of friction between coiled tubing and wellbores. The effect of hydraulic vibrations, induced by using a solenoid type valve, on the friction will be investigated. This valve interrupts the flow of water flowing inside the tube string which makes it vibrate.

Literature review of the problem, a description of the buckling facility and preliminary experimental results and analysis are presented. The results of this study are useful for non rotating strings.

Project Status

Tasks	Percentage Accomplished
Literature review	75%
Buckling facility modification	75%
Experimentation	20%
Results / Data analysis	20%
Model development	20%
Reports	20%

Objectives

- The main purpose of this study is to perform experiments under controllable conditions in order to determine the effect of hydraulic vibrations on first, the buckling forces and second, the axial force transfer in horizontal wellbores. Variables such as the frequency f (Hz), the amplitude A (psi) of the pressure pulses, the water flow rate Q (gpm) and the axial loading force F (Lb) will be controlled and varied to study their effect in our experiments.
- Develop a corresponding mechanistic model or correlations.

Statement of Problem

Since the outset of the use of Coiled Tubing (CT), some main technical issues such as improvement of axial force transfer and helical buckling have been investigated. Owing to inability to rotate coiled tubing, there will be low axial force transfer and therefore inadequate weight on bit (WOB), which in turn results in decreased rate of penetration (ROP) and, as a consequence, increasing drilling cost per foot.

Actually in horizontal wellbores, the axial force transfer along CT decreases as the friction coefficient increases. In other words the higher the friction coefficient, the less axial force submitted from the top of CT to the bottom of CT. Therefore a high friction coefficient means it would be difficult to drill any further, since WOB would be very small. The friction coefficient is a very important parameter for predicting the axial force transfer along the pipe. Therefore improving axial force transfer by decreasing frictional drag, in order to

increase WOB and thereby increase ROP, is an important issue to investigate in this field.

So, there are two issues here to study, the effect of pressure pulses on both the buckling configuration which include the sinusoidal and unstable cases, and the post buckling configuration which is known as helical buckling.

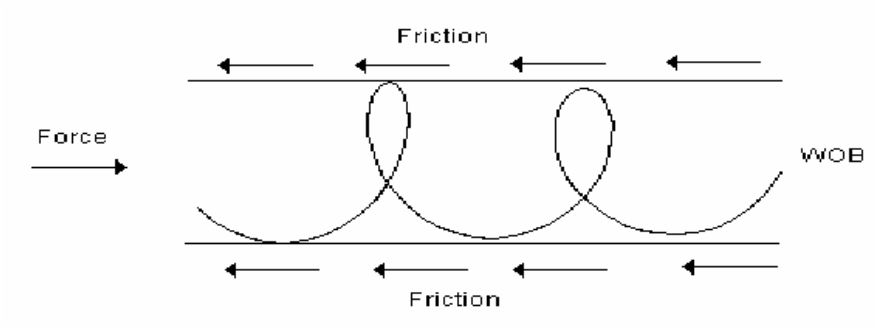

Approach

Extending the horizontal reach can be achieved by using hydraulic vibration and therefore introducing oscillations to the coiled tubing string. Thereby the effective friction factor between the coiled tubing and the wellbore will be reduced.

Oscillations are generated by pumping fluid down the CT and using a solenoid valve to interrupt the flow.

Literature review

A- Field case histories of the use of a dynamic excitation tool

A new dynamic excitation tool that reduces frictional drag adds to available options for further extending limits and capabilities of coiled tubing. This tool comprises a short positive displacement motor (PDM) which powers a valve. This valve creates pressure pulses which in turn induce axial vibration traveling outward from the tool and breaking static friction with the wellbore.

Whilst the tool has previously been used successfully in slide drilling applications, it had never been used before with coiled tubing. In order to prove the effectiveness of the coiled tubing tool, a series of trials were conducted at the Ullrig test facility in Norway. These tests confirmed the tool's ability to be very effective when used with coiled tubing.

Also, in Alaska, the excitation tool was picked up to drill the final sections to target depth (TD) of six wells when conventional drilling became difficult. The drilling engineer at the rig site of one of the wells commented that the drilling was steadier and easier with the tool compared with the previous BHA.

The tool was also used in fishing operations. At one of the wells, two perforation guns had become stuck inside the liner. Cement debris was suspected. The tool was used and the guns were recovered. The rig crew concluded that the tool was very effective and provides an additional option for removing large fish from the wellbore. These field applications demonstrated that the dynamic excitation tool is very effective.
Data is still being collected and analyzed to further improve learning and enable further improvements of the tool.

B- Buckling of pipes in inclined and horizontal wellbores

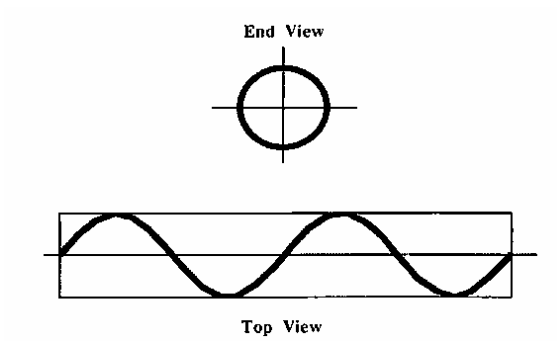

Helical buckling of pipes in wellbores

In the 1960's, Paslay and Bogy conducted a theoretical study of pipe buckling in inclined wellbores. They used a circular rod laterally constrained and in contact with a circular cylinder at the lower part. The buckling shape was assumed to be a multi-sine-wave shape along the lower side of the cylinder.

In the 1980's, based on Paslay and Bogy's research, Dawson and Paslay derived an explicit expression of sinusoidal buckling load for drillpipes in inclined wellbores. It is valid for frictionless systems and long strings.

$$Fcr = 2\sqrt{\frac{EIW \sin\alpha}{r}}$$

Where - EI is the bending stiffness.

- W is the pipe unit weight.

- α is the wellbore inclination angle.
- r is the radial clearance.

In 1962, Lubinski et al. published a paper on the prediction of forces and the movement of helically buckled pipes inside vertical wells. They assumed that the pipe would helically buckle, the system was frictionless, the pipe had no weight and the pitch was constant along the pipe. They developed the following expression for the force-pitch relationship:

$$F = \frac{8\pi^2 EI}{p^2}$$

Where - p is the pitch of the helix.

Mitchell, 1982-1986, derived the conventional beam column equations expressed in a polar coordinate system.

$$EI[-\theta^{IV} + 6(\theta')^2\theta''] - F\theta'' = 0$$

$$EI[-4\theta^{III}\theta^{I} - 3(\theta^{II})^2 + (\theta')^4] - F(\theta')^2 + \frac{N}{r} = 0$$

Where – θ is the angular coordinate
- N is the lateral contact force

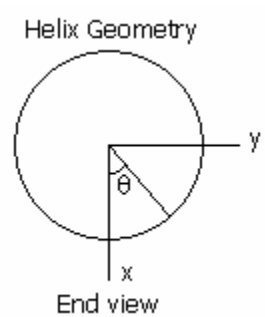

Neglecting higher order derivatives, Mitchell obtained an expression for lateral contact force exerted by helically buckled rod in a vertical well as

$$N = \frac{rF^2}{4EI}$$

In a deviated well, Miska, Qiu and Volk (1996, 1997) obtained the unit contact forces for

- A straight pipe

$$N = W \sin\alpha$$

- A buckled pipe in sinusoidal configuration

$$N = \frac{16\pi^4 EIrA^2}{p^4}(-A^2\cos^4\frac{2\pi z}{p} + 3\sin^2\frac{2\pi z}{p} - 4\cos^2\frac{2\pi z}{p}) + \frac{4\pi^2 rFA^2}{p^2}\cos^2\frac{2\pi z}{p} + W\sin\alpha\cos\theta$$

- A buckled pipe in helical configuration

$$N = \frac{rF^2}{4EI} + W\sin\alpha\cos\theta$$

Where - θ is the angular coordinate.

<u>In horizontal wells, with</u> $\alpha = 90$ <u>, these equations become</u>

- straight pipe

$$N = W$$

- A buckled pipe in sinusoidal configuration

$$N = \frac{16\pi^4 EIrA^2}{p^4}(-A^2\cos^4\frac{2\pi z}{p} + 3\sin^2\frac{2\pi z}{p} - 4\cos^2\frac{2\pi z}{p}) + \frac{4\pi^2 rFA^2}{p^2}\cos^2\frac{2\pi z}{p} + W\cos\theta$$

- A buckled pipe in helical configuration

$$N = \frac{16\pi^4 EIr}{p^4} + \frac{4\pi^2 rF}{p^2}W\cos\theta$$

Where - θ is the angular coordinate.

In 1990, Chen et al presented an energy analysis for the helical buckling of casing and tubing in horizontal wellbores, and derived the following helical buckling load equation

$$F = 2\sqrt{\frac{EIW}{r}}$$

Wu and Juvkam-Wold, in 1993, 1994, 1995, studied buckling and post-buckling behavior of pipes in deviated wellbores and developed an expression for the helical buckling load

$$F = 2(2\sqrt{2} - 1)\sqrt{\frac{EIW \sin\alpha}{r}}$$

Miska and Cunha (1995) studied the effect of axial and torsional loading in inclined wellbores. They used the principle of conservation of energy and assumed that the string was long enough, so that the end conditions do not affect the force-torque-pitch relation, the wellbore was circular and straight, and the system was frictionless. For axial load only and for a weightless string, they presented the following force-pitch relationship:

$$F = \frac{4\pi^2 EI}{p^2}$$

For a string with unit weight W and also subjected only to axial force F:

$$F = \frac{4\pi^2 EI}{p^2} + \frac{W \sin\alpha}{2\pi^2 r} p^2$$

And

$$p = \pi\sqrt[4]{\frac{8EIr}{W \sin\alpha}}$$

And the critical buckling force

$$Fcr = 2\sqrt{\frac{EIW \sin\alpha}{r}}$$

Miska and Cunha also studied the post-buckling behavior of pipes. They claimed that the external force needed to generate helical buckling is not considered constant during the change from the unstressed state to the state of equilibrium. In this case, the critical helical buckling force neglecting the effect of torque is:

$$Fcr = 4\sqrt{\frac{2EIW\sin\alpha}{r}}$$

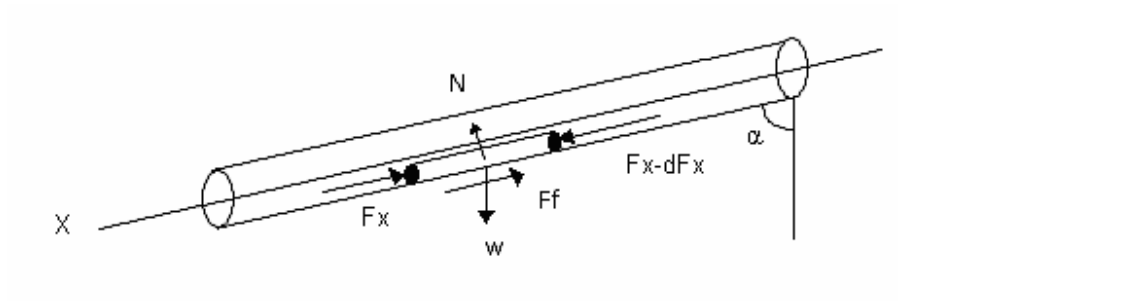

In 1993, Wu and Juvkam-Wold studied the frictional drag of helically buckled pipes in extended reach and horizontal wells. The differential equation for static axial force balance is

$$\frac{dFx}{dx} = W\cos\alpha - \mu N$$

Where x is the axial coordinate (down the positive direction), α is the inclination angle of the wellbore, $W\cos\alpha$ is the pipe unit weight component in the axial direction and N is the radial contact force as follows:

$$N = \frac{r\,F_x^2}{4EI} + W\sin\alpha$$

In summary, the following can be pointed out from this literature review:

- All the analytical studies on buckling behavior assume a pipe-wellbore system that is frictionless.
- All the analytical studies on buckling behavior assume static conditions.

These equations are not valid for our case where the friction plays an important role and where the conditions are very much dynamic.

In our literature review, we did not find any reference that deals with dynamic systems that include friction. It seems that this problem has not been researched. It is very interesting and important to see the effect of friction, vibrations and the buckling forces on axial force transfer.

Literature review of friction force

Dry friction or sliding friction occurs when one solid body slides on another. A force, called frictional force, is needed to maintain motion. The force needed to overcome friction and to drag one object over another depends upon the normal force between the two surfaces that are in contact.
Actually, the frictional force is proportional to this normal force, and has a more or less constant coefficient μ called coefficient of friction.

Empirically,

$$F = \mu N$$

The apparent friction is reduced when the lower surface vibrates very fast.

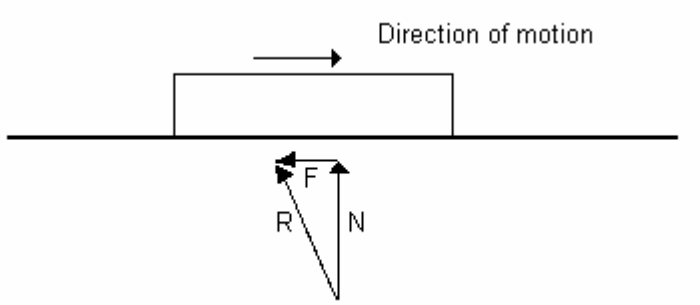

The relation between frictional force and the normal force for sliding contact.

Review of transient flow (water hammer)

Sudden closure of a control valve or stopping of a pump produces excess pressure in a pipeline.

Water hammer, or *hydraulic transient* as used more recently, refers to pressure fluctuations caused by a sudden increase or decrease in flow velocity. This unsteady state phenomenon deals with the change between kinetic energy and pressure energy. If the pressure induced exceeds the pressure rating of a pipe given by the manufacturer, the pipe may rupture.

Several common causes of hydraulic transient are:

- Sudden opening or closing of valves in a pipeline
- Starting or stopping the pumps in a pumping system
- Sudden increases in the inflow to a river or a sewer due to flash storm runoff
- Operating errors or malfunctioning of equipment.

Experimental facility

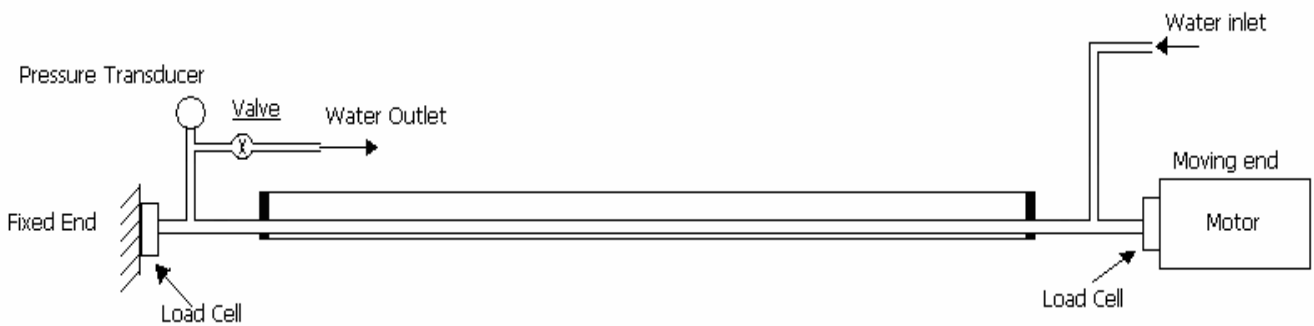

The TUDRP buckling facility is a straight horizontal wellbore composed of an inner steel pipe of outer diameter equal to 0.5 in and an acrylic tube representing the wellbore of an inner diameter of 1.9 in. The outer acrylic tube is composed of 7 sections, measuring 10 ft each. These sections are sealed by pipe repairing clamps with rubber liners. The whole tube is supported by steel stands and raised about a foot from the floor. The two ends of the buckling facility have flexible rubber seals between the outer and the inner tube to allow free movement of the inner tube. The space between the inner and outer tube is filled with water through a small hole drilled in the top part of the middle section. This water will simulate the drilling fluids in the wellbore. One end of the facility (the bottom end) is fixed. It supports the clamped connections for the inner pipe and also a load transducer (0 – 1000Lbf) for measuring the axial force transmitted to the bottom end from the top one.
The top end is composed of a horizontally moving clamped connection for the inner pipe and a top loading transducer (0 – 1000Lbf) for measuring axial force applied to the pipe. Horizontal motion of this end is provided by a screw drive mechanism sliding along two threaded rods and powered by a variable speed DC electric motor. A solenoid type valve is fixed at the end of the inner pipe in order to interrupt the flow.

Frequencies of 1 Hz and 2 Hz can be generated. Also, a pressure transducer is placed next to the valve. It measures the pressure in the inner pipe, which allows us to plot the pressure vs. time using Labview®. Data acquisition is performed by connecting the load cells and the pressure transducer to the analog/digital converting PCMXI board, which is capable of handling 12 data channels.

Preliminary experiments and analysis

The preliminary experiments were conducted using the following test matrix:

Flow rate (Gpm)	0	4	7
Frequency (Hz)	0	1	2
Top load (Lb)	200	250	300

Plots of the results

The following plots represent the case where first, the pipe is helically buckled due to the application of the various loads (200, 250, 300 lb) and then pressure pulsations are generated using the different water flow rates and frequencies.

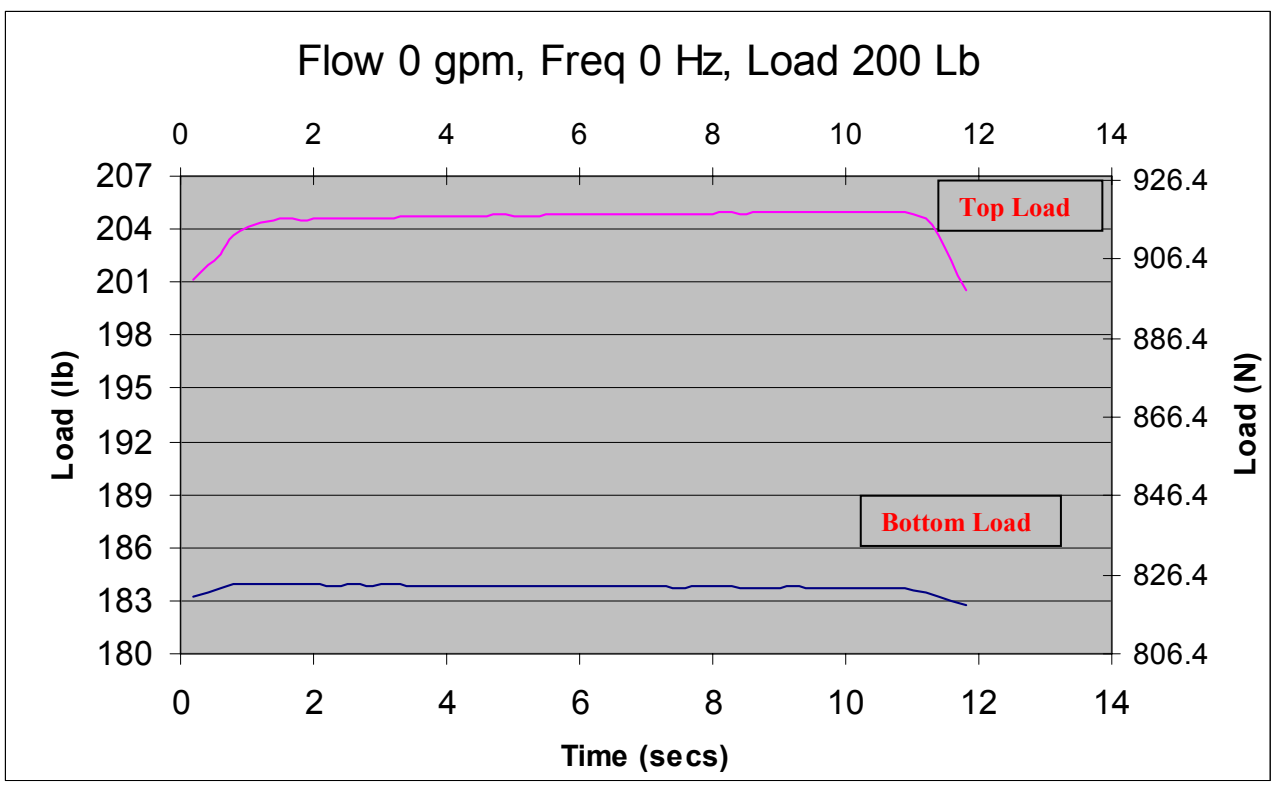

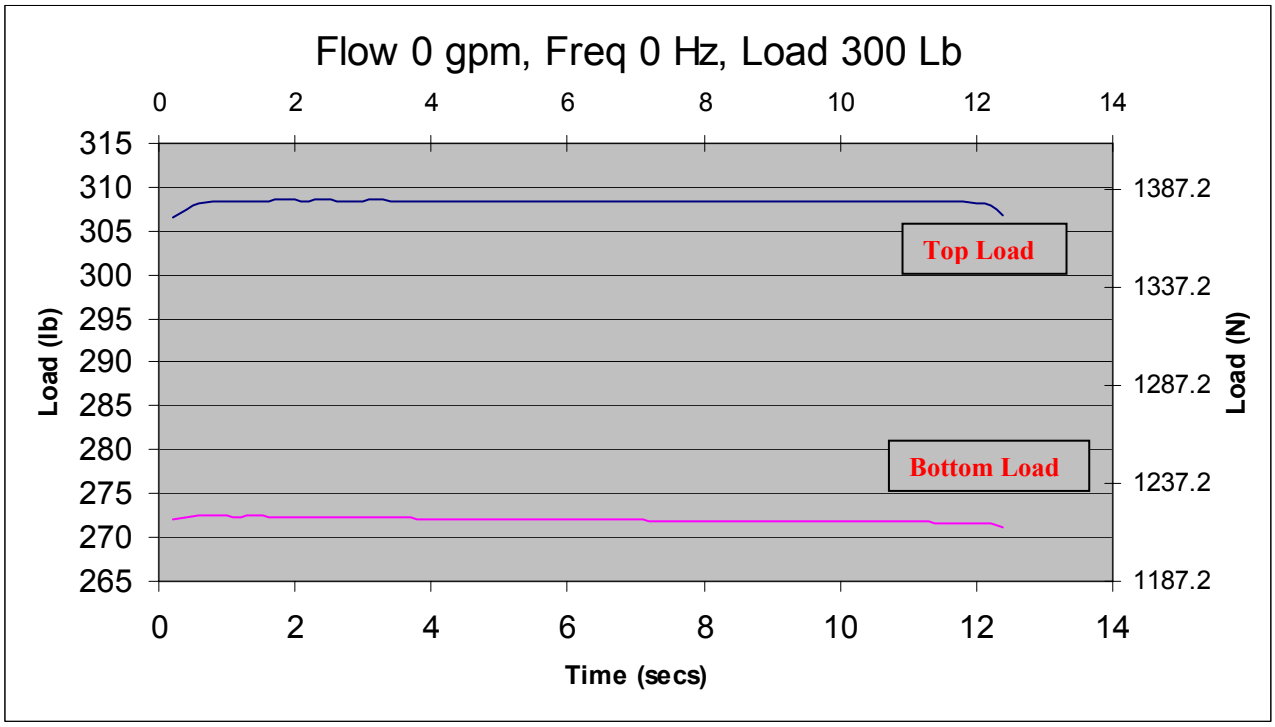
Flow 0 gpm, Freq 0 Hz, Load 300 Lb
Top Load
Bottom Load
Load (lb)
Load (N)
Time (secs)
315
310
305
300
295
290
285
280
275
270
265
1387.2
1337.2
1287.2
1237.2
1187.2
0
2
4
6
8
10
12
14

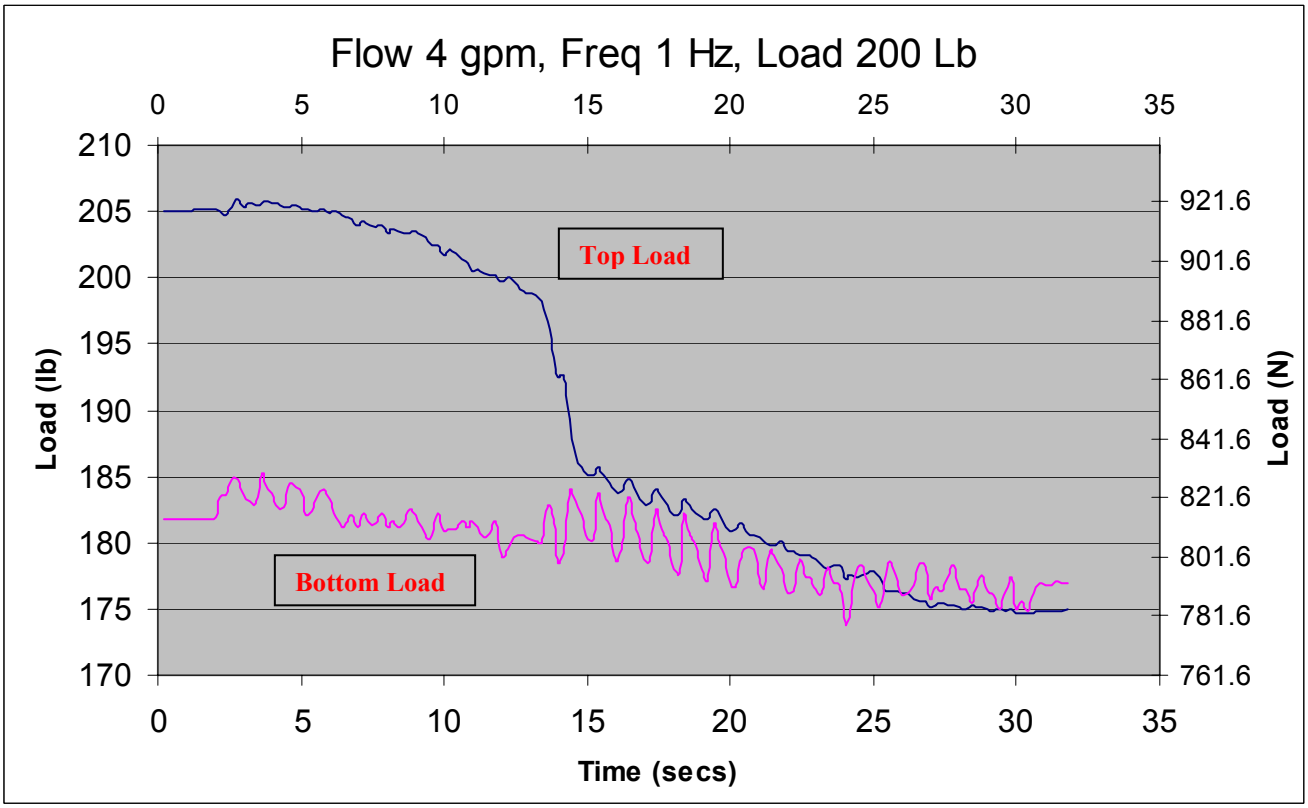
Flow 4 gpm, Freq 1 Hz, Load 200 Lb
Top Load
Bottom Load
Load (lb)
Load (N)
Time (secs)
210
205
200
195
190
185
180
175
170
921.6
901.6
881.6
861.6
841.6
821.6
801.6
781.6
761.6
0
5
10
15
20
25
30
35

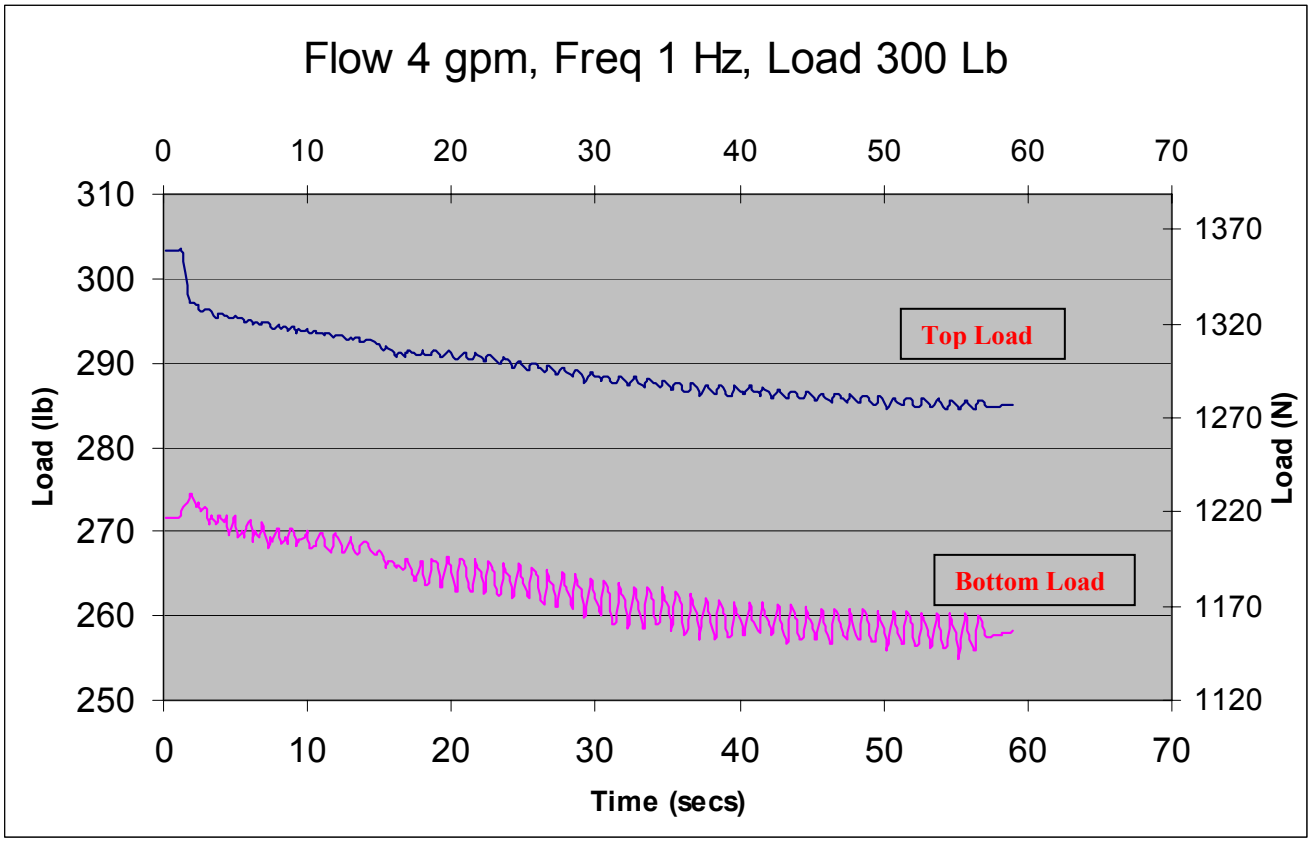
Flow 4 gpm, Freq 1 Hz, Load 300 Lb
Top Load
Bottom Load
Load (lb)
Load (N)
Time (secs)
310
300
290
280
270
260
250
1370
1320
1270
1220
1170
1120
0
10
20
30
40
50
60
70

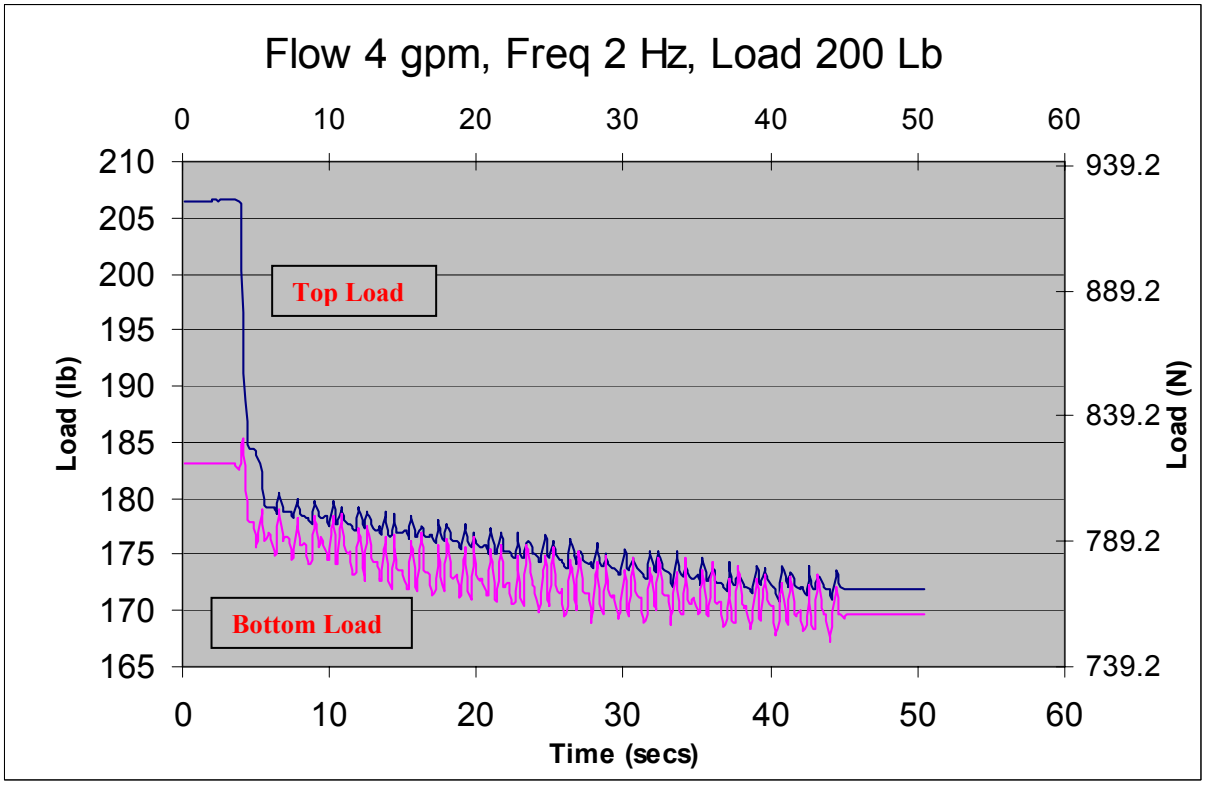
Flow 4 gpm, Freq 2 Hz, Load 200 Lb
Top Load
Bottom Load
Load (lb)
Load (N)
Time (secs)
210
205
200
195
190
185
180
175
170
165
939.2
889.2
839.2
789.2
739.2
0
10
20
30
40
50
60

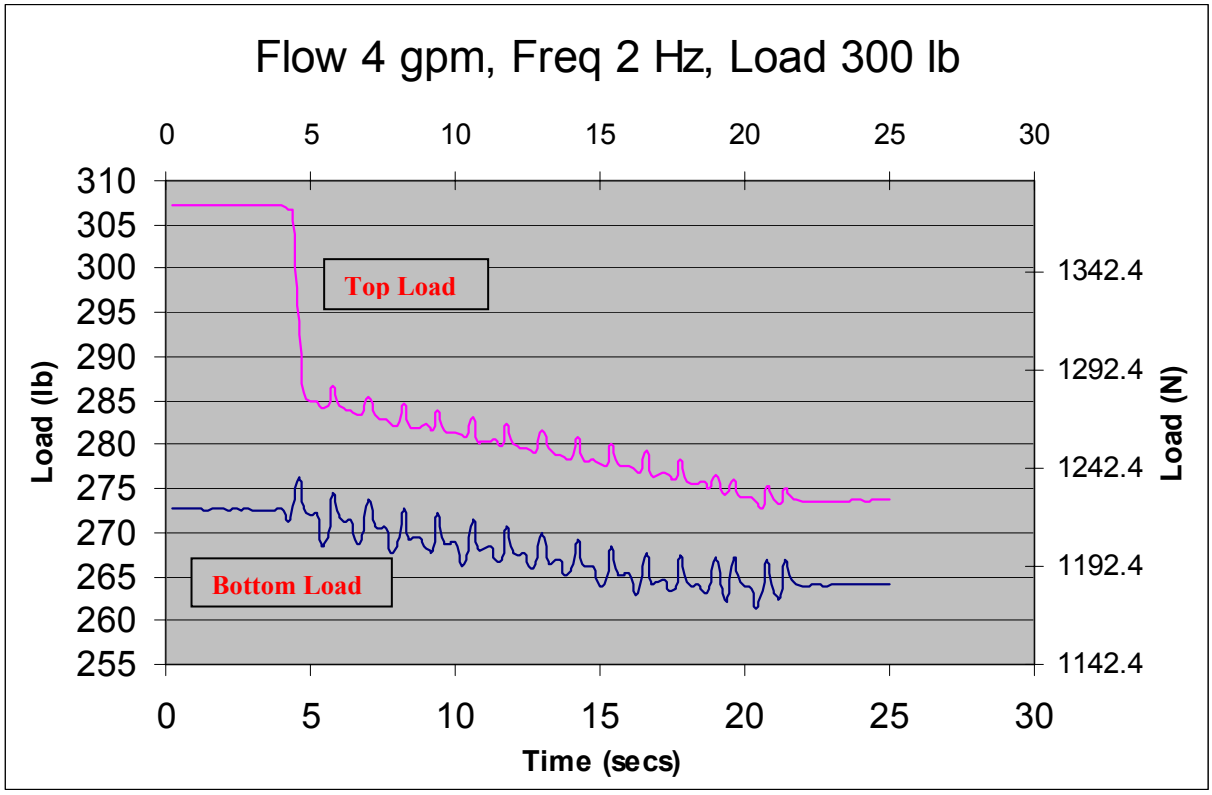
Flow 4 gpm, Freq 2 Hz, Load 300 lb
Top Load
Bottom Load
Load (lb)
Load (N)
Time (secs)
310
305
300
295
290
285
280
275
270
265
260
255
1342.4
1292.4
1242.4
1192.4
1142.4
0
5
10
15
20
25
30

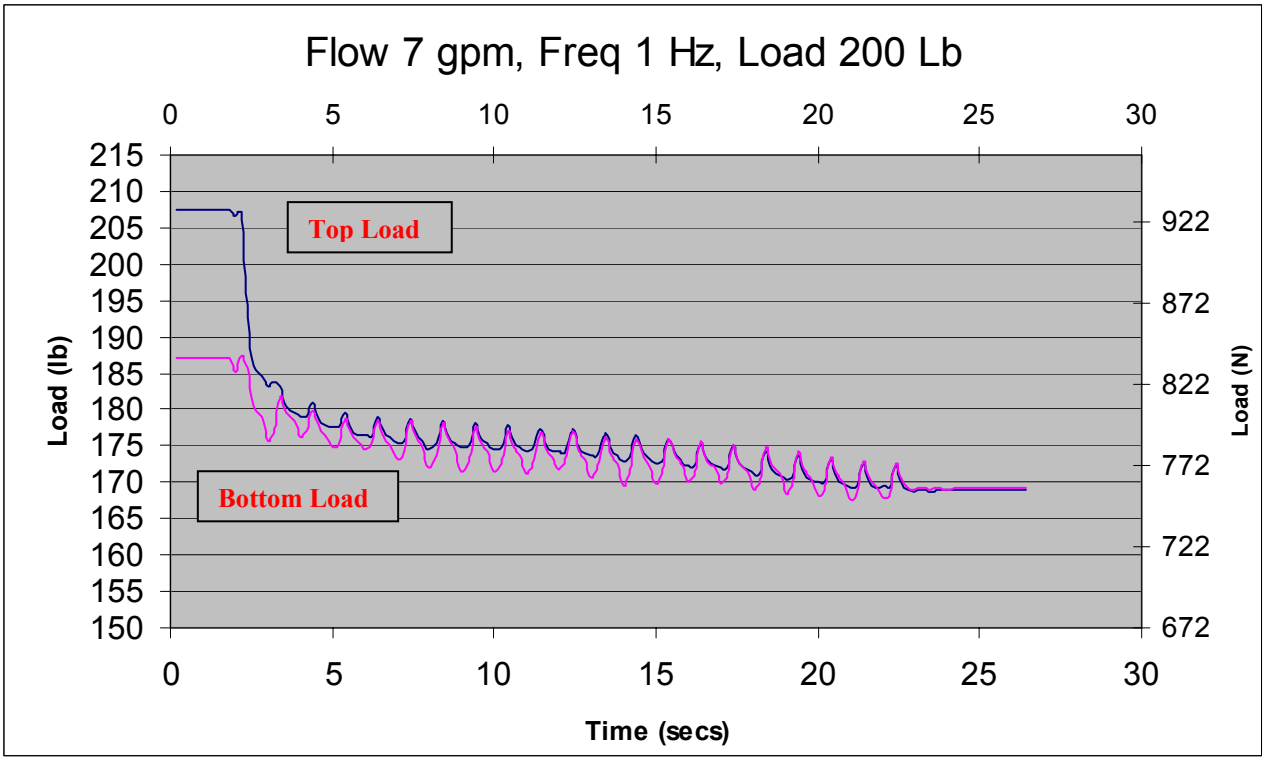
Flow 7 gpm, Freq 1 Hz, Load 200 Lb
Top Load
Bottom Load
Load (lb)
Load (N)
Time (secs)
215
210
205
200
195
190
185
180
175
170
165
160
155
150
922
872
822
772
722
672
0
5
10
15
20
25
30

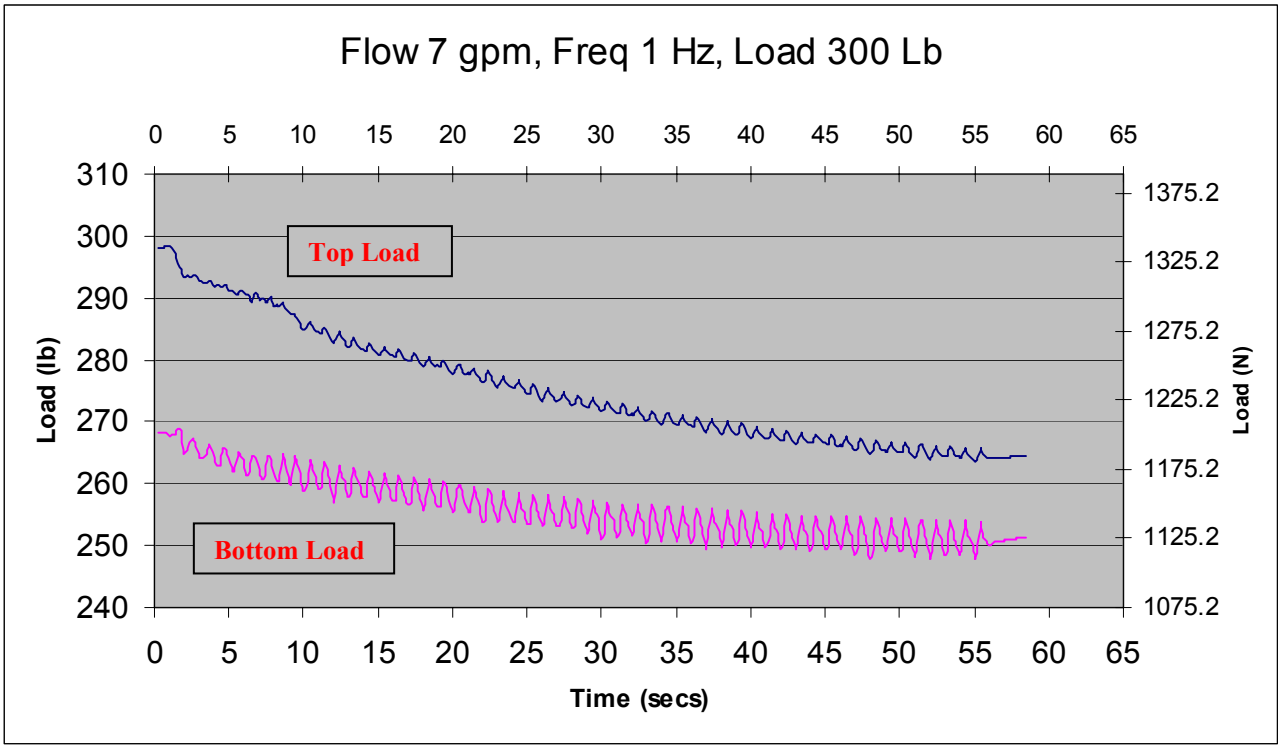
Flow 7 gpm, Freq 1 Hz, Load 300 Lb
Top Load
Bottom Load
Load (lb)
Load (N)
Time (secs)
310
300
290
280
270
260
250
240
1375.2
1325.2
1275.2
1225.2
1175.2
1125.2
1075.2
0 5 10 15 20 25 30 35 40 45 50 55 60 65

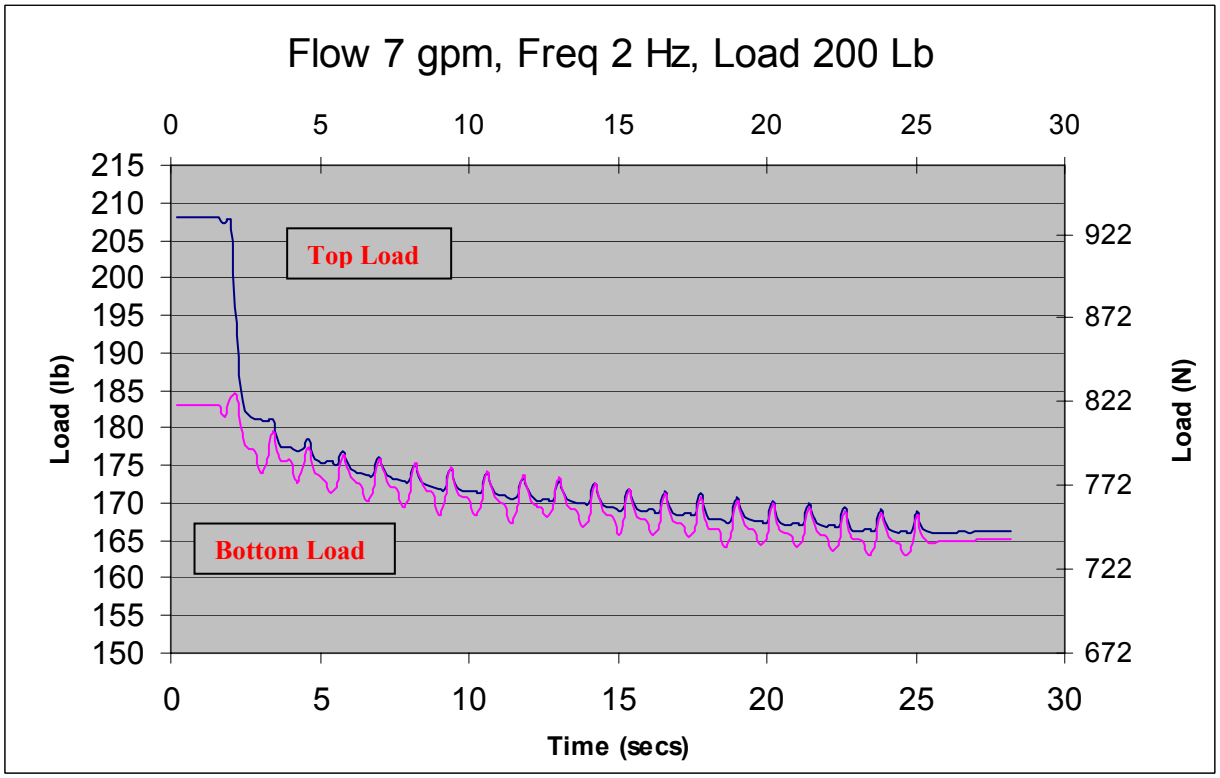
Flow 7 gpm, Freq 2 Hz, Load 200 Lb
Top Load
Bottom Load
Load (lb)
Load (N)
Time (secs)
215
210
205
200
195
190
185
180
175
170
165
160
155
150
922
872
822
772
722
672
0 5 10 15 20 25 30

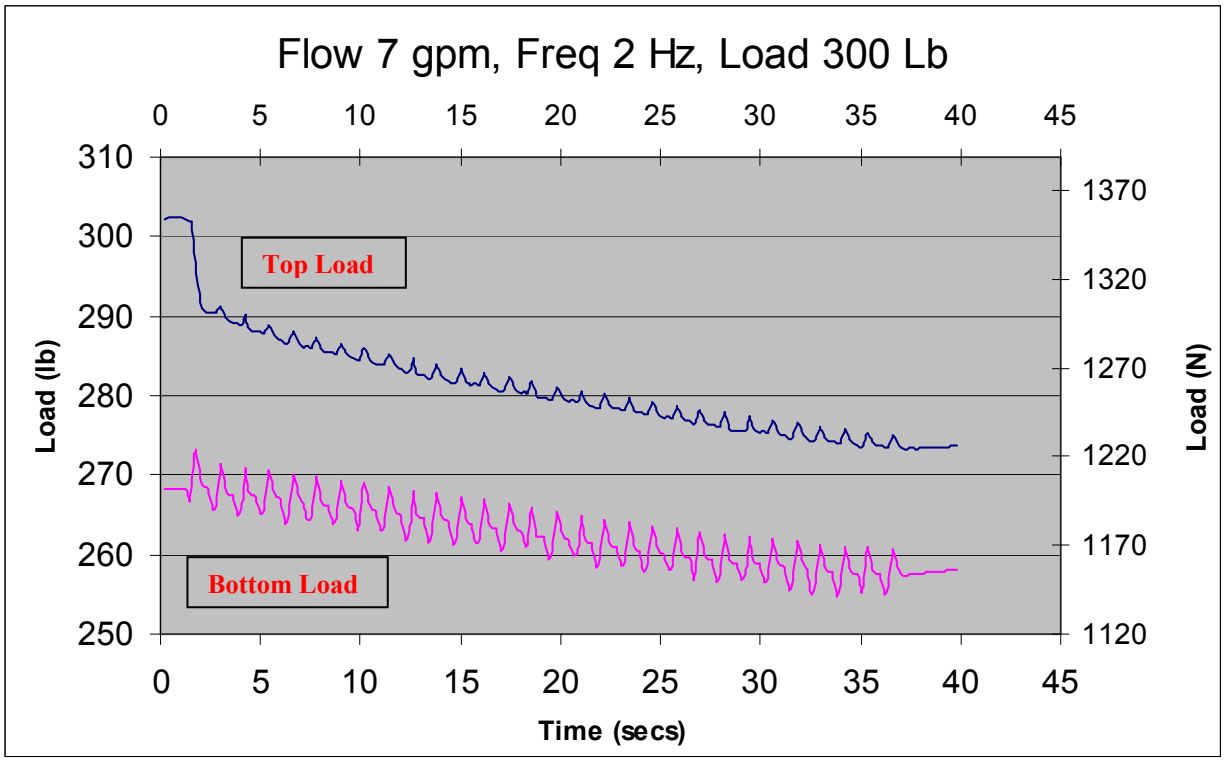

These experiments have been repeated 4 times.

Results

1) Friction Force (lb) 1 is the friction force before inducing pressure pulses.
2) Friction Force (lb) 2 is the friction force after inducing pressure pulses.
3) $E = \frac{Force.at.Bottom}{Force.at.Top} \times 100$

For 0 gpm, 0 Hz

Top load (lb)	Bottom load (lb)	Friction Force (lb) 1	Friction Force (lb) 2	Efficiency E
205	184	21	21	89.75 %
308	273	35	35	88.31 %

For 4 gpm, 1 Hz

Top load (lb)	Bottom load (lb)	Friction Force (lb) 1	Friction Force (lb) 2	Efficiency E
205	182	23	3	101.1 %
304	272	32	27	90.5 %

For 4 gpm, 2 Hz

Top load (lb)	Bottom load (lb)	Friction Force (lb) 1	Friction Force (lb) 2	Efficiency E
206	184	22	2	98.8 %
306	273	33	10	96.3 %

For 7 gpm, 1 Hz

Top load (lb)	Bottom load (lb)	Friction Force (lb) 1	Friction Force (lb) 2	Efficiency E
207	187	20	0	100 %
298	268	30	14	94.7 %

For 7 gpm, 2 Hz

Top load (lb)	Bottom load (lb)	Friction Force (lb) 1	Friction Force (lb) 2	Efficiency E
207	184	23	1	99.4 %
302	268	34	15	94.5 %

Data analysis

From the first two plots, where there is no flow and pulsations are not generated, we know the amount of load transmitted to the bottom load cell when loads of 200lb and 300lb are applied at the top end of the facility. For a 205 lb load, a load of 184 lb is transmitted whereas for 308lb a load of 273 lb is transmitted to the bottom load cell. These two lines remained constant for 10 secs, which shows that the facility is stable and reliable.

If we analyze the plots where a load of 200 lb is applied on the top cell, we observe that for a constant flow of 4 gpm, the curves came together much faster for the 2 Hz frequency than for the 1 Hz frequency. And for the 7 gpm flow, we see that the two curves are closer to each other in the case of 2 Hz than in the case of 1 Hz frequency. Therefore, a higher frequency gives a better result in bringing the curves of the top cell and bottom cell closer to each other.

In addition, if we check the 300 lb load on the top cell, we can affirm our previous remarks. For the constant flow of 4 gpm, the friction force of 32lb went down to 27lb for a frequency of 1Hz and from 33 to 10 lb for a frequency of 2 Hz. It is very important to notice that the bigger decrease in the friction force with 2 Hz was achieved in 20 secs as compared to 55 secs for 1Hz.

If we want to study the effect of the flow, we notice that for a constant frequency of 1Hz and a constant load of 300 lb, the friction force went down from 32 lb to 27 lb for a flow rate of 4 gpm and from 30 lb to 14 lb for a flow rate of 7 gpm.

Lastly, studying the effect of increasing both the flow rate from 4 gpm to 7 gpm and the frequency from 1 Hz to 2 Hz, we see that the friction decreased from 32 lb to 27 lb in 55 secs for a flow of 4 gpm and 1Hz and decreased from 34 lb to 15 lb in 35 sec for a flow of 7 gpm and 2 Hz, which means that increasing both the water flow rate and the frequency gives a better result in a faster time.

The efficiency E was defined as $E = \frac{Force.at.Bottom}{Force.at.Top} \times 100$. Our system's initial efficiency is 89.75 % when 200 lb are applied at the top end, and 88.31 % when 300 lb are applied at the top end. When we started generating the pressure pulses, the system efficiencies increased. This increase depends on the flow rate and frequency used, and ranges from around 2.2 % to around 12% in some cases. This increase in efficiency proves that more axial force is being transmitted to the bottom end. If we take a general look at our plots, we can conclude that a load of 200 lb and a corresponding friction force of 20 lb are relatively small, since the curves of the top load cell and the bottom one are converging very fast. In other words, the flow rates and frequencies used are typical for such loads. Will higher flow rates and frequencies give the same results for the 300 lb load?

In addition, we notice two main things in the shape of the curves. First, we see that a "dip" always occurs in the plot of the top load cell whenever the pulsations are first started. More experiments observing the dynamics of the pipe revealed that this is due to the fact that the tube is buckled more near the top load cell. This can be confirmed by measuring the pipe pitch along the wellbore. Considering the fact that the pipe is buckled more near the top end, when the first pressure pulses reach that section, the friction is overcome and therefore the configuration of the pipe slightly changes. This will cause the pitch length there to increase and less load will be measured on the top load cell.

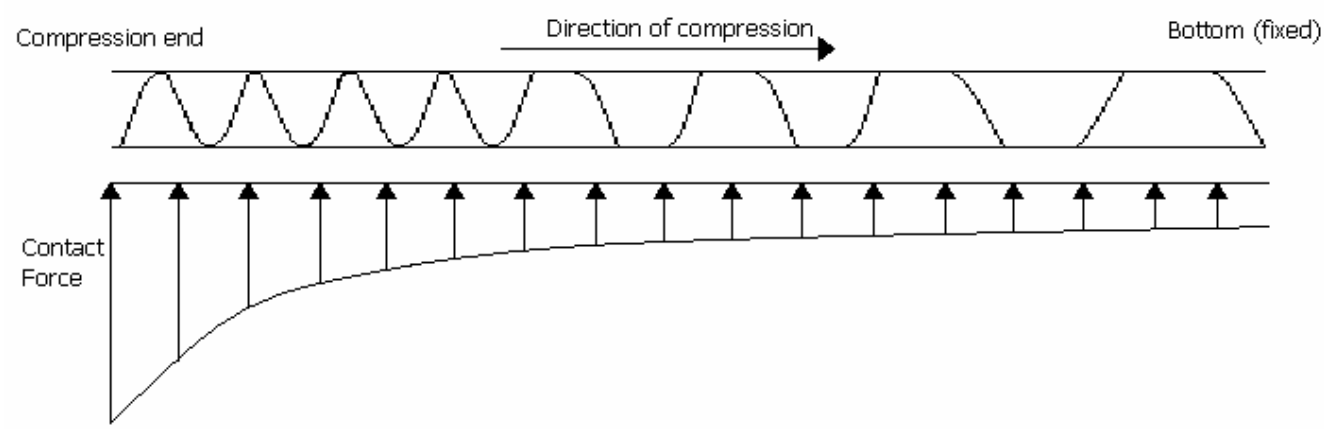

Second, the two curves representing the load on the top and the bottom cell are going down. We expected that the top load cell would remain at the initial compression load and that the bottom cell would read more load as more axial force was being transmitted to the bottom. This did not happen. First, our applied load was constant and second, we observed that the configuration of the pipe was more severely buckled. This explains the reduction in the load on the two load cells.

Conclusions

- The TUDRP buckling facility has been modified in order to be able to run water inside the drilling tube. A pressure transducer and a solenoid type valve were also added.
- Experiments have been made using top loads of 200, 250 and 300 lb and flow rates of 0, 4 and 7 gpm and frequencies of 1 Hz and 2 Hz.
- The friction force decreases when pressure pulses are induced in the drillpipe.
- The efficiency increases when pressure pulses are induced in the drillpipe.
- The bottom load cell did not read an increase in the load applied.
- The top curve and the bottom curve appear to decrease because the configuration of the pipe is changing.
- The pitch is smaller near the top end and the contact force is bigger near the top end.

Future work

Based on the preliminary results, many modifications and investigations should be made in the near future:

Technical modifications:

- The faucet pressure is not always constant, and because the inner pressure of the pipe is a critical parameter, a reservoir will be built and a pump will be used.
- We should add a flow meter in order to accurately measure the flow rate which, as we saw, it is an important parameter in our experiments.
- A new valve that can generate higher frequencies will be used.

Future work:

- More experiments using higher frequencies will be conducted. These experiments will deal with two cases: First, initiating the pressure pulses while buckling the pipe to study the effect of these pulses on buckling forces, and, second, initiating the pulses after the pipe is helically buckled to study the effect of these pulses on axial force transfer.
- A model will be generated.

References

1. L.J. Leising and K.R. Newman, "Coiled-Tubing Drilling" SPE 24594 presented at the 67th Annual Technical Conference and Exhibition of the Society of Petroleum Engineers held in Washington, DC, October 4-7, 1992

2. Dawson, R. and Pasaly, P.R:"Drillpipe Buckling in Inclined Holes", JPT (October 1984)1734; Trans., AIME, 227.

3. S. Miska, W. Qiu, L. Volk and J.C. Cunha "An Improved Analysis of Axial Force Along Coiled Tubing in Inclined/Horizontal Wellbore" Paper SPE 37056 presented at the 1996 SPE International Conference on horizontal well technology held in Calgary, Canada, 18-20 November 1996

4. Alexander Martinez "Experimental study of Axial Force Transfer Continuous Pipes-The Lateral Contact Force Effect-" MS thesis, University of Tulsa, 1999

5. S. Miska, W. Qiu, R. Samuel, A. Sanchez, I. Azouz and P. Johnson "Advanced Horizontal Coiled Tubing Drilling System" Annual Report For The Period Of January-August 1995, The University of Tulsa.

6. L. Robertson, SPE, Andergauge Ltd, C. J. Mason, SPE, A.S. Sherwood, SPE, BP plc, K. R. Newman, SPE, CTES LP," Dynamic Excitation Tool: Developmental Testing and CTD Field Case Histories", SPE 89519 presented at the SPE/ICoTA Coiled Tubing Conference and Exhibition held in Houston, Texas, U.S.A., ,23-24 March 2004.

7. Carl W. Stoesz, Joe P. DeGeare "Low-Frequency Downhole Vibration Technology Applied to Fishing Operations" Paper SPE 63129 presented at the 2000 SPE Annual Technical Conference and Exhibition held in Dallas, Texas, U.S.A., 1–4 October 2000.

8. David B. Haughton, Joe P. DeGeare "Downhole Impulse vs. Downhole Impacts Improve Recovery of Stuck Retrievable Packers", Paper SPE 90737 presented at the SPE Annual Technical Conference and Exhibition held in Houston, Texas, U.S.A., 26-29 September 2004

9. Andrey A. Zdvizhkov "Study of Induced Torsion and Axial Force Transfer in Helically Buckled Tubular", The University of Tulsa, Tulsa, Oklahoma, 2004

10. Richard P. Feynman "The Feynman, Lectures on Physics", vol.1, 1963.

11. E. P. POPOV "Mechanics of Materials", second edition, 1976.

12. Stefan Miska, J. C. Cunha "An analysis of Helical Buckling of Tubulars Subjected to Axial and Torsional Loading in inclined Wellbores", Paper SPE 29460 presented at the Production Operations Symposium held in Oklahoma City, OK, U.S.A 2-4 April 1995.

13. L. Robertson, SPE, Andergauge Ltd, C.J. Manson, SPE,A.S. Sherwood, SPE, BP plc, K. R. Newman, SPE, CTES LP "Dynamic Excitation Tool: Developmental Testing and CTD Field Case Histories" Paper SPE 89519 presented at the SPE/ICoTA Coiled Tubing Conference in Houston, TX, USA 2004.

14. Mitchell, R.F.; "Buckling Behavior of Well Tubing: The Packer Effect" SPE 9264, Society Of Petroleum Journal, 1982.

15. Mitchell, R.F.; "Frictional Forces in Helical Buckling of Tubing", SPE 13064, presented at the 59th Annual Technical Conference and Exhibition, Houston, USA, September 1984.

16. Mitchell, R.F.; "Simple Frictional Forces in Helical Buckling of Tubing", SPE 13064, SPE Drilling Engineering, December 1986.

Determination of Cutting Lag in Horizontal and Deviated Wells

Research Proposal

Augusto Garcia

Determination of Cuttings Lag in Horizontal and Deviated Wells

Investigator: Augusto Garcia

Overview

Accurate geological models are essential for oil and gas reservoirs exploration. Due to the inaccessibility of reservoirs for direct investigation, various techniques are used: 3-D seismic mapping; Logging; Coring; and Cuttings investigation.

Cuttings investigation is highly self-descriptive and quite inexpensive. This technique provides complete information on rock and fluid properties. In addition, it is continuous since cuttings must be removed from the well-bore. The most important advantage is that there is no additional cost, because cuttings must be generated at the drill bit and transported to the surface. However, it can be efficiently used only if we assign particular samples of rock to the specific locations, which is not a simple task. Accurate models of cuttings transport should be employed to estimate the difference in time between drilling mud and cuttings, traveling from the same location.

Research Objectives

1. Determine experimentally the transport velocity of cuttings in horizontal and high-angle boreholes
2. Produce a computer model for cuttings lag

Practical Applications

1. Use the lag model during the well-planning process to estimate the formation properties and lithology

Project Deliverables

1. Advisory Board Meeting (ABM) Research proposal
2. A mechanistic model to produce lag time diagram for horizontal and high inclined wells
3. The experimental data will be used to determine the cuttings velocity and compare the results with the computer lag model
4. Semi-annual Advisory Board Meetings Reports and Final Report

Determination of Cuttings Lag in Horizontal and Deviated Wells

Augusto José Garcia-Hernandez, University of Tulsa, Drilling Research Projects,
B.S. in Mechanical Engineering, Central University of Venezuela.

This proposal is prepared for TUDRP Advisory Board Meeting, May 23-24, 2005, Tulsa-Oklahoma.

Introduction:

Accurate geological models are essential for oil and gas reservoirs exploration. Due to the inaccessibility of reservoir for direct investigation, various techniques are used:

- 3-D seismic mapping
- Logging
- Coring
- Cuttings investigation.

All of them have different degree of certainty and different cost of utilization. 3-D seismic is a progressive and rapidly growing technique, but it is very expensive and does not provide high resolution. Moreover, it requires prior knowledge of lithology and rock and fluid elastic properties, which is usually provided by other techniques. Logging is another progressive technique, but it is also expensive and has limited resolution. Compare to them, coring is the best technique from the self-descriptiveness point of view. It provides wide range of information on rock and fluid properties, but it is quite expensive. Moreover, it is quite difficult to get a continuous core and some losses of information usually happen. In contrast to these techniques, cuttings investigation is highly self-descriptive and quite inexpensive. This technique provides complete information on rock and fluid properties. In addition, it is continuous since cuttings must be removed from the well-bore. The most important advantage is that there is no additional cost, because cuttings must be generated at the drill bit and transported to the surface.

Cuttings transport is an important part during the drilling process. Numerous experimental studies have been performed to investigate factors related to cuttings removal from the well-bore and to optimize drilling

efficiency. Several empirical and analytical solutions were developed in recent years. They provide good understanding of cuttings removal and allow modeling of this process. But, effective models of cuttings removal are important not only as a tool for drilling optimization. They are also a good source of geological information.

Drilled cuttings are readily available and excellent source of information about rock and fluid properties. However, it can be efficiently used only if we assign particular samples of rock to the specific locations, which is not a simple task. Accurate models of cuttings transport should be employed to estimate the difference in time between drilling mud and cuttings, traveling from the same location.

Objectives:

1. To determine experimentally the transport velocity of cuttings in horizontal and high-angle boreholes.
2. To produce a computer model for cuttings lag.

Problem Statement:

During the drilling process, cuttings are generated at the bottom of the hole and transported to the surface by the drilling fluid. Essential information about the properties of the formation (type, strength, porosity, etc) is inferred from the cuttings, but there is some uncertainty about the source depth of the cuttings during drilling operations. In addition, it is important to determine the original location where the cuttings were generated for formation characterization.

In order to know the source depth of cuttings that are collected at the surface, it is essential to determine correctly the transport velocity of the cuttings.

As we know, the cuttings transport velocity is directly related to the slip velocity. For the sake of simplicity we have divided the well-bore in three segments: horizontal, inclined and vertical, as shown in Fig. 1.

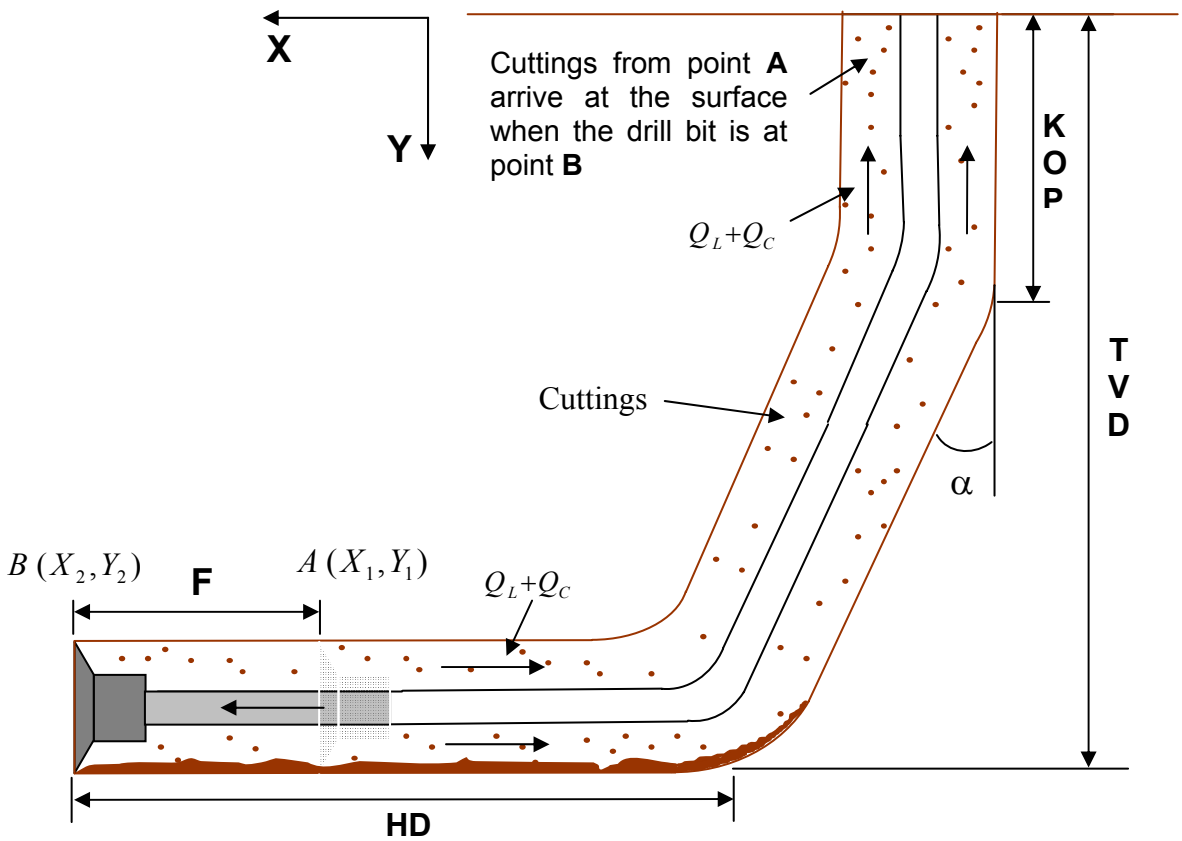

Figure 1.- Schematic representation of a well-bore

Description of the process:

Let us say that at time t=0 the bit penetrates through the formation under consideration.

As the time is progressing a footage is drilled.

The cuttings generated at the point "A" (Q_C) travel to the surface suspended in the drilling fluid (Q_L) while the bit arrives to the point "B".

Assumptions:

- No interruption of the drilling process (no connection time).
- Steady state; Transport velocity in each segment= const.

It can be shown that the relationships between the source locations and the transport velocity are given by:

Vertical segment	Inclined segment	Horizontal segment
$S_{DY(Vertical)} = \dfrac{V_{T(Vertical)} D_C}{V_{T(Vertical)} + \overline{ROP}}$	$S_{DX(Inclined)} = \dfrac{V_{T(Incllined)} L_I Sin(\alpha)}{V_{T(Inclined)} + \overline{ROP}}$	$S_{DX(Horizontal)} = \dfrac{V_{T(Horizontal)} L_H}{V_{T(Horizontal)} + \overline{ROP}}$
	$S_{DY(Inclined)} = \dfrac{V_{T(Incllined)} L_I Cos(\alpha)}{V_{T(Inclined)} + \overline{ROP}}$	

where:

V_L = *Liquid Velocity*

$S_{DX(V,I,H)}$ = *Horizontal coordinate of the cuttings Source*

$S_{DY(V,I,H)}$ = *Vertical coordinate of the cuttings Source*

D_C = *Vertical Current Depth*

L_I = *Inclined section lenght*

L_H = *Horizontal section lenght*

α = *Well inclination angle*

$\overline{ROP}$ = *Average Rate of Penetration*

V_T = *Transport Velocity*

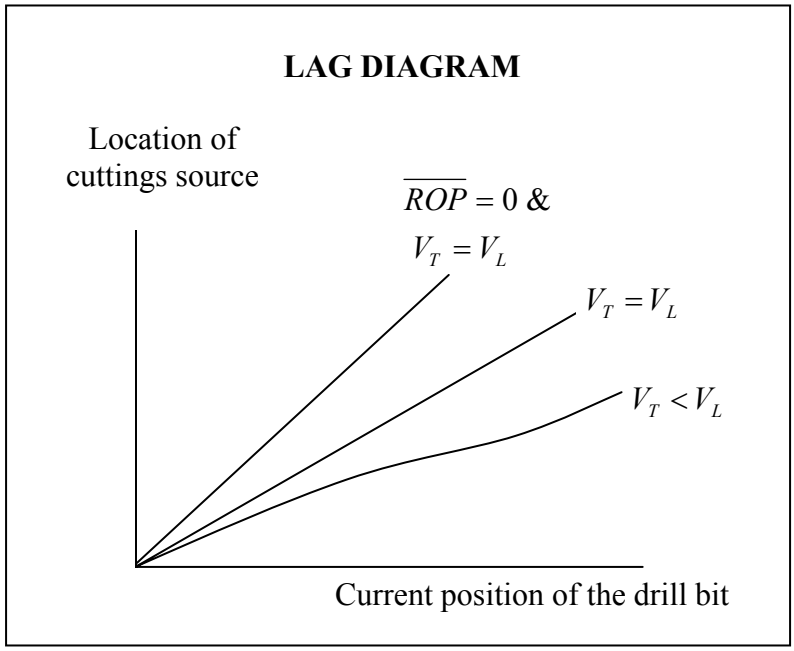

It is essential to highlight that the transport velocity is the most important parameter to consider when we compute the source depth.

Therefore the main objective of the study is to determine the transport velocity for the horizontal well-bore configuration.

Literature Review:

Over the past two decades research has been done on investigation of cuttings transport problems. Most of the methods of investigations can be categorized into three main approaches: the first is an empirical approach that begins with experimentation to obtain data from scale-up models and then correlate these data by dimensional analysis; the second is a semi-theoretical or semi-analytical methods that uses mechanistic modeling along with analytical solutions; the third is a theoretical approach which, by analyzing forces involved in the situation with the use of basic principles, develops a set of equations and then numerically solves them with certain physical or mathematical assumptions.

The experimental large-scale study done by Sifferman[1] defines the variables affecting drill cutting transport under steady-state conditions. It was mentioned that the most important factors controlling cutting transport are annular velocity and rheological properties.

Similar large-scale study of cuttings transport in directional wells was performed by Tomren, Iyoho, and Azar[3]. They determined that the major factors affecting cuttings transport are drilling fluid velocity, hole

inclination angle, and fluid rheological properties. Inclination angles of 40^0 to 50^0 were shown to be critical because of cuttings buildup and downward sliding of the bed of cuttings. They also proved the existence of three different layers that might occur during the flow of mud and cuttings in a well bore. Later Azar and Sanchez[5] extended this study by discussing factors that impact on well-bore cleaning and formulating key issues for future research.

In order to quantify influence of different factors on cuttings transport problem, several studies were performed. One of such studies was presented by Chien[18]. He performed an extensive experimental study on the settling of irregularly shaped particles. On the base of this study, he developed correlations of settling velocity for particles in both Newtonian and non-Newtonian fluids, using relationship between the drag force coefficient and particle Reynolds number. Later, Sample et. al.[2] performed evaluation of the published correlations of Moore, Chien, and Walker and Mayes, using data obtained in the laboratory under both static and flowing conditions. In addition, a new approach was developed. Results of evaluation have shown that the method proposed by Moore provided the best agreement, among three published correlations. However, the new technique was the only procedure of acceptable accuracy for the engineering design of drilling operations.

Iyoho et al.[17] presented a semi-analytical cutting transport model. They proposed computer model for predicting well-bore constituent velocities and concentrations by solving a set of finite-difference equations representing material transport through the well-bore. Iyoho et al.[17] used empirical correlations for particle slip velocity derived by Moore[21] and along with analytical solution for particles concentration within well-bore.

In spite of existence of a number of empirical and semi-empirical models existences, they are mostly the case of experimentally derived relations, limited to very specific ranges of operating conditions. Therefore, several mechanistic models were proposed by various investigators[4, 9, 10, 11, 13, 14.]

The mechanistic models are based on mass balance equations for solids plus momentum balance equations for the two or three layers resulting in a system of coupled algebraic equations. Closure relationships that describe the interaction of the two phases are needed in order to solve these equations and these are taken from published correlations.

Doron and Barnea[9] attempted to group together flow patterns which have similar behavior and refer to their most conspicuous characteristics regarding the distribution of the solids in pipe. They have employed the three-layer model (Doron & Barnea, 1993) for the drawing of flow pattern maps, which can be used to indicate the flow pattern. One year later, they have presented a new mechanistic model[10], providing an extension of their previous model to account for pipe tilt.

Kamp and Rivero[11] developed a two-layer model accounting for existence of moving cuttings bed below a heterogeneous layer of mud and cuttings.

Nguyen and Rahman[13] present a new three-layer model. They distinguished annular flow in uniformly moving at the bottom of the well-bore cuttings layer, dispersed cuttings layer on the top of first layer, and the upper layer of clear mud. The advantage of this model is adaptability for highly deviated well-bores.

Kelessidis&Bandelis[4] provided a wide review of existing two- and three-layer models. They presented the critical parameters, involved in cuttings transport, and proposed a different approach for predicting the minimum suspension velocity. Laboratory system for gathering of good quality data was also presented.

Cho et al.[14] have proposed three-segment hydraulic model. They have basically adopted tree-layer model for horizontal and near horizontal sections, modified existing two-layer model for transient (highly inclined) sections, and used one-layer model for vertical and near vertical sections. On the base of this model they also gave a discussion of various parameters that affect the efficiency of cuttings transport.

In spite of variety of solutions, proposed models are mostly similar. The main differences are whether a two or a three layer model is used and closure relationships.

Approach:

Modify the experimental facility and establish a reliable experimental method to determine the transport velocity of cuttings.

Obtain and analyze experimental data.

Mechanistic modeling for horizontal and highly deviated wells**.**

Scope of Work

1. **Proposed test matrix:**

Stage	Fluid Type	Flow Rate (GPM)	Hole Angle	Pipe Rotation (RPM)
I	Water	200 300 500	70º	0 40
			90º	
II	Polymer	200 300 500	70º	0 40
			90º	

Notes:.

- Average Cuttings size 3-5mm
- Average Specific gravity Cuttings 2.6, (Normal Gravel)
- Average rate of penetration 30ft/h, this parameter depends on the experimental technique
- Estimated Number of test runs: 24x2=48 (the test matrix will be done twice)
- The above test matrix could be modified as more information will be acquired during the tests
- Polymer:
  PAC (Poly Anionic Cellulose)

Consideration for choosing the proposed test matrix:

Flow rate, mud type, mud properties and drill pipe rotary speed affect directly the phenomena in study and can be controlled during the normal process of drilling.

2. Experimental Technique:

A video technique will be used to determine the cuttings velocity. The video acquisition system will provide a digital image of the particle immerge in the traveling fluid.

The video will be made using a CCD Hitachi Camera (KP-F120), which has the following features:

- Progressive Scan, High Resolution, 1.45 Million Pixel Digital Output Camera.
- Spectral Response Extends above 1000 nm, 2/3 inch 1.45 Million Pixel CCD.
- Frame rates of 15, 30, 60 or 120 F / sec., 1392 (H)x 1040 (V) Pixels.
- Choice of Digital Outputs, RS-232 control, Compact Size.

Experimental setup:

Experiments will be realized in the LPAT flow loop facility. It is 90 ft long and consists of an 8-in. inner diameter transparent casing with 4.5 in. outer diameter drill pipe. A 75 H.P. centrifugal pump (maximum tested capacity is 650 gpm), is used to pump fluid into the flow loop. The cuttings are injected at the inlet of the annular test section where they merge with the test section. There will be a visualization section in the middle of the flow loop that will be used to obtain the image of the particles.

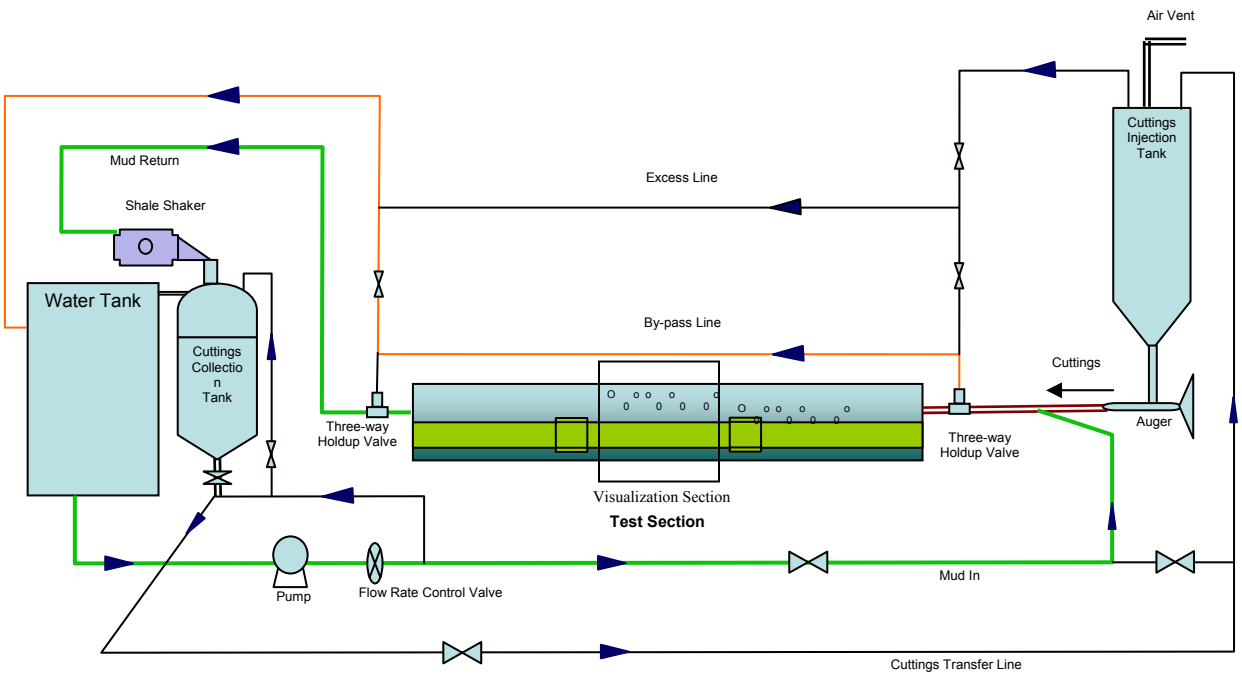

Figure 2.- Schematic diagram of the current flow loop

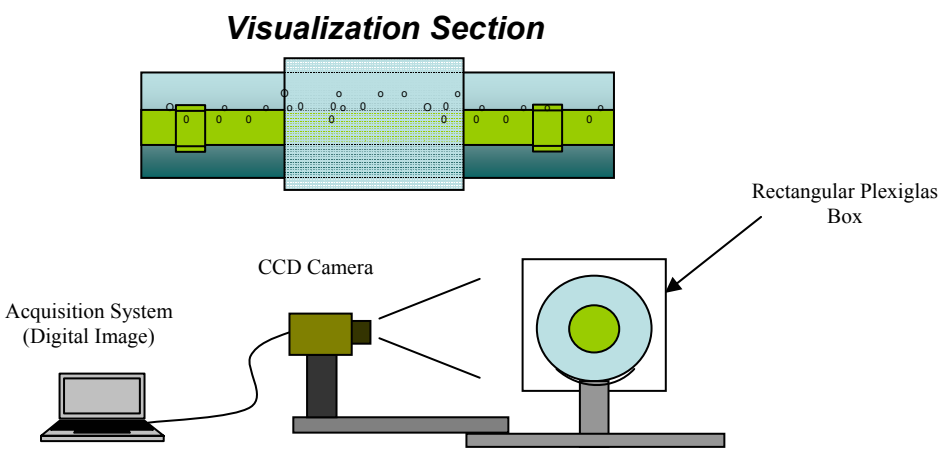

Figure 3.- The proposed modification to the flow loop

Timetable:

Activity/Time	Spring 2005	Summer 2005	Fall 2005	Spring 2006	Summer 2006	Fall 2006	Spring 2007
Literature Review							
Development of experimental technique							
Experiments							
Modeling							
Analysis of the results							
Final Report							

Deliverables:

- Advisory Board Meeting (ABM) Research proposal.
- A mechanistic model to produce lag time diagram for horizontal and highly inclined wells.
- The experimental data will be used to determine the cuttings velocity and compare the results with the computer lag model.
- Semi-annual Advisory Board Meetings Reports and Final Report.

References:

1. Sifferman, Drill Cuttings transport Vertical Annuli. SPE 4514, 1973.
2. Sample et al., An Experimental Evaluation of Correlations Used for Predicting Cutting Slip Velocity, SPE 6645, 1977.
3. Tomren, Iyoho & Azar, Experimental study of cuttings transport in directional Wells. SPE 12123, 1986.
4. Kelessidis & Bandelis, Flow Patterns and Minimum Suspension Velocity for Efficient Cuttings Transport in Horizontal and Deviated Wells in Coiled-tubing Drilling, paper SPE 81746 presented at the 2003 SPE/ICoTA Coiled Tubing Conference.
5. Azar & Sanchez, Important Issues in Cutting Transport for drilling Directional Wells. SPE 39020, 1997.
6. Leising &Walton, Cuttings transport Problems and Solutions in Coiled Tubing. IADC/SPE 39300, 2002.

7. Zeidler, An Experimental Analysis of the transport of drilled Particles, Rice University, Houston, Texas, 1970.
8. Larsen, A Study of the Critical Fluid Velocity in cuttings Transport for Inclined Well bores, Master thesis, University of Tulsa, Tulsa, Oklahoma, 1990.
9. Doron and Barnea, Flow Pattern Maps for Solid-Liquid Flow in Pipes. Int. J. Multiphase Flow Vol.22, Nº 2, pp 273-283, 1996.
10. Doron & Barnea, Flow of Solid-Liquid Mixtures in Inclined Pipes. Int. J. Multiphase Flow Vol. 23, Nº 2, pp 313-323, 1997.
11. Kamp and Rivero, Layer Modeling for Cuttings Transport in Highly Inclined Wellbores, paper SPE 53942 presented at SPE Latin American and Caribbean Petroleum Engineering Conference, 1999.
12. Iyoho, Drilled-Cuttings Transport by Non-Newtonian Drilling Fluids through Inclined, Eccentric Annuli, Ph. D thesis, University of Tulsa, Tulsa, Oklahoma, 1980.
13. Nguyen and Rahman, A Three-Layer Hydraulic Program for Effective Cuttings Transport and Hole Cleaning in Highly Deviated and Horizontal Wells, IADC/SPE 36383, 1996.
14. Cho et al., A Three-Segment Hydraulic Model for Cuttings Transport in Horizontal and Deviated Wells, SPE 65488, 2000.
15. Martings and Santana, Modeling and Simulation of Annular Axial Flow of Solids and Non-Newtonian Mixtures, papers presented at the III Encontro Nacional de Ciencias Termicas, Itapema, Brazil.
16. Gadde et al., Modeling Proppant Settling in Water-Fracs, SPE 89875, 2004.
17. Iyoho et al., A computer Model for Hole-Cleaning Analysis, SPE16694, 1987.
18. Chien, settling velocity of irregularly shaped particles, SPE 26121, 1992.
19. Patankar et al., Power law correlations for sediment transport in pressure driven channel flows, Int. J. Multiphase Flow 28, pp 1269-1292, 2002.
20. Joseph and Ocando, Slip velocity and lift, Department of Aerospace Engineering and Mechanics, University of Minnesota, 2001.
21. Bourgoyne A. et al., Applied Drilling Engineering SPE Textbook Series, Vol. 2, 1991, ISBN 1-55563-001-4.
22. Communication with Dr. Claudia Zettner, Exxon Mobil.